SCUOLA DI DOTTORATO
UNIVERSITÀ DEGLI STUDI DI MILANO-BICOCCA

Dipartimento di Biotecnologie e Bioscienze

PhD in Biotechnology and Biosciences Cycle: XXXI

Curriculum in Biology

Exploiting Nanotechnology to Improve Cancer Immunotherapy and Overcome Biological Barriers

Surname: Rizzuto Name: Maria Antonietta

Registration number: 712513

Supervisor: Prof. Davide Prosperi

Tutor: Prof. Paolo Tortora

Coordinator: Prof. Paola Branduardi

ACADEMIC YEAR 2017/2018

Exploiting Nanotechnology to Improve Cancer Immunotherapy and Overcome Biological Barriers

TABLE OF CONTENTS

ABSTRACT

The use of therapeutic monoclonal antibodies (mAbs) has revolutionized cancer treatment. During the last decades, mAbs became very appealing also for nanotechnology. Indeed, they have been exploited as targeting moieties for nanoparticles, thanks to their high binding efficacy and target selectivity. However, the functionalization of NPs with mAbs is usually performed with the aim to ameliorate targeting, rather than to overcome mAbs limitations. Moreover, the therapeutic implications of nanoconjugation are generally poorly considered.

In this thesis, I focused on the study of cancers with no efficient therapies available, such as brain cancers and triple negative breast cancer (TNBC), with the final goal to exploit nanoparticle (NP) conjugation as a tool to improve antibody-based therapies. In particular my work aimed at increasing the spectrum of action of already existing mAbs, making them suitable for new applications, either as the whole protein or as fragments.

In **Chapter 1**, I used a recombinant human ferritin (HFn) as nanovector to promote mAbs permeation across the BBB to activate the ADCC response against brain cancer. Glioblastoma and HER2+ metastatic breast cancer were selected as brain tumor models. HFn was used as delivery system thanks to the ability to cross the BBB upon interaction with its receptor. Then, cetuximab or trastuzumab were linked to HFn and the maintenance of the cytotoxic activity of NPs was confirmed by in vitro assays. Next, we tested the ability of HFn-mAb to cross an in vitro model of BBB. Results showed that HFn-mAb proved to be effective in BBB crossing and that, after permeation, mAbs retained their biological activity against the targets, as assessed by MTS and ADCC assays.

These preliminary results support the use of HFn as efficient carrier to enhance mAbs permeation into the brain, without affecting their activity.

In **Chapter 2**, half-chain fragments of cetuximab were conjugated to colloidal NPs (HC-CTX-NPs) to be investigated as surrogates of mAbs in TNBC. Three TNBC cell lines were selected according to EGFR expression and to diverse cetuximab sensitivity. The molecular mechanisms of action of HC-CTX-NPs, including cell targeting, interference with signaling pathways, proliferation, cell cycle, apoptosis and ADCC response, were investigated in TNBC cells. We found that HC-CTX-NPs were able to enhance the therapeutic efficacy and improve the target selectivity against sensitive, but unexpectedly also resistant, TNBC cells. Viability assays and signaling transduction modulation suggested that HC-CTX-NPs not only improved the antibody activity but also exerted different mechanisms of action to circumvent CTX resistance. Our results provide robust evidence of the potential of HC-CTX-NPs in the treatment of TNBC, which could improve curative efficiency, reducing dosages in both sensitive and resistant tumors.

ACRONYMS

ADCC	Antibody Dependent Cell-Mediated Cytotoxicity
ACT	Adoptive Cell Therapy
ALL	Acute Lymphoblastic Leukemia
APcs	Antigen Presenting Cells
BBB	Blood Brain Barrier
BC	Breast Cancer
BCS	Breast Conserving Surgery
BSA	Bovine Serum Albumin
CAR	Chimera Antigen Receptor
CNS	Central Nervous System
CTX	Cetuximab
DCIS	Ductal Carcinoma In Situ
DCs	Dendritic Cells
DDS	Drug Delivery System
DLS	Dynamic Light Scattering
DMEM	Dulbecco's Modified Eagle Medium
E	Effector cells
EGFR	Epidermal Growth Factor Receptor
EPR	Enhanced Permeability and Retention
ER	Estrogen Receptor
Fab	Variable Fraction
FBS	Fetal Bovin Serum
Fc	Constant Fraction
FcR	Constant Fraction Receptor

FDA	Food and Drug Administration
FITC	Isotiocianante Fluorescein
FPLC	Fast Protein Liquid Chromatography
GBM	Glioblastoma Multiforme
HC	Half Chain
HFn	Heavy chain Ferritin
HER-2	Human Epidermal Growth Factor Receptor 2
IDC	Invasive Ductal Carcinoma
IgG	Immunoglobulin G
IL-2	Interleukin 2
ILC	Invasive Lobular Carcinoma
IONPs	Iron Oxide Nanoparticles
LCIS	Lobular Carcinoma In Situ
LDH	Lactate Dehydrogenase
mAb	Monoclonal Antibody
Mal	Maleimide
MHC	Major Histocompatibility Complex
MNPs	Magnetic Nanoparticles
MDR	Multi Drug Resistance
MRI	Magnetic Resonance Imaging
NHS	N-HydroxySuccinimide
NK	Natural Killer
NPs	Nanoparticles
PEG	Polyethylene glycol
PBMC	Peripheral Blood Mononuclear Cells
PBS	Phosphate Buffered Saline

PR	Progesteron Receptor
SDS-PAGE	Sodium Dodecyl Sulphate - PolyAcrylamide Gel Electrophoresis
SEC	Size Exclusion Cromatography
SPIONs	Superparamagnetic Iron Oxide Nanoparticles
T	Target cells
TfR1	Transferrin Receptor 1
TMZ	Temozolomide
TNBC	Triple Negative Breast Cancer
TZ	Trastuzumab
WHO	World Health Organization

GENERAL INTRODUCTION

1. CANCER

The term “cancer” encloses a group of more than 100 related diseases, all characterized by an uncontrolled cell growth. It can occur everywhere in the body leading to the formation of a new mass of abnormal proliferating cells that can also acquire infiltrating behaviour spreading in other part of the body. The most validated hypothesis regarding cancer onset is the multistep clonal evolution by which cancer evolves starting from an initial mutation in a single normal cell that acquires selective growth advantages over other cells. As a consequence, the mutated cell starts to proliferate, accumulating genomic instability during generations.[1] This process leads to a step-by-step acquisition of different biological modifications that enable cells to become tumorigenic and malignant, including sustaining proliferative signaling, evading growth suppressors, resisting cell death, enabling replicative immortality, inducing angiogenesis, activating invasion, metastasis, energy metabolism reprogramming and evading immune surveillance (Fig1).[2] Over the years these cancer hallmarks were used as targets for the development of anticancer drugs. A deep understanding of all these cancer hallmarks could help in the development of new pharmacological treatments.

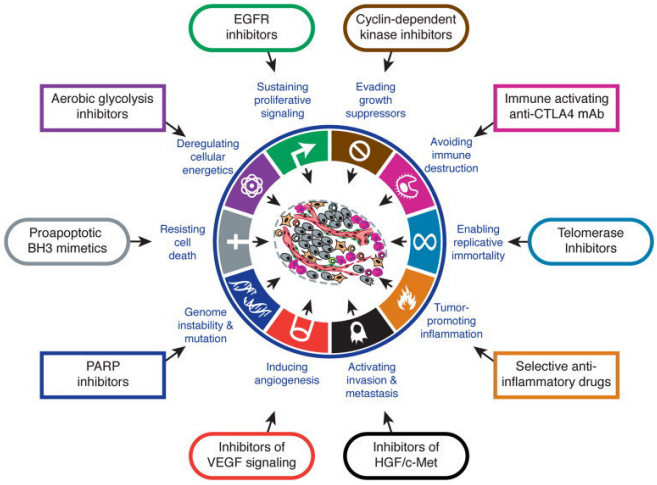

Figure 1. Cancer hallmarks and target elements for therapy. Scheme of all the modifications involved in cancer onset and progression and drugs that have been developed to target each of them.[2]

The last update about cancer incidence worldwide pointed out that cancer is increasing because of the aging of the population and the increasing of tumor-associated risk factors. Indeed, the GLOBOCAN statistics reported 8.2 million cancer deaths and 14.1 million new cancer cases in 2012 worldwide: 7.4 million (53%) in males and 6.7 million (47%) in females, giving a male:female ratio of 10:9. Moreover worldwide cancer incidence rate is predicted to increase by 68% in 2030.[3,4]

1.1. BREAST CANCER

Breast cancer (BC) is the most frequently diagnosed cancer and the leading cause of cancer death among females worldwide, with an estimated 1.7 million cases and 521,900 deaths in 2012. It is so common that BC alone accounts for 25% of all cancer cases and 15% of all cancer deaths among females.[4] From a molecular point of view, breast cancer is universally considered as a very heterogeneous disease characterized by different histopathological and biological features that necessarily lead to different clinical outcomes. Molecular dissimilarities can occur either between different patients with the same tumor type (intertumor heterogeneity), or within the same patient (intratumor heterogeneity).[5-7] In order to organize these BC dissimilarities two complementary classifications have been developed, i.e., histological and molecular classifications.

1.1.1. Histological classification of breast cancer

First, BC can be categorized into in situ carcinoma or infiltrating carcinoma, based on the invasiveness pattern. Between these two groups we can also distinguish in ductal or lobular, depending on tumor origin site (Fig2). As a result of the histological classification we can identify different BC subtypes:[8]

- **Ductal Carcinoma In Situ (DCIS)** is a commonly diagnosed breast lesion that is confined to the ducts. It is non-invasive, but can potentially evolve during time from low-grade to high-grade lesion, with infiltrating behaviour.[9,10]

- **Lobular Carcinoma In Situ (LCIS)** is a less frequent alteration, originating from the milk-producing glands (lobules). LCIS is usually confined in

this area, thus it is considered to be a risk factor rather than a precursor for invasive lobular cancer. However in some cases LCIS can infiltrate surrounding tissues becoming invasive.[11]

- **Invasive Ductal Carcinoma (IDC)** is the most common form of infiltrating breast cancer, accounting for 70-80% of all invasive lesions. IDC originates from ducts epithelial cells that penetrate through the duct wall into the stroma. Over time it can metastasize to lymph nodes and other organs. [8,10]

- **Invasive Lobular Carcinoma (ILC)** originates from the lobules epithelial cells and infiltrates lymph nodes spreading to distant site of the body. It account for 5-15% of invasive breast cancer diagnosis and usually affects older age group woman with IDC.[10]

- **Mucinous (colloid), tubular, medullary, comedo, inflammatory and papillary carcinomas** represent others invasive breast cancers with less incidences. Together they account for the 10% of all BC cases.[12]

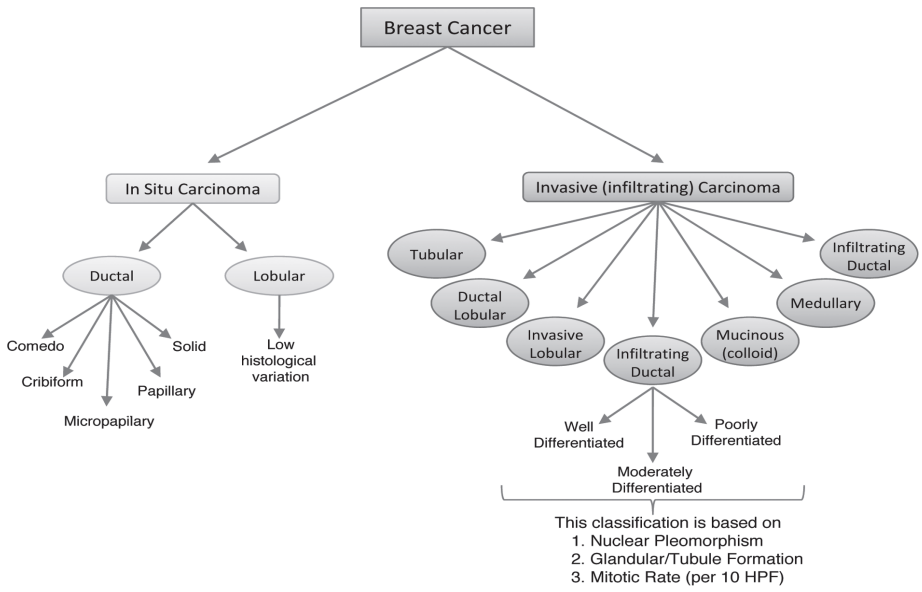

Figure 2. Histological classification of breast cancer[8]

Breast carcinomas are also identified by stages of evolution from 0 to IV that are determined based on the tumor size, the presence of the tumor in the lymph nodes and the onset of metastases (Fig3). In details:

- **Stage 0** comprises non-invasive breast cancers, such as DCIS.

- **Stage I** encloses invasive breast cancers in which cancer cells infiltrate the surrounding breast tissue. Tumor diameter is no more than 2 cm and has not infiltrated the lymph nodes.

- **Stage II** comprises invasive cancers sizing between 2 and 5 cm in diameter and cancers that are not found in the breast but are present in axillary lymph nodes or to the lymph nodes near the breastbone.

- **Stage III** includes invasive cancers with a diameter of 5 cm or more, cancers that are not found in the breast but are present in more than 4 axillary lymph nodes or to the lymph nodes near the breastbone and also cancers of any size but that have spread to axillary lymph nodes, or to the lymph nodes near the breastbone.

- **Stage IV** is also known as metastatic. At this stage cancer has spread to other parts of the body, such as brain, bones, skin, liver and lungs.

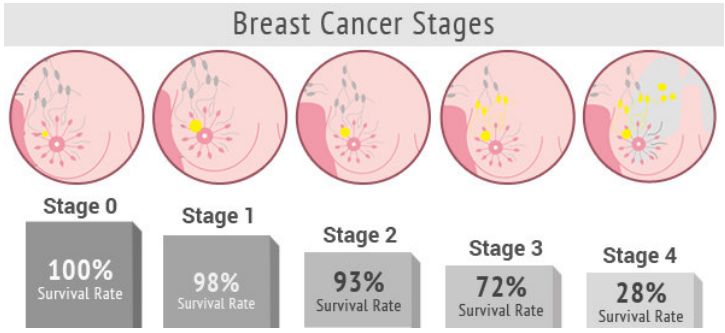

Figure 3. Stages of breast cancer and survival rates (healthonmobile.in)

Recently the American Joint Committee on Cancer (AJCC), which is responsible to oversee this breast cancer staging system, update it including other cancer characteristics, such as tumor grade, hormone-receptors status and HER2 status.[13,14] Indeed, high-throughput molecular profiling studies proved a strong heterogeneity among different BC subtypes in terms of estrogen receptor (ER), progesterone receptor (PR), and HER2 expression.[15] Furthermore these studies revealed a more complicated situation in which molecular dissimilarities occur in different area of the same tumor (spatial intratumor heterogeneity) or in different moments of tumor evolution (temporal intratumor heterogeneity).[16,6] Therefore a better understanding of the molecular heterogeneity of BCs could provide the identification of specific markers useful in the development of subtype-specific targeted therapies. The final idea for these personalized treatments is to improve the therapeutic efficacy as well as reducing side effects.[5]

1.1.2. Molecular classification of breast cancer

The previously mentioned molecular profiling studies using DNA microarray led to a deeper classification of breast cancer, identifying four different so-called intrinsic subtypes: ER+/luminal, HER2-enriched, basal-like and normal-like breast cancer.[15] Approximately 70% of invasive breast cancers are ER+ and the majority of them also express PR. Collectively all the ER+ cancers are classified as luminal. Furthermore, based on the HER2 expression and proliferation rate, these neoplasms are divided in HER2- luminal A and HER2+ luminal B subtypes.[9]

- **Luminal A** is the most common type of BC occurring with a frequency of 28 to 31%. It usually has an ER+/PR+/HER2- profile, with low pathological

grade and low proliferation rate. Among BC subtypes it is the one with the best prognosis. Current treatment includes anti-estrogen drugs, such as Tamoxifen.

- **Luminal B** is less frequent (approximately 20% of patients) and it is usually identified as ER+/PR+/HER2+, with high pathological grade and high proliferation rate. Although both luminal subtypes are associated with a good prognosis and long-term survival (approximately 80-85% 5-years survival), the luminal B is associated with a significantly worse prognosis compared to subtype A. This difference is mainly due to the higher proliferation rate, the larger tumor size and the involvement of lymph nodes. Luminal B subtype is usually treated with anti-estrogenic hormonal therapies (Tamoxifen) together with Trastuzumab (an anti-HER2 drug).

- **HER2-enriched** is characterized by the overexpression of the human epidermal growth factor receptor, HER2. This subtype is usually ER-/PR-/HER2+ and accounts approximately for 17% of all breast cancers. The amplification of HER2 in breast cancer was first reported in 1987[17]. It is generally associated with poor clinical outcomes but it is also predictive of positive responses to anti-HER2 therapy (Trastuzumab).

- **Basal-like** represent approximately 15% of all BCs and it is characterized by the expression of markers of basal-cellular origin, such as basal cytokeratins. This subtype usually doesn't express hormone receptors or HER2 (ER-/PR-/HER2- triple negative breast cancer, TNBC) being not responsive to the previously mentioned targeted therapies. It is associated with aggressive behaviour, high proliferation rate and very poor prognosis, related to a higher likelihood of relapse.

- **Claudin-low** subtype accounts for 10% of all breast cancer. It is

characterized by low expressions of cell-cell adhesion molecules, such as claudin and E-cadherin, while it is enriched for markers of epithelial-to-mesenchymal transition. Similar to basal-like cancer, claudin-low patients have low clinical outcome and very poor prognosis.

- **Normal-like** breast cancers are so called because they tend to cluster very close with the normal breast tissue.

1.1.3. Breast cancer treatment

Breast cancer treatments include surgery, radiation, chemotherapy and more. Treatment choice is usually guided by several factors, such as stage of cancer, cancer molecular profile, involvement of lymph nodes, presence of metastases. In patients with non-invasive or early-stage breast cancer, treatment is generally delivered with curative intent, involving combinations of local treatment (surgery and/or radiation therapy) and systemic treatment (chemotherapy and targeted therapy, including anti-estrogen therapy and anti-HER2 therapy).

Surgery is the first intervention to provide local control of BC, removing the tumor mass and identifying the tumor stage. Breast cancer surgery involves breast-conserving surgery (BCS, also known as partial mastectomy or lumpectomy) or mastectomy. BCS is usually used for the treatment of non-invasive DCIS, when the tumor mass is small and well confined, thus it is possible to remove only tumor tissue and a rim of the surrounding healthy tissue. Treatments for invasive BCs or big tumor masses often require neoadjunvant chemotherapy before surgery, to reduce tumor dimension. When tumor is multi-centric DCIS the removal of the entire breast is required (simple or total mastectomy), whereas for large tumors or positive margins

after BCS, surgical treatment includes also the removal of axillary lymph nodes (modified radical mastectomy).[18] Treatment given after surgery is called adjuvant therapy and may include radiation therapy, chemotherapy, targeted therapy, and/or hormonal therapy. The same treatments may be given when surgery is not possible or in case of a metastatic breast cancer recurrence. Radiation therapy involves the use of high-energy beams to kill cancer cells remaining in the breast after surgery. In the case of BCS the use of radiation shows a 50% reduction in BC recurrence.[19]

A deep understanding of the molecular profile of cancer cells is crucial in the selection of the appropriate targeted therapy. According to breast cancer subtypes, ER+/PR+ patients can be treated used hormonal therapy to block the effect of hormons on cancer cell growth. At present the standard adjuvant endocrine therapy for premenopausal woman is Tamoxifen, which leads to a 40-50% reduction of the 10-year recurrence risk and reduces BC mortality by approximately one-third.[20,21] Furthermore HER2+ breast cancer patients respond very well to treatment with Trastuzumab, a monoclonal antibody that binds to the receptor avoiding its activation. The coming of Trastuzumab has revolutionized BC chemotherapy improving long-term survivor. At present Trastuzumab is approved by the US FDA as the first-line setting for the treatment of HER2+ metastatic breast cancer, and also for the treatment of early stage breast cancer in combination with other chemotherapeutics.[22-24]

1.2. BRAIN CANCER

There are over 100 different types of brain and other central nervous system (CNS) cancers according to the WHO. The 31.5% of primary brain and other CNS tumors are malignant and 68.5% are non-malignant. The most commonly occurring types of CNS and brain cancers are: meningioma (37%), gliomas (25%), pituitary tumors (16%) and nerve sheath tumors (8%).[25,26] Cancer occurring in the brain can be distinguished in primary or secondary (metastatic). Primary tumors account for the 85-90% of all brain tumors and can be classified according to the similarity to a presumed neural or glial precursor (Fig4).[27]

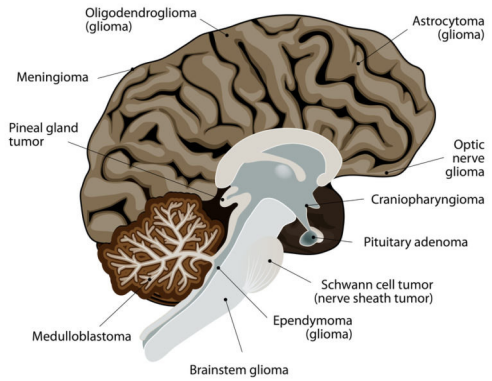

Figure 4. Primary brain tumors. Illustration of the most common primary brain tumors with indication of their origin.

The "histological similarity principle" was the leading idea behind the old Bailey and Cushing's classification system, in which they created parallels between the histological appearances of glial tumors and putative developmental stages of glia. For example, they reasoned that astrocytoma or oligodendroglioma cells microscopically resembled astrocytes or oligodendrocytes respectively. As tumors become more malignant they

resemble less differentiated precursor cells; hence malignant astrocytoma becomes astroblastoma (Fig5).[28,29] Further refinements, such as the addiction of molecular parameters to the histological evaluation, led to the universal approved WHO classification for brain cancer that better characterize tumor subtypes.[30] Secondary brain tumor is the most common cause of tumor in the intracranial cavity. It occurs when cancer cells spread to the brain from other organs. The most common cancers that metastasize to the brain are lung, breast melanoma and gastrointestinal cancers.[31,32] The exact incidence of brain metastases is unknown even though a recent study put it around 9.6% of all cancers.[32,33]

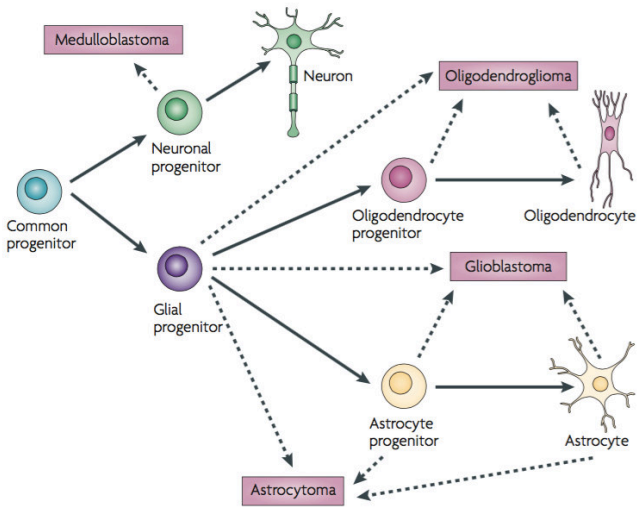

Figure 5. The probable origins of glioma variants and medulloblastoma in the neuroglial lineage tree. Although the precise cells of origin for these cancers remain largely unknown, a selection of likely candidates for each (dashed arrows) is indicated.[34]

1.2.1. Classification of brain cancer subtypes

The 2016 WHO classification for brain tumors integrates genotypic and phenotypic parameters introducing a higher level of objectivity that hopefully will help in the fine diagnosis and treatment. Indeed, in the diagnosis of oligoastrocytomas, the introduction of molecular studies allows to reveal that nearly all of the histologically defined oligoastrocytomas are genetically compatible with either astrocytomas (IDH-mutant, ATRX-mutant, 1p19q-intact) or oligodendrogliomas (IDH-mutant, ATRX-wildtype, 1p19q-codeleted).[30] However histology is still fundamental for the diagnosis of the brain tumor type, before having any molecular analysis, and in case of tumor that do not meet any defined genotype. Moreover, WHO grade determination is still made on the basis of histologic criteria: grades ranging from I to IV, where I is the least aggressive and IV the most aggressive. Among the over 100 entities identified by this classification it is possible to distinguish a big group of malignancies arising from glial cells, a group arising from non-glial cells, such as medulloblastoma, and a third group of metastatic tumors, which can originate either from brain cancers or other organs cancers.[30]

Medulloblastoma

Medulloblastoma is the most common malignant brain tumor in childhood, with a peak of incidence below 10 years old, but it may occur also in adults. Histologically childhood and adult medulloblastoma are identical and correspond to WHO malignancy grade IV. Medulloblastoma occurs in the posterior fossa of the brain, involving also the vermis and cerebellar hemispheres and often infiltrates the fourth ventricle.[35]

Metastatic brain cancers

Secondary, or metastatic, brain cancer usually arise from the bloodstream dissemination of primary cancer cells. The systemic lesions that resulted in brain metastases include lung cancer (40%), breast cancer (17%), and melanoma (11%); these accounted for two-thirds of the brain metastases. The median survival time after brain metastases diagnosis ranges from 3 to 8 months, depending on the primary tumor type.[36]

Gliomas

Gliomas arise from glial or precursor cells and account for the 81% of all malignant brain tumors, representing the most common primary intracranial cancer in adults. It is an heterogeneous disease with multiple subtypes that can occur everywhere in the central nervous system and can be distinguish in astrocytic, oligodendrocytic or both, based on the cells phenotype. Gliomas are typically classified by WHO grades I-IV, according to cell type and malignancy behaviour. In the last classification, the diffuse gliomas included the grade II and III astrocytic tumors, the grade II and III oligodendrogliomas, the grade IV glioblastomas, as well as the related diffuse gliomas of childhood.[30,37] However the absence of a consistent and commonly accepted definition of gliomas from a histological point of view leads to a very difficult definition of the incidence rate of this pathology. The most common glioma subtypes are the following:[26,35]

- **Astrocytoma** is the primary class of diffuse gliomas accounting for 75% of all cases. This group includes the astrocytomas (malignancy grade II), the anaplastic astrocytomas (malignancy grade III), and the glioblastomas (malignancy grade IV). All are more common in males and most are located in the cerebral hemispheres.

- **Oligodendroglioma** develops from glial cells called oligodendocytes. It is more common in adults rather than in children and accounts for 2% of all brain tumors and 5.7% of gliomas.
- **Oligoastrocytoma** is a mixed glioma composed by a combination of an astrocytoma and an oligodendroglioma that account for 1% of all brain tumors and 3.2% of gliomas.
- **Ependymoma** starts in the ependyma of the brain. It's common in children and in adults in their 40s-50s. It accounts for 2% of all brain tumors and 6.9% of gliomas.

1.2.2. Brain cancer treatment

Tumors of the CNS are among the most challenging malignancies to treat. Today, the standard of care in brain tumor treatment consists of cytoreductive surgery, followed by chemotherapy and radiation. However surgery is not possible in all cases and it's not curative, because brain cancer recurs almost in all patients after resection. Besides surgery only very limited options are available for primary brain cancer treatment: from the 1960s until 1998, only two drugs were approved, while in 1999 temozolomide (TMZ), a DNA alkylator, got the FDA approval for treating primary brain tumors. From that moment until now TMZ remains the standard of care.[38,39]

Brain metastases are severe complications, which represent an even stronger challenge to treatment. Indeed pharmacological treatment for primary cancers that metastasize to the brain, such as lung and breast cancers, usually involves therapeutic antibodies, cetuximab and trastuzumab respectively, which are not able to cross the blood-brain barrier and reach the brain.[39]

While treatments in other fields of medicine continue to improve remarkably, little progress has been made in brain cancer treatment and diagnosis. Indeed, many patients still have incurable cancers and suffer disabling symptoms. [38,39] This discouraging situation is mainly due to the highly aggressive nature of brain tumors as well as the presence of biological barriers that limit drugs diffusion. [39] Therefore there is still a strong clinical need to design new highly permeable drugs or to develop new strategies to deliver drugs across the blood-brain barrier.

1.3. BLOOD-BRAIN BARRIER (BBB)

The small capillaries of the brain represent unique morphological and functional units that are fundamental for the exploitation of different roles, such as supplying CNS cells with nutrients and oxygen and maintaining the correct homeostasis. Another important role for this structure is the neurons protection from all the potentially dangerous substances present in the blood. Hence this very specialized capillaries net acting like a physical barrier between brain and bloodstream is called Blood-Brain Barrier (BBB). The barrier function is ensured by the presence of tight junctions between adjacent endothelial cells that avoid the passive paracellular diffusion of molecules with a mass higher that 150 Da (or 400-600 Da for highly hydrophilic compounds). [40] However, the BBB is not only a mechanical fence, but also a dynamic biological entity, in which active metabolism and carrier-mediated transports occur. Nutrients, including glucose, amino acids, and ketone bodies, enter the brain via specific transporters, whereas receptor-mediated endocytosis mediates the uptake of larger molecules, such as neurotrophins.[40,41] Moreover endothelial cells are surrounded by pericytes and astrocytes, with a final cover

of 99%, forming the so-called neurovascular unit (Fig6).[42] The presence of these cells is determinant in the development of tight junctions, because both pericytes and astrocytes release soluble factors that educate endothelial cells to become BBB.[43-45]

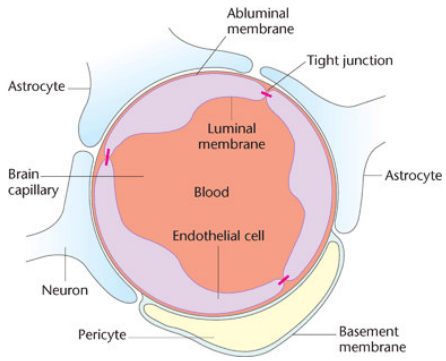

Figure 6. Schematic structure of the neurovascular unit. Blood capillaries in the brain are made of endothelial cells linked together by tight junctions. By the brain side, capillaries are surrounded by astrocytes and pericytes. All this structure is called neurovascular unit.

1.3.1. Blood-Brain Tumor Barrier (BBTB)

The functioning and organization of the BBB can be altered under pathological conditions, such as multiple sclerosis, epilepsy, autoimmune deficiency syndrome (AIDS), dementia, stroke, and brain cancer.[44] During brain tumor development the uncontrolled cell proliferation induces the rapid formation of new blood vessels to provide enough nutrients and oxygen. This abnormal angiogenesis results in the formation of imperfect vessels, with compromised structural integrity and increased permeability.[39] This structural alteration of the barrier can be exploited for the delivery of drugs to the brain thanks to the well-known EPR effect (Enhanced Permeability and Retention):[46] if small enough, drugs can cross fenestrations between adjacent endothelial cells reaching brain tissue.

Importantly, BBTB dysfunction doesn't occur anytime in brain cancer

development being often not able to ensure enough drug loading. For example, low-grade gliomas are characterized by a normal vascularization and a mostly intact BBTB, while high-grade gliomas show alteration of vessels resulting in a disrupted BBTB. However the infiltrating behaviour of high-grade gliomas causes widespread proliferation of cancer cells outside the region of disrupted BBTB and inside the surrounding normal areas, where the function of the barrier is still intact. As a consequence, both the BBB and the BBTB still represent major obstacles in brain cancer treatment, by preventing the delivery of sufficient quantities of drugs.[44]

2. CANCER IMMUNOTHERAPY

Cancer immunotherapy is a treatment that aims at re-educating the patient's own immune system to target cancer cells. The idea to exploit immunology in cancer therapy started in the 1893 with William B. Coley, who observed cases in which cancer retreats after a patient contracted infection. From that moment researchers believe that infections can trigger an immune response able to affect cancer.[47,48] Furthermore a recent discovery aware scientists that immune system is involved in cancer detection and elimination. Burnet and Thomas first developed the concept that the immune system is capable of detecting and killing nascent "non-self" malignant cells in their cancer immunosurveillance hypothesis.[49] Even if at the time this hypothesis could not be validated due to the lack of strong experimental evidences, now many studies support this concept. Among them, one of the most important was the discovery, in 1991, of the first human tumor antigen recognized by T-cells.[49,50] These studies have led to the modification of cancer immunosurveillance into the wider immunoediting hypothesis.[51] This is a

complex process in which immunosurveillance represents only one dimension of the relationship between the immune system and cancer. Cancer immunoediting is a dynamic process composed of three phases: elimination, equilibrium, and escape (Fig7).[52]

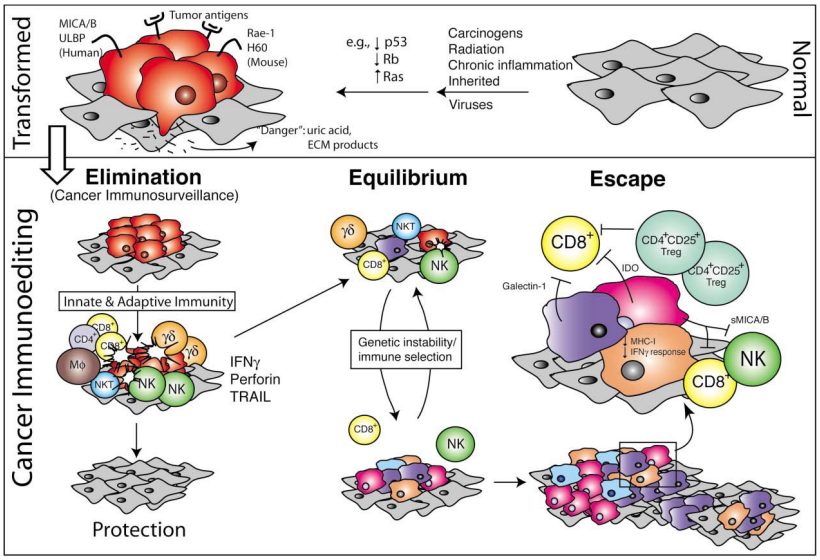

Figure 7. The three phases of cancer immunoediting process. Normal cells (grey) subject to common oncogenic stimuli undergo transformation and become tumor cells (red) (top). These cells may express distinct tumor-specific markers and generate proinflammatory signals that initiate the cancer immunoediting process (bottom). In the elimination phase, cells and molecules of innate and adaptive immunity, which comprise the cancer immunosurveillance network, may eradicate the developing tumor and protect the host from tumor formation. However, if this process is not successful, the tumor cells may enter the equilibrium phase where they may be either maintained chronically or immunologically sculpted by immune "editors" to produce new populations of tumor variants. These variants may eventually evade the immune system by a variety of mechanisms and become clinically detectable in the escape phase.[52]

The **Elimination phase** resembles the classical cancer immunosurveillance concept. It refers to an initial damage and possible destruction of tumor cells by the innate immune system, followed by presentation of the tumor antigens

to dendritic cells (DCs). DCs then process the antigen and degrade it in peptides that will translocate in the membrane creating a complex with MHC (*Major Histocompatibility Complex*) proteins for the presentation to T-cells. The complex MHC I-Ag induces the maturation of tumor-specific CD8+ cytotoxic T-cells, while when the antigen is associated to MHC II, it promotes the maturation of CD4+ T helper cells. This process ensures a strong and specific immune response against tumor cells.[49,53]

The **Equilibrium phase** occurs when any cancer cells survive the elimination phase but are not able to progress. It is a latency period in which the immune system maintains the tumor growth in a state of equilibrium.[49;52]

The **Escape phase** represents the final outgrowth of the tumor: cancer cells grow and metastasize due to the loss of control by the immune system. During escape phase cancer cells may express fewer antigens on their surface or even lose their MHC class I expression. They may also be able to protect themselves from T-cell by expressing immune checkpoint molecules like normal cells.[49]

2.1. NORMAL VS. CANCER IMMUNITY

The immune system is able to identify, eliminate and remember both external (e.g., virus, bacteria) and internal (e.g., cancer) threats. In vertebrate animals immune system has been traditionally divided in innate and adaptive, each one with a particular role (Fig8).

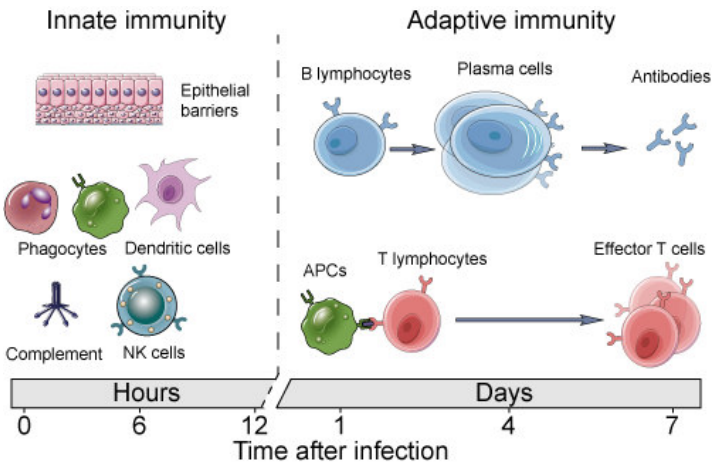

Figure 8. Schematic illustration of cells involved in innate and adaptive immunity responses, with indication of the time needed for their activation. Innate immunity is usually very fast but low specific. It involved mainly macrophages, dendritic cells and NKs. Adaptive immunity is slow but highly specific against the target. It involved B and T lymphocytes.

- **Innate immunity** is the first line of defence. It is characterized by a very fast response, within minutes to hours, due to the absence of any receptor rearrangements. Innate immunity recognition has low specificity and it's mediated by Toll-like receptors. Among the components of innate immunity are macrophages, dendritic cells, neutrophils, mononuclear phagocytes and natural killer (NK) cells, as well as their cellular products, including cytokines and chemokines.[48]

- **Adaptive immunity** is not able to respond immediately to the threat. Indeed, in the adaptive response antigens need to be processed and recognized before responding properly. This antigen presentation activates effectors cells, which in turns elaborates a highly specific response against that antigen. Moreover adaptive immunity incudes the acquisition of a memory, that makes future responses more efficient. The main actors in this process are B- and T-cells. B-cells produce and release antibodies, which can remove

pathogens and circulating antigens and activate the antibody-dependent cell-mediated cytotoxicity (ADCC) in order to kill target cells. T-cells need to recognize antigens on other immune cells, such as DCs, before get activated. After the immune response is completed, T-cells are inactivated to prevent autoimmunity.[48]

During tumor transformation a competent immune system responds by the activation of the already mentioned immunoediting process. This immune surveillance should, in principles, eradicate early malignancies. However, in some cases cancer cells acquire the ability to evade the adaptive response: the cytotoxic action of adaptive T-cells generates a selective pressure in cancer cells, forcing them to mutate to avoid elimination. In particular cancer cells can modulate either their own cellular characteristics, such as losing the MHC class I expression, or the microenvironment. Through the production of various cytokines and chemokines cancer cells may generate an immunosuppressive microenvironment by recruiting and "training" immune cells, including macrophages, regulatory T-cells, immature myeloid cells (which become "myeloid-derived suppressor cells"), T helper 17 cells, regulatory B-cells, and leukocytes.[48,49] This process of immune suppression leads to a state of unresponsiveness to antigens called "immune tolerance".[54]

Tumor cells that enhance immune tolerance either directly or indirectly have a selective survival advantage that results in their outgrowth, representing a major challenge for immunotherapy treatments. Hence, the ability of cancer cells to evade immune destruction has been recently proposed as the eighth hallmark of cancer.[2,54]

2.2. CANCER TREATMENT USING IMMUNOTHERAPY

Cancer immunotherapy is providing a new hope to revolutionize cancer treatment. Through the discovery and development of approaches aimed at stimulating effector cells or at neutralising immune-suppressive mechanisms, immunotherapy is proposing to restore an effective immune response against cancer.[48,55] Thanks to its rapid grow, cancer immunotherapy is now considered to be the "fifth pillar" of cancer therapy, together with surgery, cytotoxic chemotherapy, radiation, and targeted therapy.[49] Cancer immunotherapies can be either passive or active, based on the mechanism of action of the therapeutic agent used (Fig9).

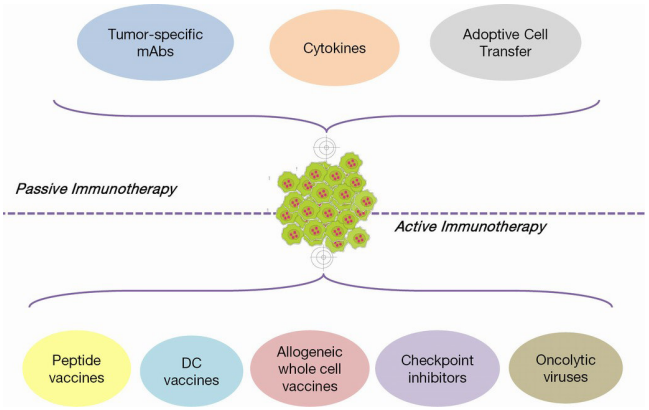

Figure 9. Cancer immunotherapies classification. Cancer immunotherapy approaches are classified into passive and active. Passive immunotherapy includes the use of tumor-specific mAbs, cytokines and adoptive cell transfer, whereas active immunotherapy refers to peptide, DC or allogeneic whole cell vaccines, checkpoint inhibitors and oncolytic viruses. DC, dendritic cell.[56]

2.2.1. Active therapy

Active therapies aim at activating the host immune system by stimulating effector functions *in vivo*. Hence, these protocols demand a competent immune system to be effective. These strategies include vaccination with tumor antigens, the use of oncolytic viruses or checkpoint inhibitors that will better present the antigen triggering an antitumor response. Moreover, by the activation of the host immune system, active therapies are able to induce the generation of an immunological memory of the antigen. Thus they create a long-lasting antitumor effect that can protect against residual cancer cells or recurrence.[47,55]

2.2.1.1. Cancer vaccines

Normally, vaccines are made of a weakened version of a disease and serve to protect people from contracting it. The idea is to present a harmless form of the antigen in order to stimulate the immune system to create an immunological memory against it. The same principle has been exploited against cancer: anti-cancer vaccines are designed to expose patients to tumor antigens inducing a tumor-specific immune response in the patient that aims at stopping the cancer growth and preventing recurrences. Anti-cancer vaccines are categorized in different classes, including antigen-based vaccines, dendritic-based vaccines and whole cell vaccines. Antigen-based vaccine exploits immunogenic peptides from tumor-specific or tumor-associated antigens to elicit the immune response. In dendritic-based vaccines, DCs from the patient are exposed to prostatic acid phosphatase and granulocyte-macrophage colony-stimulating factor (GM-CSF) and reinfused into the patient. Whole cell vaccines are prepared from tumor lysates either

autologous or allogenic thus they present the full range of neoantigens of the tumor, without having to identify them. At present the only vaccine FDA approved for clinical applications is sipuleucel-T, a dendritic-based vaccine used for the treatment of metastatic asymptomatic hormone-refractory prostate cancer.[56,57]

2.2.1.2. Oncolytic viruses

Oncolytic viruses are an emerging class of immunotherapeutics. These viruses are genetically modified to be inoffensive viral strains that selectively target and kill cancer cells, inducing also the formation of a tumor-specific immunity in the host. In detail, after infection in cancer cells, virus replicates until cells lysate releasing more viruses together with tumor antigens. Talimogene laherparepvec (T-VEC) is an oncolytic virus approved in 2015 for the treatment of advanced melanoma. T-VEC is a modified herpes simplex-1 virus, which has been transfected with GM-CSF to further stimulate immune cells proliferation. It is injected in the area of melanoma that surgery can't remove.[49,56]

2.2.1.3. Immune checkpoint inhibitors

It is a group of molecules, mainly mAbs that act during the presentation of the antigen between T-cells and antigen presenting cells (APCs) avoiding T-cells activation. Rather then killing cancer cells, their action is directed against the immunosuppressive state induced by cancer. In the process of T-cells activation there are two stimuli involved: the first one is the interaction between the T-cell receptor (TCR) on T-cells membrane and MHC molecule-tumor peptide on APC membrane, while the second stimulus occurs from the interaction of CD28 (T-cell) and B7-1 or B7-2 (APC). Activated T-cells also

express proteins cytotoxic T lymphocyte-associated 4 (CTLA-4) and programmed death-1 (PD-1). CTLA-4 is an inhibitory receptor that downregulates the initial stage of T-cells activation by competing for binding to B7, while PD-1 when interacts with its ligands PD-L1/L2 promotes the inhibition of T-cell proliferation and cytotoxicity, while enhances T-cell susceptibility to apoptosis. The immune checkpoint inhibitors are mAbs that selectively bind to CTLA-4 and PD-1 competing with their ligands thus avoiding activation. Lots of them have been approved for therapy, such as ipilimumab (against CTLA-4) for the treatment of melanoma; pembrolizumab and nivolumab (against PD-1) for the treatment of unresectable and metastatic malignant melanoma respectively and both for the treatment of NSCLC, head-and-neck squamous cell carcinoma, and Hodgkin's lymphoma; atezolizumab (against PD-1) for the treatment of bladder cancer and NSCLC.[48,55,56]

2.2.2. Passive therapy

Passive therapies are generally used in patients with weak immune responses. These strategies are based on the *ex-vivo* activation of cells or molecules that once re-injected in the body could promote the immune response. Passive therapies include the infusion of tumor-specific antibodies, the systemic administration of cytokines and the adoptive transfer of pre-activated immune cells. Generally this treatment do not generate immunologic memory in cells, thus it requires repeated injections. [47,56]

2.2.2.1. Adoptive cell therapy

Adoptive cell therapy (ACT) is an immunological treatment based on the isolation and *ex vivo* expansion of autologous T-cells, followed by the presentation of tumor antigen and the reinjection in the patient, usually together with interleukin-2 (IL-2). ACT therapies demonstrated to improve patient outcome in both solid and haematological cancers, with a particular effectiveness against metastatic melanoma. [47,56]

In 2010 Rosemberg published data about the so-called chimera antigen receptor (CAR) therapy. It can be considered as an evolution of the adoptive cell therapy, in which T-cell are genetically modified, *ex vivo*, to express CARs against cancer cells. After reinjection in the patient, CAR-T cells that meet the antigen get activated and proliferate *in vivo*, establishing also an immunological memory[54] Clinical studies involving CD19-based CARs for the treatment of acute lymphoblastic leukemia (ALL) show very encouraging results. In one of this studies 27 out of 30 children (90%) infused with autologous T-cells transduced with a CD19-directed CAR, got a complete remission of ALL.[58] However there are still some challenges to face in the use of CAR-T cells, such as the toxicity of the treatment in terms of cytokine release syndrome and neurotoxic effects,[59] as well as the autoreactivity of this system against normal cell expressing low level of the antigen.[54] Hence while researchers are still studying how modulate the system to reduce toxicity, CAR-T cells therapy has been approved by the FDA for the treatment of Relapsed and refractory B-cell acute lymphoblastic leukemia in pediatric and young adult patients.[60]

2.2.2.2. Monoclonal Antibody

Monoclonal antibodies (mAbs) are circulating proteins composed of two main functional parts: a variable fraction (Fab), which is involved in the specific interaction with the antigen, and a constant fraction (Fc) that is mainly involved in the activation of immune system (Fig10).

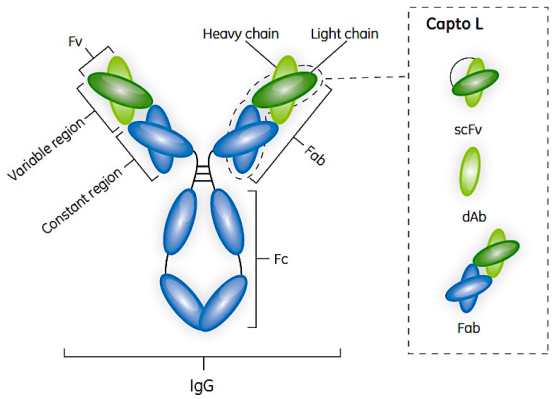

Figure 10. Scheme of monoclonal antibody structure with indication of variable region (green) and constant region (blue).

The most commonly used mAbs in clinic belong to the immunoglobulin G (IgG) class and can be distinguished in "naked," meaning that they are not combined with any other drug, and conjugated. The conjugation usually occurs between the Fc portion of the mAbs and chemotherapy drugs, radioactive particles, toxins or even enzymes that will in turn convert a prodrug in its active form only in the proximity of target cells. Hence, in the combined form mAbs are used as drug delivery system to direct the drug straight to the target reducing systemic side effects. Moreover mAbs that recognize and bind to particular receptor, avoiding the binding of the physiological ligand or the receptor dimerization, such as with tyrosine kinase receptors, are particularly appealing in cancer treatment. Hence, they are able to block specific

downstream signaling pathways and arrest cell proliferation[48,56] (Fig11).

Antibody	Trade name (company)	Target	Antibody type	Cancer type
Alemtuzumab	Campath (Genzyme)	CD52	Humanized	Chronic lymphocytic leukemia
Bevacizumab	Avastin (Roche)	VEGFA	Humanized	CRC, NSCLC, RCC, glioblastoma
Cetuximab	Erbitux (Bristol-Myers Squibb/Lilly)	EGFR	Chimeric	CRC, breast, lung
Denosumab	Xgeva/Prolia (Amgen)	RANK ligand	Human	Solid tumor bony metastases
Gemtuzumab ozogamicin	Mylotarg (Wyeth)	CD33	Humanized	Acute myeloid leukemia
Nimotuzumab	Theraloc/TheraCIM (YM Biosciences)	EGFR	Humanized	Head and neck
Ofatumumab	Arzerra (GlaxoSmithKline)	CD20	Human	Chronic lymphocytic leukemia
Panitumumab	Vectibix (Amgen)	EGFR	Human	CRC
Pertuzumab	Perjeta (Roche)	HER2	Humanized	Breast
Rituximab	Rituxan/MabThera (Biogen, Roche)	CD20	Chimeric	Non-Hodgkin's lymphoma
Tositumomab and ^{131}I-tositumomab	Bexxar (GlaxoSmithKline)	CD20	Mouse	Lymphoma
Trastuzumab	Herceptin (Roche)	HER2	Humanized	Breast

Figure 11. Monoclonal antibodies and conjugates approved for cancer treatment (update to February 2016).

Monoclonal antibodies can mediate an anticancer activity through the induction of programmed cell death upon binding to target cells by the antibody dependent cell mediated cytotoxicity (ADCC), complement cellular cytotoxicity (CDC) and antibody-dependent cellular phagocytosis (ADCP). However, it is important to consider that not all cancer types respond to the same treatment in the same way, thus mAbs are not effective in triggering an equal ADCC response in different tumors. This difference is mainly due to the fact that receptors for the Fc portion of mAbs (FcRs) are not equally sensitive to Fcs. Currently, many mAbs used in cancer treatment target and bind to a certain antigen on cancer cell surface, blocking specific downstream signaling pathways and arresting cell proliferation.[54,56] Ongoing studies are exploring ways to modify mAbs structure to enhance interactions with immune effector cells including NKs and DCs. One example is the creation of bispecific antibodies, in which the protein sequence is modified to have one arm that is specific for a tumor antigen, and the other specific for an antigen on T-cells.

The idea is to maximize the immune response by targeting both the cells and bringing them close enough each other to elicit T-cells cytotoxic activity. Examples of bispecific antibodies include anti-CD19/anti-CD20 (blinatumomab) and anti-EPCAM/anti-CD3 (catumaxomab). Despite bispecific mAbs showed promising activity against some malignancies, they still have some limitations. One of that is the rapid clearance that requires continuous infusion, which represents an issue in their clinical utility.[54,61]

Antibody dependent cell mediated cytotoxicity

Antibody dependent cell mediated cytotoxicity (ADCC) is an immune mechanism through which Fc receptor expressed on effector cells surface, recognize and kill antibody-coated target cells expressing a specific antigen on their surface[62] (Fig12).

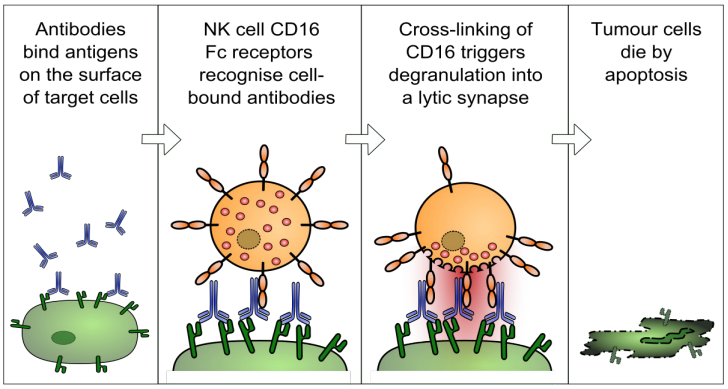

Figure 12. Schematic illustration of the antibody-dependent cell-mediated cytotoxicity mechanism.

Since this mechanism requires the presence of antibodies, it is considered part of the adaptive immune response. In principle, any immune cell capable of secreting cytotoxic proteins or chemicals could potentially drive ADCC;

however the major cell types known for catalyzing ADCC response are $CD56^{+}/CD3^{-}$ NK cells, neutrophils, monocytes and eosinophils.[63]

Nks are considered the main ADCC effectors. They bind the Fc portion of Abs trough their Fc receptor CD16 (also called FcγRIII) and then trigger the degranulation of lytic granules, and the release of cytolytic perforin and granzymes, inducing target cell death.[63]

Neutrophil-mediated ADCC is triggered upon interaction of Fc receptors FcγRI and FcγRIIa with IgG on target cell surface.

Eosinophils have been proved to recognize and kill large parasites via ADCC. Indeed, parasites that are too big to be eliminated via phagocytosis are opsonized with IgE, which binds FcεRI on eosinophils' surface, resulting in degranulation and lysis of the parasite. [63]

Monocytes also have been shown to carry out ADCC in the presence of either IgG_1 (zalutumumab) or IgG_2 (panitumumab) targeting the epidermal growth factor receptor (EGFR)[64]

In monocyte-driven ADCC FcγRIIa seems to be the key receptor for cell killing activation. However, a recent study demonstrates that there is a subpopulation of monocytes, which express FcγRIIIa (CD16). This particular subset shows a broad spectrum of ADCC capacities, suggesting that CD16+ monocytes are important effectors in the ADCC process.[65]

Among monoclonal antibodies approved for clinical practise, trastuzumab, cetuximab, rituximab, obinutuzumab are reported to elicit an effective ADCC response.[66]

Trastuzumab

Trastuzumab (TZ, also known with the trade name of Herceptin®) is a humanized mAb specific for the HER2, which is a transmembrane tyrosine kinase receptor belonging to the ErbB family. Upon dimerization with other ErbB family members, HER2 leads to the activation of proliferation and survival pathways. Thus TZ inhibits HER2 dimerization through the binding to domain IV of the extracellular segment of the HER2 receptor. Proposed mechanisms of TZ actions include inhibition of HER2 shedding, inhibition of PI3K-AKT pathway, attenuation of cell signalling, antibody-dependent cellular cytotoxicity, and inhibition of tumor angiogenesis. [67] Besides preventing HER2 from dimerization, trastuzumab is also capable to mediate ADCC against HER2-positive tumor cells.[66] It is currently approved as the first-line setting for the treatment of HER2+ metastatic breast cancer and for the treatment of early stage breast cancer in combination with other chemotherapeutics.[22-24]

Cetuximab

Cetuximab (CTX, also known with the trade name of Erbitux®) is a human-mouse chimeric mAb specific for EGFR that is approved for the treatment of EGFR-expressing metastatic colorectal cancer, metastatic non-small cell lung cancer and head and neck cancer.[66] CTX binds to the extracellular domain of EGFR competing with the endogenous ligand binding. This interaction results in the blockade of receptor-dependent signal transduction pathways, providing several antitumor effects such as cell-cycle arrest, induction of apoptosis, inhibition of angiogenesis, inhibition of metastasis, internalisation and downregulation of the EGFR and enhancement of sensitivity to radio- or chemotherapy.[68] Moreover there is evidence that CTX is also able to elicit the

ADCC immune response and clinical data confirm that CTX-mediated ADCC may contribute to its anti-tumor activity. [66]

3. NANOTECHNOLOGY

The concept of “nanotechnology” starts in the 1959 at the American Physical Society meeting with the American physicist Richard Feynman (Nobel Prize in Physics 1965). During his lecture “There's plenty of room at the bottom” Feynman raised the possibility of manipulating matter on the small-scale, interfering with the biological system at the atomic level. "*A biological system* - he said - *can be exceedingly small. Many of the cells are very tiny, but they are very active; they manufacture various substances; they walk around; they wiggle; and they do all kinds of marvelous things – all on a very small scale. Also, they store information. Consider the possibility that we too can make a thing very small which does what we want – that we can manufacture an object that maneuvers at the level!*". [69]

In 2004 the Royal Society & the Royal Academy of Engineering defined nanoscience "*as the study of phenomena and manipulation of materials at atomic, molecular and macromolecular scales, where properties differ significantly from those at a larger scale*" and nanotechnology "*as the design, characterization, production and application of structures, devices and systems by controlling shape and size at the nanometer scale*". [70] Therefore, we can fix nanotechnology as the study, the design, the production and the application of extremely small things, in order to create materials, devices, and systems with new properties and functions by engineering their structure.

Although the term "nano" theoretically refers to size ranging from 1 to 1000 nm, the most interesting range goes from 1 to 100 nm. Indeed, at this

level materials have peculiar physical properties that differ from those of the same materials at a larger size (Fig13).[71]

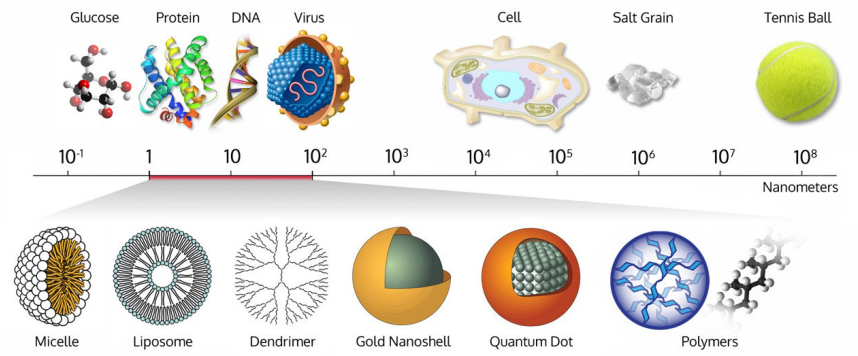

Figure 13. Nanometer Scale.

Nanoparticles (NPs) features include a remarkable high surface-to-volume ratio. As a particle decreases in size, a greater proportion of atoms are found at the surface compared to those inside. This increased surface-to-volume ratio is very important in biological systems, because it results in an improvement in chemical reactivity of NPs with molecular targets along with an increase of the surface area available for functionalization.[72] Furthermore the behavior of matter at the nano-level is dominated by the quantum effect, which affects the optical, electrical and magnetic properties of nanoparticles. Moreover, NPs dimensions fall in the typical range size of biological molecules such as proteins, DNA and others, making them appropriate tools for biomedical applications.[71]

Nanotechnology gained lots of interest in the last decades involving many research fields, such as Health and Medicine, Electronics, Transportation, Energy and Environment, Spatial exploration.[73] However, nowadays Nanomaterials, Nanoelectronics and Nanomedicine are considered to be the most important areas in which nanotechnology can bring innovations.

3.1. NANOMEDICINE

The term Nanomedicine refers to the application of nanotechnology to disease treatment, molecular imaging, diagnosis, monitoring, and to the control of biological systems.[74] Thanks to their outstanding properties and dimensions, nanoparticles may cross biological barriers and specifically interact with target molecules at the sub-cellular scale. Thus, if suitably designed, NPs may find and treat the disease, for example by locally releasing drugs. Nanoparticles able to be both diagnostic and therapeutic agents are known as *theranostic*. This potential application of nanotechnology in the biomedical field can be summarized in the "pattern of the three F" (Find, Fight & Follow), which mean detection, therapy and monitoring of the diseases and represent the stages of early diagnosis, medicine and therapy control.[75] Furthermore nanotechnology have been exploited to overcome lots of medicine limitations, especially in cancer treatment. Indeed, even though chemotherapy and radiotherapy are often effective in reducing tumor mass, they usually have significant systemic toxicities and side effects, due to their unspecific diffusion through all the body. Moreover lots of current treatments fail due to the late detection of the disease. Given that, nanotechnology aims to improve medicine by ensuring a rapid detection of the disease and a specific delivery of drugs and other therapeutics to the target tissue.[71,73,81]

3.1.1. Diagnosis

The diagnosis of a disease is a crucial point in clinic as it may determine the success of the therapy. Diagnoses are required to be quick, but must also be reliable, specific and accurate, and with minimum risk of "false positives". Nanomedicine has the potential to greatly improve the diagnostic process

thanks to the quantum effect of NPs that can be used to amplify detection signals. Thus the design of nanodevices for diagnostic purposes may improve analysis in terms of specificity, number of tests that can be done simultaneously (throughput) and read-out.[76] Some of these devices already exist such as nanosensors, which are able to detect certain substances in the bloodstream or even to identify specific cells inside the body. In details, they may recognize cancer cells over healthy cells by detecting peculiar biomolecules released or produced by such cells so that the rate of growth and development of such regions of the body is monitored. Other examples include hand held devices, such as the glucose test devices (GlucoWatch®) used by diabetics.[77] These devices can measure ions, small molecules, or proteins, or can test for specific DNA sequences that are diagnostic for a particular disease or medical condition.

3.1.2. Imaging

One of the main focuses of research in medical diagnostics is molecular imaging. The term "imaging" refers to the visualization of cellular functions and the follow up of molecular and biological processes in living organisms. Hence, molecular imaging can enable early diagnosis, as well as identify the stage of disease, provide fundamental information on pathological processes and can be applied to follow the efficacy of therapy.[78]

Nanoparticles have shown great potential as probes for tumor staining. Excellent contrast, long circulation time and the possibility to include high payloads are some of the advantages ensured by NPs. In particular, NPs have been explored as new tools both in optical imaging and magnetic resonance imaging (MRI).[78,79] Fluorescent probes are appealing due to their high

sensitivity, lack of non-ionizing radiation, cost-effectiveness and potential for real-time imaging. However, they present several limitations, such as low tissue penetration, low fluorescence intensity, photoinstability, broad emission bands and high photobleaching rates. To overcome these disadvantages, nanotechnology provide a new class of fluorescent materials, known as quantum dots (QDs). They are ultrasmall, highly stable nanocrystals with wide excitation spectra and narrow emission spectra tunable in the near infrared region (NIR). Moreover the high signal intensity and resistance to photobleaching of QDs make them interesting tool for optical imaging.[79]

Magnetic nanoparticles (MNPs) comprise metallic, bimetallic, and superparamagnetic iron oxide nanoparticles (SPIONs). Due to their intrinsic magnetic properties, these NPs have been largely studied as MRI contrast agents. Thanks to their low toxicity profile, several of these nanoformulations have been approved for clinical applications: Lumiren® for bowel imaging, Feridex IV® for liver and spleen imaging, Combidex® for lymph node metastases imaging. This first generation of SPIONs provide passive targeting of the tissue, while now studies aim at increasing targeting specificity by adding bioactive molecules to the SPION surface.[80]

3.1.3. Drug Delivery and Drug Delivery System (DDS)

Drug distribution inside the body is challenging for many reasons including poor bioavailability, in vivo stability, solubility, intestinal absorption, therapeutic effectiveness and side effects on non-specific organs. The goal of nanotechnology in drug delivery is to overcome these limitations thanks to the development and fabrication of nanostructures, which can provide several advantages. [82] The strategies used to ameliorate drug distribution through

nanoparticles design act on the improvement of pharmacokinetic and pharmacodynamic of drug molecules. In particular, therapeutic and diagnostic agents can be encapsulated, covalently attached, or adsorbed on nanocarriers, overcoming some critical issues, such as drug solubility or stability in biological fluids. [71,73,83,84] A critical issue in the design of NPs as drug delivery system is the dimension and the surface composition. Indeed, once in the bloodstream, NPs may be taken up by the mononuclear phagocytic system (MPS). The process of sequestration begins with opsonization of nanoparticles, involving the adsorption of plasma proteins. Phagocytes specifically recognize the protein corona formed around NPs inducing their elimination. To maximize circulation times, the optimal size of NPs should be less than 100 nm in diameter and the surface should be hydrophilic to circumvent clearance by macrophages. However, one of the advantages of nanoparticles synthesis is the possibility of tuning size and composition in order to make NPs invisible to the MPS avoiding the elimination.[85,87] Nanoparticles that satisfy these characteristics can circulate in the bloodstream longer, thus having higher chances to reach the tumor.

In this way, nanotechnology may revolutionize drugs efficacy as well as pharmacological treatments. Moreover, through the reformulation of existing drugs, NPs may improve the performances of some classic medicines making them more effective, increasing patient compliance, reducing healthcare costs and side effects. [83,71,73,83,84]

3.2. TARGETING

Paul Ehrilch (Nobel Prize in Physiology or Medicine in 1908) was the first to introduce the concept of drug targeting, by describing a hypothetical "magic bullet" capable to selectively act on diseased tissues without affecting normal cells.[86] Nanotechnologies offer the possibility to design such "magic bullets" that may effectively accumulate inside the tumor and ensure a controlled drug delivery. Indeed, as already mentioned, most current anticancer agents do not differentiate between cancerous and normal cells, leading to systemic toxicity and severe side effects. As a result, all these adverse effects, such as bone marrow suppression, cardiomyopathy, and neurotoxicity, strongly limit the maximal allowable dose of drug and reduce patients' compliance.

There are two main strategies by which targeting can be achieved, namely **passive** and **active** targeting. Passive targeting exploits some tumor abnormalities in order to be preferentially internalized inside the cancerous microenvironment, while in active targeting NPs are decorated with some functionalities, such as ligands or peptides, that actively recognize and interact with specific receptors on cancer cells surface (Fig14).[87,88]

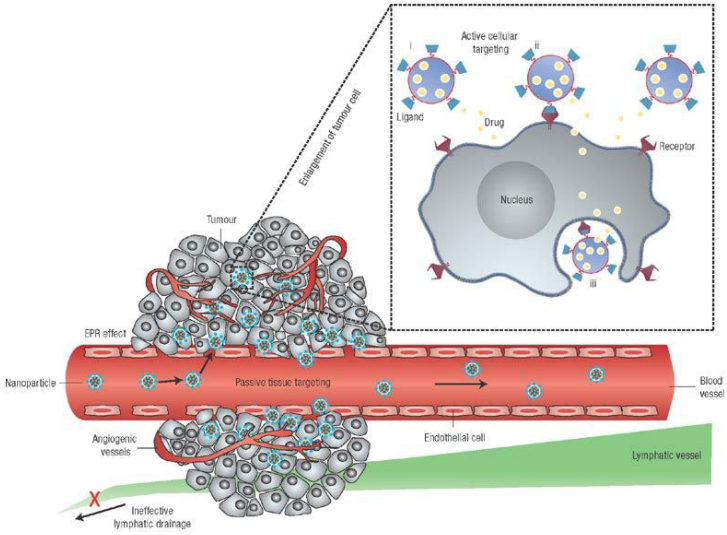

Figure 14. Schematic representation of passive and active targeting of nanoparticles to the tumor. Passive targeting is achieved by extravasation of NPs through defective vessels of tumor mass and ineffective lymphatic drainage (EPR effect). Active targeting (inset) is achieved by functionalizing the surface of NPs with ligands that promote cell-specific recognition. NPs can (i) release their contents in close proximity to the tumor cell; (ii) attach to the membrane of the cell and promote a prolonged extracellular drug release; or (iii) internalize into the cell by receptor-mediated endocytosis.[89]

3.2.1. Passive Targeting

During tumor formation, normal vascular tissues made of tight lined endothelial cells become defective and more permeable than in healthy tissues. Indeed, the increasing need of nutrients and oxygen by cancerous cells lead to the rapid formation of leaky vessels characterized by abnormal branching and enlarged inter-endothelial gaps, which allow a massive exchange of substances. Moreover tumor mass is also characterized by an impairment in lymphatic drainage, which results in a prolonged retention of these substances inside the tissue. However, together with nutrients, the leaky blood vessels allow the extravasation and accumulation of nanoparticles with

sizes of up to 400 nm in the tumor interstitial space. This well-known mechanism, called "enhanced permeability and retention" (EPR) effect,[90,91] was first described by Matsumura and Maeda in 1986: in their study authors observed that NPs better accumulate in tumor tissue compared to small molecules.[92] At present, most of the currently approved nanomedicines rely on the passive drug targeting, even though this approach still has some limitations: first, the random nature of EPR effect makes it difficult to control the process and can result in the onset of multiple-drug resistance (MDR) mechanisms; second, EPR effect is not common in all tumors and there are many large tumors cases displaying a high degree of pathophysiological heterogeneity, which limits the penetration of nanoparticles; finally although often the formulation is effectively delivered to the tumor microenvironment, internalization of the drug into the cell is not guaranteed.[93]

3.2.2. Active targeting

Active targeting involves the use of a variety of affinity moieties (such as ligands, antibodies or peptides) to direct the binding of nanoparticles to many biological targets, receptors or other surface membrane proteins overexpressed on target cells. Hence, these functionalities may promote NPs internalization in cancer cells by triggering receptor-mediated endocytosis. As a result active targeting ensure the release of drugs inside, or at least nearby, tumor cells improving therapy efficacy. Moreover, this mechanism shows the potential to suppress multidrug resistance via bypassing of P-glycoprotein-mediated drug efflux.[88,91]

Numerous targeting ligands have been employed to actively target nanoparticles including antibodies, antibody fragments, aptamers, peptides and whole proteins (e.g., transferrin) and different receptor ligands (e.g., folic

acid). Obviously, for this mechanism to be selective and successful, the antigen chosen as a target should be as much as possible exclusively, or at least preferentially, expressed on cancer cells than healthy counterparts. For example, receptors for folate and transferrin (TfR) are overexpressed on many cancer cells and have been used to make nanoparticles specific for tumor cells. However, despite the potential benefit of active targeting is widely accepted, this technology has resulted in a few clinically validated products. [87,88,91,94]

Antibody-based targeting

Antibodies were among the first agents used for targeting NPs to specific cell types. They are extremely useful either as therapeutic or target agents thanks to their high selectivity and binding affinity to the target. Currently there are over 70 among chimeric, humanized and fully human mAbs approved until 2017, with a further 50 awaiting marketing approval or under clinical trials.[95,96] However mAbs still have some limitations, such as their large size and immunogenicity, which result in a rapid clereance.[91] Hence, more recently the scientific community interest shifted to the development and use of antibody fragments (Ab-fragments) as new therapeutics.

Ab-fragments (Fig15) have very different structure and dimension each other, but in principle they are all smaller than the native mAb and lack an Fc domain. The smaller size offers different properties compared to the whole mAb, such as more binding events per mass of protein administered and the possibility to improve tissue delivery and penetration. Moreover the lack of the Fc portion avoid immunogenicity even though reduces the circulating half-life.[97] Several Ab-fragments-based therapeutics have been approved for clinical application, such as ReoPro® (abciximab), Lucentis® (ranibizumab) and Cimza® (certolizumab), with many others under development.[97]

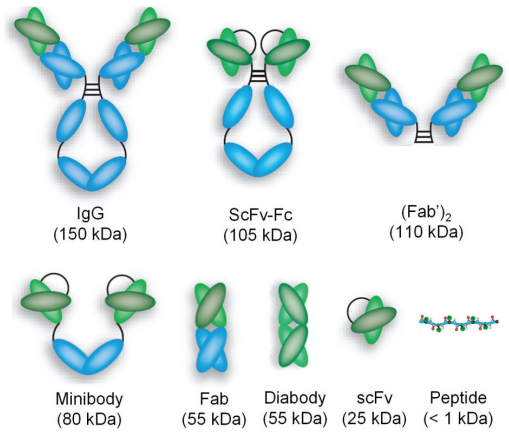

Figure 15. Schematic representations of the main antibody fragments structure. The antigen binding region, variable fraction, is in green and the constant region in blue.

3.3. NANOPARTICLES FOR CANCER TREATMENT

Cancer is a major public health problem and a leading cause of death worldwide and despite all clinical efforts lots of malignancies still have no effective treatments. Moreover cancer incidence statistics by WHO are projected to increase in the next decades.[98] Among the reasons why lots of pharmacological strategies fail, the mains are the poor selectivity of the drugs and the onset of resistance, resulting in systemic toxicity and ineffectiveness of the treatment, respectively. In this scenario, nanotechnology can help in overcoming current drug limitations: the encapsulation of cytotoxic drugs into NPs may reduce toxicity, extend blood circulation time and increase stability via the reduction of their systemic exposure. Nanocarriers can protect payload from biodegradation or excretion, influencing the pharmacokinetic profile of a compound. Moreover the encapsulation of a high quantity of drug can protect from extrusion via the MDR efflux pumps, overcoming resistance. Finally, the nanoformulation may improve biodistribution and tissue penetration and, if functionalized with targeting agents, NPs can also provide a mechanism to

deliver these drugs specifically to the tumor site.[98,99]

Therapeutic and diagnostic nanoparticles usually belong to two categories: inorganic (e.g., iron oxide, gold, silica, etc.) or organic nanoparticles (e.g., polymeric, liposomes, etc.); the first is mainly exploited for imaging and thermoablation purposes, while the second is used for a wider range of applications, such as vaccine development, delivery system for anti-cancer drugs or contrast agents. Interestingly, all of the approved nanoformulations are liposome systems encapsulating anti-cancer drugs with the only exception for Abraxane®, which is an album-bound paclitaxel nanoparticle approved for the treatment of breast, lung and pancreatic cancers. The liposome-based formulations include Doxil® (used for the treatment of ovarian cancer, HIV-associated Kaposi's sarcoma and multiple myeloma) and Myocet® (used for metastatic breast cancer treatment), which are liposomal doxorubicin nanomedicines with or without a PEG shell respectively; DaunoXome® (approved for the treatment of HIV-associated Kaposi's sarcoma) and Marqibo® (used for Philadelphia chromosome-negative acute lymphoblastic leukemia treatment), which are liposomal daunorubicin and vincristine respectively; Onivyde®, which is a liposomal formulation for irinotecan used for metastatic pancreatic cancer treatment; etc (Fig16). Moreover, despite all the advantages and clinical benefits that a targeted therapy could bring, all of the currently approved nanoformulation are passively delivered.[100]

Name	Particle type/drug	Approved application/indication	Approval (year)	Investigated application/indication	ClinicalTrials.gov identifier
Cancer Nanoparticle Medicines					
Doxil/Caelyx (Janssen)	Liposomal doxorubicin (PEGylated)	Ovarian cancer (secondary to platinum based therapies) HIV-associated Kaposi's sarcoma (secondary to chemotherapy) Multiple myeloma (secondary)	FDA (1995) EMA (1996)	Various cancers including: solid malignancies, ovarian, breast, leukemia, lymphomas, prostate, metastatic, or liver	166 studies mention Doxil 90 studies mention CAELYX
DaunoXome (Galen)	Liposomal daunorubicin (non-PEGylated)	HIV-associated Kaposi's sarcoma (primary)	FDA (1996)	Various leukemias	32 studies mention DaunoXome
Myocet (Teva UK)	Liposomal doxorubicin (non-PEGylated)	Treatment of metastatic breast cancer (primary)	EMA (2000)	Various cancers including: breast, lymphoma, or ovarian	32 studies mention Myocet
Abraxane (Celgene)	Albumin-particle bound paclitaxel	Advanced nonsmall cell lung cancer (surgery or radiation is not an option) Metastatic breast cancer (secondary) Metastatic pancreatic cancer (primary)	FDA (2005) EMA (2008)	Various cancers including: solid malignancies, breast, lymphomas, bladder, lung, pancreatic, head and neck, prostate, melanoma, or liver	295 studies mention Abraxane
Marqibo (Spectrum)	Liposomal vincristine (non-PEGylated)	Philadelphia chromosome-negative acute lymphoblastic leukemia (tertiary)	FDA (2012)	Various cancers including: lymphoma, brain, leukemia, or melanoma	23 studies mention Marqibo
MEPACT (Millennium)	Liposomal mifamurtide (non-PEGylated)	Treatment for osteosarcoma (primary following surgery)	EMA (2009)	Osteosarcomas	4 studies mention MEPACT: 3 active/recruiting
Onivyde MM-398 (Merrimack)	Liposomal irinotecan (PEGylated)	Metastatic pancreatic cancer (secondary)	FDA (2015)	Various cancers including: solid malignancies, breast, pancreatic, sarcomas, or brain	7 studies mention MM-398/ Onivyde: 6 active/recruiting
Iron-replacement nanoparticle therapies					
CosmoFer/INFeD/ Ferrisat (Pharmacosmos)	Iron dextran colloid	Iron deficient anemia	FDA (1992) Some of Europe	Iron deficient anemia	6 studies mention INFeD: 1 recruiting
DexFerrum/DexIron (American Regent)	Iron dextran colloid	Iron deficient anemia	FDA (1996)	Iron deficient anemia	6 studies mention DexFerrum
Ferrlecit (Sanofi)	Iron gluconate colloid	Iron replacement for anemia treatment in patients with chronic kidney disease	FDA (1999)	Iron deficient anemia	13 studies mention Ferrlecit: 2 recruiting
Venofer (American Regent)	Iron sucrose colloid	Iron replacement for anemia treatment in patients with chronic kidney disease	FDA (2000)	Iron deficient anemia Following autologous stem cell transplantation	44 studies mention Venofer
Feraheme (AMAG)/ Rienso (Takeda)/ Ferumoxytol	Iron polyglucose sorbitol carboxymethylether colloid	Iron deficiency in patients with chronic kidney disease	FDA (2009)	Iron deficient anemia Imaging: brain metastases, lymph node metastases, neuroinflammation in epilepsy, head and neck cancer, myocardial infarction, or multiple sclerosis	57 studies mention Ferumoxytol: 6 recruiting/active for anemia treatment 22 recruiting/active for imaging applications
Injectafter/Ferinject (Vifor)	Iron carboxymaltose colloid	Iron deficient anemia	FDA (2013)	Iron deficient anemia	50 studies mention Ferinject 8 studies mention Injectafer
Monofer (Pharmacosmos)	10% Iron isomaltoside 1000 colloid	Treating iron deficiency and anemia when oral methods do not work or when iron delivery is required immediately	Some of Europe	Iron deficient anemia	22 studies: 3 active/recruiting
Diafer (Pharmacosmos)	5% Iron isomaltoside 1000 colloid	Iron deficient anemia	Some of Europe	Iron deficient anemia	1 recruiting study

Name	Particle type/drug	Approved application/indication	Approval (year)	Investigated application/indication	ClinicalTrials.gov identifier
Nanoparticle/microparticle imaging agents					
Definity (Lantheus Medical Imaging)	Perflutren lipid microspheres	Ultrasound contrast agent	FDA (2001)	Ultrasound enhancement for: liver or breast or intraocular or pancreatic tumors, pulmonary diseases, heart function, transcranial injuries, strokes, or liver cirrhosis	58 studies mention Definity
Feridex I.V. (AMAG)/ Endorem	Iron dextran colloid	Imaging of liver lesions	FDA (1996) Discontinued (2008)	N/A: No current studies	4 studies mention Endorem 2 studies mention Feridex No current active or recruiting studies
Optison (GE Healthcare)	Human serum albumin stabilized perflutren microspheres	Ultrasound contrast agent	FDA (1997) EMA (1998)	Ultrasound enhancement for: lymph node, renal cell carcinoma, myocardial infarction, pulmonary transit times, or heart transplant rejections	11 currently active or recruiting studies
SonoVue (Bracco Imaging)	Phospholipid stabilized microbubble	Ultrasound contrast agent	EMA (2001)	Ultrasound enhancement for: liver neoplasms, prostate or breast or pancreatic cancer, or coronary/pulmonary disease	43 studies mention SonoVue
Resovist (Bayer Schering Pharma)/ Clavist	Iron carboxydextran colloid	Imaging of liver lesions	Some of Europe Discontinued (2009)	N/A No current studies	2 studies mention Resovist: No current active or recruiting studies
Ferumoxtran-10/ Combidex/Sinerem (AMAG)	Iron dextran colloid	Imaging lymph node metastases	Only available in Holland	Imaging lymph node metastases	11 studies mention ferumoxtran-10: 1 active
Nanoparticle vaccines					
Epaxal (Crucell)	Liposome with hepatitis A virus	Hepatitis A vaccine	Some of Europe (Discontinued)	Safety and immunogenicity of hepatitis A vaccine	6 studies mention Epaxal: 1 recruiting
Inflexal V (Crucell)	Liposome with trivalent-influenza	Influenza vaccine	Some of Europe (Discontinued)	Safety and immunogenicity of influenza vaccine	14 studies mention Inflexal V: All completed
Particle anesthetics					
Diprivan	Liposomal propofol	Induction and maintenance of sedation or anesthesia	FDA (1989)	General anesthesia in specific situations: morbidly obese patients, open heart surgery, or spinal surgery	110 studies mention Diprivan
Nanoparticles for fungal treatments					
AmBisome (Gilead Sciences)	Liposomal amphotericin B	Cryptococcal Meningitis in HIV-infected patients Aspergillus, Candida, and/or Cryptococcus species infections (secondary) Visceral leishmaniasis parasite in immunocompromised patients	FDA (1997) Most of Europe	Preventing or treating invasive fungal infections	50 studies mention AmBisome
Nanoparticles for macular degeneration					
Visudyne (Bausch and Lomb)	Liposomal verteporfin	Treatment of subfoveal choroidal neovascularization from age-related macular degeneration, pathologic, or ocular histoplasmosis	FDA (2000) EMA (2000)	Macular degeneration	52 studies mention Visudyne

Figure 16. List of nanoparticles approved for clinical applications, grouped by their broad indication.[100]

3.3.1. Ferritin NPs

Ferritin is a globular protein of about 450 kDa that plays a fundamental role in iron metabolism. It was discovered more than 80 years ago by Laufberger, who isolated ferritin from the horse spleen in 1937.[101] From that moment, ferritin has been found in many other organisms, such as plants, archea, bacteria, animals and fungi, with the notable exception of yeasts, as well as in different cellular compartments. Indeed, even though ferritin is mainly cytosolic, it has been found also in nuclei, animal mitochondria and plants plastids.[101-103] In 1991 crystallography studies reveal that ferritin is a round shape protein made of 24 self-assembling subunits that create a hollow cage-like structure with internal and external diameters of about 8 and 12 nm, respectively (Fig17).[104,105]

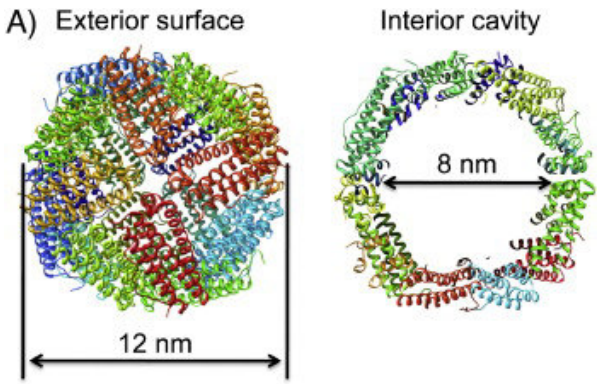

Figure 17. Ribbon diagrams of exterior surface and internal cavity of human heavy chain ferritin.

Mammalian ferritins are heteropolymers consisting of different ratios of heavy (H) chain subunits (182 amino acids) and light (L) chain subunits (174 amino acids) each of them with a specific role in iron uptake and storage: H-chain contains the ferroxidase centre, while L-chain facilitates the deposition

of Fe(III) inside ferritin cavity to form a mineral core (ferrihydrite).[102,106] In general L-rich ferritins are characteristic of iron-storing organs, such as liver and spleen, while H-rich ferritins are mainly found in brain and heart.[103] The ability of ferritin to internalize up to 4500 Fe(II) atoms transforming them into a inert mineral, makes this protein very important in protecting cells from the damage caused by reactive oxygen species, which are produced by Fe(II) oxidation during the Fenton reaction.[102,107] Thus ferritin can act as an antioxidant agent and as an iron storage system within cells.[106]

Ferritin subunits are linked together in the 3D structure by a large number of intra- and inter-subunit salt bridges and hydrogen bonds, which are responsible for its great stability, both at high temperatures (up to 80–100 °C) and in a wide range of pH values (pH 3–10).[103,108] However, when the pH goes above or below that range ferritin proteins disassemble into single subunits, which maintain the ability to reconstitute the entire protein once the pH restores to a neutral value. This ability to assemble and disassemble in response to pH variation, together with the possibility to produce a recombinant ferritin protein without the metallic core inside (Apo-ferritin), makes this protein a very interesting tool in nanomedicine and bio-nanotechnology fields.[106,109] Tuning properly the pH, ferritin cavity can be exploited to load active molecules or contrast agents, acting either as MRI agent or as drug delivery system for the diagnosis and treatment of tumors.[110,111] Moreover the external surface of ferritin can be used as a platform for the immobilization of targeting ligands via chemical reactions or genetic modifications, exploiting the numerous functional groups on the surface or the production of modified subunits with additional peptide fused at the N-terminal of the protein sequence.[108,112,113] Alternatively, the

production of ferritin nanoparticles with peptides fused at the C-terminal has been reported for the development of vaccines (Fig18).[109,114,115]

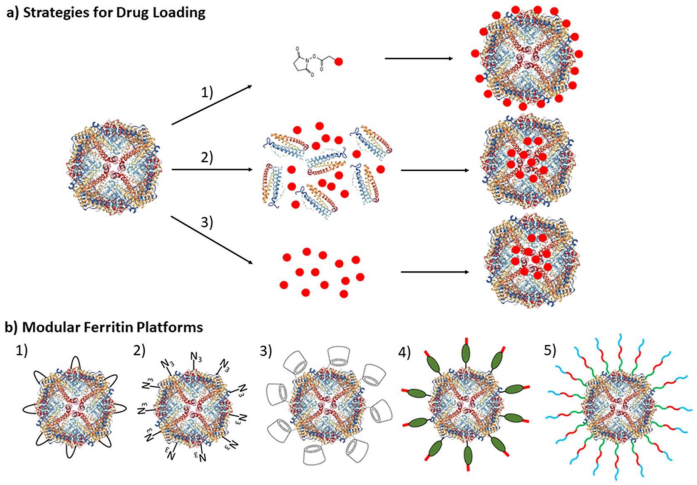

Figure 18. Schematic representation of drug loading strategies (a) and external functionalization (b). a) Different ways for ferritin drug loading: 1) chemical conjugation of drugs to ferritin surface, 2) encapsulation of drugs via the pH- or salt-based assembly and disassembly of ferritin subunits, and 3) encapsulation of small molecules by diffusion through the surface pores of ferritin. b) Examples of modular ferritin platforms such as 1) ferritin incorporating Fc-binding peptide for binding targeting antibodies, 2) incorporation of azide-bearing amino acid in ferritin for click coupling to targeting ligands or antibodies, 3) ferritin surface conjugated with β-cyclodextrins for rapid drug loading, 4) ferritin incorporating protein G and 6X-His tag for antibody or cargo binding, and 5) engineered ferritin displaying functional peptides for siRNA delivery.[108]

Other characteristics that make this natural bio-nanoparticle an excellent drug delivery system are monodispersity, small uniform size, biocompatibility, biodegradability and low cost large-scale production. Furthermore, one of the most appealing features of ferritin is its intrinsic specificity for cancer cells.[108,116] Indeed, its physiological receptor, the human transferrin receptor 1 (TfR1, also termed CD71), is a protein that has found to be overexpressed in most of solid cancers (Fig19).[116,117]

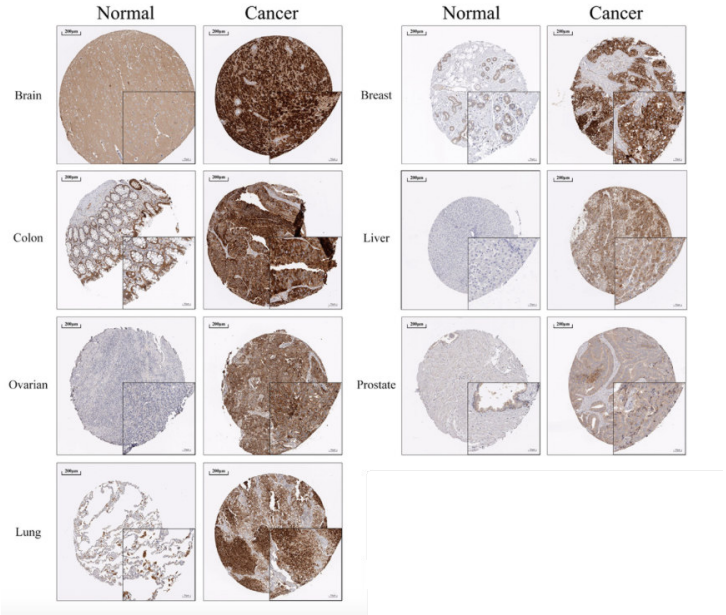

Figure 19. TfR1 expression in various normal tissues and tumor tissues. TfR1 is overexpressed in tumor tissues compared to healthy tissues. Immunohistochemical analysis was obtained from the Human Protein Atlas database.[117]

TfR1 was first characterized in 1999 with X-ray crystallography.[118] It is a transmembrane receptor made of two identical monomers joined by two disulfide bonds, each of them able to bind one molecule of transferrin. After the interaction with its ligands, transferrin or ferritin, the receptor internalizes via a clathrin-mediated endocytosis.[117]

Assuming that iron is essential for the metabolism, viability and proliferation of cells, it is not surprising that alterations of its metabolism may be involved in the development of cancer.[119,120] Indeed, despite the TfR1 ubiquitous expression, several studies have shown that TfR1 is present on malignant cells at levels many times higher than their normal counterparts and its expression can be correlated with tumor stage or cancer progression.[121,122] The significant increase in TfR1 expression makes this receptor an ideal

candidate for the targeting of cancer cells. Thus it can be successfully used to deliver cytotoxic agents into malignant cells including chemotherapeutic drugs, cytotoxic proteins, or high molecular weight compounds including liposomes, viruses, or nanoparticles[123] Indeed the functionalization of NPs with transferrin or mAbs against TfR1 (e.g., OKT9) has been largely exploited to increase target specificity.[124]

In this scenario, the ability of ferritin to naturally target TfR1 without any further functionalization, together with all its structural and chemical properties, makes this protein very promising as a NP for drug delivery and imaging of tumor. Moreover, compared with other NPs functionalized with TfR1-targeting moieties, ferritin may have an additional advantage. It is well established that once in biological systems NPs interact with circulating proteins, which cover them creating the so-called *protein corona*. Most of the time this envelope masks the targeting moieties reducing the interaction with the receptor, hence loosing the targeting ability. The use of ferritin NPs may overcome this problem thanks to its natural high affinity for the receptor in the biological environment.[125]

3.3.2. Iron oxide NPs

Iron oxide nanoparticles (IONPs) belong to the group of magnetic materials. The two primary biocompatible forms of iron oxide are magnetite (Fe_3O_4) and maghemite (γ-Fe_2O_3), both of them already approved for biomedical applications.[126] These nanoparticles can be synthetized through different mechanisms: co-precipitation, high-temperature thermal decomposition, hydrothermal and solvothermal synthesis, polyol method, microemulsion. Each of them generates IONPs with a dimension ranging from 1-1000 nm, although it's preferable to stay below 20 nm, which is the single domain critical value for iron material. Indeed, when the nanoparticles size is below that dimension, each particle becomes a single magnetic domain and shows superparamagnetic behaviour at room temperature.[126-128] Hence, on the basis of their dimensions iron oxide NPs can be classified in superparamagnetic iron oxide nanoparticles (SPIONs), which fall between 50 and 180 nm; ultrasmall superparamagnetic iron oxide nanoparticles (USPIONs) that range between 10 and 50 nm and very small SPIONs, which are smaller than 10 nm in diameter.[129]

The magnetic properties of IONPs and superparamagnetic iron oxide nanoparticles make them very attractive for a broad range of biomedical applications such as in MRI, as magnetic contrast agents; in hyperthermia treatments, where the magnetic particles (MNPs) are heated selectively by application of a high frequency magnetic field (e.g., in thermal ablation or hyperthermia of tumors); and in targeted drug delivery, where a magnetic field gradient is used to direct magnetic particles towards a certain location (Fig20).[130]

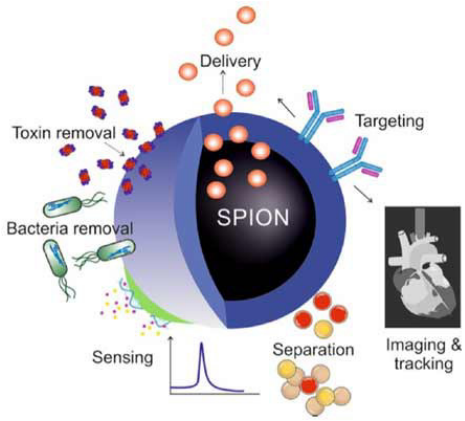

Figure 20. Schematic illustration of biomedical applications for super paramagnetic iron oxide nanoparticles (SPIONs).

However, the high reactivity and toxicity of iron oxide NPs makes them unsuitable for direct applications in biomedicine, thus these nanoparticles are usually coated by a polymer shell (e.g., polyethylene glycol, PEG) to protect them against the degradation in biological environments.[128] This biocompatible envelope can replace or being added to the surfactant used to stabilize NPs during the synthesis. Indeed, usually stabilizers such as surfactant or polymers are used to control the growth of NPs and to avoid the clusterization induced by magnetic attraction, making the formulation monodisperse in size and shape, as well as to solubilize NPs in water solution. The most commonly used surfactants are sodium dodecyl sulfate, cetyltrimethyl ammonium bromide (CTAB) and fatty acid molecules such as oleic acids. When the surfactant doesn't have a hydrophilic portion, such as for oleic acids, NPs need to be further covered with an amphiphilic polymer to ensure water solubility. The most commonly used polymers are PEG, polymethyl methacrylate (PMMA), polyethyleneimine (PEI) and polyvinyl alcohol (PVA). Besides offering long-term stabilization in biological fluids, improving blood circulation time and increasing biocompatibility, the polymer

shell is useful to further decorate nanoparticles with drugs or targeting moieties, exploiting polymer's functional groups.[131]

As already mentioned, one of the main application for IONPs in clinics is MRI. Indeed magnetic nanoparticles are able to enhance imaging resolution acting as T_2 contrast agents. Briefly, under an applied magnetic field, a magnetic moment is induced in SPIONs, which perturbs magnetic relaxation of the surrounding water protons, shortening the relaxation time T_2. Such changes result in darkening of the corresponding area in T_2-weighted MR images.[132] Moreover SPIONs can be functionalized with targeting moieties to specifically reach the desired site, or they can be driven to a precise organ by the application of an external magnetic field gradient, and once in the right place SPIONs can be used for hyperthermia or drug release. Indeed, when they are excited by an external alternating magnetic field nanoparticles can generate a local overheating leading to the death of surrounding cells (Fig21).[133,134] Another modification of SPIONs surface is the conjugation of drugs or active molecules, which, depending on the type of reaction or linker used, can be released inside or in the proximity of target cells.[130]

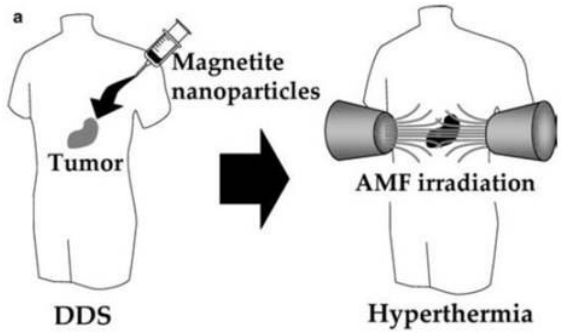

Figure 2. Scheme of hyperthermia treatment using magnetite nanoparticles. After injection NPs reach the tumor site by targeted delivery; then NPs are irradiated with an external alternating magnetic field (AMF), resulting in a tumor-specific hyperthermia.

The versatility of magnetic nanoparticles to allow both imaging and therapy (drug delivery or hyperthermia) at the same time makes them very promising theranostic agents[135] (Fig22).

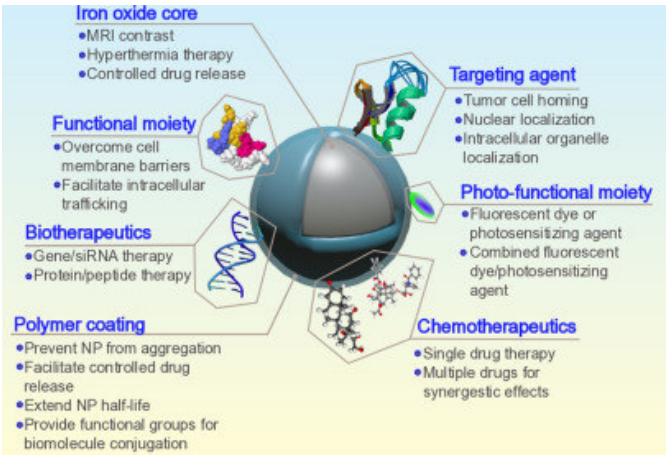

Figure 22. Schematic illustration of a theranostic iron oxide NP.

Some of the iron oxide nanoformulations, including Feridex®, Resovit®, Gastromark®, ect, got the FDA approval to be used as MRI contrast agents.[134] Moreover, Ferumoxytol (commercialized as Feraheme®), which is an ultra small SPIONs, has been approved for the treatment of iron deficiency in adult chronic kidney disease patients, although now there is an increased interest in using Ferumoxytol as MRI contrast agent, especially for vascular imaging and macrophage imaging.[136-138] Sienna+® is a suspension of organically coated SPIONs, which gained the CE approval for the detection of sentinel lymph nodes. Briefly it is injected subcutaneously where the lymphatic system filters out the nanoparticles, enabling sentinel nodes to be located. Currently, some of these approved SPIONs, such as Feridex®, are no longer commercialized due to the lack of users, while many other formulations are undergoing clinical trials.[138]

4. AIM OF THE WORK

The aim of my PhD project was the improvement of cancer immunotherapy by studing different types of nanoparticles as drug delivery systems for monoclonal antibodies or antibody fragments. In particular, starting from current antibody-based treatments restrictions, we reasoned to exploit nanotechnology to overcome some of these limitations (e.g., permeation across biological membranes), potentially widening mAbs spectrum of use in clinic.

In chapter 1 we aimed at developing a protein-based nanovector for mAbs delivery across the blood brain barrier for the treatment of brain cancers. In details, we selected brain cancers of different origins, such as glioblastoma multiforme (as primary tumor) and HER2-positive breast cancer (as secondary tumor) and Trastuzumab and Cetuximab as therapeutic agents to be delivered. To accomplish this function we chose H-chain ferritin nanoparticle, due to its already established capability to cross the BBB and its easily functionalizable surface. First, we designed our nanoparticles choosing to have one mAb covalently conjugated on each HFn molecule. Then we investigated both the direct and indirect anticancer activity of the nanoformulation by viability test, cell cycle analysis, ADCC and CD16 shedding assay. Finally we assessed also the ability of the nanoconjugates to cross an *in vitro* model of the BBB in order to evaluate their feasibility as effective delivery system.

In chapter 2 we aimed at investigating the activity of colloidal nanoparticles conjugated with the half chain (HC) of CTX compared to unconjugated CTX on three triple negative breast cancer cell lines. The selected cell lines were different in terms of CTX-treatment sensitivity, EGFR

expression levels and mutations in EGFR signaling pathway. For this study we were particularly focused on the evaluation of the effects induced by HC-CTX treatment, compared to free CTX, on cell targeting efficiency, interference with downstream signaling pathways, cell cycle and proliferation. Moreover, we investigated the capability of nanoconjugated HC-CTX to promote the ADCC response against TNBC cells, in order to assess the maintenance of the full mAb power upon half-chain nanoconjugation.

5. REFERENCES

1. Nowell P. C. The Clonal Evolution of Tumor Cell Populations. *Science*, (**1976**) 194, 23–28.
2. Hanahan. Hallmarks of cancer: the next generation. *Cell* (**2011**) 144(5), 646–74.
3. Ferlay J., Soerjomataram I., Ervik M., et al. GLOBOCAN 2012 v1.0, Cancer Incidence and Mortality Worldwide: IARC CancerBase No. 11 [Internet]. Lyon, France: International Agency for Research on Cancer; (**2013**).
4. Torre L. A., Bray F., Singel R. L., Ferlay J., Lortet-Tieulent J., Jemal A. Global cancer statistics, 2012. *CA Cancer J Clin* (**2015**) 65: 87–108.
5. Polyak K. Breast cancer origin and evolution. *J Clin Invest* (**2007**) 117(11): 3155–63.
6. Ellsworth R. E., Blackburn H. L., Shriver C. D., Soon-Shiong P., Ellsworth D. L. Molecular heterogeneity in breast cancer: state of science and implications for patient care. *Semin Cell Dev Biol* (**2016**) 64: 65–72.
7. Turashvili G. and Brogi E. Tumor heterogeneity in breast cancer. *Front Med (Lausanne)* (**2017**) 4: 227.
8. Malhotra G. K., Zhao X., Band H. & Band V. Histological, molecular and functional subtypes of breast cancers. *Cancer Biol. Ther.* (**2010**) 10, 955–960.
9. Rivenbark A. G., O'Connor S. M., Coleman W. B. Molecular and cellular heterogeneity in breast cancer: challenges for personalized medicine. *Am J Pathol* (**2013**) 183(4): 1113–1124.
10. Makki J. Diversity of breast carcinoma: Histological subtypes and clinical relevance. *Clin Med Insights Pathol* (**2015**) 8: 23–31.

11. Eheman C. R., Shaw K. M., Blythe Ryerson A., et al. The Changing Incidence of *In situ* and Invasive Ductal and Lobular Breast Carcinomas: United States, 1999-2004. *Cancer Epidemiol Biomarkers Prev* (**2009**) 18(6): 1763–69.
12. Li C. Uribe D.J., Daling J.R. Clinical characteristics of different histologic types of breast cancer. *British Journal of Cancer* (**2005**) 93: 1046–52.
13. Hortobagyi, G. N. Physician to physician. AJCC 8th Edition, Breast www.cancerstaging.org (**2018**)
14. Giuliano, A. E., Edge, S.B. & Hortobagyi, G.N. Eighth Edition of the AJCC Cancer Staging Manual: Breast Cancer. Ann Surg Oncol (**2018**) 25: 1783.
15. Perou C. M., Sørlie T., Eisen M. B., et al. Molecular portraits of human breast tumors. Nature (**2000**) 406, 747–752.
16. Zardavas D., Irrthum A., Swanton C. & Piccart M. Clinical management of breast cancer heterogeneity. Nat Rev Clin Oncol (**2015**) 12, 381–394.
17. Slamon D.J., Clark G.M., Wong S.G., Levin W.J., Ulrich A., McGuire W.L. Human breast cancer: correlation of relapse and survival with amplification of the HER-2/neu oncogene. *Science* (**1987**) 235(4785): 177–182.
18. Lester J. Local treatment of breast cancer. Semin Oncol Nurs (**2015**) 31(2): 122-133.
19. Darby S., McGale P., Correa C., Taylor C., Arriagada R., Clarke M., Cutter D., Davies C., Ewertz M., Godwin J., Gray R., Pierce L., Whelan T., Wang Y., Peto R. Effect of radiotherapy after breast-conserving surgery on 10-years recurrence and 15-year breast cancer death: meta-analysis of individual patient data for 10,801 women in 17 randomised trials. Lancet (**2011**) 378: 1707–1716.
20. Burstein H.J., Lacchetti C., Griggs J.J. Adjuvant endocrine therapy for women with hormone receptor-positive breast cancer: American society of

clinical oncology clinical practice guideline ipdate on ovarian suppression summary. Am Soc Clin Oncol (**2016**) 12(4): 390–393.

21. Davies C., Pan H., Godwin J., et al. Long-term effects of continuing adjuvant tamoxifen to 10 years versus stopping at 5 years after diagnosis of oestrogen receptor-positive breast cancer: ATLAS, a randomised trial. *Lancet* (**2013**) 381, 805–816.
22. Wilson et al. Herceptin (Trastuzumab) in HER2-positive early breast cancer: protocol for a systematic review and cumulative network meta-analysis. *Systematic Reviews* (**2017**) 6: 196.
23. Mendes D. et al. The benefit of HER2-targeted therapies on overall survival of patients with metastatic HER2-positive breast cancer – a systematic review. *Breast Cancer Research* (**2015**) 17: 140.
24. Baselga J., Perez E.A., Pienkowski T., Bell R. Adjuvant Trastuzumab: a milestone in the treatment of HER-2-positive early breast cancer. *Oncologist* (**2006**) 11 suppl 1: 4–12.
25. Kruchko C., Ostrom Q.T., Gittleman H., Barnholtz-Sloan J.S. The CBTRUS story: providing accurate population-based statistics on brain and other central nervous system tumors for everyone. *Neuro Oncology* (**2018**) 20(3):295–298.
26. Ostrom Q.T., Gittleman H., Fulop J., Liu M., Blanda R., Kromer C., Wolinsky Y., Kruchko C., Barnholtz-Sloan J.S. CBTRUS Statistical Report: Primary Brain and Central Nervous System Tumors Diagnosed in the United States in 2008-2012. *Neuro Oncology* (**2015**) 17: iv1-iv62.
27. Veganzones S., de la Orden V., Requejo L., Mediero B., Gonzalez M.L., del Prado N., Rodriguez Garcia C., Gutierrez-Gonzalez R., et al. Genetic

alterations of IDH1 and vegf in brain tumors. *Brain and Behavior* (**2017**) 7(9): e00718.

28. Bailey P. & Cushing H. A Classification of the Tumors of the Glioma Group on a Histogenic Basis with a Correlated Study of Prognosis (Lippincott, Philadelphia, **1928**).
29. Mischel P.S., Cloughesy T.F. and Nelson S.F. DNA-microarray analysis of brain cancer: molecular classification for therapy. *Nature Rev Neurosci* (**2004**) 5: 782–792.
30. Louis D.N., Perry A., Reifenberger G., et al. The 2016 world health organization classification of the central nervous system: a summary. *Acta Neuropathol* (**2016**) 131: 803.
31. Gavrilovic I.T., Posner J.B. Brain metastases: epidemiology and pathophysiology. *J Neuro Oncol* (**2005**) 75: 5–14.
32. Nayak L., Lee E.Q. & Wen P.Y. Epidemiology of brain metastases. *Curr Oncol Rep* (**2012**) 14: 48.
33. Barnholtz-Sloan J.S., Sloan A.E., Davis F.G., et al. Incidence proportions of brain metastases in patients diagnosed (1973 to 2001) in the Metropolitan Detroit Cancer Surveillance System. *J Clin Oncol.* (**2004**) 22: 2865–72.
34. Huse J.T. and Holland E.C. Targeting brain cancer: advances in the molecular pathology of malignant glioma and medulloblastoma. *Nature Rev*. (**2010**) 10: 319–31.
35. Collins V.P. Brain tumors: classification and genes. *J Neurol Neurosurg Psychiatry* (**2004**) 75(II): ii2–ii11.
36. Brem S. and Panattil J.G. An Era of Rapid Advancement: Diagnosis and Treatment of Metastatic Brain Cancer. *Neurosurgery*. (**2005**) 57(5): S4–5–S4–9.

37. Ostrom Q.T., Bauchet L., Davis F.G., Deltour I., Fisher J.L., Langer C.E., Pekmezci M., Schwartzbaum J.A., Turner M.C., Walsh K.M., Wrensch M.R., Barnholtz-Sloan J.S. The epidemiology of glioma in adults: a "state od the science" review. *Neuro Oncol* (**2014**) 16(7): 896–913
38. Mellinghoff I.K, Gilbertson R.J. Brain tumors: challenges and opportunties to cure. *J Clin Oncol* (**2017**) 35(21): 2343-45.
39. Lijubimova J.Y., Sun T., Mashouf L., Ljubimov A.V., Israel L.L., Ljubimov V.A., Falahatian V., Holler E. Covalent nano delivery systems for selective imaging and treatment of brain tumors. *Advanced Drug Delivery Reviews* (**2017**) 113: 177–200.
40. Santaguida S., Janigro D., Hossain M., Oby E., Rapp E., Cucullo L. Side by side comparison between dynamic versus static models of blood-brain barrier in vitro: a permeability study. *Brain Research* (**2006**) 1109: 1–13.
41. Zhang Y., Pardridge W.M. Conjugation of brain-derived neurotrophic factor to a blood–brain barrier drug targeting system enables neuroprotection in regional brain ischemia following intravenous injection of the neurotrophin. *Brain Research* (**2001**) 889: 49–56.
42. Abbott N.J., Ronnback L., Hansson E. Astrocyte–endothelial interactions at the blood–brain barrier. *Nat. Rev. Neurosci.* (**2006**) 7: 41–53.
43. Weiss N., Miller F., Cazaubon S., Couraud P. The blood-brain barrier in brain homeostasis and neurological diseases. *Biochim Biophys Acta.* (**2009**) 1788(4): 842–57.
44. Van Tellinger O., Yetkin-Arik B., de Gooijer M.C., Wesseling P., Wurdinger T., de Vries H.E. Overcoming the blood–brain tumor barrier for effective glioblastoma treatment. *Drug Resistance Updates* (**2015**) 19: 1–12.

45. Helms H.C., Abbott N.J., Burek M., Cecchelli R., Couraud P., Deli M.A., Förster C., Galla H.J., Romero I.A., Shusta E.V., Stebbins M.J., Vandenhaute E., Weksler B. and Brodin B. In vitro models of the blood–brain barrier: An overview of commonly used brain endothelial cell culture models and guidelines for their use. *J Cereb Blood Flow Meta*b (**2016**) 36(5): 862–890.
46. Fang J., Nakamura H., Maeda H. The EPR effect: unique features of tumor blood vessels for drug delivery factors involved, and limitations and augmentation of the effect. *Advanced drug delivery reviews* (**2011**) 63(3): 136–161.
47. Geresu M.A., Sultan A.F., Ahmed S.K., Kassa G.M. Immunotherapy against cancer: a comprehensive review. *J. Cancer Res. Exp. Oncol.* (**2016**) 8(2): 15–25.
48. Ventola C.L. Cancer Immunotherapy, Part 1: Current Strategies and Agents. *P&T* (**2017**) 42(6): 375–383.
49. Oiseth S.J., Aziz M.S. Cancer immunotherapy: a brief review of the history, possibilities, and challenges ahead. *J Cancer Metastasis Treat* (**2017**) 3: 250–61.
50. Van der Bruggen P., Traversari C., Chomez P., Lurquin C., De Plaen E., Van der Eynde B., Knuth A., Boon T. A gene encoding an antigen recognized by cytolytic T lymphocytes on a human melanoma. *Science* (**1991**) 254(5038): 1643–47.
51. Dunn G.P., Bruce A.T., Ikeda H., Old L.J., Schreiber R.D. Cancer immunoediting: from immunosurveillance to tumor escape. *Nature immunology* (**2002**) 3: 991–998.
52. Dunn G.P., Old L.J., Schreiber R.D. The immunobiology of cancer immunosurveillance and immunoediting. *Immunity*. (**2004**) 21: 137–148.

53. Sharma R., Mody N., Dubey S., Vyas S.P. Nanostructures for drug delivery 1st edition. Chapter 17 – Nanoparticulate carrier(s): an emergin paradigm in new generation vaccine development. *Micro and Nano Technologies* (**2017**) 523–550.
54. Makkouk A., Weiner G. Cancer Immunotherapy and Breaking Immune Tolerance-New Approaches to an Old Challenge. *Cancer Res*. (**2015**) 75(1): 5–10.
55. Farkona S., Diamandis E.P., Blasutig I.M. Cancer immunotherapy: the beginning of the end of cancer? *BMC Medicine* (**2016**)
56. Papaioannou N.E., Beniata O.V., Vitsos P., Tsitsilonis O., Samara P. Harnessing the immune system to improve cancer therapy. *Ann Transl Med* (**2016**) 4(14): 261.
57. Melief C.J.M., van Hall T., Arens R., Ossendorp F., van der Burg S.H. Therapeutic cancer vaccines. *J Clin Invest.* (**2015**) 125(9): 3401–3412.
58. Maude S.L., Frey N., Shaw P.A., Aplenc R.A., Barret D.M., et al. Chimeric antigen receptor T cells for susteined remissions in leukemia. *N Engl J Med* (**2014**) 371: 1507–1517.
59. Park J.H., Riviere I., Gonen M., Wang X., Sénéchal B., Kevin J.C., Sauter C., et al. Long-term follow-up of CD19-CAR therapy in acute lymphoblastic leukemia. N Engl J Med 2018; 378:449–459.
60. FDA News Release. FDA approval brings first gene therapy to the United States. Available from: https://www.fda.gov/NewsEvents/ Newsroom/PressAnnouncements/ucm574058.htm.
61. May C., Sapra P., Gerber H. Advances in bispecific biotherapeutics for the treatment of cancer. *Biochem Pharmacol*. (**2012**) 84(9): 1105–1112.
62. Román V.R.G, Murray J.C., Weiner L.M. Antibody Fc: Linking Adaptive and

Innate Immunity. Chapter 1 - antibody-dependent cellular cytotoxicity (ADCC). *MAbs* (**2014**) 6(3): 1–27.

63. Strohl W., Strohl L.M. Therapeutic antibody engineering. Current and future advances driving the strongest growth area in the pharmaceutical industry. Chapter 8: Monoclonal antibody targets and mechanism of action. *Woodhead Publishing Series in Biomedicine.* (**2012**) Pages 163–196, 459–595.
64. Scheneider-Merck T., van Bueren J.J.L., Berger S., Rossen K., van Berkel P.H.C., Derer S. Beyer T., et al. Human IgG2 antibodies against epidermal growth factor receptor effectively trigger antibody-dependent cellular cytotoxicity but, in contrast to IgG1, only by cells of myeloid lineage. *J Immunol* (**2010**) 184: 512–520.
65. Yeap W.H., Wong K.L., Shimasaki N., Teo E.C.Y. Quek J.K.S. Yong H.X., Diong C.P., et al. CD16 is indispensable for antibody-dependent cellular cytotoxicity by human monocytes. *Scientific Reports* (**2016**) 6: 34310.
66. Wang W., Erbe A.K., Hank J.A., Morris Z.S., Sondel P.M. NK cell-mediated antibody-dependent cellular cytotoxicity in cancer immunotherapy. *Front. Immunol.* (**2015**) 6: 368.
67. Kute T., Lack C.M., Willingham M., Bishwokama B., Williams H., Barrett K., Mitchell T., Vaughn J.P. "Development of Herceptin Resistance in Breast Cancer Cells". *Cytometry A*. (**2004**) 57: 86–93.
68. Blick S.K.A. and Scott L.J. Cetuximab. A review of its use in squamous cell carcinoma of the head and neck and metastatic colorectal cancer. *Drugs* (**2007**) 67(17): 2585–2607.
69. Feynman, R.P. There's Plenty of Room at the Bottom. *Eng. Sci*. 23, 22–36 (**1960**).

70. The Royal Society and Royal Academy. Nanoscience and nanotechnologies: opportunities and uncertainties. (**2004**) Available at: https://royalsociety.org/topics- policy/publications/2004/nanoscience-nanotechnologies/.
71. Liu, Y., Miyoshi, H. & Nakamura, M. Nanomedicine for drug delivery and imaging: A promising avenue for cancer therapy and diagnosis using targeted functional nanoparticles. Int. J. Cancer (**2007**) 120: 2527–2537.
72. Kim B.Y.S., Rutka J.T., Chan W.C.W. Nanomedicine. *N. Engl. J. Med.* (**2010**) 363, 243–443.
73. Nikalje A.P. Nanotechnology and its Applications in Medicine. *Med Chem* (**2015**) 5: 081–089.
74. Moghimi S.M., Moghimi A.C. Hunter, Murray J.C. (2005) Nanomedicine: current status and future prospects. The FASEB Journal 19, 311-330.
75. Riehemann, K. et al. Nanomedicine--challenge and perspectives. Angew. Chem. Int. Ed Engl. 48, 872–897 (2009).
76. Solano-Umana V., Vega-Baudrit J.R., Gonzalez-Paz R. The new field of nanomedicine. *IJAST*. (**2015**) 5.
77. Jackson T.C., Patani B.O., Ekpa D.E. Nanotechnology in diagnosis: a review. *Advances in Nanoparticles* (**2017**) 6: 93–102.
78. Cormode D.P., Skajaa T., Fayad Z.A., Mulder W.J.M. Nanotechnology in medical imaging: probe design and applications. *Arterioscler Thromb Vasc Biol* (**2009**) 29(7): 992–1000.
79. Toy R., Bauer L., Hoimes C., Ghaghada K.B., Karathanasis E. Targeted nanotechnology for cancer imaging. *Adv Drug Deliv Rev.* (**2014**) 0: 79–97.

80. Veiseh O., Gunn J.W., Zhang M. Design and fabrication of magnetic nanoparticles for targeted drug delivery and imaging. *Adv Drug Deliv Rev.* (**2010**) 62(3): 284–304.
81. Sahoo S.K., Parveen S., Panda J.J. The present and future of nanotechnology in human health care. *Nanomedicine: NBM.* (**2007**) 3:20–31.
82. Ochekpe N.A., Olorunfemi P.O., Ngwuluka N.C. Nanotechnology and drug delivery. *Trop J Pharma Res*. (**2009**) 8: 265–274.
83. Parveen S., Misra R. & Sahoo S. K. Nanoparticles: a boon to drug delivery, therapeutics, diagnostics and imaging. *Nanomedicine Nanotechnol. Biol. Med*. (**2012**) 8: 147–166.
84. Tiwari G., Tiwari R., Sriwastawa B., Bhati L., Pandey S., Pandey P., Bannerjee S.K. (**2012**) Drug delivery systems: an updated review. Int J Pharm Investig 2(1), 2-11.
85. Blanco E., Shen H. Ferrari M. Principles of nanoparticle design for overcoming biological barriers to drug delivery. *Nat. Biotechnol*. (**2015**) 33(9): 941–951.
86. Kreuter J. Nanoparticles - a historical perspective. *Int J Pharm*. (**2007**) 331(1): 1–10.
87. Nie S., Xing Y., Kim G.J., Simons J.W. Nanotechnology application in cancer. *Annu. Rev. Biomed. Eng.* (**2007**) 9: 257–88.
88. Bazak R., Houri M., El Achy S., Kamel S. & Refaat T. Cancer active targeting by nanoparticles: a comprehensive review of literature. *J. Cancer Res. Clin. Oncol.* (**2015**) 141: 769–784.
89. Peer D., Karp J.M., Hong S., Farokhzad O.C, Margalit R., Langer R. Nanocarriers as an emerging platform for cancer therapy. *Nature*

Nanotechnology (**2007**) 2: 751–760.

90. Maeda H., Nakamura H., Fang J. "The EPR effect for macromolecular drug delivery to solid tumors: improvement of tumor uptake, lowering of systemic toxicity, and distinct tumor imaging in vivo". *Advanced Drug Delivery Reviews*. (**2013**) 65: 71–79.
91. Sanna V., Pala N. & Sechi M. Targeted therapy using nanotechnology: focus on cancer. *Int. J. Nanomedicine* (**2014**) 9: 467–483.
92. Matsumura Y., Maeda H. A new concept for macromolecular therapeutics in cancer chemotherapy: Mechanism of tumoritropic accumulation of proteins and the antitumor agent smancs" *Cancer Res.* (**1986**) 46(12): 6387–92.
93. Richardson P.F. Chapter 16: Nanotechnology therapeutics in oncology – recent developments and future outlook. *Annual Reports in Medicinal Chemistry* (**2012**) 47(16): 239–251.
94. Torchilin V.P. Targeted pharmaceutical nanocarriers for cancer therapy and imaging. *AAPS Journal*. (**2007**) 9: 128–147.
95. Chames P., Van Regenmortel M., Weiss, E.; Baty, D. Therapeutic Antibodies: Successes, Limitations and Hopes for the Future. *Br. J. Pharmacol.* (**2009**) 157: 220–233.
96. Reichert J.M. Antibodies to Watch in 2017. *mAbs* (**2017**) 9: 167–181.
97. Rodrigo G., Gruvegrd M., Van Alstine J.M. Antibody fragments and their purification by protein L affinity chromatography. *Antibodies* (**2015**) 4: 259–277.
98. Wicki A., Witzigmann D., Balasubramanian V., Huwyler J. Nanomedicine in cancer therapy: challenges, opportunities, and clinical applications. *Journal of Control Release* (**2015**) 200: 138–157.

99. Goodall S., Jones M.L., Mahler S. Monoclonal antibody-targeted polymeric nanoparticles for cancer therapy – future prospects. *J Chem Technol Biotechnol* (**2015**) 90: 1169–76.

100. Anselmo A.C., Mitragotri S. Nanoparticles in the clinic. *Bioengineering & Translational Medicine* (**2016**) 1: 10–29.

101. Arosio P., Elia L., Poli M. Ferritin, cellular iron storage and regulation. *IUBMB* (**2017**) 414–422.

102. Arosio P., Ingrassia R., Cavadini P. Ferritins: A family of molecules for iron storage, antioxidation and more. *Biochim. Biophys. Acta*. (**2009**) 1790: 589–599.

103. Harrison P. M., Arosio P. The ferritins: molecular properties, iron storage function and cellular regulation. *Biochim. Biophys. Acta.* (**1996**) 1275: 161–203.

104. Lawson D. M., Artymiuk P. J., Yewdall S. J., Smith J. M., Livingstone J. C., Treffry A., Luzzago A., Levi S., Arosio P., Cesareni G. Solving the structure of human H ferritin by genetically engineering intermolecular crystal contacts. *Nature* (**1991**) 349: 541–544.

105. Uchida M., Kang S., Reichhardt C., Harlen K., Douglas T. The ferritin superfamily: Supramolecular templates for materials synthesis. *Biochim. Biophys. Acta.* (**2010**) 1800: 834–845.

106. He D. and Marles-Wright J. Ferritin family proteins and their use in bionanotechnology. *New Biotechnology* (**2015**) 32(6): 651–657.

107. Theil E.C. Ferritin protein nanocages – the story. *Nanotechnol Percept.* (**2012**) 8(1): 7–16.

108. Khoshnejad M., Parhiz H., Shuvaev V.V., Dmochowski I.J., Muzykantov V.R. Ferritin-based drug delivery systems: hybrid nanocarriers for vascular immunotargeting. *Journal of Controlled Release* (**2018**) 282: 13–24.

109. Truffi M., Fiandra L., Sorrentino L., Monieri M., Corsi F., Mazzucchelli S. Ferritin nanocages: a biological platform for drug delivery, imaging and theranostics in cancer. *Pharmacological Research* (**2016**) 107: 57-65.

110. Yang Z., Wang X., Diao H., Zhang J., Li H., Sun H., Guo Z., Encapsulation of platinum anticancer drugs by apoferritin. *Chem. Commun*. (**2007**) 33: 3453–3455.

111. Lee C.W., Choi S., Lee S.J., Oh Y.T., Park G., Park N.Y., Yoon K., Kim S., Kim D., Kim Y., Suh J. The effectiveness of ferritin as a contrast agent for cell tracking MRI in mouse cancer models. *Yonsei Med J.* (**2017**) 58(1): 51–58.

112. Uchida M., Willits D.A., Muller K., Wills A.F., Jackiw L., Jutila M., Young M.J., Porter A.E., Douglas T. Intracellular distribution of macrophage targeting ferritin-iron oxide nanocomposite. *Adv. Mater.* (**2009**) 21: 458–462.

113. Zheng Z., Tang W., Chen H., Lin X., Todd T., Wang G., Cowger T., Chen X., Xie J. RGD-modified nanoparticles for efficient drug delivery to tumors. *ACS Nano* (**2013**) 7: 4830–4837.

114. Han J.A., Kang Y.J., Shin C., Ra J.-S., Shin H.-H., Hong S.Y., Do Y., Kang S. Ferritin protein cage nanoparticles as versatile antigen delivery nanoplatforms for dendritic cell (DC)-based vaccine development. *Nanomed.: Nanotechnol. Biol. Med.* (**2014**) 10: 561–569.

115. Lee B., Ko H.K., Ryu J.H., Ahn K.Y., Lee Y., Oh S.J., Na J.H., Kim T.W., Byun Y., Kwon I.C., Kim K., Lee J. Engineered human ferritin nanoparticles

for direct delivery of tumor antigens to lymph node and cancer immunotherapy. *Scientific Reports* (**2016**) 6: 35182.

116. Fan K., Cao C., Pan Y., Lu D., Yang D., Feng J., Song L., Liang M., Yan X. Magnetoferritin nanoparticles for targeting and visualizing tumour tissues. *Nat. Nanotechnol.* (**2012**) 7: 459–464.

117. Shen Y., Li X., Dong D., Zhang B., Xue Y., Shang P. Transferrin receptor 1 in cancer: a new sight for cancer therapy. *Am J Cancer Res* (**2018**) 8(6): 916–931.

118. Lawrence C.M., Ray S., Babyonyshev M., Galluser R., Borhani D.W., Harrison S.C. Crystal structure of the ectodomain of human transferrin receptor. *Science*. (**1999**) 286: 779–782.

119. Richardson D.R., Ponka P. The molecular mechanisms of the metabolism and transport of iron in normal and neoplastic cells. *Biochimica et Biophysica Acta*. (**1997**) 1331: 1–40.

120. Prutki M., Poljak-Blazi M., Jakopovic M., Tomas D., Stipancic I., Zarkovic N. Altered iron metabolism, transferrin receptor 1 and ferritin in patients with colon cancer. *Cancer letters*. (**2006**) 238: 188–196.

121. Yang D.C., Wang F., Elliott R.L., Head J.F. Expression of transferrin receptor and ferritin H-chain mRNA are associated with clinical and histopathological prognostic indicators in breast cancer. *Anticancer Research*. (**2001**) 21: 541–549.

122. Greene C.J., Attwood K., Sharma N.J., Gross K.W., Smith G.J., Xu B., Kauffman E.C. Transferrin receptor 1 upregulation in primary tumor and downregulation in benign kidney is associated with progression and mortality in renal cell carcinoma patients. *Oncotarget* (**2017**) 8(63): 107052–107075.

123. Daniels T.R., Delgado T., Helguera G. & Penichet, M.L. The transferrin receptor part II: targeted delivery of therapeutic agents into cancer cells. *Clin. Immunol. Orlando Fla* (**2006**) 121: 159–176.

124. Wang J., Tian S., Petros R.A., Napier M.E., DeSimone J.M. The complex role of multivalency in nanoparticles targeting the transferrin receptor for cancer therapies. *J. Am. Chem. Soc.* (**2010**) 132(32): 11306–11313.

125. Salvati A., Pitek A.S., Monopoli M.P., Prapainop K., Baldelli Bombelli F., Hristov D.R., Kelly P.M., Åberg C., Mahon E., Dawson K.A. Transferrin-functionalized nanoparticles lose their targeting capabilities when a biomolecule corona adsorbs on the surface. *Nature Nanotechnology*. (**2013**) 8: 137–143.

126. Colombo M., Carregal-Romero S., Casula M.F., Gutierrez L., Morales M.P., Bohm I.B., Heverhagen J.T., Prosperi D., Parak W.J. Biological Applications of Magnetic Nanoparticles. *Chem Soc Rev.* (**2012**) 41: 4306–4334.

127. Wu W., Wu Z., Yu T., Jiang C., Kim W. Recent progress on magnetic iron oxide nanoparticles: synthesis, surface functional strategies and biomedical applications. *Sci. Technol. Adv. Mater.* (**2015**) 16 023501.

128. Lu A., Salabas E.L., Schüth F. Magnetic nanoparticles: synthesis, protection, functionalization, and application. *Angew. Chem. Int. Ed.* (**2007**) 46: 1222–1244.

129. Menon P.K., Sharma A., Lafuente J.V., Muresanu D.F., ... Sharma H.S. Nanomedicine in central nervous system injury and repair. Chapter Three - Intravenous Administration of Functionalized Magnetic Iron Oxide Nanoparticles Does Not Induce CNS Injury in the Rat: Influence of Spinal

Cord Trauma and Cerebrolysin Treatment. *International Review of Neurobiology* (**2017**) 137: 47–63.

130. Arrouebo M., Fernandez-Pacheco R., Ibarra M.R., Santamaria J. Magnetic nanoparticles for drug delivery. *Nanotoday.* (**2007**) 2(3): 22–32.

131. Wu W., Jiang C.Z., Roy V.A.L. Designed synthesis and surface engineering strategies of magnetic iron oxide nanoparticles for biomedical applications. *Nanoscale* (**2016**) 8: 19421–19474.

132. Hao R., Xing R., Xu Z., Hou Y., Gao S., Sun S. Synthesis, Functionalization, and Biomedical Applications of Multifunctional Magnetic Nanoparticles *Adv Mater* (**2010**) 22:2729–49.

133. Silva A.C., Oliveira T.R., Mamani J.B., Malheiros S.M.F., Malavolta L., Pavon L.F., Sibov T.T., … Gamarra L.F. Application of hyperthermia induced by superparamagnetic iron oxide nanoparticles in glioma treatment. *International Journal of Nanomedicine* (**2011**) 6: 591–603.

134. Revia R.A. and Zhang M. Magnetite nanoparticles for cancer diagnosis, treatment, and treatment monitoring: recent advances. *Materials Today* (**2016**) 19(3): 157–168.

135. Hola K., Markova Z., Zoppellaro G., Tucek J., Zboril R. Tailored functionalization of iron oxide nanoparticles for MRI, drug delivery, magnetic separation and immobilization of biosubstances. *Biotechnology Advances* (**2015**) 33: 1162–1176.

136. Vasanawala S.S., Nguyen K., Hope M.D., Bridges M.D., Hope T.A., Reeder S.B., Bashir M.R. Safety and technique of ferumoxytol administration for MRI. *Magn Reson Med.* (**2016**) 75(5): 2107–2111.

137. Neuwelt A., Sidhu N., Hu C.A., Mlady G., Eberhardt S.C., Sillerud L.O. Iron-based superparamagnetic nanoparticle contrast agents for MRI of

infection and inflammation. *AJR Am J Roentgenol*. (**2015**) 204(3): W302–W313.

138. Wang Y.X.J., Idée J. A comprehensive literatures update of clinical researches of superparamagnetic resonance iron oxide nanoparticles for magnetic resonance imaging. *Quant Imaging Med Surg* (**2017**) 7(1): 88–122.

CHAPTER 1

Ferritin nanoparticle-mediated delivery of antibodies across the blood brain barrier for brain tumors treatment

1. Introduction

Brain cancers are a group of neoplasms located in the brain that can be either primary, arising from neurons or glial cells, or metastatic, occurring when cancer cells from other organs spread to the brain. Glioblastoma Multiforme (GBM) is the most common and malignant brain tumor occurring in adults, while one of the main sources of brain metastasis is the HER2 positive breast cancer.[1,2] An important feature that these cancers share is their protected location. Indeed the brain represents a sanctuary for cancer cells thanks to the presence of the blood-brain barrier that controls molecules trafficking between bloodstream and neurons, avoiding the permeation of potentially harmful substances (see Introduction, paragraph 1.3).[2,3]

Glioblastoma Multiforme

Glioblastoma is either the most common and lethal glioma histology, representing the 55% of all gliomas and the 15% of all primary brain tumors, with an average survival of 15-18 months and a 5-year survival of 5%.[4,5] Current treatments consist in surgical resection of the tumor mass, radiotherapy and adjuvant chemotherapy with the alkylating agent temozolomide (TMZ).[6] However, despite TMZ has been approved as the first line therapy, most patients do not respond to the treatment due to an overexpression of the O6-methylguanine-DNA methyltransferase (MGMT) and/or lack of a DNA repair pathway in GBM cells.[7-9] Treatment with TMZ in combination with radiations has demonstrated limited efficacy also in responsive patients, with an extension of median survival by just 2.5 months when compared to radiation therapy alone.[10] Thus there is a clinical need for

developing new therapeutic agents with a good permeability across the blood-brain barrier (BBB) and new strategies to overcome drug resistance.[11]

One of the most common genetic aberrations associated with GBM oncogenesis is the amplification of the epidermal growth factor receptor (EGFR), which contributes to uncontrolled proliferation and survival of glioma cells. Indeed, overall 60% of GBM patients show EGFR copy number alterations or receptor mutations (e.g., constitutively active truncations and in-frame deletions).[12] Despite its overexpression, EGFR is poorly used as therapeutic target for GBM treatment since the most common receptor-interfering agents, such as tyrosine kinase inhibitors and monoclonal antibodies (mAbs), fail to reach the target, due to their low permeability across the blood-brain barrier.[12] Among all EGFR inhibitors, the recombinant chimeric IgG1 monoclonal antibody, Cetuximab (CTX), binds the extracellular domain of EGFR, thus preventing signal transduction by interfering with ligand binding and EGFR extracellular dimerization (see Introduction, paragraph 2.2.2.2).[13,14] Additionally, CTX is believed to trigger EGFR receptor internalization and degradation, as well as to recruit immune cells and activate the ADCC mechanism.[15]

HER2+ breast cancer brain metastases

Brain metastasis affects an estimated 10% of cancer patients with disseminated disease and the adenocarcinoma of the breast represents one of the main sources. Even though very little is known about the mechanism of insurgence of breast cancer brain metastases, some studies identified HER2 overexpression as a risk factor associated with this phenotype.[16] HER2 is a transmembrane tyrosine kinase protein overexpressed, due to gene

amplification, in 15-30% of invasive breast cancer. Together with EGFR, it belongs to the human epidermal growth factor receptor family and like all the other members is involved in the regulation of cell proliferation, differentiation and migration.[17,18] Moreover, HER2 overexpression is associated with a more aggressive disease leading to poor outcome, even though it is also predictive of positive response to anti-HER2 targeted therapies.[19,20] Among HER2 inhibitors, humanized monoclonal antibody Trastuzumab (TZ) has been approved as a first-line setting for the treatment of HER2+ metastatic breast cancer (see Introduction, paragraph 2.2.2.2).[21] Unfortunately, as in the case of GBM, pharmacological treatments become ineffective when metastases reach the brain due to the presence of the BBB. Hence there is a strong clinical need to solve the problem of drug delivery across the barrier to finally reach the brain, improving therapeutic outcome.[22] Furthermore the overcome of the delivery issue might also expand the arsenal of usable drugs.

2. Aim of the work

In this study, we use a recombinant variant of human apoferritin, all made of H-chain subunits (HFn) (see Introduction, paragraph 3.3.1) as nanovector to promote mAbs delivery across the BBB in order to affect cancer cells viability through the inhibition of ErbB signaling pathways and the activation of the ADCC response. We reasoned that HFn could be a good drug delivery system since it is internalized upon the interaction with transferrin receptor 1, a type II transmembrane protein highly expressed on brain endothelial cells to ensure iron uptake in this organ.[24,25] Several studies report the ability of HFn to cross the BBB and, recently, it has been also assessed the efficacy of HFn in deliver cytotoxic drugs to the brain for glioma treatment.[25,26] Furthermore HFn surface can be easily modified by chemical reactions with the numerous functional groups available, or by genetic modifications.[27] Hence, taking all these features together, HFn seems to be a very promising platform for the development of a new antibody-based nanoparticle able to overcome the BBB and target brain cancer cells.

The aim of this work was to investigate the feasibility of using HFn as a vector for the delivery of mAbs across the barrier in terms of preservation of target specificity and cytotoxic activity of conjugated mAbs as well as maintenance of HFn-TfR1 interaction and translocation across the BBB. Furthermore we wanted to confirm also the ability of mAbs to conserve their cytotoxic activity after BBB permeation.

3. Materials and Methods

HFn nanocage design

HFn was produced as recombinant protein made of only H-chain subunits in E. coli BL21(DE3)/pET30b and purified following our established protocol.[28] Then HFn purity was checked by SDS-PAGE analysis.

HFn_mAbs conjugation reaction

The conjugation reaction was performed adapting the protocol by *Falvo et al*. to our purpose.[29] Briefly, amine-containing mAbs (TZ or CTX) and sulfhydryl-containing HFn were covalently conjugated together by a heterobifunctional crosslinker with N-hydroxysuccinimide (NHS) ester and maleimide (Mal) groups (MW_{PEG} ≈ 5000 Da). mAb molecules reacted first with 20-fold molar excess of the crosslinker in phosphate buffer (PBS) pH 7.5 at room temperature for 1 h. After the incubation time unreacted species were removed by washing with PBS buffer in 50 kDa Amicon centrifugal devices (Millipore Corporate) and finally refine on Zeba™ Spin Desalting Columns (ThermoFisher Scientific). Then, HFn molecules were added at a final HFn:mAb molar ratio of 1:1 and incubated overnight at 4 °C under stirring. At the end of the reaction, large aggregates produced were removed by centrifugation (12,000 rpm for 30 min at 4 °C), while the nanoconjugate-containing supernatant was collected and purified using a size exclusion chromatography (SEC-FPLC) equipped with a Superose 6 increased 10/300 GL column (GE Healtcare) equilibrated with PBS. The eluted fractions were then characterized by SDS-PAGE analysis, western blot and dynamic light scattering (DLS).

Cell cultures

U-87 MG and T98 cell lines were used as EGFR-positive models of glioblastoma primary brain cancer, while SKBR3 cell line was used as HER2-positive model of metastatic breast cancer. Rat brain microvascular endothelial cells (RBMEC) were used as representative rat BBB model, while hCMEC/D3 endothelial cells were used as a representative human model of the barrier.

U-87 MG and T98 were cultured in Dulbecco's Modified Eagle's Medium (DMEM) supplemented with 10% fetal bovine serum (FBS), 2mM L-glutamine, penicillin (50 UI mL^{-1}) and streptomycin (50 mg mL^{-1}). SKBR3 cells were cultured in 50% DMEM and 50% Ham's F12, supplemented with 10% FBS, 2mM L-glutamine, penicillin (50 UI mL^{-1}) and streptomycin (50 mg mL^{-1}). RBMEC cells were purchase from Innoprot (Spain) and sub-cultured in Innoprot ECM. hCMEC/D3 cells were cultured in EBM-2 medium (Lonza, Basel, Switzerland) supplemented with 5% FBS, 1% penicillin–streptomycin, 1.4 µM hydrocortisone, 5 µg/mL ascorbic acid, 1/100 chemically defined lipid concentrate (Invitrogen), 10 mM HEPES and 1 ng/mL basic FGF (bFGF).

All cell lines were maintained at 37 °C in humidified atmosphere containing 5% CO_2 and sub-cultured prior to confluence using trypsin/EDTA.

Cell binding assay

SKBR3, RBMEC, U-87 MG and T98 cells were seeded at a concentration of 2.5×10^5 cells/well. The day after, cells were incubated 1 h at 37 °C in culture medium supplemented with 50 µg mL^{-1} of FITC-labeled HFn conjugated with CTX (HFnF-CTX) or 10 and 100 µg mL^{-1} of HFnF-TZ and HFnF-IgG. After incubations cells were washed thrice with PBS and analyzed by CytoFLEX flow cytometer (Beckman Coulter). 20,000 events were acquired for each analysis,

after gating on viable cells and on singlets. Samples of untreated cells were used to set the appropriate gates. Data were analyzed by FlowLogic software.

Competition assay

SKBR3, U-87 MG and T98 cells (5×10^5) were transferred in FACS tubes and washed twice with PBS. Then, cells were incubated with 50 μg mL^{-1} of HFnF-CTX with or without CTX as competitor (140 μg mL^{-1}) or HFnF-TZ and HFnF-IgG with or without TZ as competitor (2 mg mL^{-1}) in PBS supplemented with 2% BSA at 37 °C for 30 min. Cells were washed thrice, resuspended in PBS (500 μL) and analyzed by CytoFLEX flow cytometer (Beckman Coulter). 10,000 events were acquired for each analysis, after gating on viable cells and on singlets. Samples of untreated cells were used to set the appropriate gates. Data were analyzed by FlowLogic software.

Cell viability assay

Viability test was performed by seeding 5×10^3 SKBR3 and U-87 MG cells on a 96-well dish. Cells were incubated at 37 °C in starvation medium with different amounts of CTX (5, 10, 50, 100 μg mL^{-1}), TZ, HFn-TZ or HFn-IgG (2, 10 μg mL^{-1}). Untreated cells were used as controls. After 3, 5, 7 days of treatment, cells were washed with PBS and incubated for 3 h at 37 °C with 0.1 mL of a stock solution of 3-(4,5-dimethylthiazol-2-yl)-5-(3-carboxymethoxyphenyl)-2-(4-sulfophenyl)-2H-tetrazolium (MTS) and phenazine ethosulfate (PES) previously diluted 1:10 in DMEM medium without phenol red (CellTiter 96® AQueous One Solution Reagent; Promega). Absorbance was measured by EnSight™ multimode plate reader (Perkin Elmer, Waltham, MA, USA) setting absorbance wavelength at 490 nm. Results were normalized on viability of untreated samples and expressed as means ± s.e.

TZ-mediated HER2 phosphorylation in Y1248.

5×10^5 cells were seeded in a 6-wells plate the day before. Cells were treated for 1 h with 4 μg mL^{-1} of TZ free or nanoformulated (HFn-TZ) or with HFn-IgG as a control, in starvation medium. Negative control was represented by untreated cells. At the end of incubation, cells were washed thrice with ice cold PBS and detached with 200 mL lysis buffer (20 mM Tris HCl pH 7.6, 150 mM NaCl, 1 mM EDTA, 1% Triton X-100, 1% glycerol, 1 mM Na_3VO_4, 10 mM NaF, Protease Inhibitor Cocktail, 1 mM PMSF) using a cell scraper. Cells were transferred in tubes, vortexed and lysed incubating 30 min at 4 °C. Then, lysed cells were centrifuged 10 min at 13,000 rpm at 4 °C, the supernatants were collected. The protein content was quantified using the Coomassie Plus Protein Assay Reagent (Thermo Fisher Scientific) with BSA as standard protein. Approximately 35 μg of protein from each sample were dissolved in sample buffer 5× (125 mM Tris HCl pH 6.8, 10% SDS, 20% glycerol, 0.02% Bromophenol blue, 5% β-mercaptoethanol), denatured 5 min at 95 °C, separated by SDS-PAGE and transferred onto PVDF membrane. The membrane was blocked in 5% BSA in TBS with 0.1 % Tween 20 for 1 h. For evaluation of HER2 phosphorylated in Y1248, the membrane was incubated with rabbit-monoclonal antibody against Phospho-HER2 receptor (Y1248) (#2247; Cell Signalling) at 1:1000 dilution overnight at 4 °C with gentle shaking and with mouse monoclonal antibody anti-α-tubulin (Sigma) at 1:1000 dilution in 5% BSA in TBS with 0.1 % Tween 20 for 1 h. The membranes were washed three times with TBS with 0.1 % Tween 20 and reacted 1 h with the secondary antibody anti-rabbit conjugated with horseradish peroxidase (1:5000; Abcam). The bound antibody was revealed using ECL star reagent (Euroclone) and the chemiluminescence signal was detected using the Chemidoc System (Biorad).

Then, Phospho-HER2 Y1248 was stripped and the membrane was blocked in 5% BSA in TBS with 0.1 % Tween 20 for 1 h. For evaluation of total HER2, the membrane was incubated overnight at 4 °C with gentle shaking with rabbit-monoclonal antibody against HER2 (#4290; Cell Signalling) at 1:1000 dilution. The membranes were washed three times with TBS with 0.1 % Tween 20 and reacted 1 h with the secondary antibody anti-rabbit conjugated with horseradish peroxidase (1:5000; Abcam) and revealed as described above.

Cell cycle analysis

U-87 MG cells were seeded on a 12-well plate (2.5×10^5 cells per well) and incubated for 24 h. Then, cells were treated with CTX or HFn-CTX (10 μg mL^{-1}) in complete medium and incubated for 24, 48 and 72 h at 37 °C. Untreated cells were used as negative control. At the indicated time point, cells were collected in FACS tubes and fixed with cold ethanol 90% for 1 h. Then cellular DNA was stained with a solution of propidium iodide (10 μg mL^{-1}) and RNase A (20 μg mL^{-1}). 10,000 events were acquired for each sample, using flow cytometry equipped with a doublet discriminator module (GalliosTM Flow Cytometer - Beckman Coulter Inc.) and the DNA content was analyzed by FlowLogic software.

Effector cells isolation

Peripheral blood mononuclear cells (PBMCs) were obtained by centrifugation on Ficoll-Paque of blood samples from healthy donor (30 min at 1,500 rpm without brakes). At the end the PBMCs layer was carefully transferred to a new 50 mL tube, diluted with PBS and centrifuged for 6 min at 1,400 rpm. Then supernatant was eliminated to remove platelets and the procedure was repeated for four times decreasing the centrifugation speed up to 1,000 rpm.

Washed PBMCs were resuspended in RPMI-1640 medium with 10% of decomplemented FBS and 1,000 U mL^{-1} IL-2 (BioLegend, San Diego, CA, USA) for 24 h at 37 °C. The described procedure was approved by Ethical Committee of the University of Milano-Bicocca (prot.#351, 13th November 2017) after submission of the project together with informed consent by the healthy volunteer.

ADCC assay

ADCC was performed using CytoTox 96® Non-Radioactive Cytotoxicity Assay (Promega Corporation, Madison, WI, USA). Firstly, target cells, plated at a density of 5×10^3 in 96-well, were coated with free or nanoformulated CTX (5 and 10 µg mL^{-1}) and with free or nanoformulated TZ (0.2 and 2 µg mL^{-1}) for 30 min at 4 °C in RPMI-1640 medium. After coating, IL-2-activated PBMCs were added onto target cells at an effector:target (E:T) ratio of 40:1 and incubated 4 h at 37 °C. Then LDH release from target cells was measured by EnSight™ multimode plate reader (Perkin Elmer, Waltham, MA, USA) setting absorbance wavelength at 490 nm. Percentage of ADCC was calculated using the formula following protocol instruction:

$$\% \, Specific \, Lysis = \frac{Experimental - Effector \, Spontaneous - Target \, Spontaneous}{Target \, Maximum - Target \, Spontaneous} \times 100$$

Confocal live image microscopy of ADCC

T98 cells were selected for the confocal live image microscopy of ADCC mechanism induced by HFn-CTX. First, cells were stained with *CellTrace ™ Far Red* (ThermoFisher Scientific, USA) diluted 1:1000 in PBS and incubated for 20 minutes at 37 °C. Then 2×10^5 T98 cells were seeded in a 35 mm petri dish. Cells nuclei were stained with Hoechst (ThermoFisher Scientific, USA), while membranes were stained with WGA-Alexa 488 (*Wheat Germ Agglutinin, Alexa Fluor® 488 Conjugate,* ThermoFisher Scientific, USA). After, cells were incubated 30 minutes at 4 °C with 10 μg mL^{-1} of HFn-CTX. WGA-Alexa 488 pre-stained effector cells were added to the petri dish. Images were acquired every 15 minutes for 3 hours using a Nikon confocal microscope (A1 series).

CD16 shedding assay

SKBR3, U-87 MG and T98 cells were seeded at a concentration of 1.5×10^4 cells/well in a 48-well plate. The day after, medium was removed and cells were incubated 30 minutes at 4 °C in RPMI culture medium without FBS with 5 and 10 μg mL^{-1} of HFn-CTX or 0.2 and 2 μg mL^{-1} of HFn-TZ. After the incubation IL-2-activated PMBCs were added at an effector:target (E:T) ratio of 40:1 and incubated 4 h at 37 °C. Then 300 μL of the medium containing PBMCs were collected and transferred in FACS tubes. Effector cells were centrifuged for 5 min at 1,300 rpm and washed once with PBS before adding the AlexaFluor® 488 anti-human CD16 antibody (clone 3G8; BioLegend®) with a dilution of 1:100. The antibody was incubated 10 minutes in the dark. The amount of the not cleaved CD16 on effector cells was evaluated by FACS analysis. 10,000 events were acquired for each sample, using flow cytometry equipped with a doublet discriminator module (GalliosTM Flow Cytometer - Beckman Coulter Inc.) and data were analyzed by FlowLogic software.

In vitro model of BBB

Human cerebral microvascular endothelial cells (hCMEC/D3) were used as a BBB *in vitro* model.[30] Briefly, 0.5 mL of cell suspension containing 5×10^4 of hCMEC/D3 cells (passage 25-35) were seeded onto collagen-coated (4 μg/cm^2 rat tail collagen type 1 Invitrogen) transwell filters (polycarbonate 12-well, pore size 0.4 μm, translucent membrane insert 1.12 cm^2; Euroclone) to establish a polarized monolayer. After 48 h, glioblastoma cells (U-87 MG) were seeded in the lower compartment at a density of 1.2×10^4 cells/cm^2. Experiments were performed after 5 days of co-culture. However, before running any experiments we measured the TEER (Trans Endothelial Electrical Resistance) value of our monolayer using an EVOM Endohm chamber (World Precision Instruments, Sarasota, FL). To be considered a reliable *in vitro* model of the BBB, TEER value should be higher than 40 Ω×cm^2.

HFn-CTX ability to cross the BBB model was evaluated by measuring the endothelial permeability of the nanoformulation. Fluorescent-labeled HFn-CTX was incubated in the apical compartment of the transwell system (the concentration of each protein species in the complex was HFn = 0.35 mg mL^{-1} and CTX = 0.1 mg mL^{-1}) and the endothelial permeability was measured after 3 h. The uptake of fluorescent-labeled CTX or HFn-CTX by hCMEC/D3 was measured 3 and 24 h after the incubation in the apical chamber of the transwell system by spectrofluorometer. The uptake of HFn-CTX compared to free CTX by hCMEC/D3 cells was evaluated using Operetta High Content imaging system (Perkin Elmer).

After we evaluated the interaction of nanoformulated CTX with U-87 MG cells after BBB permeation. We assessed both the cytostatic effect of the mAb and

its ability to induce antibody-dependent cell-mediated cytotoxicity (ADCC) as indicated above.

Statistical analysis

Statistical analyses were conducted using two-tailed Student's *t*-test. All plots show mean values ± standard error (s.e.). All tests assumed normal distribution and the statistical significance threshold was set at $P<0.05$.

4. Results

Synthesis and characterization of mAbs-conjugated ferritin nanoparticles.

H-chain apoferritin nanoparticles were produced and purified as previously reported.[27] After purification HFn cages were used for the conjugation reaction with monoclonal antibodies (CTX or TZ) according to an existing protocol modified for our purposes.[28] A PEG-based heterobifunctional crosslinker (MW_{PEG} ≈ 5000 Da) was used to anchor the monoclonal antibody on HFn surface in a two steps reaction. Briefly, in the first step mAbs react with a molar excess of PEG, which binds to the amine residues on mAb molecules thanks to the N-hydroxysuccinimide (NHS) ester group. In the second step, after the addition of HFn to the reaction mix, the PEG linker anchors the mAb on HFn surface thanks to the binding between PEG maleimide (Mal) groups and sulfhydryl residues on HFn (Fig1).

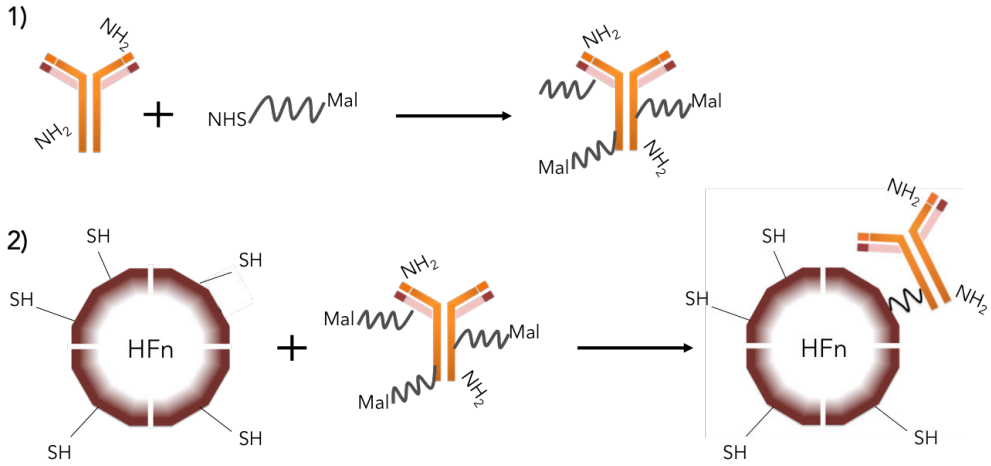

Figure 1. Schematic representation of the two steps reaction used for NPs synthesis. First PEGylation of the mAb occurs **(1)** followed by conjugation with HFn nanoparticles **(2).**

Next, reaction products were separated and characterized by size exclusion gel filtration chromatography (SEC-FPLC) that allowed identifying a peak for protein complex and others for each unreacted species (FigS1). After FPLC elution we qualitatively confirmed the presence of both protein species inside our complex by SDS-PAGE gel electrophoresis and western blot analysis (FigS2). To calculate the amount of mAbs on HFn surface we repeated the reaction using double labeled samples: before using them in the conjugation reaction, mAb and HFn were labeled with AlexaFluor660 (AF660) and Fluorescein Isotiochianate (FITC), respectively. These dyes avoided interfering with each other thanks to the almost total absence of spectra overlapping. Starting from fluorescence species we created calibration curves before performing the reaction, which were used after nanoconjugate peak isolation, for the quantification of single proteins concentration (FigS3). As a result we obtained a batch of HFn NPs with 1 non-oriented immobilized mAb on the surface. The hydrodynamic diameter of HFn-mAb nanoconjugates was measured by DLS, obtaining an overall dimension of less then 30 nm (HFn-TZ = 26.2 ± 9.6 nm; HFn-CTX= 28.8 ± 10.8 nm) (FigS4).

Determination of HFn-mAbs binding to target receptors

The choice of having just one monoclonal antibody on each particle was made in order to create a nanoformulation in which both the protein species maintained the intrinsic ability to bind their targets. Hence, theoretically HFn-mAb should interact with BBB endothelial cells, exploiting the HFn-TfR1 interaction, but also with cancer cells exploiting the TZ-HER2 or CTX-EGFR interactions. To confirm the maintenance of these interactions, flow cytometry experiments were performed. Binding efficiency was estimated incubating cells with HFn-mAb nanoconjugates for 1 h at 37 °C. First we assessed the

binding of two different concentrations of HFn-TZ (10 and 100 μg mL^{-1}) on both endothelial cells (RBMEC, used as cellular model of blood-brain barrier) and HER2 positive breast cancer cells (SKBR3), in comparison to nonspecific HFn-IgG. SKBR3 cells treated with 100 μg mL^{-1} showed signal saturation with both the formulations, while a lower concentration (10 μg mL^{-1}) allowed us to discriminate between specific and nonspecific binding. Indeed we observed a 2-fold increase in the binding capability of HFn-TZ complex compared to the nonspecific HFn-IgG (Fig2a A). This difference confirmed that TZ was still able to interact with HER2 despite its conjugation with HFn. Moreover our nanoconjugate turned out to be able to bind RBMEC cells, but no significant differences in binding efficiency were detected between the treatment with HFn-TZ and the nonspecific control HFn-IgG at both concentrations. Thus we can speculate that the binding capability of the nanoconjugate on endothelial cells was mediated by the interaction of HFn with its specific receptor TfR1 (Fig2a B). The specific interaction of our nanoconjugate with HER2 was also confirmed by repeating the binding assay in presence of free TZ (2 mg mL^{-1}) as a competitor for the receptor (Fig2a C): the difference in binding capability to SKBR3 cells between HFn-TZ and the nonspecific HFn-IgG was completely abolished in presence of free TZ, suggesting that the difference was actually due to the contribution of TZ specific interaction in HFn-conjugated TZ with HER2 receptor.

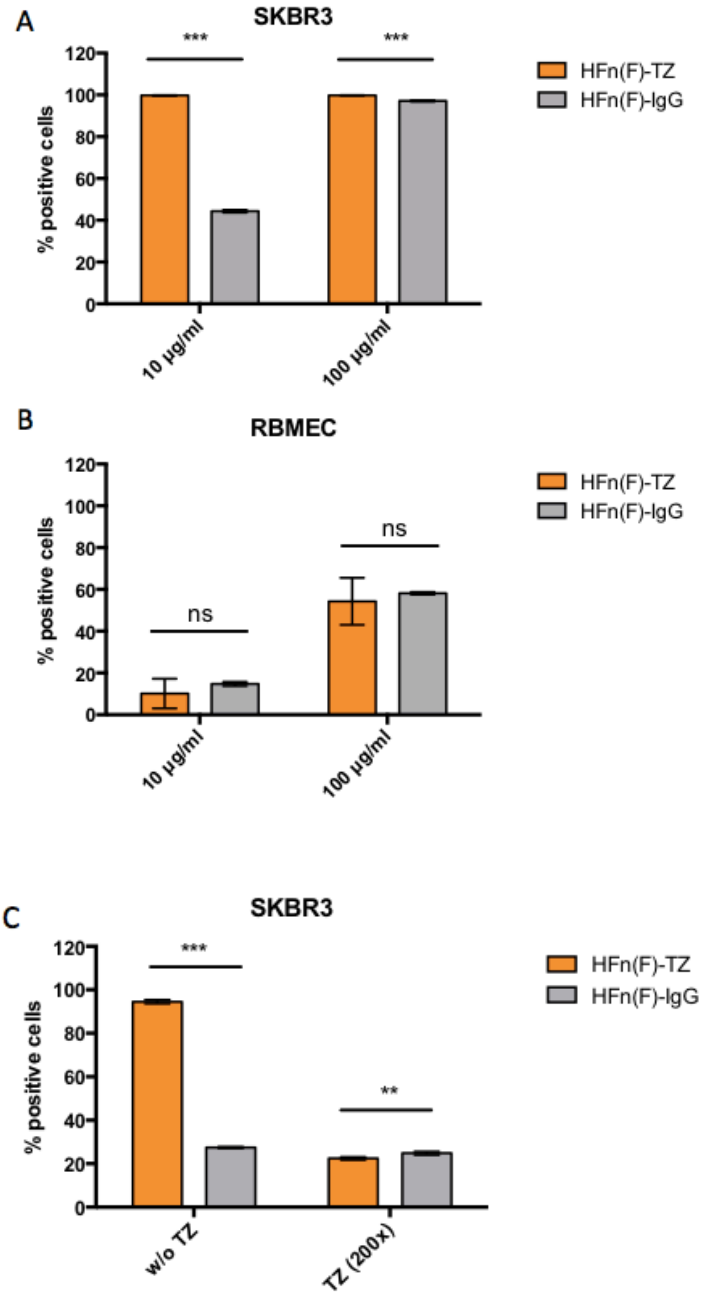

Figure 2a. Evaluation of HFn-TZ ability to bind breast cancer cells (SKBR3) and endothelial cells (RBMEC). SKBR3 (A) and RBMEC (B) were treated with 10 and 100 µg mL^{-1} of FITC-labeled HFn-TZ and HFn-IgG and incubated 1 h at 37 °C. Untreated cells were used to set the positive region and the singlet gate. C) Competition assay. SKBR3 cells were pre-incubated with 2 mg

mL^{-1} of TZ at 37 °C for 30 min. Then 10 µg mL^{-1} of FITC-labeled HFn-TZ and HFn-IgG were added and incubated 1 h at 37 °C. Untreated cells were used to set the positive region and the singlet gate. Reported values are means of 3 replicates ± se. Ns = non significant; ** = $p < 0.01$; *** = $p < 0.001$ (Student's *t*-test).

Furthermore we evaluated also the ability of HFn-conjugated CTX to efficiently bind EGFR in glioblastoma cells, with or without the presence of free CTX as a competitor (Fig2b). Glioblastoma cells (U-87 MG and T98) were incubated with 50 µg mL^{-1} HFn-CTX nanoconjugates for 1 h at 37 °C to estimate the amount of binding and confirm the ability of nanoconjugated CTX to interact with EGFR. The different levels of binding recorded agreed with the EGFR expression levels of the cell lines used.[31] Then we repeated the experiment pre-treating cells with 140 µg mL^{-1} of free CTX for 30 min at 37 °C before adding the nanocomplex. Our results showed that once in presence of free CTX, the amount of HFn-CTX binding to EGFR was at least halved in both cell lines (−66% in T98 cells and −52% in U-87 MG cells). Hence, also in the case of HFn-conjugated CTX, we can assume that nanoformulation didn't affect specific interaction between CTX and EGF receptor.

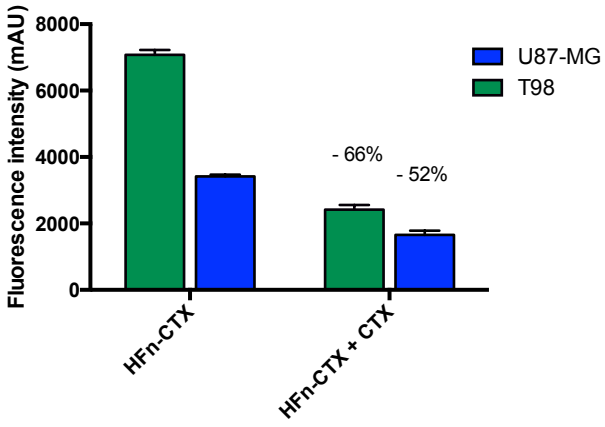

Figure 2b. HFn-CTX binding to glioblastoma multiforme cells. U-87 MG and T98 cells were treated with 50 µg mL^{-1} of FITC-labeled HFn-CTX and incubated 1 h at 37 °C. For the

competition assay, U-87 MG and T98 cells were pre-incubated with 140 μg mL^{-1} of CTX at 37 °C for 30 min. Untreated cells were used to set the positive region and the singlet gate. Reported values are means of 3 replicates ± se.

Antitumor efficacy of HFn-mAb nanoconjugates compared to free mAb.

Next, we assessed the ability of nanoconjugates to impair cancer cell proliferation. Regarding this, it's important to consider that not all monoclonal antibodies affect cancer cells through the same mechanisms. Indeed, it is well known that, for instance, Trastuzumab is a highly active molecule, thus it is able to inhibit cell proliferation and induce apoptosis, affecting tumor growth,[32,33] while Cetuximab has a cytostatic effect, which results in the cell cycle arrest.[34,35] Hence, we evaluated the ability of HFn-TZ to affect breast cancer cell viability in comparison to free TZ and the inhibition of cell cycle induced by HFn-CTX compared to CTX in glioblastoma cells.

SKBR3 cells were treated with free TZ, HFn-TZ or HFn-IgG at two different concentrations of the antibodies (2 and 10 μg mL^{-1}). Since the nanoconjugate is made by 1 HFn and 1 antibody, we were able to quantify the concentration of each protein by dividing the absorbance ($A_{280\ nm}$) of the complex by the overall molecular weight (MW) and multiply it by the MW of each protein species.

After treatments, SKBR3 cells were incubated at 37 °C for 3, 5 and 7 days. At each time point, the MTS reagent was added to the cell culture medium and incubated for 3 h at 37 °C in the dark to allow the reduction of MTS in formazan. The formazan dye produced was quantified measuring the absorbance at 490 nm, which is directly proportional to the number of living cells in culture.

Our results showed that HFn-IgG doesn't affect cell viability at both the concentrations tested. On the other hand the treatment with 2 μg mL^{-1} HFn-TZ exhibited a significant antiproliferative effect that became comparable to the one induced by TZ when we increased the concentration (10 μg mL^{-1}) (Fig3a).

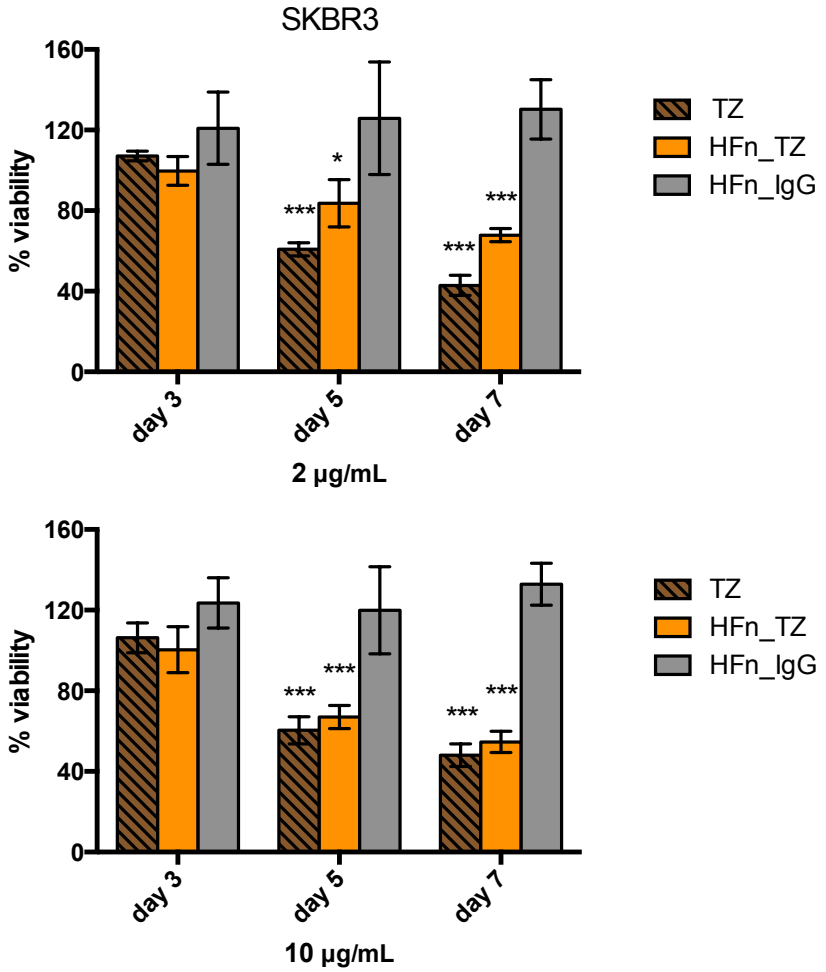

Figure 3a. Antiproliferative effect induced by HFn-TZ compared to TZ. Cells were incubated at 37 °C for 3, 5 and 7 days with 2 and 10 μg mL^{-1} of HFn-TZ, HFn-IgG and TZ. Data are means ± se (n = 6). Statistical significance of treated *vs*. non-treated cells (100% viability) * = $P < 0.05$; *** = $p < 0.001$ (Student's *t*-test).

Evaluation of HER2 phosphorylation

Since one of the modifications specifically induced by trastuzumab treatment is the HER2 phosphorilation on tyrosin 1248 residue, we investigated the effect of our nanoformulation on receptor phosphorylation (Fig3b). SKBR3 cells were treated with 4 µg mL^{-1} of free or nanoformulated TZ or with nanoformulated IgG, for 1 hour in serum starvation. After incubation, cells were lysed and membrane proteins isolated and used for Western Blot analysis. We quantify the ratio between phospho Y-1248 and total HER2 in our samples, using α-tubulin as a reference for normalization. Our data showed that HFn-conjugated TZ was able to induce about the same level of Y1248 phosphorylation of free TZ and that this phosphorylation was significantly higher compared to untreated cells; while HFn-IgG showed no variation in HER2 phosphorylation compared to UNTR. This result, together with what obtained in MTS assay, confirmed that after nanoconjugation, TZ maitained the same activity against its target.

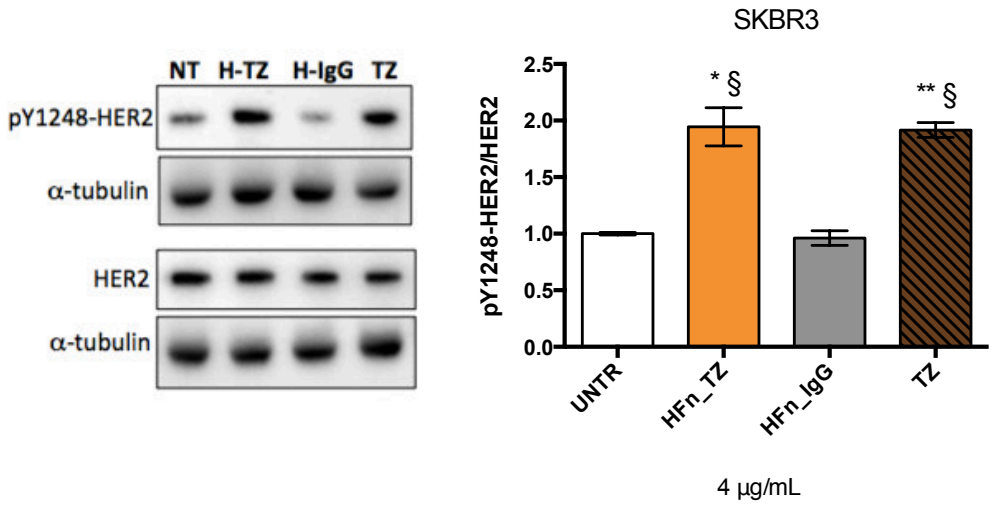

Figure 3b. HER2 phosphorylation assay. SKBR3 cells were treated with μ4 g mL^{-1} of TZ, HFn-TZ or HFn-IgG in starvation medium for 1 h. Untreated cells were used as negative control. At the end of incubation, cells were lysed, subjected to western blot analysis (left) and the ratio of phosphorylated/total HER2 were quantified by densitometry using imageJ software (right). Reported values are the mean of 3 samples ± s.e. Statistical significance *P<0.05, **P<0.01 vs. NT; §p<0.05 vs. HFn-IgG (Student's *t*-test).

Effect of HFn-CTX on cell cycle progression

An important activity of Cetuxumab is the ability to block the cell cycle. Indeed, it is well documented that CTX is able to induce cell cycle arrest in G1 phase by reducing ciclin D1 level and increasing p27 level.[34,35] This activity results in the inhibition of G1/S transition that, in some cases, could lead to apoptosis. Thus, to evaluate if the conjugation on HFn nanoparticles altered the cytostatic effect of CTX, we analyzed the effect on cell cycle progression of HFn-CTX treatment compared to free CTX treatment. U-87 MG cells were treated with 10 μg mL^{-1} of free or nanoformulated CTX at different time points (24, 48 and 72 h). Our data showed that HFn-CTX was more efficient in inducing cell cycle arrest in G1 phase in U-87 MG cells compared to free CTX at the concentration tested (Fig4). We speculated that the higher effect induced by the nanoformulation can be explained by a more stable interaction between EGFR and the nanoparticle, which in turns may lead to a prolonged internalization and sequestration of the receptor.

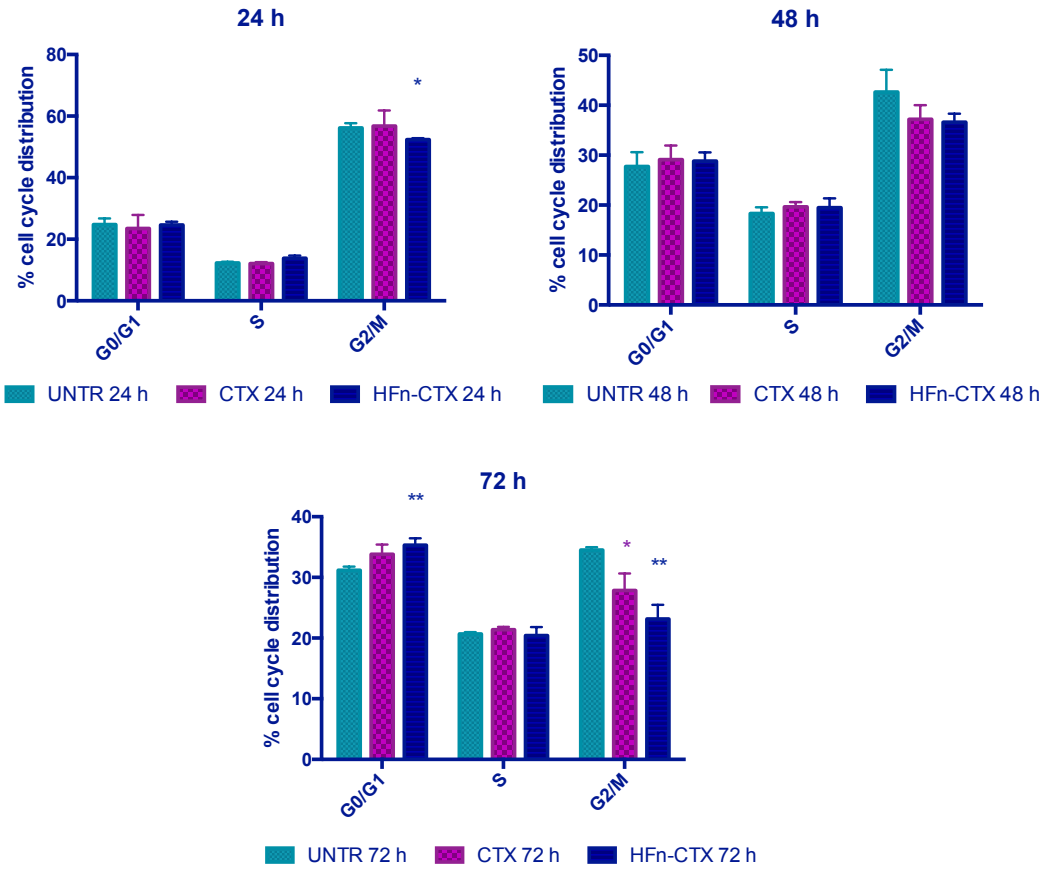

Figure 4. HFn-CTX vs. CTX treatments effect on cell cycle progression. Cells were incubated at 37 °C for 24, 48 and 72 h with 10 μg mL^{-1} of HFn-CTX or free CTX. Graphs represented the mean percentage of events in G1, S and G2/M phase, respectively, ± s.e. (n = 3). Statistical significance of CTX or HFn-CTX *vs*. non-treated cells (UNTR), * = $P < 0.05$; ** = $p < 0.01$ (Student's *t*-test).

Evaluation of ADCC induced by HFn-TZ and HFn-CTX treatment by *in vitro* assay and live image confocal microscopy.

After the evaluation of the direct effect of our nanoconjugates on receptors cascade, we investigated their ability to recruit immune cells. Indeed, if direct effect of mAbs is mediated just by the physical interaction between the mAb and the receptor, the antibody-dependent cell-mediated cytotoxicity (ADCC) requires the recruitment of immune effector cells to be activated. The importance of the interaction between the Fc portion of mAbs and its receptor (FcγR, CD16) has been investigated in several studies, so that now it is considered to be crucial for the *in vivo* antitumor effects of certain monoclonal antibodies.[36,37] However, it is known that not all monoclonal antibodies are able to elicit the same immune response, due to differences in their affinity for CD16.[38] For both the monoclonal antibodies investigated in our study there are evidences that ADCC activation contributes to their overall anticancer activity.[38-40] To evaluate the amount of ADCC response induced by HFn-mAb treatment on cancer cells, we incubated cells with freshly isolated PBMCs, containing around 5% of NK cells, at an effector-to-target cell (E:T) ratio of 40:1. Before running the experiment, PBMCs were incubated 24 h with IL-2 to allow their activation. SKBR3 cells were pre-incubated with 2 μg mL^{-1} of TZ and HFn-TZ at 4 °C for 30 minutes and then IL-2-activated-effector cells were added and incubated at 37 °C for 4 hours to give enough time for ADCC reaction to occur (Fig5 A). In the same way T98 and U-87 MG cells were pre-treated with 10 μg mL^{-1} of CTX or HFn-CTX at 4 °C for 30 minutes, before the addition of activated PBMCs. After 4 hours of incubation, lysis of tumor cells induced by NK cells was quantified using a lactate dehydrogenase (LDH) assay, which correlates the release of LDH enzymes by target cells to cytolytic activity

of NK cells. We observed that compared to free antibodies, our nanocomplexes showed a lower activation of ADCC response, which is not surprising considering that the conjugation reaction we used doesn't orient mAbs on HFn surface. Hence, inside the batch of NPs that we used not all the immobilized mAbs had the Fc portion available for the interaction with effector cells receptor CD16. In detail, we obtain 43.6% of ADCC by treating SKBR3 cells with HFn-TZ, compared to the 80.2% induced by free TZ. A similar behavior was observed also for glioblastoma cells: T98 and U-87 MG cells treated with HFn-CTX showed 37.3% and 21% of ADCC, respectively, while the treatment with free CTX was able to induce 57.8% and 36.3% of toxicity (Fig5 B).

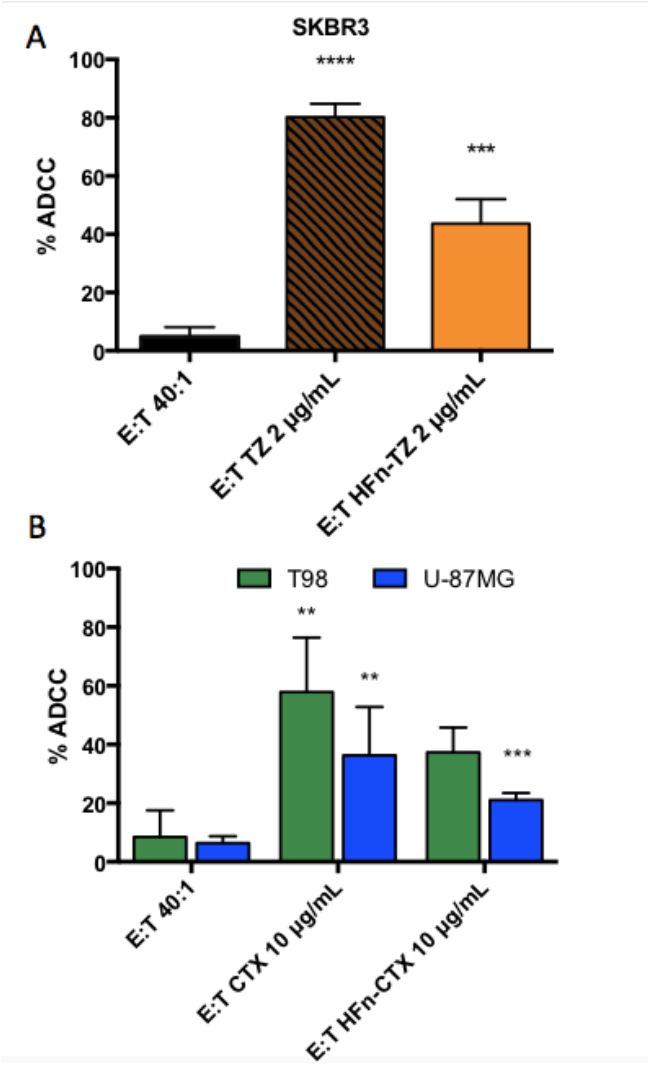

Figure 5. ADCC response induced by HFn-mAb treatment on cancer cells. SKBR3 cells (A) were pre-coated with 2 µg mL^{-1} of TZ and HFn-TZ, while T98 and U-87 MG cells (B) were pre-coated with 10 µg mL^{-1} of free and nanoformulated CTX for 30 min at 4 °C. Next, IL-2-activated PBMCs were added to the target cells with a E:T ratio of 40:1 and incubated 4 h at 37 °C. The percentage of ADCC response activated was calculated from the LDH released by target cell lysis. Graphs represent the mean percentage of ADCC ± s.e. (n=3). Statistical significance of treatments *vs*. non-treated cells (E:T), ** = $p < 0.01$; *** $p < 0.001$; **** $p < 0.0001$ (Student's *t*-test).

As mentioned above, the reduced cytotoxic activity of nanoformulations was expected. However, what was important according to our final purposes was to demonstrate that even when conjugated to HFn nanoparticles, monoclonal antibodies are still able to elicit the immune response. Indeed, the great advantage that HFn-mAbs nanoparticles could have over free mAbs treatment, is the ability to across the blood-brain barrier reaching the brain, thus delivering mAbs in an organ that they are not able to reach.[12]

To further demonstrate that the nanoformulation is able to activate immune cells, we performed a live image confocal microscopy analysis (Fig6). For this experiment we selected T98 cells and repeated the treatment that we tested for the ADCC assay (HFn-CTX 10 μg mL^{-1}). Briefly T98 cells were stained with *CellTrace* ™ *Far Red* and seeded (2×10^5) in a 35 mm petri dish. Then IL-2-activated effector cells were added and the ADCC response was live monitored under the microscope, recording frames every 15 minutes up to 3 hours. All cells used were pre-stained with WGA-Alexa 488. Effector cells, smaller in size compared to cancer cells, appeared like small green spots. Frames in figure 6 showed that during time effector cells attacked target cells inducing cell death (one example is indicated by the white circle).

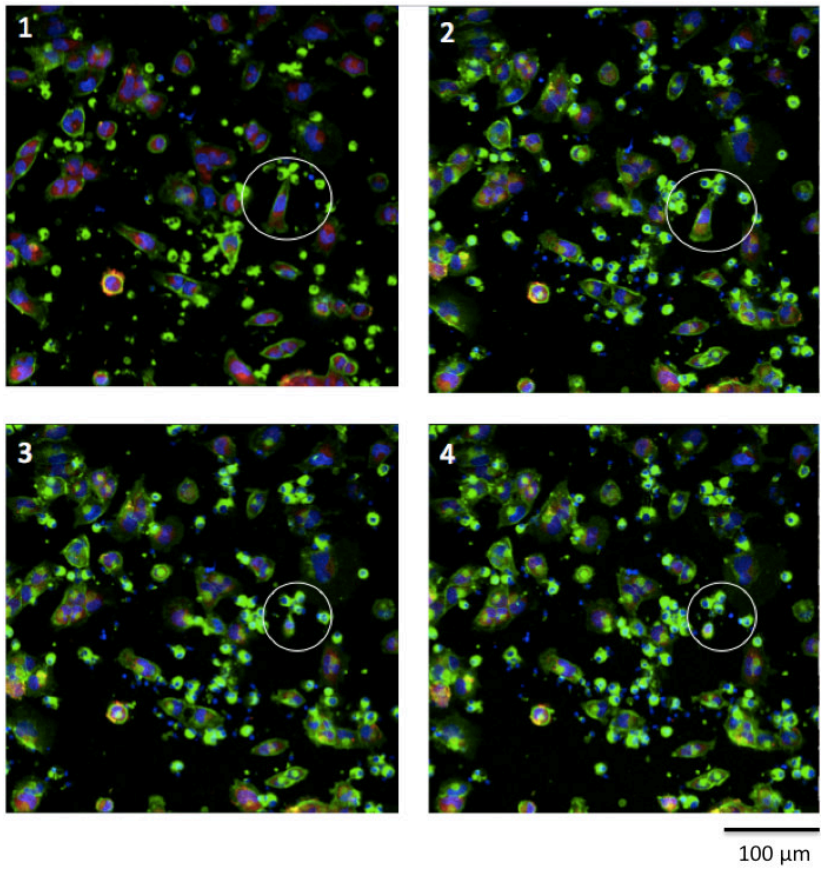

Figure 6. Live image confocal microscopy. T98 cells were stained with *CellTrace ™ Far Red* (red signal) before seeding them. Cells nuclei were stained with Hoechst (blu signal) while membranes were stained with WGA-Alexa 488 (green signal). After, cells were incubated 30 minutes at 4 °C with 10 µg mL^{-1} of HFn-CTX. WGA-Alexa 488 pre-stained effector cells were added to the petri dish and images were acquired every 15 minutes for 3 hours. During this period of time we saw the activation of ADCC, which lead to cancer cell death (see white circle). Scale bar = 100 µm.

Shedding of CD16 receptor

Among the immune cells able to activate the ADCC response, NK cells are considered to be the main effectors.[41] These innate immune cells represent only the 5-15% of circulating lymphocytes in humans and, unless appropriately activated, naïve NK cells exhibit limited cytotoxicity. Indeed, NK cells function is tightly controlled by a balance between activating and inhibitory signals.[42] Thus, a strong limitation for NK-based therapies resides in the induction of a "self-inhibition" process involving the proteolytic cleavage of the CD16 receptor mediated by a metalloproteinase expressed on NK surface, ADAM17, which is activated upon the interaction of Fc with CD16.[43] This inactivation process is also called CD16 shedding.

In order to better investigate the cytotoxic effect induced by our nanoformulations we checked the amount of CD16 shedding. So, if with the ADCC assay we evaluated the effect of our treatment on target cells, now we can appreciate the effect of the same treatment on effector cells. Figure 7 offers a schematic representation of the NK "self-inhibition" process: upon binding of mAb to the cancer cell surface receptor, NK cells are recruited and bind to the Fc through the CD16, which in turn promotes the ADCC and activates ADAM17 metalloproteinase, leading to the cleavage of CD16 and the inhibition of the cytotoxic response. Briefly, SKBR3 and U-87 MG cells were seeded in a 48-well plate and treated with mAbs or HFn-mAbs samples at the same concentrations used for the ADCC assay. After 30 minutes coating, the medium was removed and replaced with RPMI containing the IL-2-activated PBMCs (E:T ratio of 40:1) and cells were incubated 4 hours at 37 °C. Then effectors-containing medium was collected and incubated with AF488 anti-human CD16 antibody before FACS analysis. We observed that effectors

previously incubated with glioblastoma cells and HFn-CTX induced a lower reduction of CD16 expression, compared to CTX treatment. On the other hand HFn-TZ treatment was able to affect CD16 expression on effector cells in the same way as TZ treatment (Fig7). Our results showed that all the nanoformulations tested were able to significantly reduce the amount of extracellular CD16 on effector cells membrane, thus confirming that the result obtained in ADCC assays was indeed attributable to NK activation.

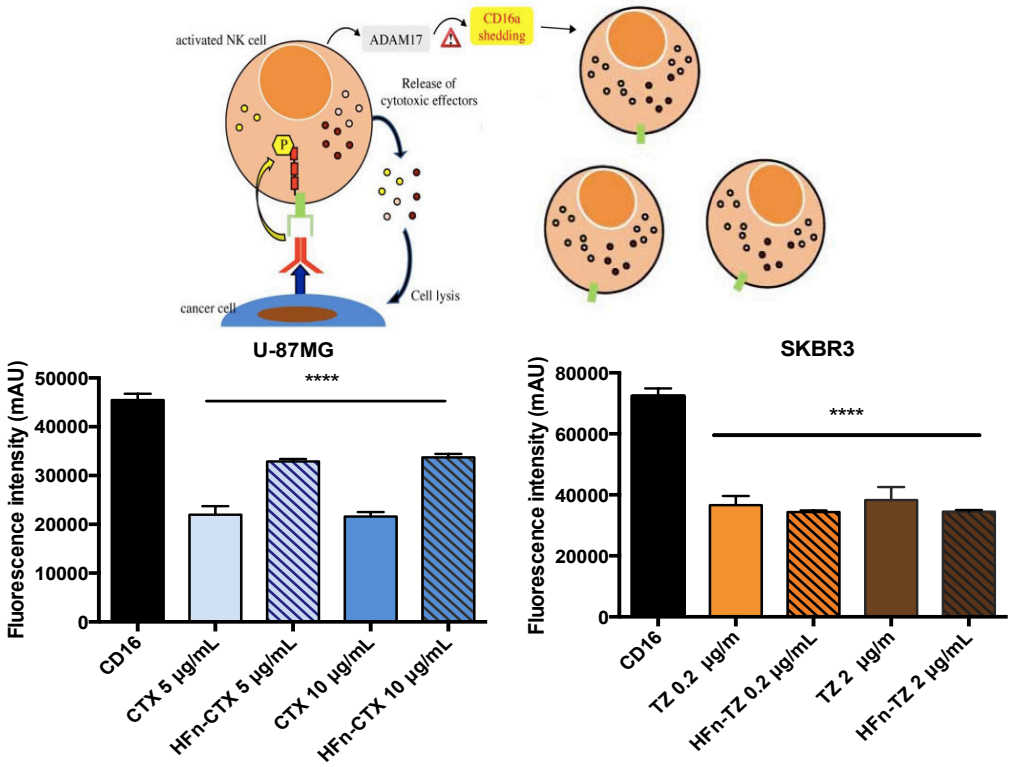

Figure 7. Evaluation of CD16 shedding. (Above) Schematic illustration of the process of ADCC inactivation, mediated by the cleavage of CD16. (Below) U-87 MG and SKBR3 cells were treated with HFn-mAbs and free mAbs as previously described for ADCC assay. After incubation with PBMCs, the medium was collected and incubated with labeled anti-human CD16 antibody. FACS analysis revealed that both the nanoformulations were able to significantly reduce CD16 expression on effector cells. Untreated cells were used to set the

positive region and the singlet gate. Reported values are means of 3 replicates ± se. **** = $p < 0.0001$ (Student's *t*-test).

Evaluation of HFn-mAb permeability across an *in vitro* model of BBB

The blood-brain barrier is a peculiar structure, which acts as a physical obstacle preventing brain contact with harmful blood-circulating substances.[44] Several studies reported that ferritin is able to cross the BBB thanks to its interaction with the TfR1, which is highly expressed on brain endothelial cells due to its role in maintaining iron homeostasis.[25,26,45] Thus we reasoned that HFn could be a good candidate for the delivery of mAbs to the brain. To investigate if this assumption was correct we tested the ability of fluorescent-labeled HFn-CTX to cross an *in vitro* model of BBB and to target glioblastoma cells. In details we seeded immortalized human cerebral microvascular endothelial cells (hCMEC/D3)[30,46] and glioblastoma cells (U-87 MG) in a co-culture transwell system (Fig8): hCMEC/D3 were seeded on the insert filter, while U-87 MG cells were seeded at the bottom of the well. Both the chambers (apical and basolateral) were filled up with culture medium and the transwell was incubated at 37 °C until cells confluence. At day 7 of culture, before performing the experiment, we checked the formation of tight junctions by measuring the TEER (the recorded value was 40.3±2.1 $\Omega \times cm^2$). Then fluorescent-labeled HFn-CTX was incubated in the apical compartment of the transwell system with a concentration of proteins in the complex of HFn = 0.35 mg mL^{-1} and CTX = 0.1 mg mL^{-1}. The endothelial permeability measured after 3 hours incubation was $1.23 \pm 0.02 \times 10^{-4}$ cm min^{-1} (Fig8 A). We evaluated also the uptake of fluorescent-labeled CTX or HFn-CTX by hCMEC/D3. Briefly, we incubated hCMEC/D3 cells with labeled HFn-CTX and free CTX at the same concentration of CTX (0.1 mg mL^{-1}). Proteins uptake was measured after 3 and

24 hours of incubation in the apical chamber of the transwell system by spectrofluorometer. Results showed an increased internalization of HFn-CTX compared to free CTX. In details, after 24 hours of incubation HFn-CTX, showed a more than 2.5 fold higher internalization compared to free CTX (Fig8 B). Fluorescence data obtained by transwell experiments were confirmed by confocal analysis: hCMEC/D3 cells were treated with 0.1 mg mL^{-1} of free or nanoformulated CTX for 24 hours. HFn-CTX (left panel) showed higher uptake by hCMEC/D3 cells compared to free CTX (right panel) and was mainly observed at the perinuclear region of cells (Fig9). Taken together, these data demonstrate that the conjugation to HFn nanoparticles could increase monoclonal antibodies permeability across the blood brain barrier.

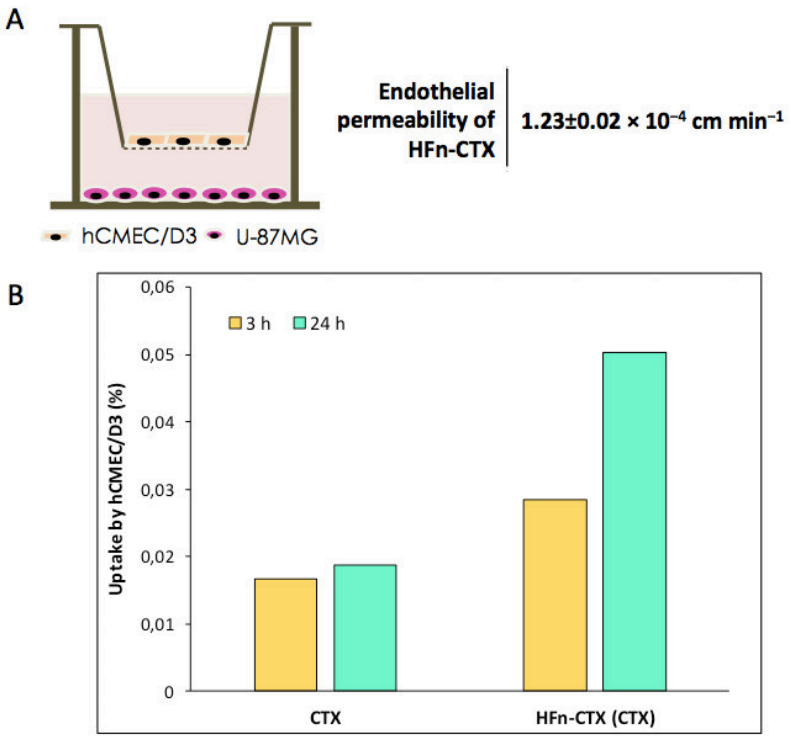

Figure 8. (A) Schematic illustration of a transwell system. The endothelial permeability of fluorescent-labeled HFn-CTX recorded was 1.23±0.02 × 10^{-4} cm min^{-1}. **(B) Percentage of**

uptake of fluorescent-labeled CTX or HFn-CTX by hCMEC/D3. After incubating the transwell system with 0.1 mg mL^{-1} of free or nanoformulated CTX, we observed an increased internalization of HFn-CTX compared to free CTX at both the time points.

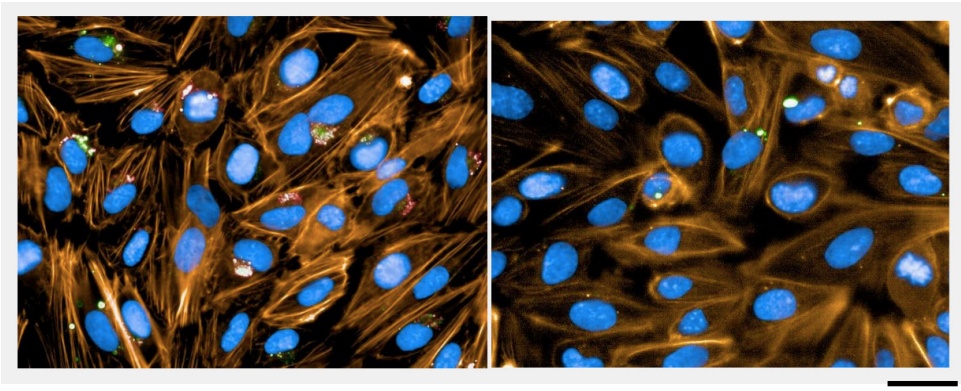

Figure 9. Confocal images of HFn-CTX and free CTX uptake by hCMEC/D3. hCMEC/D3 cells were treated with HFn-CTX or CTX at the concentration of 0.1 mg mL^{-1}. Images were acquired after 24 hours using Operetta high content system. Nuclei were stained with Dapi (blue); Cytoskeleton was stained with Phalloidin Texas-Red (orange); free and nanoformulated CTX was labeled with FITC (green). Scale bar = 50 µm.

mAbs anticancer activity after BBB crossing

Using the transwell system we could assess that, once nanoformulated, the monoclonal antibody permeate more efficiently across the barrier. However, the permeation ability doesn't give any information about the maintenance of mAb anticancer activity. Thus, in order to demonstrate if, after crossing the BBB, the nanoformulated-mAb was still capable of activating its cytotoxic mechanisms, we tested permeated samples ability to reduce cancer cell proliferation, activate ADCC response and induce CD16 shedding.

The inhibition of cancer cell proliferation was assessed directly on U-87 MG cells seeded in co-culture with hCMEC/D3 cells in the traswell system. HFn-CTX, free CTX or free HFn were added in parallel in the apical compartment of

the transwell as described above, with proteins concentration of HFn = 0.35 mg mL^{-1} and CTX = 0.1 mg mL^{-1} (only for the nanoconjugate we tested also a doubled concentration, named HFn-CTX1 in Fig10 A). After 24 hours incubation, to evaluate the effect of each treatment on cells proliferation, we counted the nuclei using Operetta high content system function *find nuclei.* Results showed that permeated HFn-CTX was still able to affect glioblastoma cells proliferation and that its activity was dose dependent (Fig 10 A). Furthermore, to evaluate HFn-CTX ability to activate immune system after BBB crossing, we collected the medium from lower chambers and incubated it with U-87 MG cells for 30 minutes at 4 °C before adding IL-2-activated effector cells. ADCC and CD16 shedding experiments were performed as previously indicated. Our results showed that after crossing the endothelial cell monolayer, conjugated-CTX retains its biological activity against glioblastoma cells. Hence, it was able to significantly induce ADCC-mediated cell lysis as well as significantly reduce the amount of the CD16 on effector cells membrane (Fig10 B, C).

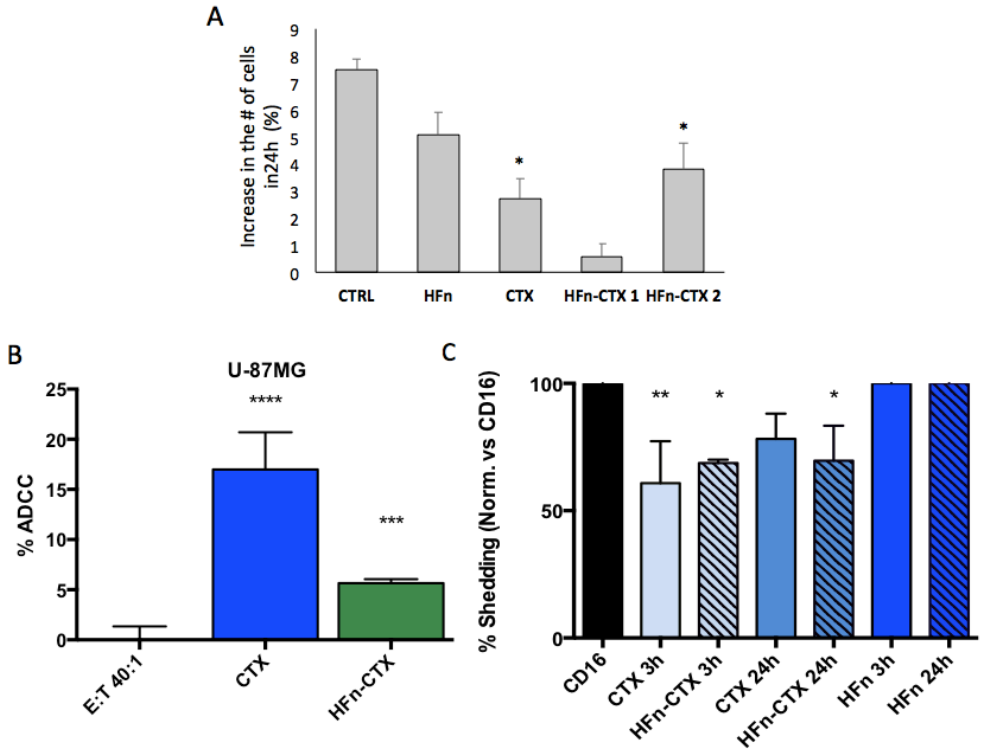

Figure 10. Anticancer activity of nanoconjugated-mAbs after BBB crossing. (A) Evaluation of cancer cell proliferation upon 24 h treatment with BBB permeated samples. 0.35 mg mL^{-1} of HFn and 0.1 mg mL^{-1} of CTX (free or conjugated) were incubated in the apical compartment of transwell system. For HFn-CTX1 we incubated a doubled concentration. Results obtained from nuclei counting showed that our nanoconjugate was still active after BBB crossing and that its effect was dose dependent. Reported values are means of 3 replicates ± se. * = $p < 0.05$ vs. CTRL (Student's *t*-test). **ADCC (B) and CD16 Shedding (C) assays after BBB permeation.** ADCC and shedding analysis confirmed that, after crossing the BBB, HFn-conjugated CTX maintains its capability to recruit and activate immune cells. Reported values are means of 3 replicates ± se. **** = $p < 0.001$ and *** = $p < 0.01$ vs. E:T; ** = $p < 0.05$ and * = $p < 0.1$ vs. UNTR (CD16) (Student's *t*-test). Untreated cells were used to set the positive region and the singlet gate in the shedding analysis.

5. Discussion

In this study we have developed fully biocompatible and biodegradable nanoformulations of monoclonal antibodies, made of H-chain apoferritin, externally monofunctionalized with TZ or CTX. These nanoconjugates were tested both as antibody delivery system across the BBB and as therapeutic agents for brain cancers treatment. The choice of having only one monoclonal antibody immobilized on HFn surface was made with the aim to preserve the specificity of both the proteins for their targets. Indeed mAb-receptor interaction should be well-maintained in order to exert the cytotoxic activity, as well as HFn-TfR1 interaction, which is fundamental for the BBB crossing.[25] For this study we focused on a model of primary (glioblastoma, U-87 MG and T98) and metastatic (HER2 positive breast cancer, SKBR3) brain tumor, in which we investigated the effect of HFn-mAbs treatment in terms of a direct toxicity, induced by inhibition of the receptor pathways, and an indirect toxicity, mediated by immune cells recruitment. Performing some binding assays, we confirmed that the rational behind nanoparticles design was correct, thus HFn-mAbs maintained the ability to bind both endothelial cells of the BBB and cancer cells (GBM cells or SKBR3). However, some concerns might arise about the capability of conjugated-mAbs to exert their cytotoxic activity. Hence, starting from literature data that documented CTX ability to arrest cell cycle in G1/S phase[34,35], we evaluated the effect of HFn-CTX on cell cycle progression. We obtained that, at the concentrations tested, our nanoformulation worked even better than free CTX, inducing an arrest in G1 phase after 72 h treatment. One possible explanation for this higher effect might be a more stable interaction between EGFR and the nanoparticle, which

in turns may lead to a prolonged internalization and sequestration of the receptor, avoiding its translocation into the nucleus and the activation of ciclin D1 transcription.[34,35] The maintenance of cytotoxic activity was confirmed also for HFn-conjugated TZ. Indeed, viability assay showed that TZ has an almost identical cytotoxic effect when it is free or nanoformulated. This result was further confirmed by the evaluation of the TZ-specific HER2 phosphorylation on Y1248 residue, which suggested tha nanoformulated TZ could affect HER2 signaling by activating the same molecular mechanism of free TZ. Another well-known mechanism of action of monoclonal antibodies is the toxicity mediated by immune cells. Even though ADCC is not induced by all monoclonal antibodies, for TZ and CTX there are lots of evidences.[38-40] Thus, we checked if also this mechanism was preserved after the conjugation. Our results showed that for both the nanoformulations (HFn-TZ and HFn-CTX) the ADCC response was maintained, albeit to a smaller extent. This reduction in activity was not surprising, since during NPs synthesis, mAbs were chemically linked on HFn surface in a non-oriented manner. As a result, our batches of nanoconjugates were intrinsically heterogeneous in terms of antibodies orientation and surface available for accomplishing their functions. Consequently, the reduction in ADCC activity, observed for HFn-mAbs, could be attributed to the lower amount of Fc portions available for the interaction with immune cells. This assumption could explain also the results obtained in the evaluation of CD16 shedding, in which NPs treatment showed a similar reduction in activity compared to free mAbs. Anyway all these experiments confirmed that our nanoconjugation method preserved all mAbs activities, even increasing the direct effect. Furthermore, considering that our final goal was the treatment of brain cancers, we investigated the ability of HFn-mAb to cross an *in vitro*

model of BBB and to target cancer cells. Indeed, even if there are several studies reporting the ability of ferritin to cross the barrier (both with or without cargo molecules inside),[25,26] it is still unknown if ferritin could deliver to the brain also molecules attached on its surface. So we performed a set of permeability and uptake experiments using a transwell system, which proved HFn-mAb to be effective in BBB crossing. Cellular uptake of HFn-mAb by human cerebral microvascular endothelial cells (hCMEC/D3) was demonstrated by confocal microscopy. After crossing the endothelial cell monolayer, mAbs conjugated to HFn retains their biological activity against their targets, as assessed by MTS and ADCC assays.

These preliminary data provide a proof of concept that HFn is as an efficient carrier to enhance the BBB crossing of mAbs, without affecting their toxic activity on cancer cells. Moreover, our results support that HFn-conjugated TZ and CTX can represent promising approaches for brain cancers treatment.

6. Supporting Information

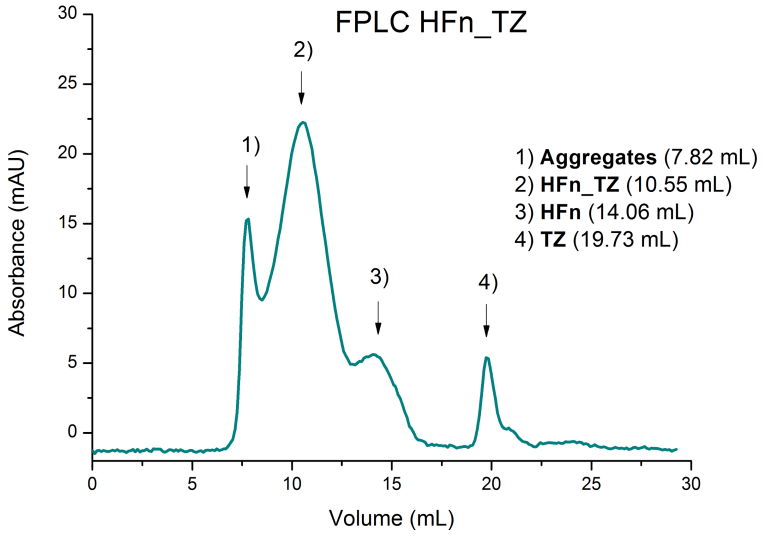

Figure S1. Elution profile of the nanoconjugate by SEC-FPLC.

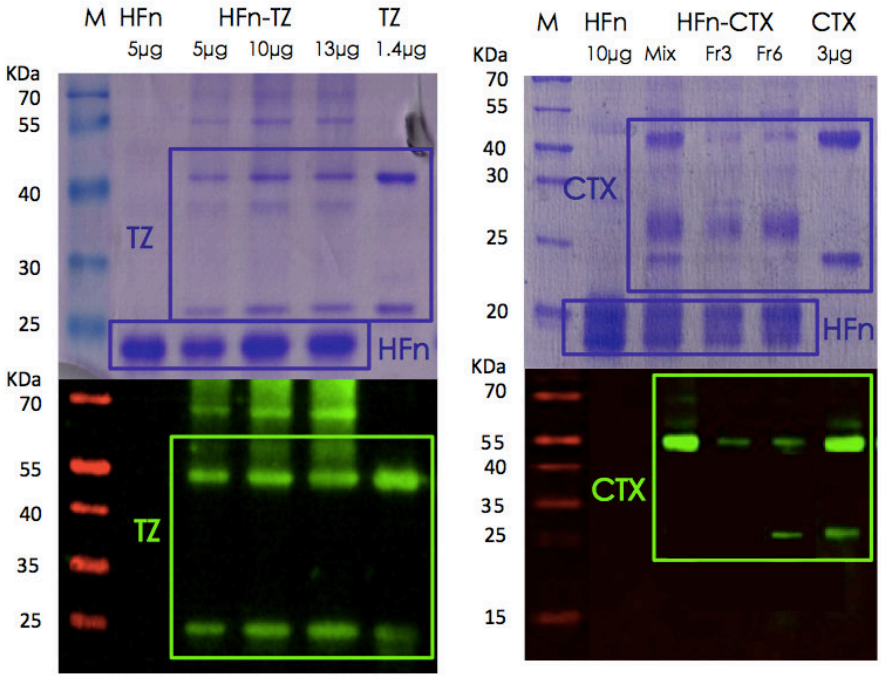

Figure S2. Qualitative evaluation of the presence of both the proteins (HFn and mAbs) in the complex, after FPLC elution. The presence of HFn, TZ and CTX in the nanoformulations was qualitatively checked via 12% SDS-PAGE separation. Starting from the left, the protein marker is in the first lane, then standards of HFn and mAb were loaded in second and last lane, respectively. Different samples of HFn-mAb complex were loaded in the central lanes. For WB analysis membranes were incubated over night with rabbit-monoclonal antibody against ferritin heavy chain (EPR3005Y; Abcam) at 1:1000 dilution in 5% BSA in TBS with 0.1% tween 20. After, membranes were washed thrice with TBS with 0.1% tween 20 and reacted 1 h with rabbit polyclonal anti-human IgG secondary antibody (A80-118P; Bethyl) at 1:20000 dilution in 5% BSA in TBS with 0.1% tween 20. After washing again the membranes, the bound antibodies were revealed using ECL star reagent (Euroclone) and the chemiluminescence signal was detected using Odyssey Fc Imaging System (Licor).

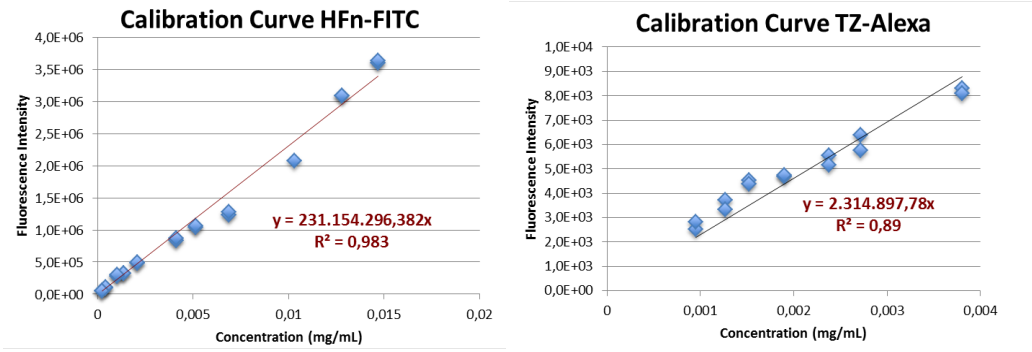

Figure S3. Quantification of protein species in the nanoformulation using double-labeled samples. HFn and mAb were labelel using FITC and AF660, respectively and calibration curves were obtained for each of them before the reaction took place. After the reaction, the fluorescence intensity of each dye was recorded and used to calculate the protein concentration. Thanks to this quantification we obtained that HFn was functionalized with one monoclonal antibody on the surface (HFn:mAb ratio of 1.2).

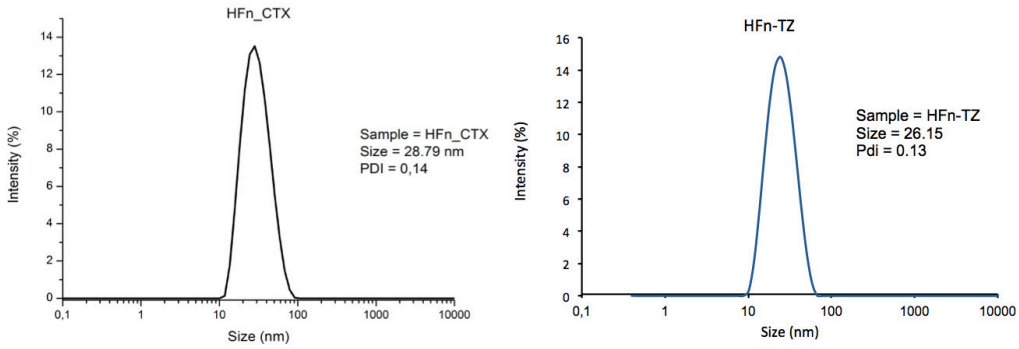

Figure S4. Nanoparticle characterization. Hydrodynamic diameter size of HFn-CTX (28.8±10.8 nm, left) and HFn-TZ (26.2±9.6 nm, right) nanoparticles was evaluated by dynamic light scattering.

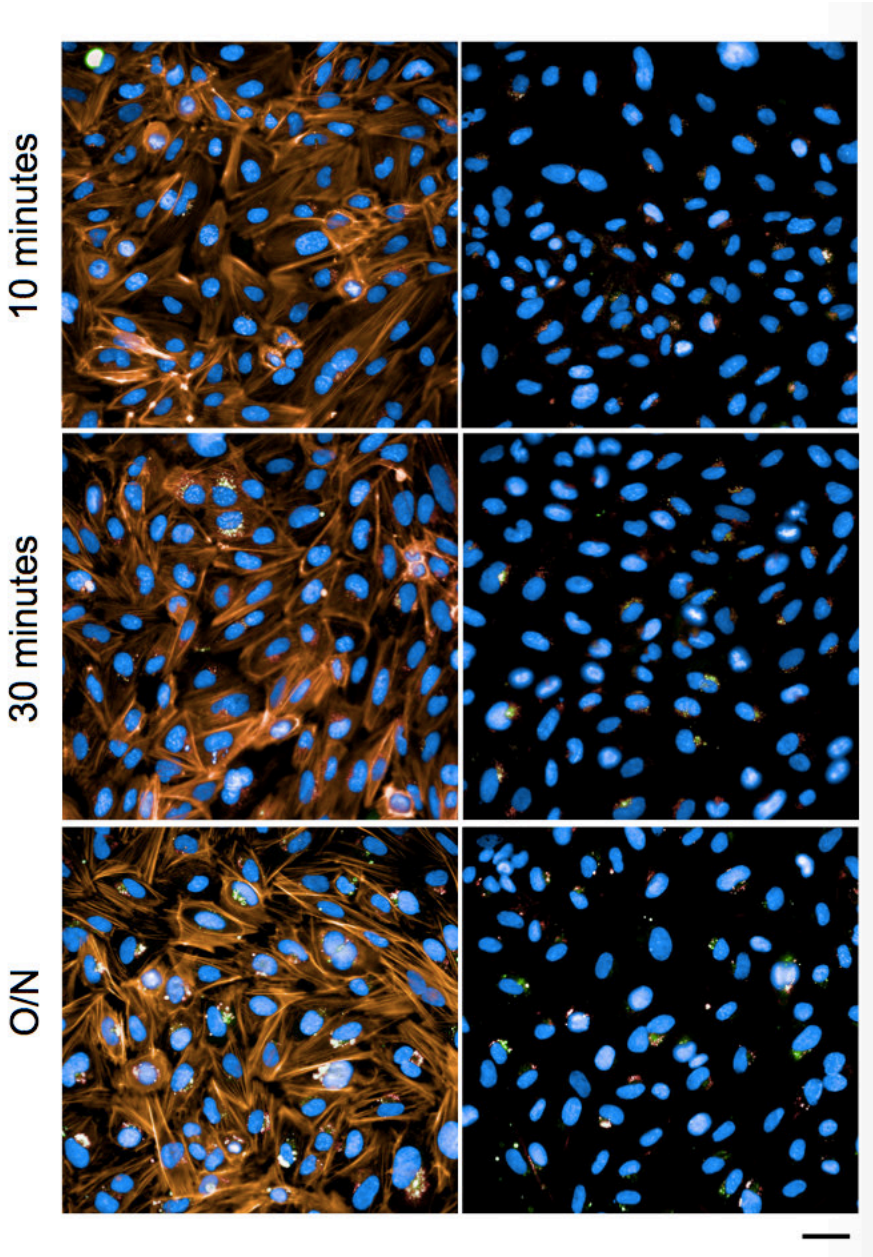

Figure S5. Confocal images of HFn-CTX uptake by hCMEC/D3. hCMEC/D3 cells were treated with HFn-CTX (HFn = 0.35 mg mL^{-1} and CTX = 0.1 mg mL^{-1}). Images were acquired after 10 minutes, 30 minutes and over night (O/N) using Operetta high content system. We observed that NPs uptake was very fast and time dependent. Nuclei were stained with Dapi (blue); Cytoskeleton was stained with Phalloidin Texas-Red (orange); HFn was labeled with FITC (green); CTX was labeled with AF660 (red). Scale bar = 50 µm.

7. References

1. Bos P.D., Zhang X., Nadal C., Shu W., Gomis R.R., Nguyen D.X., Minn A.J., van de Vijver M.J., Gerald W.L., Foekens J.A., Massague J. Genes that mediate breast cancer metastasis to the brain. *Nat Lett* (**2009**) 459: 1005.
2. Wilhelm I., Molnár J., Fazakas C., Haskó J., Krizbai I.A., Role of the Blood-Brain Barrier in the formation of brain metastases. *Int. J. Mol. Sci.* (**2013**) 14: 1383–1411.
3. Van Tellinger O., Yetkin-Arik B., de Gooijer M.C., Wesseling P., Wurdinger T., de Vries H.E. Overcoming the blood–brain tumor barrier for effective glioblastoma treatment. *Drug Resistance Updates* (**2015**) 19: 1–12.
4. Ostrom Q.T., Gittleman H., Fulop J., Liu M., Blanda R., Kromer C., Wolinsky Y., Kruchko C., Barnholtz-Sloan J.S. CBTRUS Statistical Report: Primary Brain and Central Nervous System Tumors Diagnosed in the United States in 2008-2012. *Neuro Oncology* (**2015**)
5. Ostrom Q.T., Bauchet L., Davis F.G., Deltour I., Fisher J.L., Langer C.E., Pekmezci M., Schwartzbaum J.A., Turner M.C., Walsh K.M., Wrensch M.R., Barnholtz-Sloan J.S. The epidemiology of glioma in adults: a "state od the science" review. *Neuro Oncol* (**2014**) 16(7): 896–913
6. Wick W., Osswald M., Wick A. and Winkler F. Treatment of glioblastoma in adults. *Ther Adv Neurol Disord* (**2018**) 11: 1–13.
7. Lee S.Y. Temozolomide resistance in glioblastoma multiforme. *Genes & Diseases* (**2016**) 3(3): 198–210.
8. Bocangel D.B., Finkelstein S., Schold S.C., Bhakat K.K., Mitra S., Kokkinakis D.M. Multifaceted resistance of gliomas to temozolomide. *Clin Cancer Res*. (**2002**) 2: 2725–2734.

9. Gaspar N., Marchall L., Perryman L., Bax D.A., Little S.E., Viana-Pereira M., Sharp S.Y., Vassal G., Pearson A.D.J., Reis R.M., Hargrave D., Workman P., and Jones C. MGMT-Independent Temozolomide Resistance in Pediatric Glioblastoma Cells Associated with a PI3-Kinase–Mediated HOX/Stem Cell Gene Signature. *Cancer Res.* (**2010**) 70(22): 9243–9252.
10. Chamberlain M.C. Temozolomide: therapeutic limitations in the treatment of adult high-grade gliomas. *Expert Rev. Neurother*. (**2010**) 10: 1537–1544.
11. Kim S.S., Harford J.B., Pirollo K.F., Chang E.H. Effective treatment of glioblastoma requires crossing the blood-brain barrier and targeting tumors including cancer stem cells: The promise of nanomedicine**.** *Biochem Biophys Res Commun*. (**2015**) 468(3): 485-9.
12. Westphal M., Maire C.L., Lamszus K. EGFR as a target for glioblastoma treatment: an unfulfilled promise. *CNS Drugs* (**2017**) 31:723–735.
13. Sunada H., Magun B. E., Mendelsohn J. & MacLeod C. L. Monoclonal antibody against epidermal growth factor receptor is internalized without stimulating receptor phosphorylation. *Proc. Natl Acad. Sci.* (**1986**) 83: 3825–3829.
14. Li S. et al. Structural basis for inhibition of the epidermal growth factor receptor by cetuximab. *Cancer Cell* (**2005**) 7: 301–311.
15. Blick S.K.A. and Scott L.J. Cetuximab. A review of its use in squamous cell carcinoma of the head and neck and metastatic colorectal cancer. *Drugs* (**2007**) 67(17): 2585–2607.
16. Chang X., Hung M. Breast cancer brain metastases. *Cancer Metastasis Rev.* (**2007**) 26:635–643.
17. Iqbal N., Iqbal N. human epidermal growth factor receptor overexpression

and therapeutic implications. *Molecular Biology International* (**2014**) 852748.

18. Yarden Y., Sliwkowski M.X. Untangling the ErbB signalling network. *Nature Rev.* (**2001**) 2: 127–137.
19. Slamon D.J., Clark G.M., Wong S.G., Levin W.J., Ulrich A., McGuire W.L. Human breast cancer: correlation of relapse and survival with amplification of the HER-2/neu oncogene. *Science* (**1987**) 235(4785): 177–182.
20. Tafe L.J., Janjigian Y.Y., Zaidinski M., Hedvat C.V., Hameed M.R., Tang L.H., Hicks J.B., Shah M.A., Barbashina V. Human epidermal growth factor receptor 2 testing in gastroesophageal cancer: correlation between immunohistochemistry and fluorescence *in situ* hybridization. *Archives of Pathology & Laboratory Medicine*. (**2011**) 135: 1460–1465.
21. Dawood S., Broglio K., Buzdar A.U., Hortobagyi G.N., Giordano S.H. Prognosis of women with metastatic breast cancer by her2 status and trastuzumab treatment: an institutional based review. *Journal of Clinical Oncology*. (**2010**) 28: 92–98.
22. Pardridge W.M. Blood-brain barrier drug targeting: the future of brain drug development. *Molecular Interventions.* (**2003**) 3(2): 90–105.
23. Loscher W., Potschka H. Role of drug efflux transporters in the brain for drug disposition and treatment of brain diseases. *Prog. Neurobiol.*, (**2005**) 76: 22–76.
24. Bien-Ly N., Yu Y.J., Bumbaca D., Elstrott J., Boswell C.A., Zhang Y., Luk W., LuY., Dennis M.S., Weimer R.M., Chung I., Watts R.J. Transferrin receptor (Tf R) trafficking determines brain uptake of Tf R antibody affinity variants. *J Exp Med.* (**2014**) 211(2): 233–244.

25. Fan K., Jia X., Zhou M., Wang K., Conde J., He J., Tian J., Yan X. Ferritin nanocarrier traverses the blood brain barrier and kills glioma. *ACS Nano* (**2018**) 12(5): 4105–4115.

26. Fisher J., Devraj K., Ingram J., Slagle-Webb B., Madhankumar A.B., Liu X., Klinger M., Simpson I.A., Connor J.R. Ferritin: a novel mechanism for delivery of iron to the brain and other organs. *Am J Physiol Cell Physiol.* (**2007**) 293(2): C641–9.

27. Wang Z., Gao H., Zhang Y., Liu G., Niu G., Chen X. Functional ferritin nanoparticles for biomedical applications. *Front. Chem. Sci. Eng.* (**2017**) 11(4): 633–646.

28. Bellini M., Mazzucchelli S., Galbiati E., Sommaruga S., Fiandra L., Truffi M., Rizzuto M.A., Colombo M., Tortora P., Corsi F., Prosperi D. Protein nanocages for self-triggered nuclear delivery of DNA-targeted chemotherapeutics in Cancer Cells. *J Control Release* (**2014**) 196: 184–196.

29. Falvo E., Tremante E., Fraioli R., Leonetti C., Zamparelli C., Boffi A., Morea V., Ceci P., Giacomini P. Antibody-drug conjugates: targeting melanoma with cisplatin encapsulated in protein-cage nanoparticles based on human ferritin. *Nanoscale* (**2013**) 5: 12278–12285.

30. Weksler B., Romero I.A. and Couraud P.O. The hCMEC/ D3 cell line as a model of the human blood brain barrier. *Fluids Barriers CNS* (**2013**) 10: 16.

31. Carrasco-Garcia E., Saceda M., Grasso S., Rocamora-Reverte L., Conde M., Gomez-Martinez A., et Al. Small tyrosine kinase inhibitors interrupt EGFR signaling by interacting with erbB3 and erbB4 in glioblastoma cell lines. *Experimental Cell Research* (**2011**) 1476–1489.

32. Nahta R., Hung M., Esteva F. The HER-2 targeting antibodies Trastuzumab and Pertuzumab synergistically inhibit the survival of breast cancer cells.

Cancer Research (**2004**) 64: 2343–2346.

33. Hudis C.A. Trastuzumab: mechanism of action and use in clinical practice. *N Engl J Med* (**2007**) 357: 39–51.
34. Vincenzi, B., Schiavon, G., Silletta, M., Santini, D., Tonini G. The Biological Properties of Cetuximab. *Crit. Rev. Oncol. Hematol*. (**2008**) 68: 93–106.
35. Wu, X., Rubin, M., Fan, Z., DeBlasio, T., Soos, T., Koff, A., Mendelsohn, J. Involvement of $p27^{KIP1}$ in G1 Arrest Mediated by an Anti-Epidermal Growth Factor Receptor Monoclonal Antibody. *Oncogene* (**1996**) 12: 1397–1403.
36. Weiner L.M., Surana R., Wang S. Monoclonal antibodies: versatile platforms for cancer immunotherapy. *Nat Rev* (**2010**) 10: 317–327.
37. Mellor J.D., Brown M.P., Irving H.R., Zalcberg J.R., Dobrovic A. A critical review of the role of Fc gamma receptor polymorphisms in the response to monoclonal antibodies in cancer. *Journal of Hematology & Oncology* (**2013**) 6:1.
38. Monteverde M., Milano G., Strola G., Maffi M., Lattanzio L., Vivenza D., Tonissi F., Merlano M., Lo Nigro C. The relevance of ADCC for EGFR targeting: a review of the literature and a clinically-applicable method of assessment in patients. *Crit Rev Oncol Hematol* (**2015**) 95: 179–190.
39. Musolino, a. et al. Immunoglobulin G. fragment C receptor polymorphisms and clinical efficacy of trastuzumab-based therapy in patients with HER-2/ neu-positive metastatic breast cancer. *J. Clin. Oncol.* (**2008**) 26: 1789–1796.
40. Bibeau, F. et al. Impact of FcγRIIa–FcγRIIIa polymorphisms and KRaS mutations on the clinical outcome of patients with metastatic colorectal cancer treated with cetuximab plus irinotecan. *J. Clin. Oncol.* (**2009**) 27:

1122–1129.

41. Wang W., Erbe A.K., Hank J.A., Morris Z.S., Sondel P.M. NK cell-mediated antibody-dependent cellular cytotoxicity in cancer immunotherapy. *Front. Immunol.* (**2015**) 6: 368.
42. Lanier LL. Up on the tightrope: natural killer cell activation and inhibition. *Nat Immunol.* (**2008)**: 9(5): 495–502.
43. Romee R., Foley B., Lenvik T., Wang Y., Zhang B., Ankarlo D., Luo X., Cooley S., Verneris M., Walcheck B., Miller J. NK cell CD16 surface expression and function is regulated by a disintegrin and metalloprotease-17 (ADAM17). *Blood*. (**2013**) 121(18): 3599–3608.
44. Abbott N.J., Patabendige A.A., Dolman D.E., et al. Structure and function of the blood-brain barrier. *Neurobiol Dis*. (**2010**) 37: 13–25.
45. Rouault T.A., Cooperman S. Brain iron metabolism. *Semin Pediatr Neurol.* (**2006**) 13(3): 142–148.
46. Helms H.C., Abbott N.J., Burek M., Cecchelli R., Couraud P., Deli M.A., Förster C., Galla H.J., Romero I.A., Shusta E.V., Stebbins M.J., Vandenhaute E., Weksler B. and Brodin B. In vitro models of the blood–brain barrier: An overview of commonly used brain endothelial cell culture models and guidelines for their use. *J Cereb Blood Flow Meta*b (**2016**) 36(5): 862–890.

CHAPTER 2

Half-Chain Cetuximab Nanoconjugates Allow Multitarget Therapy of Triple Negative Breast Cancer

1. Introduction

The concept of using therapeutic antibodies as “magic bullets” to target cancer was first suggested by Paul Ehrlich early at the beginning of the past Century.[1] Since then, continuous advances in the development of monoclonal antibodies (mAbs) have led to the availability of over 70 among chimeric, humanized and fully human mAbs approved until 2017, with a further 50 awaiting market approval or under clinical trials.[2,3] The technology progress in mAbs engineering allowed researchers to address some of the adverse issues that limited the clinical impact of such biological therapeutics, including high immunogenicity in humans and poor efficacy in triggering the human immune effector response.[4] Over the past two decades, the use of mAbs directed either to specific antigens overexpressed by tumor cells or to the tumor microenvironment, including angiogenesis and checkpoint inhibition, has provided great benefit in the treatment of certain cancers.[5-8] Antibodies conjugated to chemotherapeutics or radioisotopes proved to be effective against hematological malignancies, whereas unconjugated mAbs have been especially employed for the treatment of non-leukemic tumors.[2,9-11] Among the latter class of therapeutic mAbs, those targeting growth factor receptors, including the epidermal growth factor receptor (EGFR) and the human epidermal growth factor receptor 2 (HER2), have demonstrated well recognized efficacy.

Cetuximab (CTX) is a chimeric mAb in use as second- or third-line therapy for the treatment of EGFR-positive colorectal cancer and head-and-neck squamous cell cancer.[12,13] Although CTX does not exhibit primary cytotoxic

activity,[14] this mAb exerts a cytostatic antitumor action by competing the binding of EGFR with the activating ligand (EGF)[15] and by preventing receptor dimerization.[16] These events were associated with EGFR-mediated signaling transduction typical of tyrosine kinase receptors family.[17] In addition, CTX is able to promote the antibody-dependent cell-mediated cytotoxicity (ADCC). Improved efficacy has been suggested in combination with chemotherapy or co-administration of tyrosine kinase inhibitors.[18,19]

However, a few constrains, including low tissue penetration, short circulation half-life and onset of resistance, limit the conventional therapy with unconjugated CTX as well as with other mAbs intended for use against solid tumors.[20,21] As a consequence, CTX-based chemotherapy failed to demonstrate a significant clinical benefit in triple negative breast cancer (TNBC) in early phase clinical trials.[22]

The advent of nanotechnology in biomedicine has offered new opportunities to challenge some of these limitations. The conjugation of mAbs to nanoparticles (NPs) or their incorporation within suitable nanocarriers have shown satisfactory preservation of the structural and functional features of the antibody, improved tissue penetration and enhanced permanence in the blood circulation.[23-25] Hitherto, antibodies in nanoconjugates have been conceived as tumor homing ligands to improve the targeting efficiency of NPs to selected cell populations exploiting the unique affinity and selectivity of mAbs toward specific molecular receptors. Actually, several reports have established the efficacy of mAb conjugation in enhancing the active targeting capability of colloidal NPs. In several instances, antibody fragments including Fab, single chain variable fragments (scFv), nanobodies, and half-chain

antibodies (HC-mAbs) proved to be valuable alternatives to the nanoconjugation of entire mAbs for targeting applications.[26-28]

Only very recently, interest has been also attributed to the investigation of the therapeutic implications of mAb conjugation to NPs, highlighting the incidence of selected parameters, including ligand density,[29] orientation,[30] and structure,[31] on the biofunctionality of the attached therapeutic antibody. In addition, the conjugation of mAbs to drug nanocarriers allowed the simultaneous delivery of cytotoxic chemotherapeutics useful for bimodal combination in adjuvant and neoadjuvant therapy.[32,33] The advantages provided by antibody nanoconjugation are estimated to lead to a reappraisal of the great potential of therapeutic mAbs also in the treatment of highly aggressive and refractory tumors.

Among poorly manageable malignancies for which treatment improvement is strongly demanded, here we focused on TNBC to assess the potential of CTX conjugation to NPs. Breast cancer is the most commonly diagnosed cancer in women and, despite the great benefits deriving from early diagnosis, adjuvant therapy and lowered rates of usage of hormone replacement therapies, it remains a major cause of death.[34,35] Due to the huge heterogeneity, genomic instability and capability to resume features usually observed in cancer, breast cancer is considered a good model for assessing innovative therapeutic strategies and for the development of novel anticancer agents. TNBC, which accounts for 15% of breast neoplasms, represents an unsolved issue in oncology owing to poor prognosis deriving from its aggressive phenotype and absence of a targeted therapy, as it is defined by lack of estrogen receptor (ER), progesterone receptor (PR) and HER2.[36] In recent years, TNBC classification has been revised pointing out four molecular subtypes to better

reflect different response rates to neoadjuvant chemotherapy. TNBCs include luminal androgen receptor (LAR), mesenchymal (MES), basal-like immune activated (BLIA), and basal-like immune-suppressed (BLIS). Basal-like subtypes account for 55-80% of TNBCs.[37] Although TNBC displays higher chemosensitivity compared to other breast cancers, patients harboring TNBC generally retain unfavorable clinical outcome, mainly due to the onset of chemoresistance, which is a direct consequence of TNBC intrinsic genomic instability.[38] Up to 80% of TNBC cells are p53-deficient, which can be explained by the involvement of alternative survival pathways for DNA repair from damages caused by cytotoxic drugs, ensuring replication and metastatic proliferation.[39] On the other hand, around 60% of TNBCs are characterized by overexpression of EGFR, which regulates activation of its downstream signaling, including the mitogen-activated protein kinases cascade (originally called extracellular signal-regulated kinases, ERK) or MAPK/ERK (also known as Ras/Raf/MEK/ERK) and the phosphatidylinositol-3 kinases (PI3K/Akt) pathways. Activation of these pathways induces signal migration from cell membrane into the nucleus to increase proliferation and mediate chemoresistance by influencing DNA damage repair, DNA replication, and oncogene transcription.[19,40] As EGFR overexpression is normally associated with poor prognosis, this tyrosine kinase receptor has been envisaged as an emerging therapeutic target for the treatment of TNBC.[38,39]

The use nanotechnology was estimated to improve the therapeutic outcome of TNBC treatment by increasing antitumor efficacy due to NP delivery of drugs, reducing off-target toxicity and preventing chemoresistance.[41,42] Most of these studies have indicated EGFR as a preferential surface target to address chemotherapy to the malignant cells. In the present study, we

explored the impact of conjugation of half-chain cetuximab (HC-CTX) to colloidal NPs on the therapeutic efficacy of the antibody in TNBC cells.

2. Aim of the work

The aim of this study was to investigate the molecular mechanisms of action of the nanoconjugated HC-CTX in comparison with unconjugated CTX, evaluating the effect of nanoconjugation on cell targeting efficiency, interference with downstream signaling pathways, cell cycle and proliferation in different TNBC cell subtypes, including both CTX-sensitive and resistant cell lines. In addition, to assess the maintenance of the full mAb power upon half-chain nanoconjugation, we explored the capability of nanoconjugated HC-CTX to promote the ADCC mechanism of immune response against TNBC cells.

3. Materials and Methods

Synthesis and characterization of nanoparticles

All HC-mAb-NPs used in this study were synthesized following the protocol that we have previously published.[27] Briefly, mAb (CTX or IgG) dissolved in EDTA–PBS buffer (1 mg mL^{-1}) was added to the 2-mercaptoethanolamine kit (MEA, Thermo Fisher Scientific) in order to obtain thiol groups from the disulfide bridges reduction between the two heavy chains of the mAb (HCs). HCs were rapidly added to PDP-NPs (1 mg) and incubated 1 h at room temperature (RT). Nanoparticles surface was saturated with PEG_{500}-SH. The reagents excess was removed by dialysis, and HC-mAb-NPs were collected. PEG-NPs, used as control, were prepared incubating 1 mg of PDP-NPs with an excess of PEG_{500}-SH according to the protocol above. Hydrodynamic size and

surface charge of HC-CTX-NPs were measured using a Malvern Zetasizer Nano ZS ZEN3600 (Worcestershire, UK). The measurements were performed in triplicate after dilution with MilliQ® water. SDS-PAGE electrophoresis was carried out using a 12% running gel and a 4% stacking gel and run for 2 h at 20 mA with a pH 8.3 running buffer (Buffer 10X: 1 L deionized water, 30.28 g Tris HCl, 144 g Glycine, final concentration SDS 0.1 %). Proteins were revealed by Coomassie staining (Imperial protein staining, Euroclone).

Cell culture

MDA-MB-468 and BT-474 cells were cultured in Dulbecco's Modified Eagle's Medium High Glucose (DMEM), supplemented with 10% FBS, L-glutamine (2 mM), penicillin (50 UI mL^{-1}) and streptomycin (50 mg mL^{-1}). MDA-MB-231 and HCC1937 cells were cultured in MEM Medium or in RPMI 1640 medium supplemented with 10% FBS, 2 mM L-glutamine, penicillin (50 UI mL^{-1}) and streptomycin (50 mg mL^{-1}), respectively. All cell lines grew at 37 °C and 5% CO_2 in a humidified atmosphere and were subcultured prior to confluence using trypsin/EDTA. Buffers, chemicals and plastic disposables for cell culture were purchased from Euroclone.

EGFR expression

MDA-MB-231, MDA-MB-468, HCC1937 and BT-474 cells (5×10^5) were immunodecorated in FACS tubes with cetuximab (CTX, 1 µg/tube;) in phosphate buffer saline (PBS), 2% bovine serum albumin (BSA; Sigma) and 2% goat serum (Euroclone) for 30 min at room temperature (RT). Then, cells were washed thrice with PBS and immunodecorated with AlexaFluor488 (AF488) goat anti-human secondary antibody (1 µL/tube; Thermo Fischer Scientific) in PBS, 2% BSA and 2% goat serum for 30 min at RT. After three washes with PBS

cells were analyzed by CytoFLEX flow cytometer (Beckman Coulter). 20,000 events were acquired for each analysis, after gating on viable cells and on singlets. A sample of cells immunodecorated with the secondary antibody only was used to set the region of positivity.

Cell binding assay

MDA-MB-231, MDA-MB-468, HCC1937 and BT-474 cells were seeded at a concentration of 2.5×10^5 cells/well. The day after, cells were incubated 1 h at 37 °C in culture medium supplemented with 5, 10 and 50 μg mL^{-1} of HC-CTX-NPs or HC-IgG-NPs. After incubation, cells were incubated in PBS, 2% Bovine Serum Albumin (BSA; Sigma) and 2% goat serum (Euroclone) for 15 min at RT. Then, cells were immunodecorated with AF488 antibody (1 μL/tube; Thermo Fischer Scientific) in PBS, 2% BSA and 2% goat serum for 30 min at RT. AF488 anti-human and AF488 anti-rabbit antibodies have been used for samples treated with HC-CTX-NPs and HC-IgG-NPs, respectively. After three washes with PBS cells were analyzed by CytoFLEX flow cytometer (Beckman Coulter). 20,000 events were acquired for each analysis, after gating on viable cells and on singlets. Samples of cells immunodecorated with the secondary antibodies only were used to set the regions of positivity.

Competition assay

MDA-MB-231, MDA-MB-468, HCC1937 and BT-474 cells (5×10^5) were transferred in FACS tubes and washed twice with PBS. Then, cells were incubated with 10 μg mL^{-1} of HC-CTX-NPs labeled with FITC with or without CTX as competitor (1 mg mL^{-1}, 1 mL) in PBS supplemented with 2% BSA at 37 °C for 30 min. Cells were washed thrice and resuspended in PBS (500 μL) and analyzed by a CytoFLEX flow cytometer (Beckman Coulter). 10,000 events

were acquired for each analysis, after gating on viable cells and on singlets. A sample of untreated cells was used to set the appropriate gates.

Immunofluorescence and confocal laser scanning microscopy

Cells were seeded at 2×10^5 cell density and cultured on 22 mm^2 cover glass slides pre-coated with collagen (10%, 1 h at RT). The day after, cells have been incubated with 100 μg mL^{-1} of HC-CTX-NPs X for 15 min, 30 min, 1, 4, 24 and 48 h at 37 °C. After incubations, cells were washed with PBS, fixed for 5 min with 4% paraformaldehyde (Sigma) and then treated for 5 min with 0.1% Triton X-100 (Sigma). A blocking step was performed for 1 h at RT with a solution containing 2% BSA (Sigma), 2% goat serum (Euroclone) and 0.2 μg mL^{-1} DAPI (4',6-diamino-2-phenylindole; Thermo Fischer Scientific) in PBS. Golgi apparatus, lysosomes and early and recycling endosomes were stained for 2 h at RT with Golgi marker 130 (GM-130; at a 1:100 dilution; clone 35; BD Biosciences), Cathepsin D (CatD; 1:50; clone BC011; Calbiochem), Early Endosomes Antigen-1 (EEA-1; 1:1000; clone 14; BD Biosciences) and Transferrin (Tf; 1:100; clone 5G2; Abcam) antibodies, respectively, and revealed by AF546-conjugated antibody against murine IgGs (Thermo Fischer Scientific) at a 1:300 dilution by incubating for 2 h at RT in PBS, 2% BSA, 2% goat serum. EGFR was stained over night at 4 °C with EGFR antibody (1:50; D38B1, Cell Signaling) and revealed by AF546-conjugated antibody against rabbit IgGs (Thermo Fischer Scientific) at a 1:500 dilution by incubating for 1 h at RT in PBS, 2% BSA, 2% goat serum. Glass slides were washed thrice with PBS and mounted with Prolong Gold (Thermo Fischer Scientific). Images of NPs intracellular trafficking were acquired with Leica SP8 microscope confocal system equipped with laser excitation lines 405, 488, 535 and 633 nm. Images for EGFR localization were acquired with Nikon A1 laser microscope confocal

system equipped with laser excitation lines 405, 488, 535 and 633 nm. Images were acquired with 63× magnification oil immersion lenses at 1024×1024 pixel resolution.

Transmission electron microscopy

Cells were seeded at 1×10^6 cells/well, and the day after have been incubated with 100 μg mL^{-1} of HC-CTX-NPs for 15 min, 30 min, 1, 4, 24 and 48 h at 37 °C. After incubations, cells were washed with PBS, detached with trypsin-EDTA, and transferred in 0.5 mL tubes. Cells have been washed thrice by centrifugation (5 min at 13,000 rpm) and the resulting pellets have been fixed for 2 h in 2.5% glutaraldehyde in 0.1 M phosphate buffer, pH 7.2. After one rinsing with PBS, pellets were post-fixed in 1.5% osmium tetroxide for 2 h, dehydrated by 50, 70, 90, and 100% EtOH, and embedded in epoxy resin (PolyBed 812 Polysciences Inc.). Ultrathin sections were cut with an ultramicrotome (Ultracut E (Reichert-Jung)), stained with uranyl acetate and lead citrate and examined by TEM (Tecnai Siprit, FEI).

Cell viability assay

MDA-MB-231, MDA-MB-468 and HCC1937 cells were seeded on a 96-well dish at the density of 5000 cells cm^{-1}. Then, cells were incubated in starvation medium with different amounts of CTX (CTX: 35, 70, 700 and 3500 nM; HC-CTX-NPs: 35, 70, 700 and 3500 nM). PEG-NPs were used as specificity control in equal amount to that used for HC-CTX-NPs. Untreated cells were used as controls. After 24, 48 and 72 h of treatment, cells were washed with PBS and incubated for 3 h at 37 °C with 0.1 mL of a stock solution of 3-(4,5-dimethylthiazol-2-yl)-5-(3-carboxymethoxyphenyl)-2-(4-sulfophenyl)-2H-tetrazolium (MTS) and phenazine ethosulfate (PES) previously diluted 1:10 in

DMEM medium without phenol red (CellTiter 96® AQueous One Solution Reagent; Promega). Absorbance was read in a microplate reader (BioTek) using a testing wavelength of 490 nm and a reference wavelength of 620 nm. The results were normalized on viability of untreated samples and expressed as means ± s.e.

Cell death assay

Cells seeded on a 12-well plate at 2×10^5 cells/well were treated for 24 h with increasing concentration of CTX free or nanoformulated (70, 700, 3500 nM) in starvation medium. Negative control was represented by untreated cells. Then, cells were collected, washed thrice with PBS and treated for FACS analysis according to Annexin V-PE-Cy5 Apoptosis Detection Kit manufacturer's protocol (BioVision). Briefly, cells were suspended in Binding Buffer and incubated 5 min with 5 µL of Annexin V-PE-Cy5. Cells were analyzed within 1 h on CytoFLEX flow cytometer (Beckman Coulter). 20,000 events were acquired for each analysis.

Cell cycle analysis

2.5×10^5 cells were seeded on a 12-well dish the day before. Then, cells were incubated with different amounts of CTX free or nanoformulated (70, 700, 3500 nM). MDA-MB-468 and MDA-MB-231 cells were incubated for 24 h in starvation medium, while HCC1937 cells were incubated up to 72 h in complete medium. Untreated cells were used as negative control. PEG-NPs were used as specificity control in equal amount to that used for HC-CTX-NPs. At the end of the incubation time, cells were washed twice with PBS, detached with trypsin/EDTA solution and transferred in FACS tubes. Then, cells were fixed with cold ethanol 95% for 1 h, labeled with staining solution (PBS

supplemented with 80 µg mL^{-1} Iodide Propidium (Sigma), 100 µg mL^{-1} RNAseA (Sigma) and 0.1% Triton X-100 (Sigma)) and acquired with flow cytometer. MDA-MB-468 and MDA-MB-231 were analyzed by CytoFLEX (Beckman Coulter), while HCC1937 were analyzed by Gallios flow cytometer (Beckman Coulter).

CTX-mediated EGFR phosphorylation in Y1068

5×10^5 cells were seeded in a 6-well plate the day before. Cells were treated for 24 h with increasing concentration of CTX free or immobilized in HC-CTX-NPs (0.2, 2 and 20 µg mL^{-1}) in starvation medium. Negative control was represented by untreated cells. At the end of incubation, cells were washed thrice with ice cold PBS and detached with 200 µL lysis buffer (20 mM Tris HCl pH 7.6, 150 mM NaCl, 1 mM EDTA, 1% Triton X-100, 1% glycerol, 1 mM Na_3VO_4, 10 mM NaF, Protease Inhibitor Cocktail, 1 mM PMSF) using a cell scraper. Cells were transferred in tubes, vortexed and lysed incubating 30 min at 4 °C. Then, lysed cells were centrifuged 10 min at 13,000 rpm at 4 °C, the supernatants were collected. The protein content was quantified using the Coomassie Plus Protein Assay Reagent (Thermo Fisher Scientific) with BSA as standard protein. Approximately 35 µg of protein from each sample were dissolved in sample buffer 5× (125 mM Tris HCl pH 6.8, 10% SDS, 20% glycerol, 0.02% Bromophenol blue, 5% β-mercaptoethanol), denatured 5 min at 95 °C, separated by SDS-PAGE and transferred onto PVDF membrane. The membrane was blocked in 5% BSA in TBS with 0.1 % Tween 20 for 1 h. For evaluation of EGFR phosphorylated in Y1068, the membrane was incubated 2 h with rabbit-monoclonal antibody against Phospho-EGFR receptor (Y1068) (#3777; Cell Signalling) at 1:1000 dilution and with mouse monoclonal antibody anti-α-tubulin (Sigma) at 1:1000 dilution in 5% BSA in TBS with 0.1 % Tween 20 for 1

h. The membranes were washed three times with TBS with 0.1 % Tween 20 and reacted 1 h with the secondary antibody anti-rabbit conjugated with horseradish peroxidase (1:5000; Abcam). The bound antibody was revealed using ECL star reagent (Euroclone) and the chemiluminescence signal was detected using the Chemidoc System (Biorad). Then, EGFR Y1068 pho was stripped and the membrane was blocked in 5% BSA in TBS with 0.1 % Tween 20 for 1 h. For evaluation of total EGFR, the membrane was incubated 2 h with rabbit-polyclonal antibody against EGFR (EGFR (1005): sc-03; Santa Cruz) at 1:1000 dilution. The membranes were washed three times with TBS with 0.1 % Tween 20 and reacted 1 h with the secondary antibody anti-rabbit conjugated with horseradish peroxidase (1:5000; Abcam) and revealed as described above.

CTX-mediated p38 phosphorylation

5×10^5 cells were seeded in a 6-well plate the day before. Cells were treated for 24 h with increasing concentration of CTX free or immobilized in HC-CTX-NPs (10, 50 and 100 μg mL^{-1}) in starvation medium. Negative control was represented by untreated cells. At the end of incubation, cells were washed with ice cold PBS, detached Trypsin- EDTA and harvested by centrifugation. Then, the pellet was resuspended in 100 μL lysis buffer (10 mM Hepes pH 7.5, 10 mM KCl, 0.1 mM EDTA, 1 mM DTT, 0.5% NP-40, 1 mM Na_3VO_4, 10 mM NaF, Protease Inhibitor Cocktail, 0.5 mM PMSF) and incubated 20 min at 4 °C. Then, cells were vortexed and centrifuged 10 min at 12,000 ×g at 4 °C. The supernatants were collected and stored as cytoplasmic extracts. The pellet was washed thrice with lysis buffer, resuspended in 60 μL of nuclear extraction buffer (20 mM Hepes pH 7.5, 400 mM NaCl, 1 mM EDTA, 1 mM DTT, 1 mM PMSF, 1 mM Na_3VO_4, 10 mM NaF, Protease Inhibitor Cocktail) and incubated

30 min at 4 °C. Then, the samples were centrifuged 15 min at 12,000 ×g at 4 °C. the supernatant was collected as nuclear extract and processed for SDS-PAGE. Samples were separated by SDS-PAGE and transferred onto PVDF membrane. The membrane was blocked in 5% BSA in TBS for 1 h. For evaluation of phosphorylated p38, the membrane was incubated 2 h with rabbit-monoclonal antibody against phospo-p38 MAP kinase (Y180/Y182) (#9211; Cell Signalling) at 1:1000 dilution in 5% BSA in TBS with 0.1 % Tween 20 for 1 h. The membranes were washed three times with TBS with 0.1 % Tween 20 and reacted 1 h with the secondary antibody anti-rabbit conjugated with horseradish peroxidase (1:5000; Abcam) or with the secondary antibody anti-mouse conjugated with horseradish peroxidase (1:5000; Abcam), respectively. The bound antibody was revealed using ECL star reagent (Euroclone) and the chemiluminescence signal was detected using the Chemidoc System (Biorad).

Effector cells isolation

Peripheral blood mononuclear cells (PBMCs) were obtained by centrifugation on Ficoll-Paque of blood samples from healthy donor (30 min at 1,500 rpm without brakes). At the end the PBMC layer was carefully transferred to a new tube, diluted with PBS and centrifuged for 6 min at 1,400 rpm. Then supernatant was eliminated to remove platelets and the procedure was repeated for four times decreasing the centrifugation speed up to 1,000 rpm. Washed PBMCs were resuspended in RPMI-1640 medium with 10% of decomplemented FBS and 1,000 U mL^{-1} IL-2 (BioLegend, San Diego, CA, USA) for 24 h at 37 °C. The described procedure was approved by Ethical Committee of the University of Milano-Bicocca (prot.#351, 13th November 2017) after

submission of the project together with informed consent by the healthy volunteer.

ADCC assay

ADCC was performed using CytoTox 96® Non-Radioactive Cytotoxicity Assay (Promega Corporation, Madison, WI, USA). Firstly, target cells, plated at a density of 5×10^3 in 96-well plates, were coated with increasing concentration of CTX and IgG (0.5, 10 and 20 μg mL^{-1}) and with 5 μg mL^{-1} of PEG-NPs, HC-CTX-NPS and HC-IgG-NPS for 30 min at 4 °C in RPMI-1640 medium. After coating, IL-2-activated PBMCs were added onto target cells at an effector:target (E:T) ratio of 20:1 and 40:1 and incubated 4 h at 37 °C. Then LDH release from target cells was measured by EnSight™ multimode plate reader (Perkin Elmer, Waltham, MA, USA) setting absorbance wavelength at 490 nm. Percentage of ADCC was calculated using the formula following protocol instruction:

$$\%\ Specific\ Lysis = \frac{Experimental - Effector\ Spontaneous\ - Target\ Spontaneous}{Target\ Maximum - Target\ Spontaneous} \times 100$$

Statistical analysis

Statistical analyses were conducted using two-tailed Student's *t*-test. All plots show mean values ± standard error (s.e.). All tests assumed normal distribution and the statistical significance threshold was set at $P<0.05$.

4. Results

Synthesis and characterization of half-chain mAb-conjugated colloidal nanoparticles. The NPs used in this study were 12 nm iron oxide nanocrystals coated with a biocompatible amphiphilic polymer (PMA) that conferred excellent colloidal stability to the NP dispersion and provided several carboxylic functional groups useful for bioconjugation.[43] HC-mAb-NPs were synthesized according to an optimized procedure derived from Fiandra et al. with some adjustments.[27] Briefly, PMA-coated NPs obtained by established protocols were modified with 2,2-(ethylenedioxy)bis(ethylamine) (EDBE) to introduce amino functionalities that were next converted into thiol-reactive groups with *N*-succinimidyl-3-[2-pyridyldithio]-propionate (SPDP) leading to PDP-NPs, with ~70% efficiency.[44] PDP-NPs were reacted with HC-mAb, obtained by mild reduction of the antibody using 2-mercaptoethanolamine,[27] and the residual PDP groups were saturated with excess PEG_{500}-SH ($MW_{PEG} \approx$ 500 Da) (see Scheme 1). This procedure was followed both with CTX and with a negative control mAb (a nonspecific antirabbit IgG), obtaining HC-CTX-NPs and HC-IgG-NPs, respectively. Control unconjugated NPs were prepared by pegylation of PDP-NPs using PEG_{500}-SH, obtaining PEG-NPs. One of the advantages of using HC fragment is that free thiol groups are generated selectively on the constant portion of the antibody heavy chain by mild reducing agents, which induce the conjugation to the NP surface through the Fc moiety allowing the presentation of the Fab fragment in the optimal orientation for binding with the receptor. The hydrodynamic size of mAb-conjugated NPs was measured by dynamic light scattering (DLS, Figure S1 in the Supporting Information), obtaining 38.0 ± 1.7 nm (HC-CTX-NPs), and 35.1 ±

2.0 nm (HC-IgG-NPs), while the zeta potential was −66.0 ± 0.6 and −66.5 ± 0.1 mV, respectively. In both cases, the number of bound half-chain antibodies was adjusted to ~5 per NP (5.3 ± 0.7 and 5.1 ± 0.9, respectively), as determined by a pyridine 2-thione assay.[45] Determining mAb loading on NPs allowed us to accurately define the mAb concentration in biological experiments using nanoconjugates. Coomassie staining of electrophoresis gel performed on mAb-conjugated NPs, using CTX as positive control and PEG-NPs as negative control, qualitatively confirmed the presence of the antibody attached to the NPs (Figure S2). Collectively, the data from DLS, zeta potential and calculation of mAbs number, let us conclude that HC-CTX-NPs and HC-IgG-NPs had very similar chemical-physical properties, differing only in the nature of the attached antibody molecule.

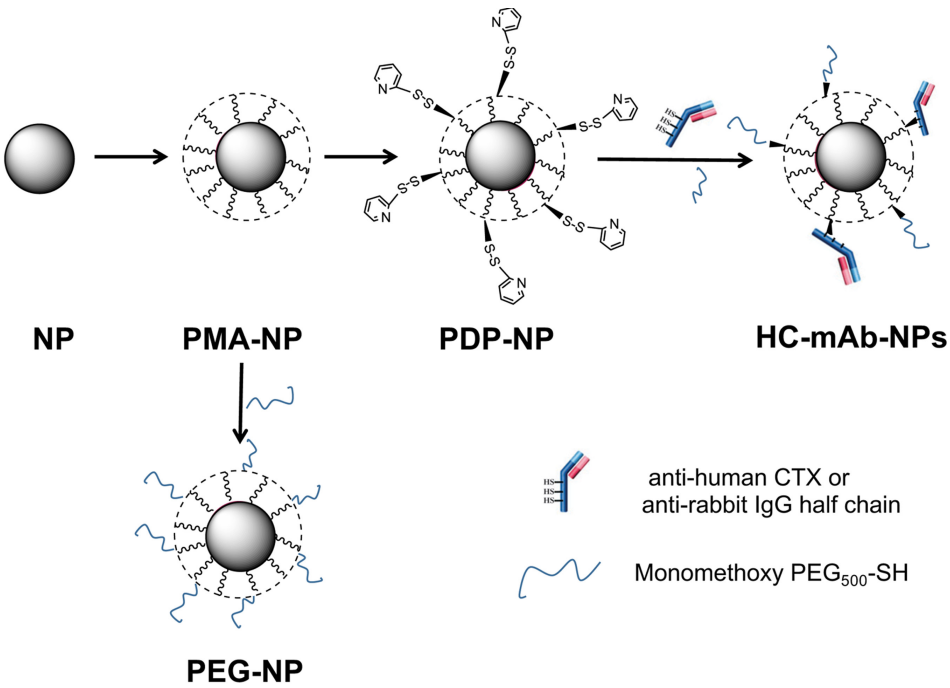

Scheme 1. Schematic representation of NPs synthesis.

TNBC cells selection and determination of HC-CTX-NP binding. Among the 27 available human cancer cell lines classified in the literature as TNBC cells,[40] we identified CTX-sensitive MDA-MB-468 (EGFR amplification, PTEN deletion) and CTX-resistant MDA-MB-231 (mutations in KRAS and BRAF, predictors of CTX resistance) cell lines,[46] – which do or do not harbor, respectively, the activating mutations of the main EGFR pathways – along with HCC1937 (PTEN deletion), a CTX-resistant, basal cell line that is homozygous for the *BRCA1* 5382insC mutation.[47,48] Among them, CTX was reported to be therapeutically active only in MDA-MB-468 cells.[19] Although CTX activity has been poorly characterized in vitro, the sensitivity to mAb treatments was associated to stimulation or inhibition of specific regulators of cell cycle, in turn activated or inactivated by signaling transduction induced by PI3K/Akt and RAS/MAPK pathways, resulting in cell cycle arrest in G1 phase followed by apoptosis.[19,49]

The above mentioned three TNBC cell lines along with a BT-474 invasive ductal breast carcinoma cell line, used as a triple positive control, and a nontumoral human umbilical vascular endothelial cell (HUVEC) line were first assessed by flow cytometry to estimate the EGFR expression. MDA-MB-468 cells exhibited very high EGFR levels (score +++) with a threefold higher fluorescence intensity compared to MDA-MB-231 (+) and HCC1937 (+). By contrast, HUVEC showed very low EGFR expression supporting the opportunity of targeting EGFR to discriminate between TNBC and healthy cells (Figure S3). EGFR expression in BT-474 was recovered on the same levels of HUVEC and could be used as negative breast cancer cell control for binding experiments.

Binding efficiency of HC-CTX-NPs in TNBC cell lines and in BT-474 cells was estimated by flow cytometry at 37 °C at different mAb concentrations in comparison to nonspecific HC-IgG-NPs (Figure 1). All TNBC cell lines showed

full signal saturation at all concentrations tested, confirming that 100% living cells could be efficiently labeled between 5 and 50 μg mL^{-1} nanoconjugated HC-CTX. However, slight differences in targeting efficiency between MDA-MB-468 and MDA-MB-231/HCC1937 cells were recovered at the highest HC-IgG-NPs concentrations. Indeed, MDA-MB-468 binding by HC-IgG-NPs was negligible even at 50 μg mL^{-1} (Figure 1A), whereas MDA-MB-231 and HCC1937 exhibited increasing binding up to around 15 and 20%, respectively (Figure 1B,C). The slightly increased nonspecific binding observed with the latter two cell lines could be attributed to their lower EGFR expression, allowing for a higher contribution of Fc receptor in membrane interaction. In contrast, flow cytometry of $EGFR^{low}$ BT-474 cells treated with HC-CTX-NPs showed around 50% positive cells independent of HC-CTX-NPs concentration, with a nonspecific contribution that increased with concentration (Figure 1D). To better appreciate the involvement of mAb-EGFR interaction in HC-CTX-NP binding to TNBC cells, a competition assay using MDA-MB-468, MDA-MB-231, HCC1937 and BT-474 cells was conducted (Figure 1E). Flow cytometry of cells treated with HC-CTX-NPs at 37 °C after preincubation with CTX for 30 min revealed a 15% nonspecific binding in $EGFR^{low}$ BT-474 cells, whereas $EGFR^{high}$ TNBC cells exhibited negligible signal. Residual 4% binding observed in MDA-MB-468 cells could be attributed to a very high EGFR expression of this cell line, making full and persistent saturation of membrane receptors very difficult to achieve with competing CTX.

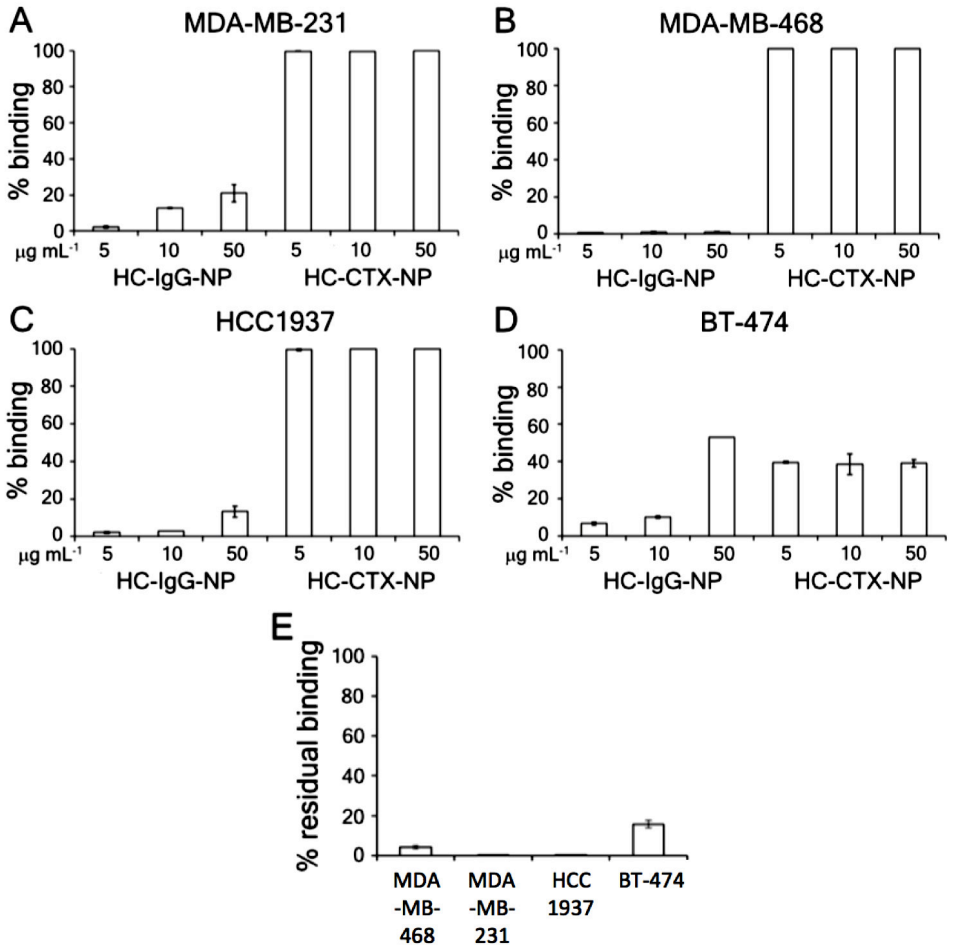

Figure 1. HC-CTX-NP binding to breast cancer cells. MDA-MB-468 (A), MDA-MB-231 (B), HCC1937 (C) TNBC cells, and BT-474 cells (D) were incubated at 4 °C for 2 h in PBS buffer and 0.3% BSA with different amounts of HC-IgG-NPs or HC-CTX-NPs (5, 10 and 50 μg mL^{-1}). Next, cells were processed for flow cytometry. HC-IgG-NPs were revealed using AF488-labeled anti-rabbit secondary antibody, while HC-CTX-NPs were labeled with AF488 anti-human antibody. Untreated cells were used to set the positive region and the singlet gate. Reported values are the mean ± s.e. (n = 3). (E) Competition assay. MDA-MB-468, MDA-MB-231, HCC1937 TNBC cells and BT-474 cells were incubated 1 h at 37 °C with 50 μg mL^{-1} of FITC-labeled HC-CTX-NPs with or without excess of unlabeled CTX (i.e., 5 mg) as competitor. Cells were then detached and treated for flow cytometry. Untreated cells have been used to set the singlet gate and the positive region. Reported values are the mean ± s.e. (n = 3).

Intracellular trafficking of HC-CTX-NPs. We were interested in investigating trafficking and fate of HC-CTX-NPs following their cellular uptake, considering that 1) MDA-MB-231, MDA-MB-468 and HCC1937 TNBC cell lines exhibited high binding affinity for HC-CTX-NPs independent of the extent of EGFR levels and of sensitivity to CTX; 2) ligand-receptor complex internalization is normally favored at 37 °C and processed through an endolysosomal intracellular pathway; 3) HC-CTX conjugation with NPs was presumed to promote the activation of endocytic mechanisms via clathrin-mediated uptake. Figure 2A shows confocal microscopy images of TNBC cells acquired after 15 min, 1, 3, 24 and 48 h treatment with HC-CTX-NPs. Untreated cells stained with DAPI were used as negative control. All three cell lines exhibited excellent binding capability, uptake and long-term internalization of HC-CTX-NPs confining persistently the nanoconjugates into endosomes and lysosomes, as clearly evidenced by spotted fluorescence emission typical of microvesicle compartmentalization of NPs. Transmission electron microscopy (TEM) images of a time course of representative MDA-MB-468 cells treated with HC-CTX-NPs at the same points were consistent with confocal microscopy results (Figure 2B). At 15 min, nanoconjugates were gathered adjacent to the cell membrane. At 1 h, they were preferentially confined inside early endosomes, whereas after 3 h they were found progressively distributed within late endosomes, which induced the recruitment of lysosomes initiating the fusion processes. At longer time points, the NPs accumulated in mature lysosomes at least for 48 h, presumably inducing receptor degradation and preventing recycling of EGFR engaged in the complex formation with mAb nanoconjugate.

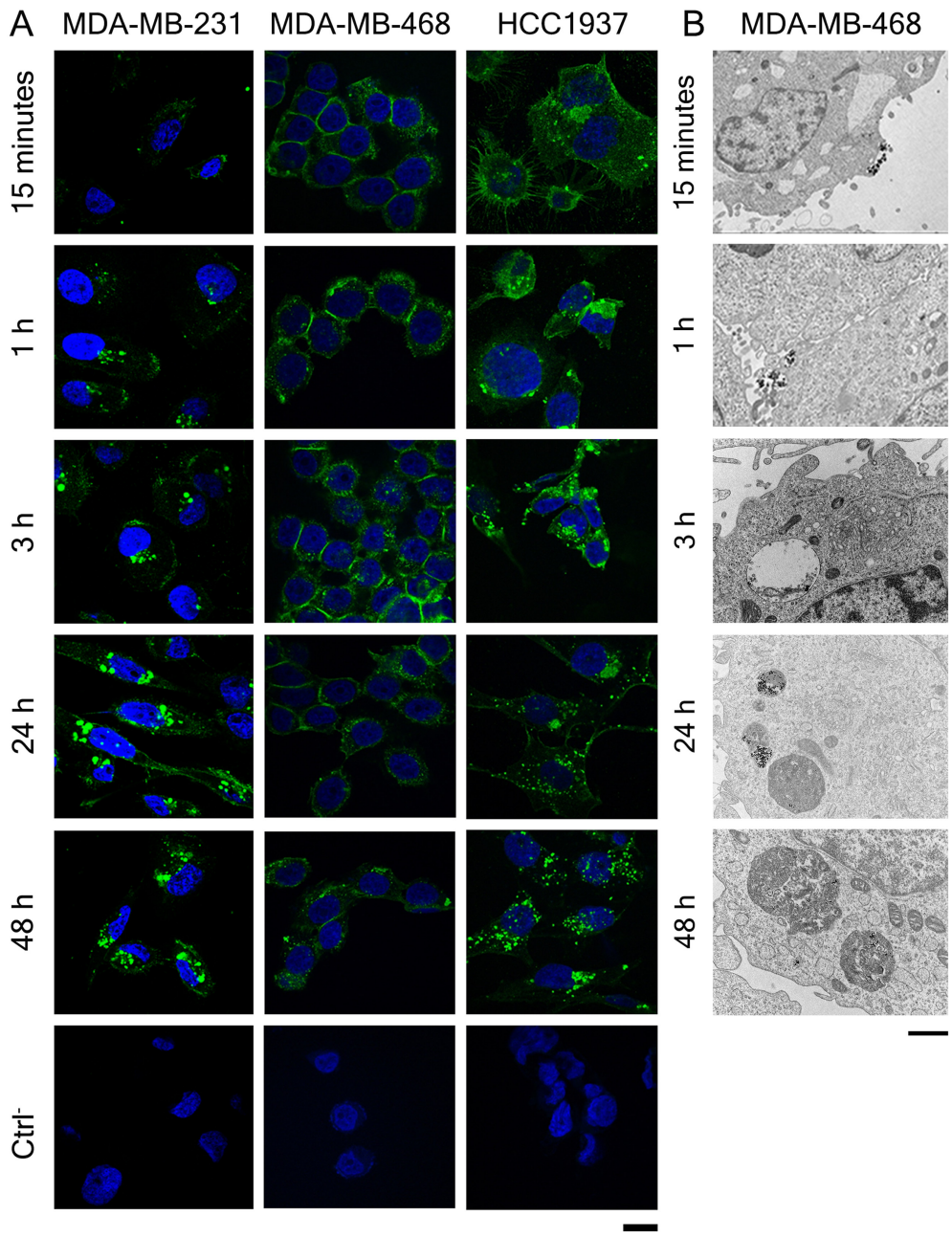
A
MDA-MB-231
MDA-MB-468
HCC1937
B
MDA-MB-468
15 minutes
1 h
3 h
24 h
48 h
Ctrl-

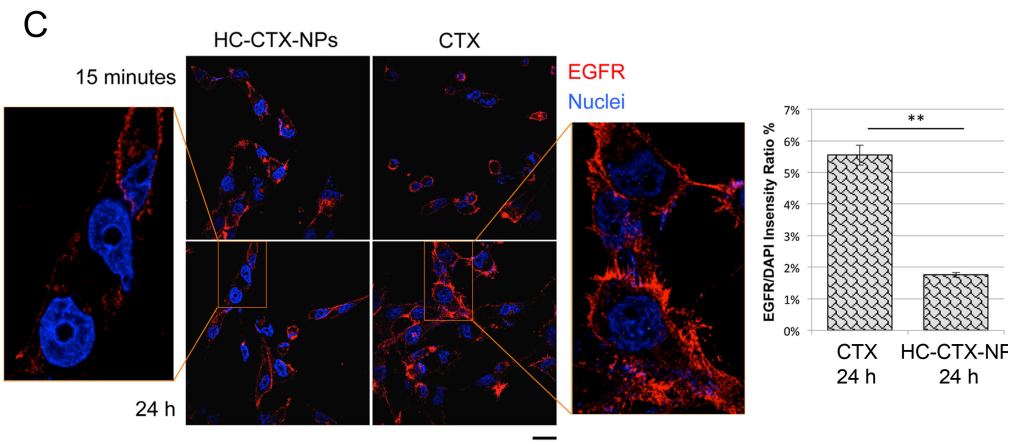

Figure 2. HC-CTX-NPs intracellular trafficking. A) Internalization of HC-CTX-NPs in TNBC cells. Confocal microscopy images of MDA-MB-231, MDA-MB-468 and HCC1937 incubated 15 min, 1, 3, 24 and 48 h at 37 °C in complete cell culture medium with HC-CTX-NPs (100 μg mL^{-1}). Nuclei were stained with DAPI (blue). CTX was recognized with anti-human secondary antibody conjugated with AF488 (green). Scale bar: 10 μm. B) Representative intracellular trafficking of HC-CTX-NPs in MDA-MB-468 cells by TEM. Scale bar: 1 μm. C) Magnification of HCC1937 cells treated with CTX or HC-CTX-NPs for 24 h. The quantification of EGFR in the nucleus was performed by the selection of cell nuclei as regions of interest (ROI) for the detection of the mean fluorescence intensity of EGFR (left). The quantification (right) revealed that cells treated with CTX for 24 h showed a 3.15-fold higher amount of EGFR in nuclei compared to cells treated with HC-CTX-NPs. Nuclei were stained with DAPI (Blue) while EGFR was recognized by anti-EGFR antibody and labeled with an anti-rabbit secondary antibody conjugated with AF546 (red). Scale bar: 20 μm. Reported values are mean of measurement performed with ImageJ software on nucleus of 20 different cells normalized to their areas ± s.e.

Enhanced antitumor activity of HC-CTX conjugated to NPs in TNBC cells. All TNBC cell lines were treated in parallel with HC-CTX-NPs and with CTX at increasing mAb concentrations between 35 nM and 3.5 μM and incubated for up to 216 h. Cells were also treated at lower CTX concentrations (down to 7 nM), but no antiproliferative effect was detected by viability assay based on tetrazolium salts (MTS). In general, MTS assay revealed that nanoconjugation had remarkably higher impact on proliferation in all TNBC cell lines compared to unconjugated CTX, statistically significant at low dosages and longer times of incubation (Figure 3 and Figure S4). In detail, CTX alone weakly inhibited proliferation in MDA-MB-468 (PTEN-null, p53-mutant, BRCA1-wt) and MDA-MB-231 (PTEN-wt, p53-mutant, BRCA1-wt) only at high dosages (0.7 and 3.5 μM) and without apparent progression after 144 h. HC-CTX-NPs exhibited appreciable effect (40% viability loss) at concentration as low as 35 nM at 216 h in MDA-MB-468, showing a dose-dependent increase in activity reaching 53% viability loss at 3.5 μM (Figure 3A). Such increase in activity associated with nanoconjugation was recovered in MDA-MB-231 (Figure 3B). Paradoxically, the apparently higher activity observed in MDA-MB-231 compared to MDA-MB-468 cells could be explained in terms of lower EGFR expression. Indeed, cancer cell viability is affected by the extent of EGFR receptor internalization upon complexation with targeted antibodies.[50] In order to rule out the possible nonspecific contribution of NPs, we repeated the assay treating the cells with PEG-NPs. However, no apparent activity was recovered as compared to HC-CTX-NPs in these two cell lines. As expected, HCC1937 (PTEN-mutated, p53-null, BRCA1-mutated) cells proved highly resistant to CTX with minimal effect even at the highest concentrations. Surprisingly, HC-CTX-NPs showed statistically significant, progressive increase

in cytotoxicity compared to CTX, already observed after 72 h (Figure 3C). Such a potent activity could not be ascribed to a sensitivity of HCC1937 to colloidal NPs, as confirmed by viability experiment using PEG-NPs (Figure 3C). Hence, this result should be attributed to CTX nanoconjugation, which advocated a role of long-lasting receptor sequestration by means of the EGFR/HC-CTX-NPs complex through the endolysosomal route. We initially interpreted this effect in terms of possible EGFR degradation, as also observed using entire antibodies.[30] Uptake kinetics analyzed by confocal microscopy (Figure 2A) and ultrastructural analysis by TEM (Figure 2B) showed prolonged residence of the antibody nanoconjugate compartmentalized within the endolysosomal evolution pathway, supporting our preliminary hypothesis. Such receptor sequestration by means of the nanoconjugate reversed the resistance mechanism, which, in absence of nanoconjugation, is otherwise exerted by BRCA1 mutation after EGFR autophosphorylation that initiates the RAS/MAPK signaling cascade (see Scheme 2).

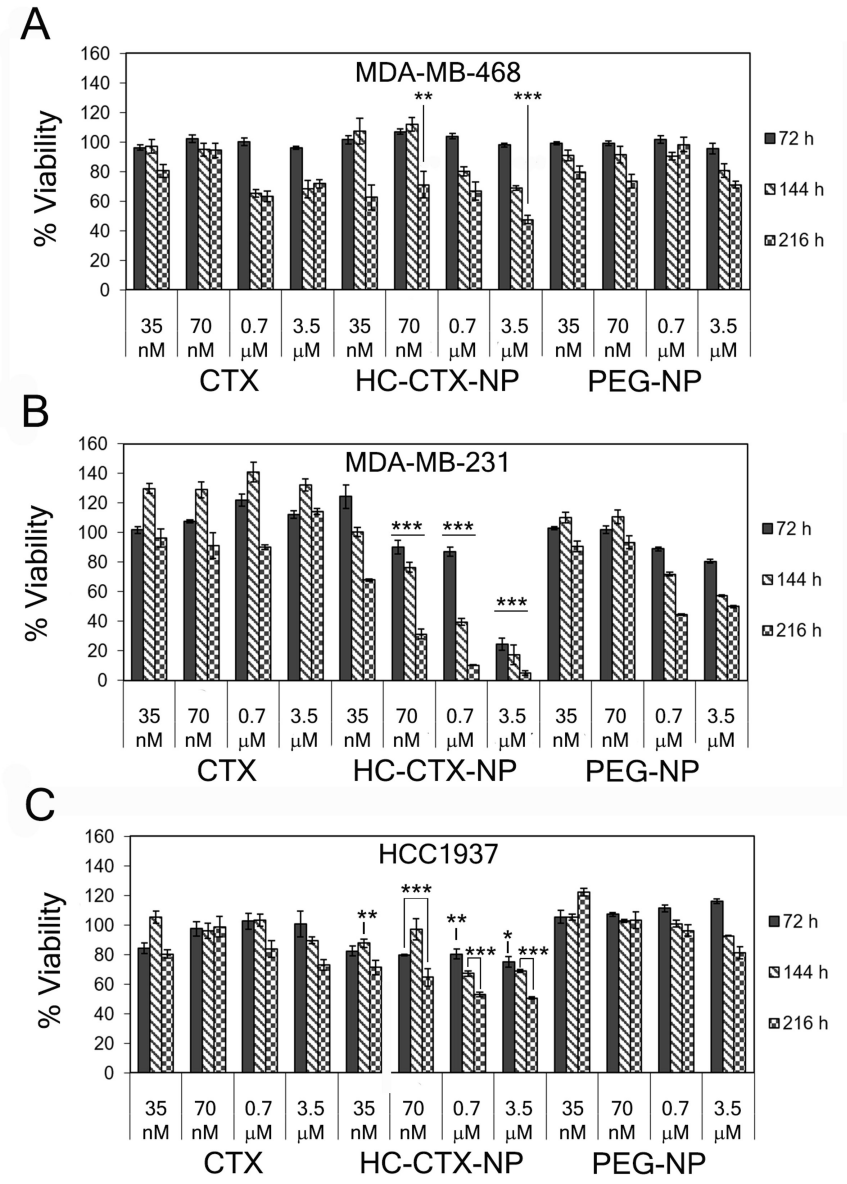

Figure 3. Antitumor activity in EGFR positive cells. Viability of TNBC cells treated with CTX, HC-CTX-NPs or PEG-NPs. MDA-MB-468 (A), MDA-MB-231 (B), and HCC1937 (C) cells were treated with increasing concentration of CTX or HC-CTX-NPs (from 35 nM to 3.5 µM) up to 216 h. PEG-NPs were used as negative control. Viability was assessed by measuring the conversion of MTS into formazan. Reported values are the mean of six replicates ± s.e., normalized on cell proliferation of untreated cells, respectively. Statistical significance of HC-CTX-NPs *vs.* free drug, * P<0.05; **P<0.001; ***P<0.0005 (Student's *t*-test).

It is worth noting that the nuclear fraction of EGFR in TNBC cells derives from trans-cytoplasmic migration of activated membrane EGFR. Nuclear EGFR was demonstrated to exert multiple functions in the nucleus, operating as a tyrosine kinase to activate the cyclin D1 and the proliferating cell nuclear antigen (PCNA), which promote the G1/S phase transition, and as a co-transcription factor for genes involved in cell proliferation and angiogenesis (see Scheme 2).[51,52] For this reason, nuclear localized EGFR was identified as an hallmark of disease progression, worse prognosis and enhanced resistance to radiation, chemotherapy, and treatment with CTX. To explore the hypothesis that HC-CTX-NPs could interfere with nuclear translocation of activated EGFR, we performed immunofluorescence analysis of EGFR localization in HCC1937 cells treated with CTX or HC-CTX-NPs. Confocal images acquired at 15 min, 1, 3 and 24 h post-treatment, corresponding to maximal EGFR localization into endosomes (15 min) and to expected recycling time (3 to 24 h),[53] showed a progressive EGFR degradation over time in samples treated with HC-CTX-NPs compared to those treated with CTX, thus preventing receptor recycling (Figure S5). Importantly, quantitative analysis of nuclear EGFR revealed that levels of EGFR in nuclei of cells treated with HC-CTX-NPs were 3.15-fold lower than those of cells treated with unconjugated CTX (Figure 2C and Figure S5). Hence, a comprehensive explanation for the observed inhibition of cancer proliferation in BRCA1-mutated TNBC cells resided in the stable complexation of EGFR by HC-CTX-NPs, which resulted in receptor downregulation and prevented EGFR nuclear translocation through its sequestration into the endolysosomal pathway.

Impact of CTX nanoconjugation on TNBC cells apoptosis and cell cycle. With the aim to investigate the mechanism of action of HC-CTX-NPs in the different TNBC cell lines, we first analyzed the early apoptotic effect of nanoconjugate compared to CTX at 24 h. Flow cytometry allowed us to monitor phosphatidylserine reversal in the plasma membrane mediated by apoptosis through a quantitative affinity assay using Annexin-V-pE-Cy5.5 exposure on cell surface.[54] Figure 4A shows a 2.5-fold increase in apoptosis in MDA-MB-468 cells from both CTX and HC-CTX-NPs at 0.7 μM compared to untreated cells, on the same levels reported for CTX alone in previous studies.[19] However, a significant increase in intracellular activity of HC-CTX-NPs (7.5-fold relevant to untreated cells) compared to CTX (3-fold relevant to control) could be appreciated at 3.5 μM. This value was even higher than the apoptotic effect of CTX alone previously documented at 10 μM after 48 h.[19] Once again, the remarkable increase in proapoptotic activity of HC-CTX-NPs over CTX could be attributed to an alteration of the recycling process caused by mAb nanoconjugation. Similarly, a twofold increase in apoptotic activity of HC-CTX-NPs compared to CTX was recovered in MDA-MB-231 cells (Figure 4B). An absolute value around 16% cell death at 3.5 μM HC-CTX-NPs, 2-fold higher than in MDA-MB-468 cells, could be interpreted in terms of higher impact of the treatment due to lower EGFR expression, the same effect observed in viability assays.[50] In contrast, HC-CTX-NPs did not exhibit significant proapoptotic activity in strongly resistant HCC1937 cells (Figure 4C), corroborating the hypothesis that the antiproliferative effect observed in viability assay in BRCA1-mutated cells could not be attributed to a mAb involvement in an apoptotic pathway of the nanoconjugate.

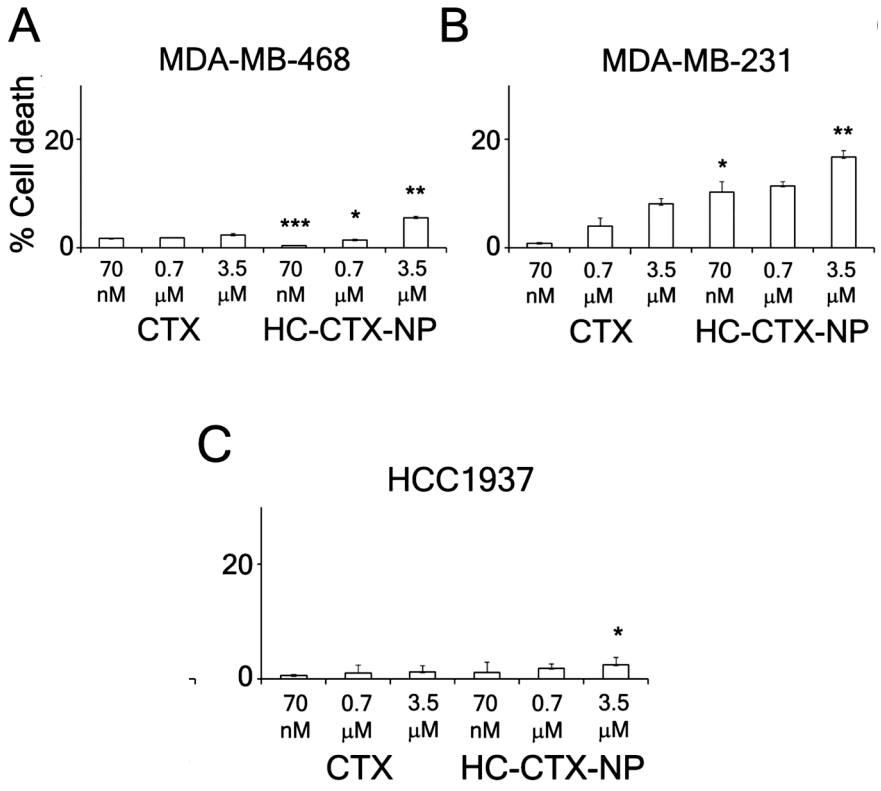

Figure 4. HC-CTX-NPs induce cell death in TNBC cells. Cell death assay of MDA-MB-468 (A), MDA-MB-231 (B), and HCC1937 (C) cells were incubated at 37 °C for 24 h with 70 nM, 0.7 and 3.5 μM of CTX or HC-CTX-NPs. Untreated cells were used as negative control to set region of analysis. Reported values represent the mean ± s. e. of three replicates. (Statistical significance of HC-CTX-NPs *vs.* free drug, *P<0.05; **P<0.001; ***P<0.0005 (Student's *t*-test).

In breast cancer, G1 cell phase progression into S phase is dependent on the activation of cyclin-dependent kinases, including CDK4/6,[55] by complexation with nuclear cyclin D1 and regulated by growth factors and intracellular checkpoints.[50] Deregulation of G1/S transition in TNBC is usually associated with cyclin D1 overexpression, which is activated by interaction of nuclear EGFR.[52] This process can be reversed reducing EGFR levels in the nucleus resulting in cell cycle arrest in G0/G1. In addition, there is evidence that

apoptosis induced by inhibition of EGF ligand interaction with EGFR is normally associated to cell cycle arrest in various cancer cell lines, including TNBC,[19] implicating upregulation of kinase inhibitory protein $p27^{KIP1}$.[50,55] In this light, increased levels of $p27^{KIP1}$ correlate with blockade of EGF/EGFR signal transduction, also associated with cell cycle arrest in G1. Thus, to confirm the direct involvement of conjugated HC-CTX in the increased activity of HC-CTX-NPs over CTX alone inferred by MTS and apoptosis assays, we analyzed the effect of treating TNBC cells with HC-CTX-NPs or CTX on cell cycle (Figure 5). Our data demonstrated that HC-CTX-NPs were more efficient in inducing cell cycle arrest in G1 decreasing the cell population in S-phase in MDA-MB-468 cells compared to free CTX, remarkably higher than untreated cells even at the lowest concentration tested (Figure 5A). In MDA-MB-231 cells, HC-CTX conjugation to NPs showed an appreciable increase in the G1/S phase ratio compared to CTX only at high concentration (Figure 5B). As expected, cell cycle in HCC1937 cells was unaffected by CTX at the highest concentration, consistent with the results from apoptosis assay. However, while no significant effect was recovered within the first 24 h, HC-CTX-NPs were able to induce statistically significant dose- and time-dependent arrest in G0/G1 phase in these cells at longer times (Figure 5C-E). Cell cycle experiment conducted using PEG-NPs ruled out a possible contribution of the NPs alone (Figure S6). Altogether, these results are important in view of a definition of the action mechanism of HC-CTX-NPs. Indeed, cell cycle arrest in G1 phase is presumed to occur in response to DNA damage associated to cyclin transcription caused by constitutive activation of ERK1/2 genes.[19] Thus, inhibition of G1/S phase transition normally associated to ERK1/2 activation represents a marker of TNBC cell sensitivity to CTX, confirming the direct involvement of HC-CTX in

the apoptotic activity of HC-CTX-NPs in BRCA1-wt MDA-MB-468 and MDA-MB-231 cells, and the key role of HC-CTX-NPs in reducing nuclear EGFR levels in BRCA1-mutated HCC1937 cells.

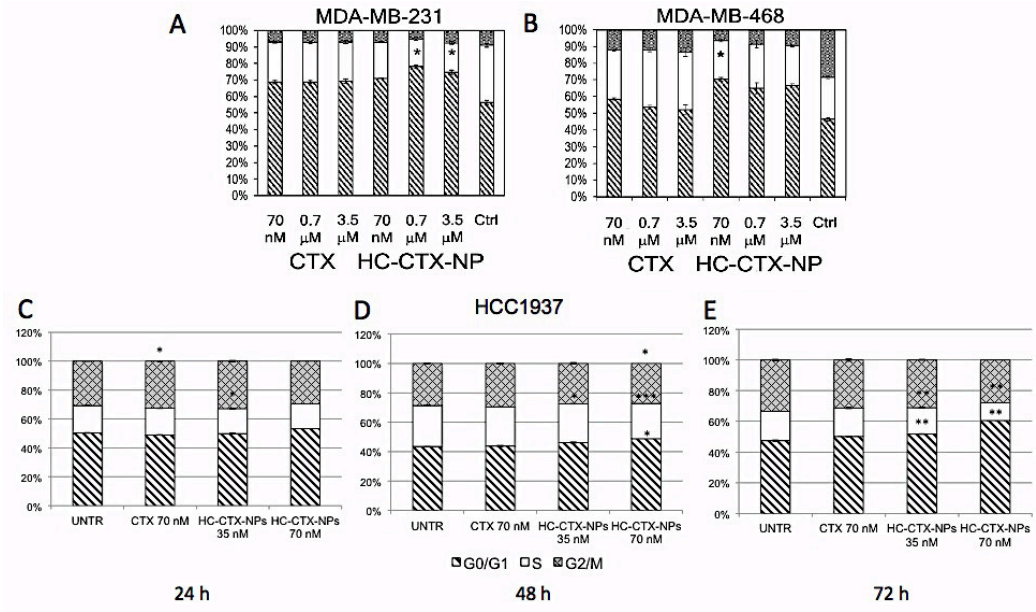

Figure 5. HC-CTX-NPs impact on cell cycle of TNBC cells. MDA-MB-468 (A) and MDA-MB-231 (B) cells were incubated at 37 °C for 24 h with 70 nM, 0.7 and 3.5 µM of CTX or HC-CTX-NPs. Then, cells were processed for flow cytometry and stained with propidium iodide. Untreated cells were used as controls. Graphs represented the mean percentage of events in G1, S and G2/M phase, respectively, ± s.e. (n = 3). Statistical significance of CTX *vs.* HC-CTX-NPs, *P<0.05 (Student's *t*-test). In addition, HCC1937 cells were incubated at 37 °C with 70 nM of CTX or 35 nM and 70 nM of HC-CTX-NPs for 24 h (C), 48 h (D) and 72 h (E). Cells were processed as described for panels A and B. Statistical significance of CTX or HC-CTX-NPs *vs.* UNTR, *p<0.05; **P<0.01; ***P<0.001 (Student's *t*-test).

Blockade of site-specific EGFR phosphorylation upon exposure to HC-CTX-NPs. The levels of total and activated (i.e., phosphorylated) EGFR was assessed by Western blotting in the three TNBC cell lines, using α-tubulin as a housekeeping reference for normalization (Figure 6).

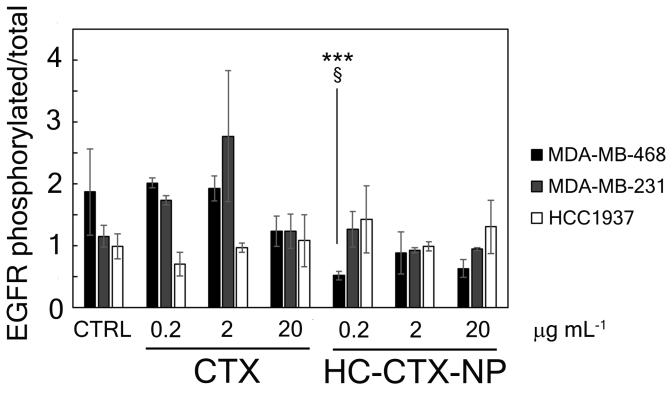

Figure 6. HC-CTX-NPs block EGFR-Y1068 phosphorylation in TNBC cells. MDA-MB-468, MDA-MB-231, and HCC1937 cells were treated with increasing concentrations of CTX or HC-CTX-NPs (0.2, 2 and 20 μg mL^{-1} CTX) in starvation medium for 24 h. Untreated cells were used as negative control. At the end of incubation, cells were lysed, subjected to western blot analysis and the ratio of phosphorylated/total EGFR were quantified by densitometry using ImageJ Software. Reported values are the mean of 6 samples ± s.e. Statistical significance *vs.* CTX, *P<0.05, **P<0.01, *** P<0.005 (Student's *t*-test). Collected p-values are reported in Table S1.

Autophosphorylation of Y1068 tyrosine residue in the kinase domain of EGFR represents the initiation event of a signaling cascade resulting in activation of transcriptional regulation of genes involved in cell proliferation, survival and drug resistance.[47] MDA-MB-468 cells revealed an increase in Y1068 phosphorylation in untreated samples, confirming the role of EGFR autophosphorylation in activating the PI3K/Akt and RAS/MAPK downstream signaling pathways in this cell line associated with PTEN deletion (see Scheme 2).[49] Results from the treatment of TNBC cell lines with 0.2, 2 or 20 μg mL^{-1}

unconjugated CTX or nanoconjugated HC-CTX evidenced that only HC-CTX-NPs in MDA-MB-468 cells was able to reduce the Y1068 phosphorylation levels in EGFR, especially at low concentrations, whereas the other two cell lines were almost completely unaffected. We were not surprised of maintenance of phosphorylated EGFR levels in the two CTX-resistant TNBC cell lines, especially HCC1937, in which BRCA1 mutation is responsible of inducing stable overexpression of activated cytosolic EGFR and constitutive enhancement of EGFR nuclear translocation even in absence of EGF.[48] Collectively, these results suggested a function of conjugated HC-CTX underlying the inhibitory activity of EGFR pathway by HC-CTX-NPs in CTX-sensitive TNBC cells.

Increase of p38 phosphorylation. To confirm the mechanism of cytostatic activity of conjugated HC-CTX, we explored the incidence of HC-CTX-NPs interaction with TNBC cells on the RAS/MAPK downstream key pathway of EGFR. There is strong evidence in support of the role played by RAS/MAPK signaling pathway in cell proliferation and apoptosis prevention.[56] Although the downstream cellular targets of CTX are not fully characterized, CTX was recently demonstrated to activate the transcription factor FOXO3a promoting its nuclear translocation through the MAPK p38 phosphorylation. As a result of this process, it has been proposed that an involvement of the upregulation of $p27^{KIP1}$ and BIM target genes would lead to apoptosis induction and proliferation inhibition.[57] Thus, we decided to determine the extent of nuclear p38 phosphorylation upon treatment with HC-CTX-NPs (Figure 7). HC-CTX-NPs induced potentiated p38 activation in sensitive MDA-MB-468 cells, confirming that nanoconjugation improved the effect of CTX in these cells. CTX alone exhibited more pronounced effect in mildly resistant MDA-MB-231 cells compared to sensitive cells. However, HC-CTX-NPs did not affect p38

phosphorylation in these cells, suggesting a different antiproliferative mechanism not involving FOXO3a activation. Inertness of HCC1937 cells toward p38 activation using HC-CTX-NPs confirmed the refractory behavior of this TNBC cells, in line with the results obtained with CTX, excluding also the involvement of this alternative pathway in the observed antiproliferative activity.

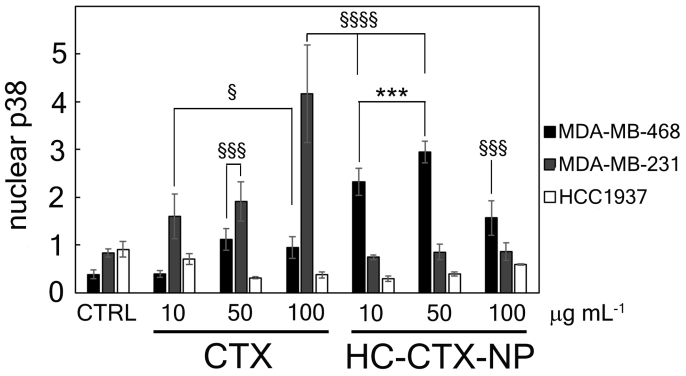

Figure 7. HC-CTX-NPs treatment increase p38 phosphorylation and its nuclear translocation in sensitive TNBC cells. MDA-MB-468, MDA-MB-231, and HCC1937 cells were treated with increasing concentration of CTX or HC-CTX-NPs (10, 50 and 100 μg μL^{-1} CTX) in starvation medium for 24 h. Untreated cells were used as negative control. At the end of incubation, nuclei were purified, lysed, subjected to western blot and the amount nuclear phosphorylated p38 were quantified by densitometry using ImageJ Software. Reported values are the mean of 6 samples ± s.e. Statistical significance *vs.* CTRL, §P<0.05, §§P<0.01, §§§ P<0.005, §§§§ P<0.0005; *vs*. CTX, *P<0.05, **P<0.01, *** P<0.005, **** P<0.0005 (Student's *t*-test). Collected p-values are reported in Table S2.

HC-CTX-NPs is capable to promote ADCC in TNBC cells. Besides a well-documented cytostatic efficacy associated to the intracellular inhibitory activity of CTX, the immunologic implications of antineoplastic efficacy of this mAb have been poorly explored. A few seminal works exploiting CTX for ADCC

against lung cancer cell lines or nontumor EGFR-transfected cell lines have been carried out. The results of these studies suggested that CTX could be effective in activating ADCC mechanism toward target cells using fresh peripheral blood mononuclear cells (PBMCs) at CTX concentration as low as 0.25 μg mL^{-1}, involving the recruitment of cytotoxic host effector cells such as monocytes and natural killer (NK) cells.[58,59]

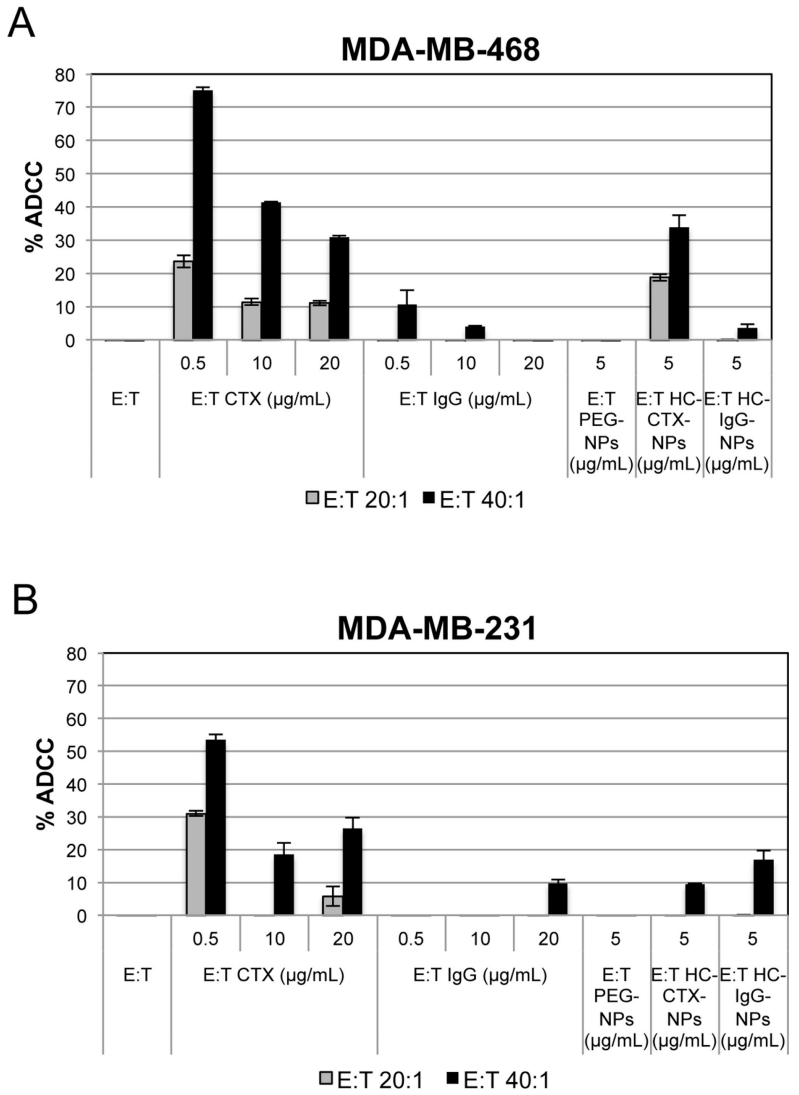

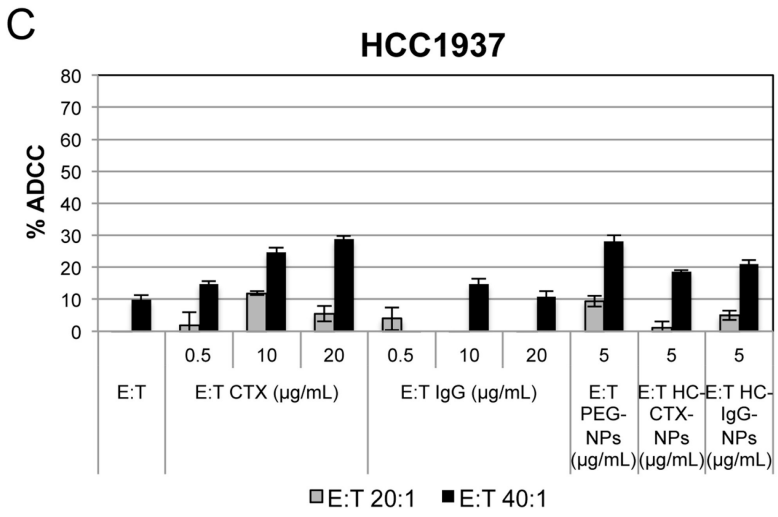

Figure 8. ADCC response induced by HC-CTX-NPs treatment on TNBC cells. MDA-MB-468 (A), MDA-MB-231 (B) and HCC1937 (C) cells were pre-coated with 0.5, 10 or 20 µg mL^{-1} of CTX or nonspecific IgG, and with 5 µg mL^{-1} of HC-CTX-NPs at 37 °C for 30 min. Next, IL-2-activated PBMCs were added to the target cells and incubated at 37 °C for 4 h. The amount of LDH released by target cells revealed the ADCC response induced by treatment. Graphs represent the mean percentage of ADCC ± s.e. (n = 3). Statistical significance of CTX or HC-CTX-NPs *vs.* E:T, *P<0.05; **P<0.01; ***P< 0.001 (Student's *t*-test).

In our study, the three selected TNBC cell lines were treated with isolated PBMCs, containing around 5% NK cells in each sample, at an effector-to-target cell (E:T) ratio of 20:1 or 40:1. PBMCs were activated for ADCC using either CTX at increasing concentrations (0.5, 10 or 20 µg mL^{-1}) or 5 µg mL^{-1} HC-CTX-NPs. Although dosages usually reported in the literature are in the range 10-20 µg mL^{-1}, unexpectedly we found that the best performing concentration for unconjugated CTX was 0.5 µg mL^{-1}. Considering that the average antibody density was 5 HC-CTX per NP corresponding to about 1/10 of the overall NP weight, we could conclude that the mAb concentration used in the experiment with HC-CTX-NPs was comparable to 0.5 µg mL^{-1} CTX in terms of mAb

concentration. Free nonspecific IgG and HC-IgG-NPs were used as negative controls to investigate the contribution of the Fc fragment interaction with CD16a on NK cells in absence of antibody binding with target receptor on cancer cells. In addition, PEG-NPs were also evaluated to assess the possible interference of NPs alone with ADCC assay. MDA-MB-468 cells proved to be sensitive to ADCC in the presence of CTX, showing a 24% and 75% cell death at E:T of 20:1 and 40:1, respectively, as determined by Lactate Dehydrogenase (LDH) assay at 0.5 μg mL^{-1} and 12% and 40%, respectively, at 10 μg mL^{-1}. HC-CTX-NPs exhibited an efficiency around 20% at 20:1 E:T and 40% at 40:1, showing good efficiency in activating ADCC compared to the therapeutic antibody alone (Figure 8A). We were surprised of this unprecedented result for several reasons. CTX was presented on NPs in an appropriate arrangement for binding to the EGFR target receptor, however the Fcγ portion responsible for activation of CD16a on NK cells was expected to be obstructed by nanoconjugation. In addition, it is common belief that a whole Fcγ fragment is necessary for optimal binding with CD16a, while in our study only half chains were available on the surface of the interacting NPs. Therefore, it is plausible that the unpredicted ADCC efficacy promoted by HC-CTX-NPs could be at least partly attributable to multivalent presentation of HC-CTX that was able to amplify NK activation triggering ADCC response. In contrast to CTX and its nanoconjugate, control IgG, HC-IgG-NPs and PEG-NPs at relevant concentrations did not activate ADCC in these cells. CTX exhibited good activity (around 54% at 40:1 E:T) also in MDA-MB-231, although less effective than MDA-MB-468, while gave inconsistent results at higher concentrations. However, HC-CTX-NPs exhibited only negligible effect below 10%, on the same level of control IgG, HC-IgG-NPs and PEG-NPs (Figure 8B). This result suggested

that nanoconjugation was able to maintain the ADCC efficiency only in selected malignant cells expressing high EGFR levels. HCC1937 showed mild activation of ADCC by both CTX and HC-CTX-NPs compared to control IgG and HC-IgG-NPs. However, LDH levels were not significantly higher than PEG-NPs (Figure 8C).

5. Discussion

In this study, we have developed therapeutic antibody nanoconjugates consisting of colloidally stable polymer-coated iron oxide nanoparticles decorated with CTX. The resulting mAb-functionalized NPs were used to investigate the impact of nanoconjugation on the therapeutic efficacy of CTX in TNBC cells. Although entire mAbs could be used for conjugation in principle,[30] our choice here was to conjugate half-chain CTX to colloidal NPs with the aim to improve the chemical-physical properties of the nanoconjugates, particularly in terms of colloidal stability in biological media, and to take advantage of the improved circulation half-life and targeting efficiency compared to whole antibody nanoconjugates in view of future in vivo experiments.[27] However, the use of half-chain antibodies raised several questions relating to the therapeutic effectiveness of nanoconjugates, both in terms of maintenance of mAb efficacy in actively interfering with signaling transduction pathways of cancer cells and of their capability to promote ADCC response, which are putatively considered the two main mechanisms of antitumor activity of therapeutic CTX. For this study, we have selected three representative cell lines, all derived from high grade human tumors with histologic features typical of TNBC, differing in the characteristic molecular profiling. We focused our investigation on EGFR amplification along with KRAS,

PTEN and BRCA1 mutations, associated with different sensitivity to CTX treatment. Phosphatase and tensin homolog (PTEN) protein represents the main tumor suppressor regulating the PI3K/Akt survival pathway of cancer cells, so that its deletion in MDA-MB-468 cells results in inhibition of apoptotic processes,[60] which however can be reestablished by tyrosine kinase phosphorylation blockade making these cells sensitive to treatment with CTX. RAS mutation is responsible for resistance in MDA-MB-231 cells and is normally associated to resistance to matrix deprivation-induced apoptosis (anoikis), which is a crucial process that promotes cell growth independent of extracellular matrix anchorage, leading to enhanced metastatic and invasive character in cancer cells.[61] On the other hand, BRCA1 oncogene expression rather than mutation or deletion were reported to correlate with EGFR expression and functionality. In HCC1937 cells, BRCA1 mutation resulted in intrinsically high levels of nuclear EGFR leading to cyclin D1 activation associated with G1/S transition-dependent overproliferation.[48]

HC-CTX-NPs were not intrinsically cytotoxic, consistent with the data from the literature referred to CTX alone.[14,30] However, our results demonstrated that HC-CTX-NPs were able to inhibit CTX-sensitive MDA-MB-468 and resistant MDA-MB-231 proliferation more pronouncedly than unconjugated CTX, but could also alter the viability in HCC1937 cells, suggesting a role of nanoconjugation in interfering with strong resistance to CTX associated to BRCA1 mutations in HCC1937. This result was unpredicted considering that BRCA1-deficient cells used to exhibit increased Y1068 autophosphorylation in EGFR, responsible of mediating the interaction of EGFR with Grb2 resulting in activation of RAS/MAPK cascade.[50] The extent of antiproliferative activity of HC-CTX-NPs in MDA-MB-468 and MDA-MB-231 cells reflected their effect on

cell cycle and proliferation,[19] thus proving that the functionality causing the cytostatic activity of the nanoconjugate was indeed the HC antibody fragment. We were surprised to notice higher persistent antitumor efficacy of HC-CTX-NPs compared to therapeutic CTX, which could be ascribed to an alteration of the receptor recycling process usually permitted both with EGF affinity ligand and with anti-EGFR antibodies.[62] The observed increase in activity of HC-CTX-NPs was also corroborated by solid evidence of their capability to interfere with downstream signaling pathways of EGFR involved in cell cycle regulation. In particular, only MDA-MB-468 cells treated with HC-CTX-NPs exhibited decreased levels of Y1068 phosphorylation in EGFR, affecting PI3K/Akt and RAS/MAPK downstream signaling pathways consistent with p38 activation in sensitive cells. These results substantiate the hypothesis that HC-CTX nanoconjugation amplifies the effect of CTX proapoptotic molecular mechanism in TNBC cells. Indeed, p38 can regulate the transcription factor FOXO3a phosphorylation in wild-type KRAS cancer cells contributing to its nuclear localization and activation,[63] bypassing the inhibition by the PI3K/Akt and MAPK/ERK pathways.[64,65] FOXO3a nuclear localization and activation promotes cell cycle arrest and apoptosis through $p27^{KIP1}$ upregulation.[66] Different from unconjugated CTX, cell cycle in HCC1937 cells was significantly affected by treatment with HC-CTX-NPs , supporting our conclusion that the significant decrease in proliferation of this strongly refractory cell line was mainly attributable to EGFR-nanocomplex formation, blocking the fast receptor recycling and preventing its nuclear translocation, rather than to direct inhibition of PI3K/Akt pathway.

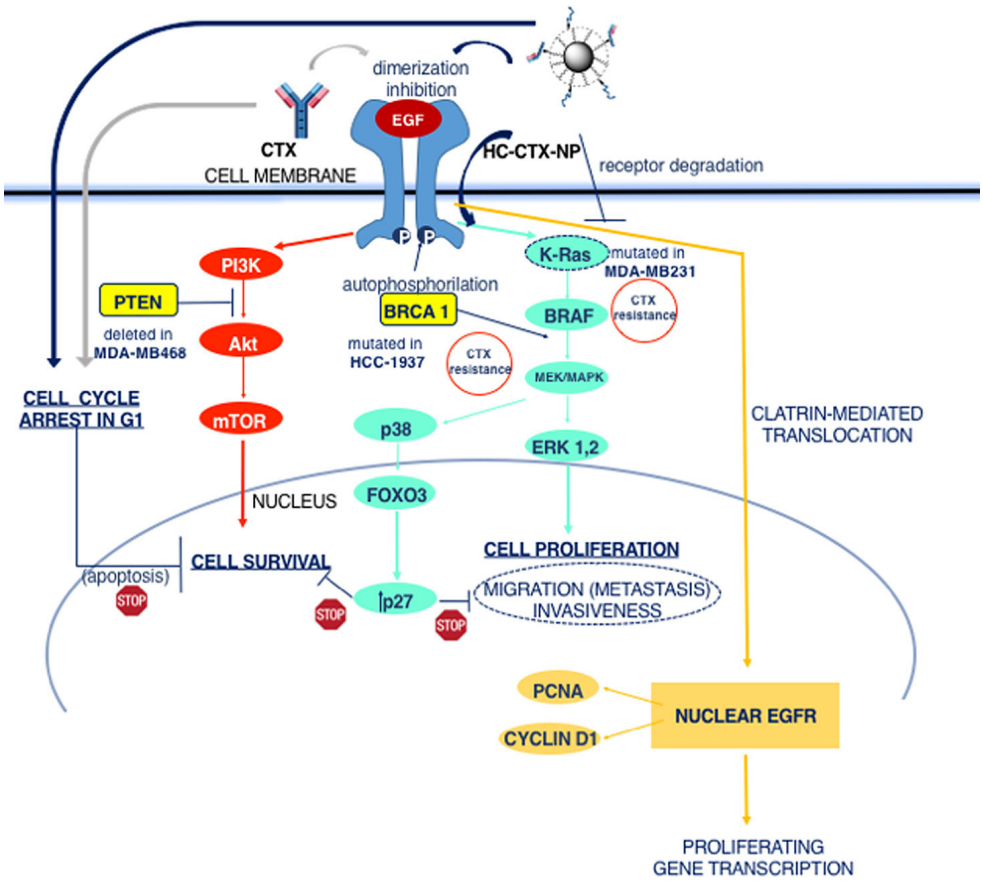

Scheme 2. Interactions of CTX or HC-CTX-NPs with EGFR activation pathways. PI3K/At and MAPK/ERK pathways are normally activated in TNBC cells either by interaction with EGF ligand or by EGFR autophosphorylation. Activated EGFR is partly translocated into the nucleus where it can exert aberrant functions inducing cell cycle deregulation, proliferation, migration and apoptosis inhibition. CTX or HC-CTX-NP can interfere with these pathways in different ways depending on the specific molecular profiles associated to the three different cell types.

Scheme 2 recapitulates the complex network of interactions of the PI3K/Akt and MAPK/ERK pathways regulating cell survival and proliferation, which are actively interfered by HC-CTX-NPs in the three different TNBC cell lines. Under aberrant conditions associated with cancer progression, binding of EGF ligand to EGFR triggers receptor dimerization and phosphorylation leading to

activation of PI3K/Akt and RAS/MAPK pathways resulting in increased cell survival and proliferation, respectively. Indeed, enhancement of PI3K/Akt pathway localizes Akt in the plasma membrane,[67] leading to $p27^{KIP1}$ inhibition and FOXO3a confinement in the cytoplasm.[68] PI3K/Akt pathway is regulated by PTEN, while BRCA1 contributes in controlling MAPK/ERK signaling cascade and in increasing expression and nuclear localization of activated EGFR. CTX binding to the extracellular domain of EGFR in TNBC cells interferes with receptor homo- and hetero-dimerization and inhibits the intracellular tyrosine kinase domain at Y1068 resulting in increased apoptosis.[19] In addition, CTX promotes p38 phosphorylation that leads to FOXO3 phosphorylation and nuclear translocation inducing $p27^{KIP1}$ upregulation, which results in decreased invasiveness and metastasis of cancer cells.[57] However, BRCA1 mutation activates Y1068 autophosphorylation conferring HCC1937 cells resistance to CTX.[48] In this picture, HC-CTX-NPs were able to exert multiple action by 1) reestablishing apoptotic events exploiting cell cycle arrest in G1 even under PTEN deletion, such as in MDA-MB-468 cells, reflecting the mechanism of CTX action, and 2) allowing MAPK pathway-mediated inhibition of cell proliferation and migration also in BRCA1 mutated TNBC cells that are normally nonresponsive to CTX, by exploiting the beneficial effect of nanoconjugation in inducing EGFR degradation preventing its fast recycling, which resulted in decrease of nuclear EGFR levels. On these bases, we are able to offer a comprehensive interpretation for the therapeutic effect of HC-CTX-NPs also in strongly resistant TNBC cells, which could be achieved exclusively through antibody nanoconjugation. Hence, our results allowed us to propose HC-CTX-NPs as a promising nanodrug suitable for widening the spectrum of TNBC responder patients.

Finally, the conjugation of HC-CTX to NPs did not negatively affect the antibody efficiency in promoting the PBMC-mediated ADCC response showing antitumor activity and improved selectivity toward CTX-sensitive TNBC cells, which is of great relevance in view of a future clinical translation. In conclusion, the results of our study provide robust evidence of the potential of compact HC-CTX-NPs in the treatment of TNBC, which could offer new therapeutic options for this highly aggressive life-threatening disease. Future directions of this work will be aimed to compare the results of this study with nanoconjugates bearing entire antibodies and to explore the effects of combining HC-CTX-NPs with conventional chemotherapy in vitro and in vivo.

6. Supporting Information

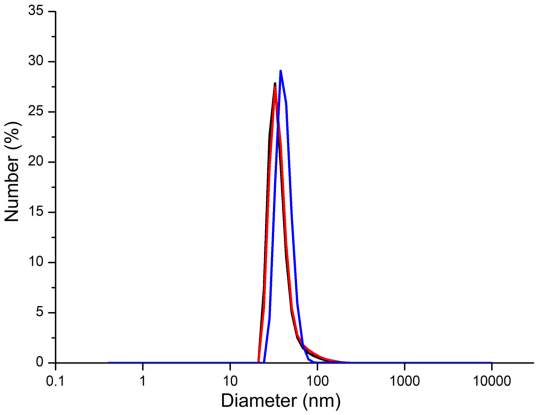

Fig. S1. Hydrodynamic diameter size of HC-CTX-NPs (38.0 ± 1.7 nm, blue) and HC-IgG-NPs (35.1 ± 2.0 nm, red) measured by DLS.

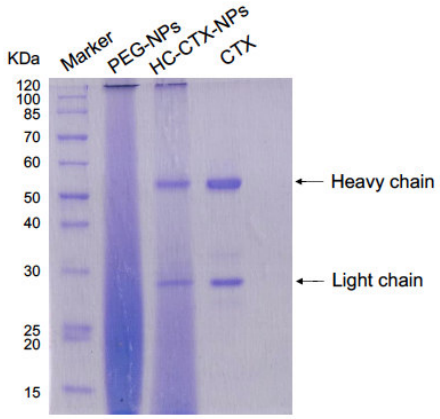

Fig. S2. Qualitative evaluation of HC-CTX presence on NPs. The presence of HC-CTX on nanoparticles was qualitatively checked via 12% SDS-PAGE separation. Starting from the left, the protein marker is in the first lane, then 100 µg of PEG-NPs and HC-CTX-NPs were loaded in second and third lane, respectively. CTX (1 µg) was loaded in the last lane as a standard.

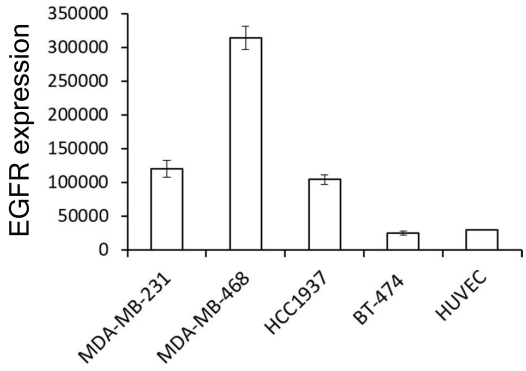

Fig. S3. EGFR expression in TNBC cells. MDA-MB-231, MDA-MB-468, HCC1937 (for TNBC), BT-474 cells and HUVEC cells were tested by flow cytometry to assess membrane EGFR expression. Cells were immunodecorated with the anti-mouse secondary antibody conjugated with AF488 and used to set the gate on viable cells, on singlets and the region of positivity.

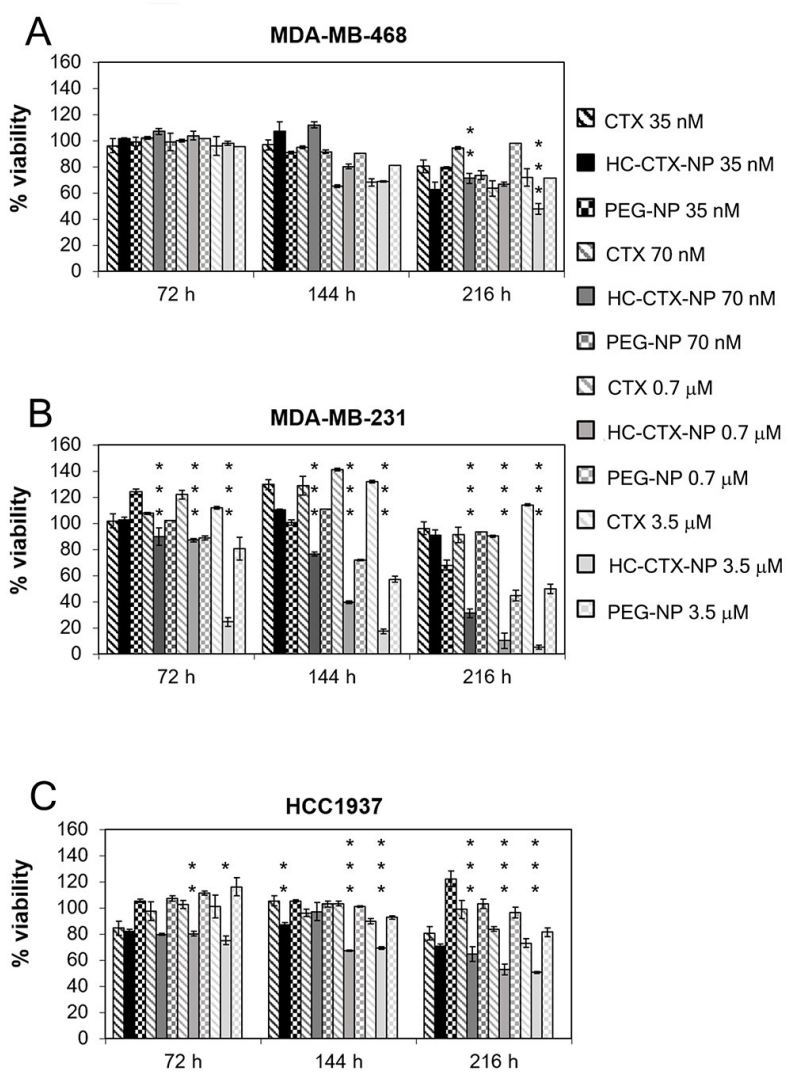

Fig. S4. Viability of TNBC cells treated with CTX, HC-CTX-NPs or PEG-NPs. This figure reproduces the same data reported in Figure 3. Here CTX, HC-CTX-NPs, and PEG-NPs were grouped together for each concentration and time tested. MDA-MB-468 (A), MDA-MB-231 (B), and HCC1937 (C) cells were treated with increasing concentration of CTX or HC-CTX-NPs (from 35 nM to 3.5 mM) up to 216 h. PEG-NPs were used as negative control. Viability was assessed by measuring the conversion of MTS into formazan. Reported values are the mean of six replicates ± s.e., normalized on cell proliferation of untreated cells, respectively. Statistical significance of HC-CTX-NPs *vs.* free drug, * $P<0.05$; ** $P<0.001$; *** $P<0.0005$ (Student's *t*-test).

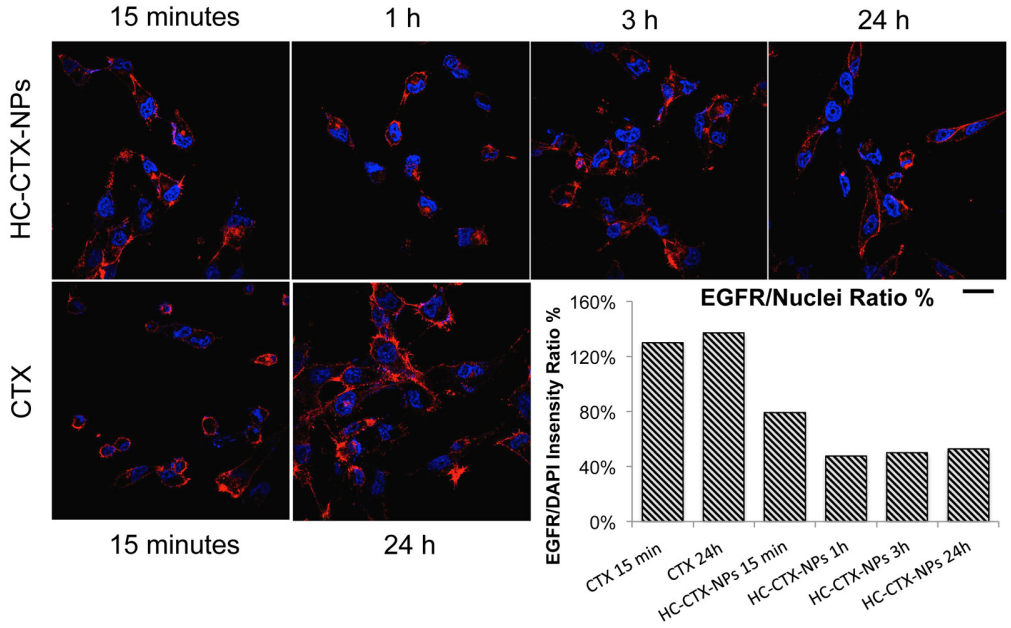

Fig. S5. Time course distribution of EGFR in HCC1937 cells after CTX or HC-CTX-NPs treatment. HCC1937 cells were incubated with 100 μg mL^{-1} of HC-CTX-NPs or 70 nM of CTX at 37 °C for 15 min up to 24 h. The average fluorescence intensity of intracellular EGFR in CTX-treated cells gave constant values at both time points: EGFR/DAPI MFI ratios in CTX-treated cells were 130% at 15 min and 137% at 24 h. EGFR signal detected in cells treated with HC-CTX-NPs was significantly lower, compared to CTX-treated cells, at all time points. The EGFR/DAPI MFI ratio was 80% after 15 min treatment and progressively decreased down to a mean value of around 50% over the following time points (1 h, 3 h, 24 h). Nuclei were stained with DAPI (Blue) while EGFR was recognized by anti-EGFR antibody and labeled with an anti-rabbit secondary antibody conjugated with AF546 (red). Scale bar 20 μm.

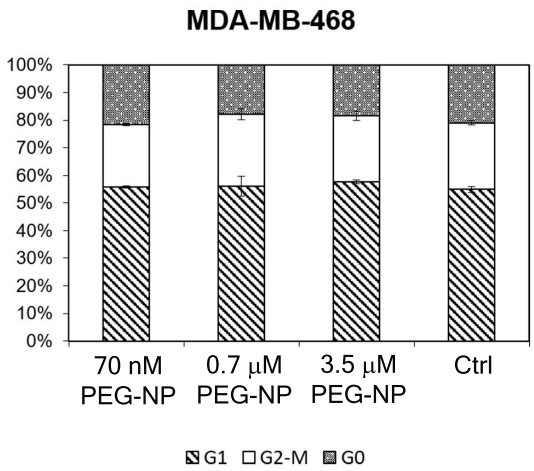

Fig. S6. Effect of PEG-NPs on cell cycle. Representative MDA-MB-468 cells were incubated at 37 °C for 24 h with an amount of PEG-NPs corresponding to 70 nM, 0.7 and 3.5 μM HC-CTX-NPs. Cells were processed for flow cytometry and stained with propidium iodide. Untreated cells were used as control. Graphs represented the mean percentage of events in G1, S and G2/M phase, respectively, ± s.e. (n = 3).

Table S1. Collected p-values from EGFR-Y1068 phosphorylation in TNBC cells.

		μg mL^{-1}	p-value vs CTRL	p-value vs CTX
MDA-MB-468	CTX	0.2	0,420903029	
		2	0,469989827	
		20	0,206581023	
	HC-CTX-NP	0.2	0,046572812	0,001381149
		2	0,119406312	0,040911896
		20	0,060894324	0,180316518
		μg mL^{-1}	p-value vs CTRL	p-value vs CTX
MDA-MB-231	CTX	0.2	0,020281511	
		2	0,131932158	
		20	0,297360802	
	HC-CTX-NP	0.2	0,384775809	0,20328451
		2	0,164183071	0,111593364
		20	0,181711626	0,170885428
		μg mL^{-1}	p-value vs CTRL	p-value vs CTX
HCC1937	CTX	0.2	0,161390606	
		2	0,451526317	
		20	0,420576919	
	HC-CTX-NP	0.2	0,185232013	0,144983227
		2	0,498965697	0,287416297
		20	0,213220605	0,35757756

Table S2. Collected p-values from quantification of nuclear p38

		µg mL^{-1}	p-value vs CTRL	p-value vs CTX
MDA-MB-468	CTX	10	0,453976089	
		50	0,004015345	
		100	0,012115753	
	HC-CTX-NP	10	2,79108E-05	0,00129647
		50	1,93439E-06	0,002444018
		100	0,001572583	0,109512068
		µg mL^{-1}	p-value vs CTRL	p-value vs CTX
MDA-MB-231	CTX	10	0,027803888	
		50	0,004395484	
		100	0,000865991	
	HC-CTX-NP	10	0,268896363	0,073716717
		50	0,448414326	0,038259798
		100	0,443665449	0,016501409
		µg mL^{-1}	p-value vs CTRL	p-value vs CTX
HCC1937	CTX	10	0,224084962	
		50	0,020417351	
		100	0,031304432	
	HC-CTX-NP	10	0,018581153	0,015589554
		50	0,034646504	0,065319698
		100	0,115219125	0,016087601

7. References

1. Ehrlich, P. *Collected Studies on Immunity*; J. Wiley & Sons: New York, 1906.
2. Chames, P.; Van Regenmortel, M.; Weiss, E.; Baty, D. Therapeutic Antibodies: Successes, Limitations and Hopes for the Future. *Br. J. Pharmacol.* **2009**, *157*, 220–233.
3. Reichert, J. M. Antibodies to Watch in 2017. *mAbs* **2017**, *9*, 167–181.
4. Weiner, L. M.; Surana, R.; Wang S. Monoclonal Antibodies: Versatile Platforms for Cancer Immunotherapy. *Nat. Rev. Immunol.* **2010**, *10*, 317–327.
5. Carter, P. J.; Lazar, G. A. Next Generation Antibody Drugs: Pursuit of the 'High-Hanging Fruit'. *Nat. Rev. Drug Discov.* **2018**, *17*, 197–223.
6. Jubb, A. M.; Oates, A. J.; Holden, S.; Koeppen, H. Predicting benefit from anti-angiogenic agents in malignancy. *Nat. Rev. Cancer* **2006**, *6*, 626–635.
7. Jubb, A. M.; Harris, A. L. Biomarkers to predict the clinical efficacy of bevacizumab in cancer. *Lancet Oncol.* **2010**, *11*, 1172–1183.
8. Wang, C.; Wang, J. Q.; Zhang, X. D.; Yu, S. J.; Wen, D.; Hu, Q. Y.; Ye, Y. Q.; Bomba, H.; Hu, X. L.; Liu, Z.; Dotti, G.; Gu, Z. In situ formed reactive oxygen species-responsive scaffold with gemcitabine and checkpoint inhibitor for combination therapy. *Sci. Transl. Med.* **2018**, *10*, eaan3682.
9. Foster, J. B.; Maude, S. L. New developments in immunotherapy for pediatric leukemia. *Curr. Opin. Pediatrics* **2018**, *30*, 25–29.
10. Ansell, S. M.; Lesokhin, A. M.; Borrello, I.; Halwani, A.; Scott, E. C.; Gutierrez, M.; Schuster, S. J.; Millenson, M. M.; Cattry, D.; Freeman, G. J.; Rodig, S. J.; Chapuy, B.; Ligon, A. H.; Zhu, L. L.; Grosso, J. F.; Kim, S. Y.; Timmerman, J. M.; Shipp, M. A.; Armand, P. PD-1 Blockade with

Nivolumab in Relapsed or Refractory Hodgkin's Lymphoma. *N. Engl. J. Med*. **2015**, *372*, 311–319.

11. Smaglo, B. G.; Aldeghaither, D.; Weiner, L. M. The development of immunoconjugates for targeted cancer therapy. *Nat. Rev. Clin. Oncol.* **2014**, *11*, 637–648.
12. Jonker, D. J.; O'Callaghan, C. J.; Karapetis, C. S.; Zalcberg, J. R.; Tu, D.; Au, H.-J.; Berry, S. R.; Krahn, M.; Price, T.; Simes, R. J.; Tebbutt, N. C.; van Hazel, G.; Wierzbicki, R.; Langer, C.; Moore, M. J. Cetuximab for the Treatment of Colorectal Cancer. *N. Engl. J. Med.* **2007**; *357*, 2040–2048.
13. J. B. Vermorken, R. Mesia, F. Rivera, E. Remenar, A. Kawecki, S. Rottey, J. Erfan, D. Zabolotnyy, H.-R. Kienzer, D. Cupissol, F. Peyrade, M. Benasso, I. Vynnychenko, D. De Raucourt, C. Bokemeyer, A. Schueler, N. Amellal, R. Hitt, Platinum-Based Chemotherapy plus Cetuximab in Head and Neck Cancer. *N. Engl. J. Med.* **2008**, *359*, 1116–1127.
14. Meira, D. D.; Nóbrega, I.; de Almeida, V. H.; Mororó, J. S.; Cardoso, A. M.; Silva, R. L.; Albano, R. M.; Ferreira, C. G. Different Antiproliferative Effects of Matuzumab and Cetuximab in A431 Cells Are Associated with Persistent Activity of the MAPK Pathway. *Eur. J. Cancer* **2009**, *45*, 1265–1273.
15. Sunada, H.; Magun, B. E.; Mendelsohn, J.; MacLeod, C. L. Monoclonal Antibody Against Epidermal Growth Factor Receptor Is Internalized Without Stimulating Receptor Phosphorylation. *Proc. Natl Acad. Sci. USA* **1986**, *83*, 3825–3829.
16. Li, S. Schmitz, K. R.; Jeffrey, P. D.; Wiltzius, J. J.; Kussie, P.; Ferguson, K.M. Structural basis for inhibition of the epidermal growth factor receptor by cetuximab. *Cancer Cell* **2005**, *7*, 301–311.
17. Wiley, H. S. Trafficking of the ErbB Receptors and its Influence on

Signaling. *Exp. Cell Res.* **2003**, *284*, 78–88.

18. Van Cutsem, E.; Köhne, C.-H.; Hitre, E.; Zaluski, J.; Chien, C.-R. C.; Makhson, A.; D'Haens, G.; Pintér, T.; Lim, R.; Bodoky, G.; Roh, J. K.; Folprecht, G.; Ruff, P.; Stroh, C.; Tejpar, S.; Schlichting, M.; Nippgen, J.; Rougier, P. Cetuximab and chemotherapy as initial treatment for metastatic colorectal cancer. *N. Engl. J. Med.* **2009**, *360*, 1408–1417.
19. El Guerrab, A.; Bamdad, M.; Kwiatkowski, F.; Bignon, Y.-J.; Penault-Llorca, F.; Aubel, C. Anti-EGFR Monoclonal Antibodies and EGFR Tyrosine Kinase Inhibitors as Combination Therapy for Triple-Negative Breast Cancer. *Oncotarget* **2016**, *7*, 73618–73637.
20. Weiner, G. J. Building Better Monoclonal Antibody-Based Therapeutics. *Nat. Rev. Cancer* **2015**, *15*, 361–370.
21. Montagut, C.; Dalmases, A.; Bellosillo, B.; Crespo, M.; Pairet, S.; Iglesias, M.; Salido, M.; Gallen, M.; Marsters, S.; Ping Tsai, S.; Minoche, A.; Somasekar, S.; Serrano, S.; Himmelbauer, H.; Bellmunt, J.; Rovira, A.; Settleman, J.; Bosch, F.; Albanell, J. Identification of a Mutation in the Extracellular Domain of the Epidermal Growth Factor Receptor Conferring Cetuximab Resistance in Colorectal Cancer. *Nat. Med.* **2012**, *18*, 221–223.
22. Costa R, Shah, A. N.; Santa-Maria, C. A.; Cruz, M. R.; Mahalingam, D.; Carneiro, B. A.; Chae, Y. K.; Cristofanilli, M.; Gradishar, W. J.; Giles, F. J. Targeting Epidermal Growth Factor Receptor in Triple Negative Breast Cancer: New Discoveries and Practical Insights for Drug Development. *Cancer Treat Rev*. **2017**, *53*, 111–119.
23. Occhipinti, E.; Verderio, P.; Natalello, A.; Galbiati, E.; Colombo, M.; Mazzucchelli, S.; Salvade, A.; Tortora, P.; Doglia, S. M.; Prosperi, D. Investigating the Structural Biofunctionality of Antibodies Conjugated to

Magnetic Nanoparticles. *Nanoscale* **2011**, *3*, 387–390.

24. Sousa, F.; Castro, P.; Fonte, P.; Kennedy, P. J.; Neves-Petersen M. T.; Sarmento, B. Nanoparticles for the Delivery of Therapeutic Antibodies: Dogma or Promising Strategy? *Expert Opin. Drug Deliv*. **2016**, *29*, 1–14.
25. Colzani, B.; Pandolfi, L.; Hoti, A.; Iovene, P. A.; Natalello, A.; Avvakumova, S.; Colombo, M.; Prosperi, D. Investigation of Antitumor Activities of Trastuzumab Delivered by PLGA Nanoparticles. *Int. J. Nanomed.* **2018**, 13, 957–973.
26. Alibakhshi, A.; Kahaki, F. A.; Ahangarzadeh, S.; Yaghoobi, H.; Yarian, F.; Arezumand, R.; Ranjbari, J.; Mokhtarzadeh, A.; de la Guardia, M. Targeted Cancer Therapy through Antibody Fragments-Decorated Nanomedicines. *J. Controlled Rel.* **2017**, *268*, 323–334.
27. Fiandra, L.; Mazzucchelli, S.; De Palma, C.; Colombo, M.; Allevi, R.; Sommaruga, S.; Clementi, E.; Bellini, M.; Prosperi, D.; Corsi, F. Assessing the in Vivo Targeting Efficiency of Multifunctional Nanoconstructs Bearing Antibody-Derived Ligands. ACS Nano **2013**, *7*, 6092–6102.
28. Colombo, M.; Sommaruga, S.; Mazzucchelli, S.; Polito, L.; Verderio, P.; Galeffi, P.; Corsi, F.; Tortora, P.; Prosperi, D. Site-Specific Conjugation of ScFvs Antibodies to Nanoparticles by Bioorthogonal Strain-Promoted Alkyne-Nitrone Cycloaddition. *Angew. Chem. Int. Ed*. **2012**, *51*, 496–499.
29. Colombo, M.; Fiandra, L.; Alessio, G.; Mazzucchelli, S.; Nebuloni, M.; De Palma, C.; Kantner, K.; Pelaz, B.; Rotem, R.; Corsi, F.; Parak, W. J.; Prosperi D. Tumor Homing and Therapeutic Effect of Colloidal Nanoparticles Depend on the Number of Attached Antibodies. *Nat. Commun.* **2016**, *7*, 13818.
30. García-Fernández, L.; Garcia-Pardo, J.; Tort, O.; Prior, I.; Brust, M.; Casals,

E.; Lorenzo, J.; Puntes, V. F. Conserved Effects and Altered Trafficking of Cetuximab Antibodies Conjugated to Gold Nanoparticles with Precise Control of their Number and Orientation. *Nanoscale* **2017**, *9*, 6111–6121.

31. Truffi, M.; Colombo, M.; Sorrentino, L.; Pandolfi, L.; Mazzucchelli, S.; Pappalardo, F.; Pacini, C.; Allevi, R.; Bonizzi, A.; Corsi, F.; Prosperi, D. Multivalent exposure of trastuzumab on iron oxide nanoparticles improves antitumor potential and reduces resistance in HER2-positive breast cancer cells. *Sci. Rep.* **2018**, *8*, 6563.
32. Ahmed, S.; Sami, A.; Xiang, J. HER2-Directed Therapy: Current Treatment Options for HER2-Positive Breast Cancer. *Breast Cancer* **2015**, *22*, 101–116.
33. Ning, S. T.; Lee, S. Y.; Wei, M. F.; Peng, C. L.; Lin, S. Y. F.; Tsai, M. H.; Lee, P. C.; Shih, Y. H.; Lin, C. Y.; Luo, T. Y.; Shieh, M. J. Targeting Colorectal Cancer Stem-Like Cells with Anti-CD133 Antibody-Conjugated SN-38 Nanoparticles. *ACS Appl. Mater. Interfaces* **2016**, *8*, 17793–17804.
34. Berry, D. A.; Cronin, K. A.; Plevritis, S. K.; Fryback, D. G.; Clarke, L.; Zelen, M.; Mandelblatt, J. S.; Yakovlev, A. Y.; Habbema, J. D. F.; Feuer, E. J. Effect of Screening and Adjuvant Therapy on Mortality from Breast Cancer. *N. Engl. J. Med.* **2005**, *353*, 1784–1792.
35. Ravdin, P. M.; Cronin, K. A.; Howlader, N.; Berg, C. D.; Chlebowski, R. T.; Feuer, E. J.; Edwards, B. K.; Berry, D. A. The Decrease in Breast-Cancer Incidence in 2003 in the United States. *N. Engl. J. Med.* **2007**, *356*, 1670–1674.
36. Brenton, J. D.; Carey L. A.; Ahmed A. A.; Caldas, C. Molecular Classification and Molecular Forecasting of Breast Cancer: Ready for Clinical Application? *J. Clin. Oncol.* **2005**, *23*, 7350–7360.

37. Bianchini, G.; Balko, J. M.; Mayer, I. A.; Sanders, M. E.; Gianni, L. Triple-Negative Breast Cancer: Challenges and Opportunities of a Heterogeneous Disease. *Nat. Rev. Clin. Oncol*. **2016**, *13*, 674–690.
38. Foulkes, W. D.; Smith, I. E.; Reis-Filho, J. S. Triple-Negative Breast Cancer. *N. Engl. J. Med*. **2010**, *363*, 1938–1948.
39. Jhan, J. R.; Andrecheck, E. R. Triple-Negative Breast Cancer and the Potential for Targeted Therapy. *Pharmacogenomics* **2017**; *18*, 1595–1609.
40. Chavez, K. J.; Garimella, S. V.; Lipkowitz, S. Triple Negative Breast Cancer Cell Lines: One Tool in the Search for Better Treatment of Triple Negative Breast Cancer. *Breast Dis.* **2010**, *32*, 35–48.
41. Wang, Y. Y.; Wang, Y. D.; Chen, G. J.; Li, Y. T.; Xu, W.; Gong, S. Q. Quantum-Dot-Based Theranostic Micelles Conjugated with an Anti-EGFR Nanobody for Triple-Negative Breast Cancer Therapy. *ACS Appl. Mater. Inter.* **2017**, *9*, 30297–30305.
42. Mazzucchelli, S.; Bellini, M.; Fiandra, L.; Truffi, M.; Rizzuto, M. A.; Sorrentino, L.; Longhi, E.; Nebuloni, M.; Prosperi, D.; Corsi F. Nanometronomic Treatment of 4T1 Breast Cancer with Nanocaged Doxorubicin Prevents Drug Resistance and Circumvents Cardiotoxicity. *Oncotarget* **2017**, *8*, 8383–8396.
43. Pellegrino, T.; Manna, L.; Kudera, S.; Liedl, T.; Koktysh, D.; Rogach, A. L.; Keller, S.; Rädler, J.; Natile, G.; Parak, W. J. Hydrophobic Nanocrystals Coated With an Amphiphilic Polymer Shell: a General Route to Water Soluble Nanocrystals. *Nano Lett*. **2004**, *4*, 703–707.
44. Mazzucchelli, S.; Colombo, M.; Verderio. P.; Rozek, E.; Andreata, F.; Galbiati, E.; Tortora, P.; Corsi, F.; Prosperi D. Orientation-Controlled Conjugation of HALO-Fused Homing Peptides to Multifunctional

Nanoparticles for Specific Recognition of Cancer Cells. *Angew. Chem. Int. Ed*. **2013**, *52*, 3121–3125.

45. Mazzucchelli, S.; Colombo, M.; De Palma, C.; Verderio, P.; Coghi, M. D.; Clementi, E.; Tortora, P.; Corsi, F.; Prosperi, D. Synthesis of Single-Domain Protein A-Engineered Magnetic Nanoparticles: Toward a Universal Strategy to Site-Specific Labeling of Antibodies for Targeted Detection of Tumor Cells. *ACS Nano* **2010**, *4*, 5693–5702.
46. Hsu, H. C.; Thiam, T. K.; Lu, Y. J.; Yeh, C. Y.; Tsai, W. S.; You, J. F.; Hung, H. Y.; Tsai, C. N.; Hsu, A.; Chen, H. C.; Chen, S. J.; Yang, T. S. Mutations of KRAS/NRAS/BRAF predict cetuximab resistance in metastatic colorectal cancer patients. *Oncotarget* **2016**, *7*, 22257–22270.
47. Schlessinger, J. Cell Signaling by Receptor Tyrosine Kinases. *Cell* **2000**, *103*, 211–25.
48. Kumaraswamy, E.; Wendt, K. L.; Augustine, L. A.; Stecklein, S. R.; Sibala, E. C.; Li, D.; Gunewardena, S.; Jensen, R. A. BRCA1 Regulation of Epidermal Growth Factor Receptor (EGFR) Expression in Human Breast Cancer Cells Involves Microrna-146a and Is Critical for Its Tumor Suppressor Function. *Oncogene* **2015**, *34*, 4333–4346.
49. Jorissen, R. N.; Walker, F.; Pouliot, N.; Garrett, T. P.; Ward, C. W.; Burgess, A. W. Epidermal Growth Factor Receptor: Mechanisms of Activation and Signalling. *Exp. Cell Res*. **2003**, *284*, 31–53.
50. Vincenzi, B.; Schiavon, G.; Silletta, M.; Santini, D.; Tonini G. The Biological Properties of Cetuximab. *Crit. Rev. Oncol. Hematol*. **2008**, *68*, 93–106.
51. Lin, S.-Y.; Makino, K.; Xia, W.; Matin, A.; Wen, Y.; Kwong, K. Y.; Bourguignon, L.; Hung M.-C. Nuclear Localization of EGF Receptor and Its Potential New Role as a Transcription Factor. *Nat. Cell Biol*. **2001**, *3*, 802–

808.

52. Brand, T. M.; Iida, M.; Luthar, N.; Starr, M. M.; Huppert, E. J.; Wheeler, D. L. Nuclear EGFR as a Molecular Target in Cancer. *Radiother. Oncol.* **2013**, *108*, 370–377.
53. Roepstorff, K.; Grandal, M. V.; Henriksen, L.; Knudsen, S. L. J.; Lerdrup, M.; Grøvdal, L.; Willumsen, B. M.; van Deurs, B. Differential Effects of EGFR Ligands on Endocytic Sorting of the Receptor. *Traffic* **2009**, *10*, 1115–1127.
54. van Tilborg, G. A. F.; Mulder, W. J. M.; Chin, P. T. K.; Storm, G.; Reutelingsperger, C. P.; Nicolay, K.; Strijkers, G. J. Annexin A5-Conjugated Quantum Dots with a Paramagnetic Lipidic Coating for the Multimodal Detection of Apoptotic Cells. *Bioconjugate Chem.* **2006**, *17*, 865−868.
55. Wu, X.; Rubin, M.; Fan, Z.; DeBlasio, T.; Soos, T.; Koff, A.; Mendelsohn, J. Involvement of $p27^{KIP1}$ in G1 Arrest Mediated by an Anti-Epidermal Growth Factor Receptor Monoclonal Antibody. *Oncogene* **1996**, *12*, 1397–1403.
56. Schlessinger J. Cell Signaling by Receptor Tyrosine Kinases. *Cell* **2000**, *103*, 211–225.
57. McCubrey, J. A.; Steelman, L. S.; Chappell, W. H.; Abrams, S. L.; Wong, E. W.; Chang, F.; Lehmann, B.; Terrian, D. M.; Milella, M.; Tafuri, A.; Stivala, F.; Libra, M.; Basecke, J.; Evangelisti, C.; Martelli, A. M.; Franklin, R. A. Roles of the Raf/MEK/ERK Pathway in Cell Growth, Malignant Transformation and Drug Resistance. *Biochim. Biophys. Acta* **2007**, *1773*, 1263–1284.
58. Marzi, L.; Combes, E; Vié, N.; Ayrolles-Torro, A; Tosi, D.; Desigaud, D.; Perez-Gracia, E.; Larbouret, C.; Montagut, C.; Iglesias, M.; Jarlier, M.; Denis, V.; Linares, L. K.; Lam, E. W.-F.; Martineau, P.; Del Rio, M.; Gongora

C. FOXO3a and the MAPK p38 Are Activated by Cetuximab to Induce Cell Death and Inhibit Cell Proliferation and their Expression Predicts Cetuximab Efficacy in Colorectal Cancer. *Br. J. Cancer* **2016**, *115*, 1223–1233.

59. Kurai, J.; Chikumi, H.; Hashimoto, K. Antibody-Dependent Cellular Cytotoxicity Mediated by Cetuximab against Lung Cancer Cell Lines. *Clin. Cancer Res.* **2007**, *13*, 1552–1561.
60. Kimura, H.; Sakai, K.; Arao, T.; Shimoyama, T.; Tamura, T.; Nishio, K. Antibody-Dependent Cellular Cytotoxicity of Cetuximab against Tumor Cells with Wild-Type or Mutant Epidermal Growth Factor Receptor. *Cancer Sci.* **2007**, *98*, 1275–1280.
61. Georgescu, M.-M. PTEN Tumor Suppressor Network in PI3K-Akt Pathway Control. *Genes Cancer* **2010**, *1*, 1170–1177.
62. Eckert, L. B.; Repasky, G. A.; Ülkü, A. S.; McFall, A.; Zhou, H.; Sartor, C. I.; Der, C. J. Involvement of Ras Activation in Human Breast Cancer Cell Signaling, Invasion, and Anoikis. *Cancer Res*. **2004**, *64*, 4585–4592.
63. Jaramilloa, M. L.; Leona, Z.; Grothea, S.; Paul-Roca, B.; Abulrobc, A.; O'Connor McCourt, M. Effect of the Anti-Receptor Ligand-Blocking 225 Monoclonal Antibody on EGF Receptor Endocytosis and Sorting. *Exp. Cell Res*. **2006**, *312*, 2778–2790.
64. Ho, K.-K.; McGuire, V. A.; Koo, C.-Y.; Muir, K. W.; de Olano, N.; Maifoshie, E.; Kelly, D. J.; McGovern, U. B.; Monteiro, L. J.; Gomes, A. R.; Nebreda, A. R.; Campbell, D. G.; Arthur, J. S.; Lam, E. W. Phosphorylation of FOXO3a on Ser-7 by p38 Promotes Its Nuclear Localization in Response to Doxorubicin. *J. Biol. Chem*. **2012**, *287*, 1545–1555.
65. Yang J.-Y.; Zong, C. S.; Xia, W.; Yamaguchi, H.; Ding, Q.; Xie, X.; Lang, J. Y.;

Lai, C. C.; Chang, C. J.; Huang, W. C.; Huang, H.; Kuo, H. P.; Lee, D. F.; Li, L. Y.; Lien, H. C.; Cheng, X.; Chang, K. J.; Hsiao, C. D.; Tsai, F. J.; Tsai, C. H.; Sahin, A. A.; Muller, W. J.; Mills, G. B.; Yu, D.; Hortobagyi, G. N.; Hung, M. C. ERK Promotes Tumorigenesis by Inhibiting FOXO3a via MDM2-Mediated Degradation. *Nat. Cell Biol*. **2008**, *10*, 138–148.

66. Biggs, W. H.; Meisenhelder, J.; Hunter, T.; Cavenee, W. K; Arden, K. C. Protein Kinase B/Akt-Mediated Phosphorylation Promotes Nuclear Exclusion of the Winged Helix Transcription Factor FKHR1. *Proc. Natl. Acad. Sci. USA* **1999**, *96*, 7421–7426.
67. van der Vos, K. E.; Coffer, P. J. The Extending Network of FOXO Transcriptional Target Genes. *Antioxid. Redox Signal.* **2011**, *14*, 579–592.
68. King, D; Yeomanson, D; Bryant, H. E. PI3King the Lock: Targeting the PI3K/Akt/mTOR Pathway as a Novel Therapeutic Strategy in Neuroblastoma. *J. Pediat. Hematol. Onc.* **2015**, *37*, 245–251.
69. Rafalski, V. A.; Brunet, A. Energy metabolism in adult neural stem cell fate". *Prog. Neurobiol.* **2011**, *93*, 182–203.

Paper

Bioconjugate Chemistry

Article

Cite This: Bioconjugate Chem. XXXX, XXX, XXX−XXX

pubs.acs.org/bc

Half-Chain Cetuximab Nanoconjugates Allow Multitarget Therapy of Triple Negative Breast Cancer

Miriam Colombo,[†] Maria Antonietta Rizzuto,[†] Chiara Pacini,[†] Laura Pandolfi,[†,⊥] Arianna Bonizzi,[§] Marta Truffi,[‡] Matteo Monieri,[‡] Francesco Catrambone,[†,‡] Marco Giustra,[†] Stefania Garbujo,[†] Luisa Fiandra,[†] Fabio Corsi,[‡,§,∥] Davide Prosperi,*[,†,§] and Serena Mazzucchelli*[,‡]

[†]NanoBioLab, Dipartimento di Biotecnologie e Bioscienze, Università di Milano-Bicocca, Piazza della Scienza 2, 20126 Milano, Italy

[‡]Department of Biomedical and Clinical Sciences "L. Sacco", University of Milano, via G. B. Grassi 74, 20157 Milano, Italy

[§]Nanomedicine Laboratory, ICS Maugeri S.p.A. SB, via S. Maugeri 10, 27100 Pavia, Italy

[∥]Surgery Department, Breast Unit, ICS Maugeri S.p.A. SB, via S. Maugeri 10, 27100 Pavia, Italy

Supporting Information

ABSTRACT: The use of therapeutic monoclonal antibodies (mAbs) has revolutionized cancer treatment. The conjugation of mAbs to nanoparticles has been broadly exploited to improve the targeting efficiency of drug nanocarriers taking advantage of high binding efficacy and target selectivity of antibodies for specific cell receptors. However, the therapeutic implications of nanoconjugation have been poorly considered. In this study, half-chain fragments of the anti-EGFR mAb cetuximab were conjugated to colloidal nanoparticles originating stable nanoconjugates that were investigated as surrogates of therapeutic mAbs in triple negative breast cancer (TNBC). Three TNBC cell lines were selected according to EGFR expression, which regulates activation of MAPK/ERK and PI3K/Akt pathways, and to distinctive molecular profiling including KRAS, PTEN, and BRCA1 mutations normally associated with diverse sensitivity to treatment with cetuximab. The molecular mechanisms of action of nanoconjugated half-chain mAb, including cell targeting, interference with downstream signaling pathways, proliferation, cell cycle, and apoptosis, along with triggering of ADCC response, were investigated in detail in sensitive and resistant TNBC cells. We found that half-chain mAb nanoconjugation was able to enhance the therapeutic efficacy and improve the target selectivity against sensitive, but unexpectedly also resistant, TNBC cells. Viability assays and signaling transduction modulation suggested a role of BRCA1 mutation in TNBC resistance to cetuximab alone, whereas its effect could be circumvented using half-chain cetuximab nanoconjugates, suggesting that nanoconjugation not only improved the antibody activity but also exerted different mechanisms of action. Our results provide robust evidence of the potential of half-chain antibody nanoconjugates in the treatment of TNBC, which could offer a new paradigm for therapeutic antibody administration, potentially allowing improved curative efficiency and reduced minimal effective dosages in both sensitive and resistant tumors.

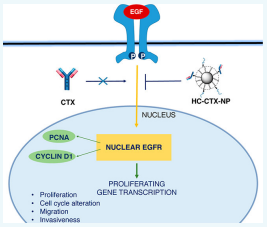

INTRODUCTION

The concept of using therapeutic antibodies as "magic bullets" to target cancer was first suggested by Paul Ehrlich at the beginning of the past century.[1] Since then, continuous advances in the development of monoclonal antibodies (mAbs) have led to the availability of over 70 among chimeric, humanized, and fully human mAbs approved until 2017, with a further 50 awaiting market approval or under clinical trials.[2,3] The technology progress in mAbs engineering allowed researchers to address some of the adverse issues that limited the clinical impact of such biological therapeutics, including high immunogenicity in humans and poor efficacy in triggering the human immune effector response.[4] Over the past two decades, the use of mAbs directed either to specific antigens overexpressed by tumor cells or to the tumor microenvironment, including angiogenesis and checkpoint inhibition, has provided great benefit in the treatment of certain cancers.[5−8] Antibodies conjugated to chemotherapeutics or radioisotopes proved to be effective against hematological malignancies, whereas unconjugated mAbs have been especially employed for the treatment of nonleukemic tumors.[5,9−11] Among the latter class of therapeutic mAbs, those targeting growth factor receptors, including the epidermal growth factor receptor (EGFR) and the human epidermal growth factor receptor 2 (HER2), have demonstrated well recognized efficacy.

Cetuximab (CTX) is a chimeric mAb in use as second- or third-line therapy for the treatment of EGFR-positive colorectal cancer and head-and-neck squamous cell cancer.[12,13] Although CTX does not exhibit primary cytotoxic activity,[14] this mAb exerts a cytostatic antitumor action by competing the binding of EGFR with the activating ligand (EGF)[15] and by

Received: September 20, 2018
Published: October 10, 2018

DOI: 10.1021/acs.bioconjchem.8b00667
Bioconjugate Chem. XXXX, XXX, XXX−XXX

preventing receptor dimerization.[16] These events were associated with EGFR-mediated signaling transduction typical of tyrosine kinase receptors family.[17] In addition, CTX is able to promote the antibody-dependent cell-mediated cytotoxicity (ADCC). Improved efficacy has been suggested in combination with chemotherapy or coadministration of tyrosine kinase inhibitors.[18,19]

However, a few constraints, including low tissue penetration, short circulation half-life, and onset of resistance, limit the conventional therapy with unconjugated CTX as well as with other mAbs intended for use against solid tumors.[20,21] As a consequence, CTX-based chemotherapy failed to demonstrate a significant clinical benefit in triple negative breast cancer (TNBC) in early phase clinical trials.[22]

The advent of nanotechnology in biomedicine has offered new opportunities to challenge some of these limitations. The conjugation of mAbs to nanoparticles (NPs) or their incorporation within suitable nanocarriers has shown satisfactory preservation of the structural and functional features of the antibody, improved tissue penetration, and enhanced permanence in the blood circulation.[23−25] Hitherto, antibodies in nanoconjugates have been conceived as tumor homing ligands to improve the targeting efficiency of NPs to selected cell populations exploiting the unique affinity and selectivity of mAbs toward specific molecular receptors. Actually, several reports have established the efficacy of mAb conjugation in enhancing the active targeting capability of colloidal NPs. In several instances, antibody fragments including Fab, single chain variable fragments (scFv), nanobodies, and half-chain antibodies (HC-mAbs), proved to be valuable alternatives to the nanoconjugation of entire mAbs for targeting applications.[26−28]

Only very recently, interest has been also attributed to the investigation of the therapeutic implications of mAb conjugation to NPs, highlighting the incidence of selected parameters, including ligand density,[29] orientation,[30] and structure,[31] on the biofunctionality of the attached therapeutic antibody. In addition, the conjugation of mAbs to drug nanocarriers allowed the simultaneous delivery of cytotoxic chemotherapeutics useful for bimodal combination in adjuvant and neoadjuvant therapy.[32,33] The advantages provided by antibody nanoconjugation are estimated to lead to a reappraisal of the great potential of therapeutic mAbs also in the treatment of highly aggressive and refractory tumors.

Among poorly manageable malignancies for which treatment improvement is strongly demanded, here we focused on TNBC to assess the potential of CTX conjugation to NPs. Breast cancer is the most commonly diagnosed cancer in women, and, despite the great benefits deriving from early diagnosis, adjuvant therapy, and lowered rates of usage of hormone replacement therapies, it remains a major cause of death.[34,35] Due to the huge heterogeneity, genomic instability, and capability to resume features usually observed in cancer, breast cancer is considered a good model for assessing innovative therapeutic strategies and for the development of novel anticancer agents. TNBC, which accounts for 15% of breast neoplasms, represents an unsolved issue in oncology owing to poor prognosis deriving from its aggressive phenotype and absence of a targeted therapy, as it is defined by lack of estrogen receptor (ER), progesterone receptor (PR), and HER2.[36] In recent years, TNBC classification has been revised pointing out four molecular subtypes to better reflect different response rates to neoadjuvant chemotherapy. TNBCs include luminal androgen receptor (LAR), mesenchymal (MES), basal-like immune activated (BLIA), and basal-like immune-suppressed (BLIS). Basal-like subtypes account for 55−80% of TNBCs.[37] Although TNBC displays higher chemosensitivity compared to other breast cancers, patients harboring TNBC generally retain unfavorable clinical outcome, mainly due to the onset of chemoresistance, which is a direct consequence of TNBC intrinsic genomic instability.[38] Up to 80% of TNBC cells are p53-deficient, which can be explained by the involvement of alternative survival pathways for DNA repair from damages caused by cytotoxic drugs, ensuring replication and metastatic proliferation.[39] On the other hand, around 60% of TNBCs are characterized by overexpression of EGFR, which regulates activation of its downstream signaling, including the mitogen-activated protein kinases cascade (originally called extracellular signal-regulated kinases, ERK) or MAPK/ERK (also known as Ras/Raf/MEK/ERK) and the phosphatidylinositol-3 kinases (PI3K/Akt) pathways. Activation of these pathways induces signal migration from cell membrane into the nucleus to increase proliferation and mediate chemoresistance by influencing DNA damage repair, DNA replication, and oncogene transcription.[19,40] As EGFR overexpression is normally associated with poor prognosis, this tyrosine kinase receptor has been envisaged as an emerging therapeutic target for the treatment of TNBC.[38,39]

The use of nanotechnology was estimated to improve the therapeutic outcome of TNBC treatment by increasing antitumor efficacy due to NP delivery of drugs, reducing off-target toxicity, and preventing chemoresistance.[41,42] Most of these studies have indicated EGFR as a preferential surface target to address chemotherapy to the malignant cells. In the present study, we explored the impact of conjugation of half-chain cetuximab (HC-CTX) to colloidal NPs on the therapeutic efficacy of the antibody in TNBC cells. The aim of this study was to investigate the molecular mechanisms of action of the nanoconjugated HC-CTX in comparison with unconjugated CTX, evaluating the effect of nanoconjugation on cell targeting efficiency, interference with downstream signaling pathways, cell cycle, and proliferation in different TNBC cell subtypes, including both CTX-sensitive and resistant cell lines. In addition, to assess the maintenance of the full mAb power upon half-chain nanoconjugation, we explored the capability of nanoconjugated HC-CTX to promote the ADCC mechanism of immune response against TNBC cells.

RESULTS AND DISCUSSION

Synthesis and Characterization of Half-Chain mAb-Conjugated Colloidal Nanoparticles. The NPs used in this study were 12 nm iron oxide nanocrystals coated with a biocompatible amphiphilic polymer (PMA) that conferred excellent colloidal stability to the NP dispersion and provided several carboxylic functional groups useful for bioconjugation.[43] HC-mAb-NPs were synthesized according to an optimized procedure derived from Fiandra et al. with some adjustments.[27] Briefly, PMA-coated NPs obtained by established protocols were modified with 2,2-(ethylenedioxy)bis-(ethylamine) (EDBE) to introduce amino functionalities that were next converted into thiol-reactive groups with *N*-succinimidyl-3-[2-pyridyldithio]propionate (SPDP) leading to PDP-NPs, with ∼70% efficiency.[44] PDP-NPs were reacted with HC-mAb, obtained by mild reduction of the antibody using 2-mercaptoethanolamine,[27] and the residual PDP groups

DOI: 10.1021/acs.bioconjchem.8b00667
Bioconjugate Chem. XXXX, XXX, XXX−XXX

Scheme 1. Schematic Representation of NPs Synthesis

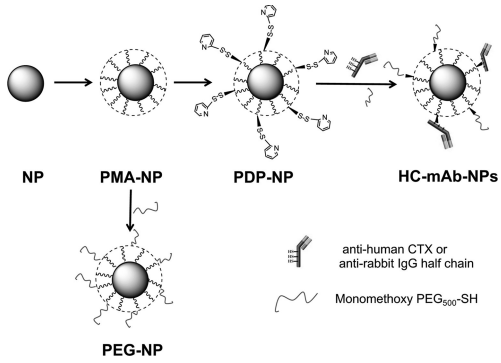

were saturated with excess PEG_{500}-SH ($MW_{PEG} \approx 500$ Da) (see Scheme 1). This procedure was followed both with CTX and with a negative control mAb (a nonspecific anti-rabbit IgG), obtaining HC-CTX-NPs and HC-IgG-NPs, respectively. Control unconjugated NPs were prepared by pegylation of PDP-NPs using PEG_{500}-SH, obtaining PEG-NPs. One of the advantages of using HC fragment is that free thiol groups are generated selectively on the constant portion of the antibody heavy chain by mild reducing agents, which induce the conjugation to the NP surface through the Fc moiety allowing the presentation of the Fab fragment in the optimal orientation for binding with the receptor. The hydrodynamic size of mAb-conjugated NPs was measured by dynamic light scattering (DLS, Figure S1 in the Supporting Information), obtaining 38.0 ± 1.7 nm (HC-CTX-NPs) and 35.1 ± 2.0 nm (HC-IgG-NPs), while the zeta potential was −66.0 ± 0.6 and −66.5 ± 0.1 mV, respectively. In both cases, the number of bound half-chain antibodies was adjusted to ∼5 per NP (5.3 ± 0.7 and 5.1 ± 0.9, respectively), as determined by a pyridine 2-thione assay.[45] Determining mAb loading on NPs allowed us to accurately define the mAb concentration in biological experiments using nanoconjugates. Coomassie staining of electrophoresis gel performed on mAb-conjugated NPs, using CTX as positive control and PEG-NPs as negative control, qualitatively confirmed the presence of the antibody attached to the NPs (Figure S2). Collectively, the data from DLS, zeta potential, and calculation of mAbs number let us conclude that HC-CTX-NPs and HC-IgG-NPs had very similar chemical-physical properties, differing only in the nature of the attached antibody molecule.

TNBC Cells Selection and Determination of HC-CTX-NP Binding. Among the 27 available human cancer cell lines classified in the literature as TNBC cells,[40] we identified CTX-sensitive MDA-MB-468 (EGFR amplification, PTEN deletion) and CTX-resistant MDA-MB-231 (mutations in KRAS and BRAF, predictors of CTX resistance) cell lines,[46] – which do or do not harbor, respectively, the activating mutations of the main EGFR pathways – along with HCC1937 (PTEN deletion), a CTX-resistant, basal cell line that is homozygous for the *BRCA1* 5382insC mutation.[47,48] Among them, CTX was reported to be therapeutically active only in MDA-MB-468 cells.[19] Although CTX activity has been poorly characterized in vitro, the sensitivity to mAb treatments was associated with stimulation or inhibition of specific regulators of cell cycle, in turn activated or inactivated by signaling transduction induced by PI3K/Akt and RAS/MAPK pathways, resulting in cell cycle arrest in the G1 phase followed by apoptosis.[19,49]

The above-mentioned three TNBC cell lines along with a BT-474 invasive ductal breast carcinoma cell line, used as a triple positive control, and a nontumoral human umbilical vascular endothelial cell (HUVEC) line were first assessed by flow cytometry to estimate the EGFR expression. MDA-MB-468 cells exhibited very high EGFR levels (score +++) with a 3-fold higher fluorescence intensity compared to MDA-MB-231 (+) and HCC1937 (+). By contrast, HUVEC showed very low EGFR expression supporting the opportunity of targeting EGFR to discriminate between TNBC and healthy cells (Figure S3). EGFR expression in BT-474 was recovered on the same levels of HUVEC and could be used as negative breast cancer cell control for binding experiments.

Binding efficiency of HC-CTX-NPs in TNBC cell lines and in BT-474 cells was estimated by flow cytometry at 37 °C at different mAb concentrations in comparison to nonspecific HC-IgG-NPs (Figure 1). All TNBC cell lines showed full signal saturation at all concentrations tested, confirming that 100% living cells could be efficiently labeled between 5 and 50 $\mu g\ mL^{-1}$ nanoconjugated HC-CTX. However, slight differences in targeting efficiency between MDA-MB-468 and MDA-MB-231/HCC1937 cells were recovered at the highest HC-IgG-NPs concentrations. Indeed, MDA-MB-468 binding by HC-IgG-NPs was negligible even at 50 $\mu g\ mL^{-1}$ (Figure 1A), whereas MDA-MB-231 and HCC1937 exhibited increasing binding up to around 15 and 20%, respectively (Figure 1B,C). The slightly increased nonspecific binding observed with the latter two cell lines could be attributed to their lower EGFR expression, allowing for a higher contribution of Fc receptor in membrane interaction. In contrast, flow cytometry of $EGFR^{low}$ BT-474 cells treated with HC-CTX-NPs showed around 50% positive cells independent of HC-CTX-NPs concentration, with a nonspecific contribu-

DOI: 10.1021/acs.bioconjchem.8b00667
Bioconjugate Chem. XXXX, XXX, XXX−XXX

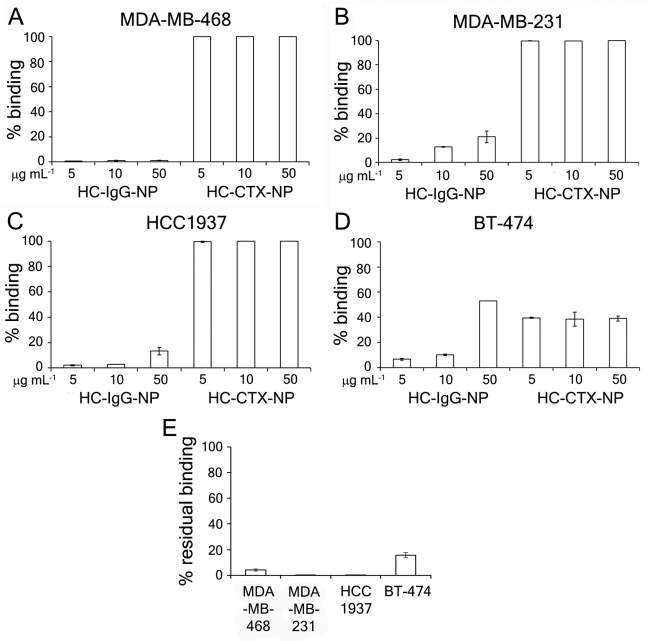

Figure 1. HC-CTX-NP binding to breast cancer cells. MDA-MB-468 (A), MDA-MB-231 (B), HCC1937 (C) TNBC cells, and BT-474 cells (D) were incubated at 4 °C for 2 h in PBS buffer and 0.3% BSA with different amounts of HC-IgG-NPs or HC-CTX-NPs (5, 10, and 50 μg mL^{-1}). Next, cells were processed for flow cytometry. HC-IgG-NPs were revealed using AF488-labeled anti-rabbit secondary antibody, while HC-CTX-NPs were labeled with AF488 anti-human antibody. Untreated cells were used to set the positive region and the singlet gate. Reported values are the mean ± s.e. (n = 3). (E) Competition assay. MDA-MB-468, MDA-MB-231, HCC1937 TNBC cells, and BT-474 cells were incubated 1 h at 37 °C with 50 μg mL^{-1} of FITC-labeled HC-CTX-NPs with or without excess of unlabeled CTX (i.e., 5 mg) as competitor. Cells were then detached and treated for flow cytometry. Untreated cells have been used to set the singlet gate and the positive region. Reported values are the mean ± s.e. (n = 3).

tion that increased with concentration (Figure 1D). To better appreciate the involvement of mAb-EGFR interaction in HC-CTX-NP binding to TNBC cells, a competition assay using MDA-MB-468, MDA-MB-231, HCC1937, and BT-474 cells was conducted (Figure 1E). Flow cytometry of cells treated with HC-CTX-NPs at 37 °C after preincubation with CTX for 30 min revealed a 15% nonspecific binding in EGFR^{low} BT-474 cells, whereas EGFR^{high} TNBC cells exhibited negligible signal. Residual 4% binding observed in MDA-MB-468 cells could be attributed to a very high EGFR expression of this cell line, making full and persistent saturation of membrane receptors very difficult to achieve with competing CTX.

Intracellular Trafficking of HC-CTX-NPs. We were interested in investigating trafficking and the fate of HC-CTX-NPs following their cellular uptake, considering that 1) MDA-MB-231, MDA-MB-468, and HCC1937 TNBC cell lines exhibited high binding affinity for HC-CTX-NPs independent of the extent of EGFR levels and of sensitivity to CTX; 2) ligand−receptor complex internalization is normally favored at 37 °C and processed through an endolysosomal intracellular pathway; and 3) HC-CTX conjugation with NPs was presumed to promote the activation of endocytic mechanisms via clathrin-mediated uptake. Figure 2A shows confocal microscopy images of TNBC cells acquired after 15 min, 1, 3, 24, and 48 h treatment with HC-CTX-NPs. Untreated cells stained with DAPI were used as negative control. All three cell lines exhibited excellent binding capability, uptake, and long-term internalization of HC-CTX-NPs confining persistently the nanoconjugates into endosomes and lysosomes, as clearly evidenced by spotted fluorescence emission typical of microvesicle compartmentalization of NPs. Transmission electron microscopy (TEM) images of a time course of representative MDA-MB-468 cells treated with HC-CTX-NPs at the same time points were consistent with confocal microscopy results (Figure 2B). At 15 min, nanoconjugates were gathered adjacent to the cell membrane.

DOI: 10.1021/acs.bioconjchem.8b00667
Bioconjugate Chem. XXXX, XXX, XXX−XXX

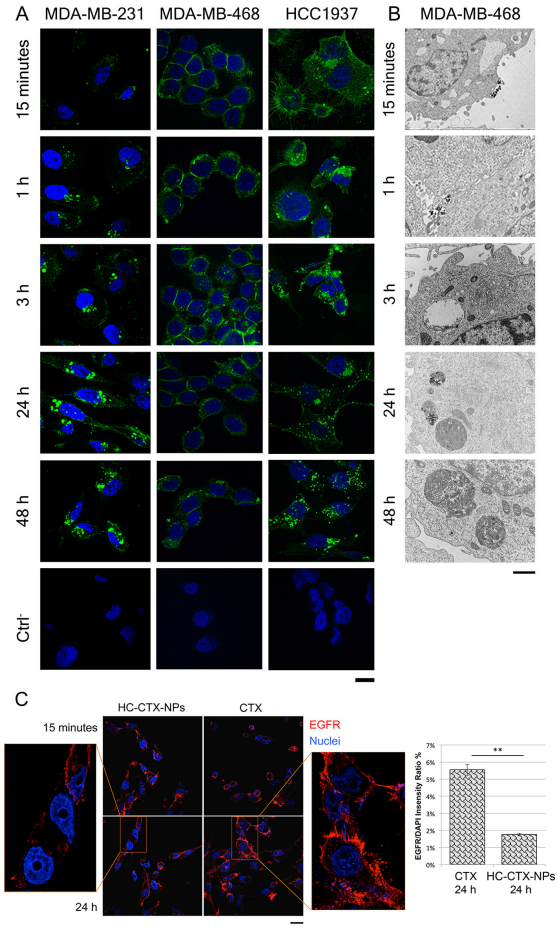

Figure 2. HC-CTX-NPs intracellular trafficking. A) Internalization of HC-CTX-NPs in TNBC cells. Confocal microscopy images of MDA-MB-231, MDA-MB-468, and HCC1937 incubated 15 min, 1, 3, 24, and 48 h at 37 °C in complete cell culture medium with HC-CTX-NPs (100 μg mL^{-1}). Nuclei were stained with DAPI (blue). CTX was recognized with anti-human secondary antibody conjugated with AF488 (green). Scale bar: 10 μm. B) Representative intracellular trafficking of HC-CTX-NPs in MDA-MB-468 cells by TEM. Scale bar: 1 μm. C) Magnification of HCC1937 cells treated with CTX or HC-CTX-NPs for 24 h. The quantification of EGFR in the nucleus was performed by the selection of cell nuclei as regions of interest (ROI) for the detection of the mean fluorescence intensity of EGFR (left). The quantification (right) revealed that cells treated with CTX for 24 h showed a 3.15-fold higher amount of EGFR in nuclei compared to cells treated with HC-CTX-NPs. Nuclei were stained with DAPI (blue), while EGFR was recognized by anti-EGFR antibody and labeled with an anti-rabbit secondary antibody conjugated with AF546 (red). Scale bar: 20 μm. Reported values are mean of measurement performed with ImageJ software on the nucleus of 20 different cells normalized to their areas ± s.e.

DOI: 10.1021/acs.bioconjchem.8b00667
Bioconjugate Chem. XXXX, XXX, XXX−XXX

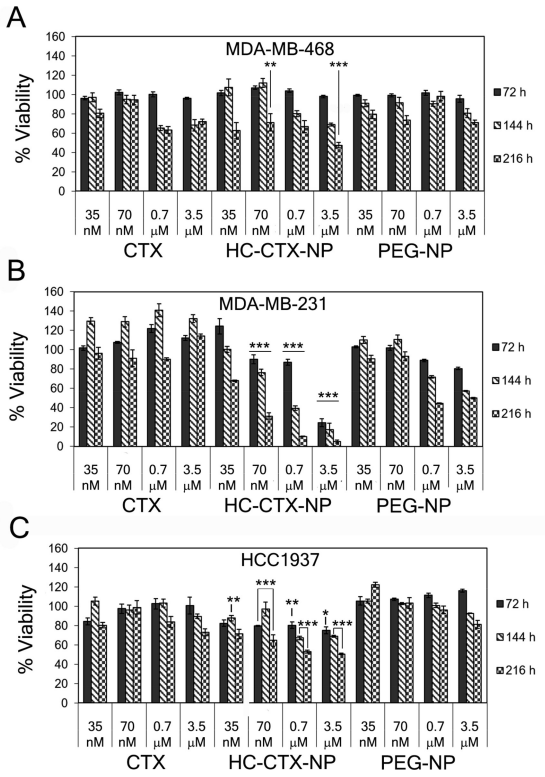

Figure 3. Antitumor activity in EGFR positive cells. Viability of TNBC cells treated with CTX, HC-CTX-NPs, or PEG-NPs. MDA-MB-468 (A), MDA-MB-231 (B), and HCC1937 (C) cells were treated with increasing concentration of CTX or HC-CTX-NPs (from 35 nM to 3.5 μM) up to 216 h. PEG-NPs were used as negative control. Viability was assessed by measuring the conversion of MTS into formazan. Reported values are the mean of six replicates ± s.e., normalized on cell proliferation of untreated cells, respectively. Statistical significance of HC-CTX-NPs vs free drug, $^{*}P < 0.05$; $^{**}P < 0.001$; $^{***}P < 0.0005$ (Student's t-test).

At 1 h, they were preferentially confined inside early endosomes, whereas after 3 h they were found progressively distributed within late endosomes, which induced the recruitment of lysosomes initiating the fusion processes. At longer time points, the NPs accumulated in mature lysosomes at least for 48 h, presumably inducing receptor degradation and preventing recycling of EGFR engaged in the complex formation with mAb nanoconjugate.

Enhanced Antitumor Activity of HC-CTX Conjugated to NPs in TNBC Cells. All TNBC cell lines were treated in parallel with HC-CTX-NPs and with CTX at increasing mAb concentrations between 35 nM and 3.5 μM and incubated for up to 216 h. Cells were also treated at lower CTX concentrations (down to 7 nM), but no antiproliferative effect was detected by viability assay based on tetrazolium salts (MTS). In general, MTS assay revealed that nanoconjugation had a remarkably higher impact on proliferation in all TNBC cell lines compared to unconjugated CTX, statistically significant at low dosages and longer times of incubation (Figure 3 and Figure S4). In detail, CTX alone weakly inhibited proliferation in MDA-MB-468 (PTEN-null, p53 mutant, BRCA1-wt) and MDA-MB-231 (PTEN-wt, p53 mutant, BRCA1-wt) only at high dosages (0.7 and 3.5 μM) and without apparent progression after 144 h. HC-CTX-NPs exhibited appreciable effect (40% viability loss) at concentration as low as 35 nM at 216 h in MDA-MB-468, showing a dose-dependent increase in activity reaching 53% viability loss at 3.5 μM (Figure 3A). Such increase in activity associated

DOI: 10.1021/acs.bioconjchem.8b00667
Bioconjugate Chem. XXXX, XXX, XXX−XXX

Scheme 2. Interactions of CTX or HC-CTX-NPs with EGFR Activation Pathways[a]

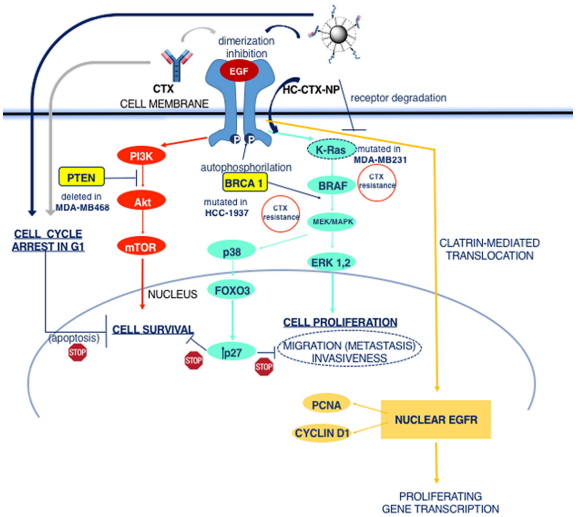

[a]PI3K/At and MAPK/ERK pathways are normally activated in TNBC cells either by interaction with EGF ligand or by EGFR autophosphorylation. Activated EGFR is partly translocated into the nucleus where it can exert aberrant functions inducing cell cycle deregulation, proliferation, migration, and apoptosis inhibition. CTX or HC-CTX-NP can interfere with these pathways in different ways depending on the specific molecular profiles associated with the three different cell types.

with nanoconjugation was recovered in MDA-MB-231 (Figure 3B). Paradoxically, the apparently higher activity observed in MDA-MB-231 compared to MDA-MB-468 cells could be explained in terms of lower EGFR expression. Indeed, cancer cell viability is affected by the extent of EGFR receptor internalization upon complexation with targeted antibodies.[50] In order to rule out the possible nonspecific contribution of NPs, we repeated the assay treating the cells with PEG-NPs. However, no apparent activity was recovered as compared to HC-CTX-NPs in these two cell lines. As expected, HCC1937 (PTEN-mutated, p53-null, BRCA1-mutated) cells proved highly resistant to CTX with minimal effect even at the highest concentrations. Surprisingly, HC-CTX-NPs showed statistically significant, progressive increase in cytotoxicity compared to CTX, already observed after 72 h (Figure 3C). Such a potent activity could not be ascribed to a sensitivity of HCC1937 to colloidal NPs, as confirmed by viability experiment using PEG-NPs (Figure 3C). Hence, this result should be attributed to CTX nanoconjugation, which advocated a role of long-lasting receptor sequestration by means of the EGFR/HC-CTX-NPs complex through the endolysosomal route. We initially interpreted this effect in terms of possible EGFR degradation, as also observed using entire antibodies.[30] Uptake kinetics analyzed by confocal microscopy (Figure 2A) and ultrastructural analysis by TEM (Figure 2B) showed prolonged residence of the antibody nanoconjugate compartmentalized within the endolysosomal evolution pathway, supporting our preliminary hypothesis. Such receptor sequestration by means of the nanoconjugate reversed the resistance mechanism, which, in the absence of nanoconjugation, is otherwise exerted by BRCA1 mutation after EGFR autophosphorylation that initiates the RAS/MAPK signaling cascade (see Scheme 2).

It is worth noting that the nuclear fraction of EGFR in TNBC cells derives from trans-cytoplasmic migration of activated membrane EGFR. Nuclear EGFR was demonstrated to exert multiple functions in the nucleus, operating as a tyrosine kinase to activate the cyclin D1 and the proliferating cell nuclear antigen (PCNA), which promote the G1/S phase transition, and as a cotranscription factor for genes involved in cell proliferation and angiogenesis (see Scheme 2).[51,52] For this reason, nuclear localized EGFR was identified as an hallmark of disease progression, worse prognosis, and enhanced resistance to radiation, chemotherapy, and treatment with CTX. To explore the hypothesis that HC-CTX-NPs could interfere with nuclear translocation of activated EGFR, we performed immunofluorescence analysis of EGFR localization in HCC1937 cells treated with CTX or HC-CTX-NPs. Confocal images acquired at 15 min, 1, 3, and 24 h post-treatment, corresponding to maximal EGFR localization into endosomes (15 min) and to expected recycling time (3 to 24 h),[53] showed a progressive EGFR degradation over time in samples treated with HC-CTX-NPs compared to those treated with CTX, thus preventing receptor recycling (Figure S5). Importantly,

DOI: 10.1021/acs.bioconjchem.8b00667
Bioconjugate Chem. XXXX, XXX, XXX−XXX

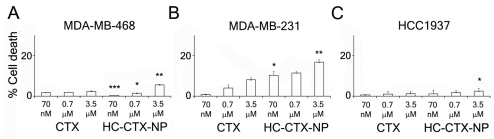

Figure 4. HC-CTX-NPs induce cell death in TNBC cells. Cell death assay of MDA-MB-468 (A), MDA-MB-231 (B), and HCC1937 (C) cells was incubated at 37 °C for 24 h with 70 nM, 0.7 and 3.5 μM of CTX or HC-CTX-NPs. Untreated cells were used as negative control to set region of analysis. Reported values represent the mean ± s.e. of three replicates. Statistical significance of HC-CTX-NPs vs free drug, $*P < 0.05$; $**P < 0.001$; $***P < 0.0005$ (Student's *t*-test).

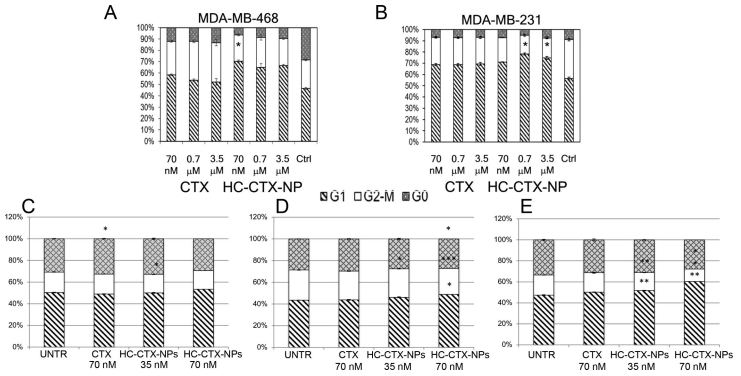

Figure 5. HC-CTX-NPs impact on cell cycle of TNBC cells. MDA-MB-468 (A) and MDA-MB-231 (B) cells were incubated at 37 °C for 24 h with 70 nM, 0.7 and 3.5 μM of CTX or HC-CTX-NPs. Then, cells were processed for flow cytometry and stained with propidium iodide. Untreated cells were used as controls. Graphs represented the mean percentage of events in G1, S, and G2/M phases, respectively, ± s.e. ($n = 3$). Statistical significance of CTX vs HC-CTX-NPs, $*P < 0.05$ (Student's *t*-test). In addition, HCC1937 cells were incubated at 37 °C with 70 nM of CTX or 35 nM and 70 nM of HC-CTX-NPs for 24 h (C), 48 h (D), and 72 h (E). Cells were processed as described for panels A and B. Statistical significance of CTX or HC-CTX-NPs vs UNTR, $*P < 0.05$; $**P < 0.01$; $***P < 0.001$ (Student's *t*-test).

quantitative analysis of nuclear EGFR revealed that levels of EGFR in nuclei of cells treated with HC-CTX-NPs were 3.15-fold lower than those of cells treated with unconjugated CTX (Figure 2C and Figure S5). Hence, a comprehensive explanation for the observed inhibition of cancer proliferation in BRCA1-mutated TNBC cells resided in the stable complexation of EGFR by HC-CTX-NPs, which resulted in receptor downregulation and prevented EGFR nuclear translocation through its sequestration into the endolysosomal pathway.

Impact of CTX Nanoconjugation on TNBC Cells Apoptosis and Cell Cycle. With the aim to investigate the mechanism of action of HC-CTX-NPs in the different TNBC cell lines, we first analyzed the early apoptotic effect of nanoconjugate compared to CTX at 24 h. Flow cytometry allowed us to monitor phosphatidylserine reversal in the plasma membrane mediated by apoptosis through a quantitative affinity assay using Annexin-V-pE-Cy5.5 exposure on cell surface.[54] Figure 4A shows a 2.5-fold increase in apoptosis in MDA-MB-468 cells from both CTX and HC-CTX-NPs at 0.7 μM compared to untreated cells, on the same levels reported for CTX alone in previous studies.[19] However, a significant increase in intracellular activity of HC-CTX-NPs (7.5-fold relevant to untreated cells) compared to CTX (3-fold relevant to control) could be appreciated at 3.5 μM. This value was even higher than the apoptotic effect of CTX alone previously documented at 10 μM after 48 h.[19] Once again, the remarkable increase in proapoptotic activity of HC-CTX-NPs over CTX could be attributed to an alteration of the recycling process caused by mAb nanoconjugation. Similarly, a 2-fold increase in apoptotic activity of HC-CTX-NPs compared to CTX was recovered in MDA-MB-231 cells (Figure 4B). An absolute value around 16% cell death at 3.5 μM HC-CTX-NPs, 2-fold higher than in MDA-MB-468 cells, could be interpreted in terms of higher impact of the treatment due to lower EGFR expression, the same effect observed in viability assays.[50] In contrast, HC-CTX-NPs did not exhibit significant proapoptotic activity in strongly resistant HCC1937 cells (Figure 4C), corroborating the hypothesis that the antiproliferative effect observed in viability assay in BRCA1-mutated cells could not be attributed to a mAb involvement in an apoptotic pathway of the nanoconjugate.

In breast cancer, G1 cell phase progression into S phase is dependent on the activation of cyclin-dependent kinases,

DOI: 10.1021/acs.bioconjchem.8b00667
Bioconjugate Chem. XXXX, XXX, XXX−XXX

including CDK4/6,[55] by complexation with nuclear cyclin D1 and regulated by growth factors and intracellular checkpoints.[50] Deregulation of G1/S transition in TNBC is usually associated with cyclin D1 overexpression, which is activated by interaction of nuclear EGFR.[52] This process can be reversed reducing EGFR levels in the nucleus resulting in cell cycle arrest in G0/G1. In addition, there is evidence that apoptosis induced by inhibition of EGF ligand interaction with EGFR is normally associated with cell cycle arrest in various cancer cell lines, including TNBC,[19] implicating upregulation of kinase inhibitory protein $p27^{KIP1}$.[50,55] In this light, increased levels of $p27^{KIP1}$ correlate with a blockade of EGF/EGFR signal transduction, also associated with cell cycle arrest in G1. Thus, to confirm the direct involvement of conjugated HC-CTX in the increased activity of HC-CTX-NPs over CTX alone inferred by MTS and apoptosis assays, we analyzed the effect of treating TNBC cells with HC-CTX-NPs or CTX on cell cycle (Figure 5). Our data demonstrated that HC-CTX-NPs were more efficient in inducing cell cycle arrest in G1 decreasing the cell population in S-phase in MDA-MB-468 cells compared to free CTX, remarkably higher than untreated cells even at the lowest concentration tested (Figure 5A). In MDA-MB-231 cells, HC-CTX conjugation to NPs showed an appreciable increase in the G1/S phase ratio compared to CTX only at high concentration (Figure 5B). As expected, cell cycle in HCC1937 cells was unaffected by CTX at the highest concentration, consistent with the results from apoptosis assay. However, while no significant effect was recovered within the first 24 h, HC-CTX-NPs were able to induce statistically significant dose- and time-dependent arrest in G0/G1 phase in these cells at longer times (Figure 5C-E). Cell cycle experiment conducted using PEG-NPs ruled out a possible contribution of the NPs alone (Figure S6). Altogether, these results are important in view of a definition of the action mechanism of HC-CTX-NPs. Indeed, cell cycle arrest in G1 phase is presumed to occur in response to DNA damage associated with cyclin transcription caused by constitutive activation of ERK1/2 genes.[19] Thus, inhibition of G1/S phase transition normally associated with ERK1/2 activation represents a marker of TNBC cell sensitivity to CTX, confirming the direct involvement of HC-CTX in the apoptotic activity of HC-CTX-NPs in BRCA1-wt MDA-MB-468 and MDA-MB-231 cells, and the key role of HC-CTX-NPs in reducing nuclear EGFR levels in BRCA1-mutated HCC1937 cells.

Blockade of Site-Specific EGFR Phosphorylation upon Exposure to HC-CTX-NPs. The levels of total and activated (i.e., phosphorylated) EGFR were assessed by Western blotting in the three TNBC cell lines, using α-tubulin as a housekeeping reference for normalization (Figure 6).

Autophosphorylation of Y1068 tyrosine residue in the kinase domain of EGFR represents the initiation event of a signaling cascade resulting in activation of transcriptional regulation of genes involved in cell proliferation, survival, and drug resistance.[47] MDA-MB-468 cells revealed an increase in Y1068 phosphorylation in untreated samples, confirming the role of EGFR autophosphorylation in activating the PI3K/Akt and RAS/MAPK downstream signaling pathways in this cell line associated with PTEN deletion (see Scheme 2).[49] Results from the treatment of TNBC cell lines with 0.2, 2, or 20 μg mL^{-1} unconjugated CTX or nanoconjugated HC-CTX evidenced that only HC-CTX-NPs in MDA-MB-468 cells was able to reduce the Y1068 phosphorylation levels in EGFR,

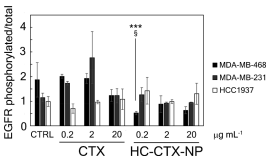

Figure 6. HC-CTX-NPs block EGFR-Y1068 phosphorylation in TNBC cells. MDA-MB-468, MDA-MB-231, and HCC1937 cells were treated with increasing concentrations of CTX or HC-CTX-NPs (0.2, 2, and 20 μg mL^{-1} CTX) in starvation medium for 24 h. Untreated cells were used as negative control. At the end of incubation, cells were lysed and subjected to Western blot analysis, and the ratio of phosphorylated/total EGFR was quantified by densitometry using ImageJ Software. Reported values are the mean of 6 samples ± s.e. Statistical significance vs CTX, $*P < 0.05$, $**P < 0.01$, $***P < 0.005$ (Student's *t*-test). Collected p-values are reported in Table S1.

especially at low concentrations, whereas the other two cell lines were almost completely unaffected. We were not surprised of the maintenance of phosphorylated EGFR levels in the two CTX-resistant TNBC cell lines, especially HCC1937, in which BRCA1 mutation is responsible for inducing stable overexpression of activated cytosolic EGFR and constitutive enhancement of EGFR nuclear translocation even in the absence of EGF.[48] Collectively, these results suggested a function of conjugated HC-CTX underlying the inhibitory activity of EGFR pathway by HC-CTX-NPs in CTX-sensitive TNBC cells.

Increase of p38 Phosphorylation. To confirm the mechanism of cytostatic activity of conjugated HC-CTX, we explored the incidence of HC-CTX-NPs interaction with TNBC cells on the RAS/MAPK downstream key pathway of EGFR. There is strong evidence in support of the role played by the RAS/MAPK signaling pathway in cell proliferation and apoptosis prevention.[56] Although the downstream cellular targets of CTX are not fully characterized, CTX was recently demonstrated to activate the transcription factor FOXO3a promoting its nuclear translocation through the MAPK p38 phosphorylation. As a result of this process, it has been proposed that an involvement of the upregulation of $p27^{KIP1}$ and BIM target genes would lead to apoptosis induction and proliferation inhibition.[57] Thus, we decided to determine the extent of nuclear p38 phosphorylation upon treatment with HC-CTX-NPs (Figure 7). HC-CTX-NPs induced potentiated p38 activation in sensitive MDA-MB-468 cells, confirming that nanoconjugation improved the effect of CTX in these cells. CTX alone exhibited a more pronounced effect in mildly resistant MDA-MB-231 cells compared to sensitive cells. However, HC-CTX-NPs did not affect p38 phosphorylation in these cells, suggesting a different antiproliferative mechanism not involving FOXO3a activation. Inertness of HCC1937 cells toward p38 activation using HC-CTX-NPs confirmed the refractory behavior of these TNBC cells, in line with the results obtained with CTX, excluding also the involvement of this alternative pathway in the observed antiproliferative activity.

HC-CTX-NPs Are Capable To Promote ADCC in TNBC Cells. Besides a well-documented cytostatic efficacy associated with the intracellular inhibitory activity of CTX, the immunologic implications of antineoplastic efficacy of this mAb have been poorly explored. A few seminal works

DOI: 10.1021/acs.bioconjchem.8b00667
Bioconjugate Chem. XXXX, XXX, XXX−XXX

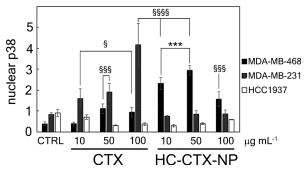

Figure 7. HC-CTX-NPs treatment increase p38 phosphorylation and its nuclear translocation in sensitive TNBC cells. MDA-MB-468, MDA-MB-231, and HCC1937 cells were treated with increasing concentration of CTX or HC-CTX-NPs (10, 50, and 100 μg mL^{-1} CTX) in starvation medium for 24 h. Untreated cells were used as negative control. At the end of incubation, nuclei were purified, lysed, and subjected to Western blot, and the amount of nuclear phosphorylated p38 was quantified by densitometry using ImageJ Software. Reported values are the mean of 6 samples ± s.e. Statistical significance vs CTRL, §P < 0.05, §§P < 0.01, §§§P < 0.005, §§§§P < 0.0005; vs CTX, *P < 0.05, **P < 0.01, ***P < 0.005, ****P < 0.0005 (Student's t-test). Collected p-values are reported in Table S2.

exploiting CTX for ADCC against lung cancer cell lines or nontumor EGFR-transfected cell lines have been carried out. The results of these studies suggested that CTX could be effective in activating the ADCC mechanism toward target cells using fresh peripheral blood mononuclear cells (PBMCs) at CTX concentration as low as 0.25 μg mL^{-1}, involving the recruitment of cytotoxic host effector cells such as monocytes and natural killer (NK) cells.[58,59]

In our study, the three selected TNBC cell lines were treated with isolated PBMCs, containing around 5% NK cells in each sample, at an effector-to-target cell (E:T) ratio of 20:1 or 40:1. PBMCs were activated for ADCC using either CTX at increasing concentrations (0.5, 10, or 20 μg mL^{-1}) or 5 μg mL^{-1} HC-CTX-NPs. Although dosages usually reported in the literature are in the range 10−20 μg mL^{-1}, unexpectedly we found that the best performing concentration for unconjugated CTX was 0.5 μg mL^{-1}. Considering that the average antibody density was 5 HC-CTX per NP corresponding to about 1/10 of the overall NP weight, we could conclude that the mAb concentration used in the experiment with HC-CTX-NPs was comparable to 0.5 μg mL^{-1} CTX in terms of mAb concentration. Free nonspecific IgG and HC-IgG-NPs were used as negative controls to investigate the contribution of the Fc fragment interaction with CD16a on NK cells in the absence of antibody binding with target receptor on cancer cells. In addition, PEG-NPs were also evaluated to assess the possible interference of NPs alone with ADCC assay. MDA-MB-468 cells proved to be sensitive to ADCC in the presence of CTX, showing a 24% and 75% cell death at E:T of 20:1 and 40:1, respectively, as determined by Lactate Dehydrogenase

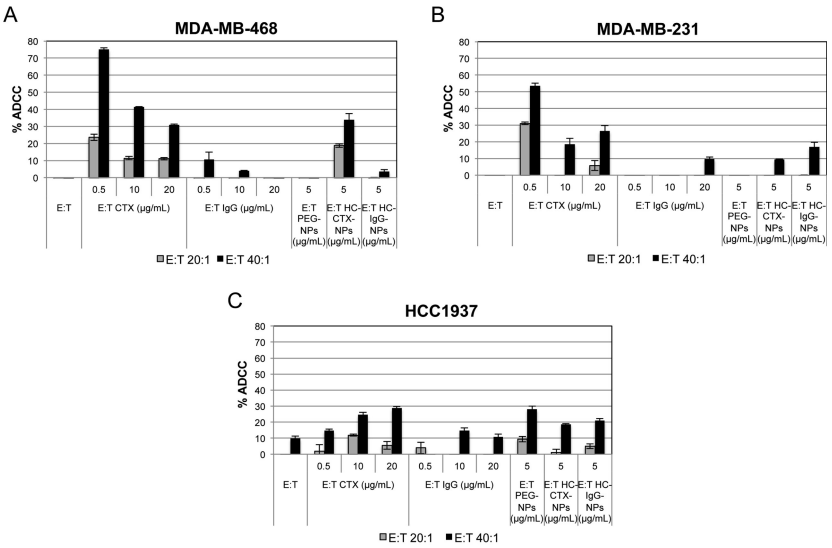

Figure 8. ADCC response induced by HC-CTX-NPs treatment on TNBC cells. MDA-MB-468 (A), MDA-MB-231 (B), and HCC1937 (C) cells were precoated with 0.5, 10, or 20 μg mL^{-1} of CTX or nonspecific IgG and with 5 μg mL^{-1} of HC-CTX-NPs at 37 °C for 30 min. Next, IL-2-activated PBMCs were added to the target cells and incubated at 37 °C for 4 h. The amount of LDH released by target cells revealed the ADCC response induced by treatment. Graphs represent the mean percentage of ADCC ± s.e. (n = 3). Statistical significance of CTX or HC-CTX-NPs vs E:T, *P < 0.05; **P < 0.01; ***P < 0.001 (Student's t-test).

DOI: 10.1021/acs.bioconjchem.8b00667
Bioconjugate Chem. XXXX, XXX, XXX−XXX

(LDH) assay at 0.5 μg mL^{-1} and 12% and 40%, respectively, at 10 μg mL^{-1}. HC-CTX-NPs exhibited an efficiency around 20% at 20:1 E:T and 40% at 40:1, showing good efficiency in activating ADCC compared to the therapeutic antibody alone (Figure 8A). We were surprised of this unprecedented result for several reasons. CTX was presented on NPs in an appropriate arrangement for binding to the EGFR target receptor; however, the Fcγ portion responsible for activation of CD16a on NK cells was expected to be obstructed by nanoconjugation. In addition, it is a common belief that a whole Fcγ fragment is necessary for optimal binding with CD16a, while in our study only half chains were available on the surface of the interacting NPs. Therefore, it is plausible that the unpredicted ADCC efficacy promoted by HC-CTX-NPs could be at least partly attributable to the multivalent presentation of HC-CTX that was able to amplify NK activation triggering ADCC response. In contrast to CTX and its nanoconjugate, control IgG, HC-IgG-NPs, and PEG-NPs at relevant concentrations did not activate ADCC in these cells. CTX exhibited good activity (around 54% at 40:1 E:T) also in MDA-MB-231, although less effective than MDA-MB-468, while giving inconsistent results at higher concentrations. However, HC-CTX-NPs exhibited only a negligible effect below 10%, on the same level of control IgG, HC-IgG-NPs, and PEG-NPs (Figure 8B). This result suggested that nanoconjugation was able to maintain the ADCC efficiency only in selected malignant cells expressing high EGFR levels. HCC1937 showed mild activation of ADCC by both CTX and HC-CTX-NPs compared to control IgG and HC-IgG-NPs. However, LDH levels were not significantly higher than PEG-NPs (Figure 8C).

DISCUSSION

In this study, we have developed therapeutic antibody nanoconjugates consisting of colloidally stable polymer-coated iron oxide nanoparticles decorated with CTX. The resulting mAb-functionalized NPs were used to investigate the impact of nanoconjugation on the therapeutic efficacy of CTX in TNBC cells. Although entire mAbs could be used for conjugation in principle,[30] our choice here was to conjugate half-chain CTX to colloidal NPs with the aim to improve the chemical-physical properties of the nanoconjugates, particularly in terms of colloidal stability in biological media, and to take advantage of the improved circulation half-life and targeting efficiency compared to whole antibody nanoconjugates in view of future in vivo experiments.[27] However, the use of half-chain antibodies raised several questions relating to the therapeutic effectiveness of nanoconjugates, both in terms of maintenance of mAb efficacy in actively interfering with signaling transduction pathways of cancer cells and of their capability to promote ADCC response, which are putatively considered the two main mechanisms of antitumor activity of therapeutic CTX. For this study, we have selected three representative cell lines, all derived from high grade human tumors with histologic features typical of TNBC, differing in the characteristic molecular profiling. We focused our investigation on EGFR amplification along with KRAS, PTEN, and BRCA1 mutations, associated with different sensitivity to CTX treatment. Phosphatase and tensin homologue (PTEN) protein represents the main tumor suppressor regulating the PI3K/Akt survival pathway of cancer cells, so that its deletion in MDA-MB-468 cells results in inhibition of apoptotic processes,[60] which however can be re-established by tyrosine kinase phosphorylation blockade making these cells sensitive to treatment with CTX. RAS mutation is responsible for resistance in MDA-MB-231 cells and is normally associated with resistance to matrix deprivation-induced apoptosis (anoikis), which is a crucial process that promotes cell growth independent of extracellular matrix anchorage, leading to enhanced metastatic and invasive character in cancer cells.[61] On the other hand, BRCA1 oncogene expression rather than mutation or deletion was reported to correlate with EGFR expression and functionality. In HCC1937 cells, BRCA1 mutation resulted in intrinsically high levels of nuclear EGFR leading to cyclin D1 activation associated with G1/S transition-dependent overproliferation.[48]

HC-CTX-NPs were not intrinsically cytotoxic, consistent with the data from the literature referred to CTX alone.[14,30] However, our results demonstrated that HC-CTX-NPs were able to inhibit CTX-sensitive MDA-MB-468 and resistant MDA-MB-231 proliferation more pronouncedly than unconjugated CTX but could also alter the viability in HCC1937 cells, suggesting a role of nanoconjugation in interfering with strong resistance to CTX associated with BRCA1 mutations in HCC1937. This result was unpredicted considering that BRCA1-deficient cells used to exhibit increased Y1068 autophosphorylation in EGFR, responsible for mediating the interaction of EGFR with Grb2 resulting in activation of RAS/MAPK cascade.[50] The extent of antiproliferative activity of HC-CTX-NPs in MDA-MB-468 and MDA-MB-231 cells reflected their effect on cell cycle and proliferation,[19] thus proving that the functionality causing the cytostatic activity of the nanoconjugate was indeed the HC antibody fragment. We were surprised to notice higher persistent antitumor efficacy of HC-CTX-NPs compared to therapeutic CTX, which could be ascribed to an alteration of the receptor recycling process usually permitted both with EGF affinity ligand and with anti-EGFR antibodies.[62] The observed increase in activity of HC-CTX-NPs was also corroborated by solid evidence of their capability to interfere with downstream signaling pathways of EGFR involved in cell cycle regulation. In particular, only MDA-MB-468 cells treated with HC-CTX-NPs exhibited decreased levels of Y1068 phosphorylation in EGFR, affecting PI3K/Akt and RAS/MAPK downstream signaling pathways consistent with p38 activation in sensitive cells. These results substantiate the hypothesis that HC-CTX nanoconjugation amplifies the effect of CTX proapoptotic molecular mechanism in TNBC cells. Indeed, p38 can regulate the transcription factor FOXO3a phosphorylation in wild-type KRAS cancer cells contributing to its nuclear localization and activation,[63] bypassing the inhibition by the PI3K/Akt and MAPK/ERK pathways.[64,65] FOXO3a nuclear localization and activation promotes cell cycle arrest and apoptosis through p27^{KIP1} upregulation.[66] Different from unconjugated CTX, cell cycle in HCC1937 cells was significantly affected by treatment with HC-CTX-NPs, supporting our conclusion that the significant decrease in proliferation of this strongly refractory cell line was mainly attributable to EGFR-nanocomplex formation, blocking the fast receptor recycling and preventing its nuclear translocation, rather than to direct inhibition of the PI3K/Akt pathway.

Scheme 2 recapitulates the complex network of interactions of the PI3K/Akt and MAPK/ERK pathways regulating cell survival and proliferation, which are actively interfered by HC-CTX-NPs in the three different TNBC cell lines. Under aberrant conditions associated with cancer progression,

DOI: 10.1021/acs.bioconjchem.8b00667
Bioconjugate Chem. XXXX, XXX, XXX−XXX

binding of EGF ligand to EGFR triggers receptor dimerization and phosphorylation leading to activation of PI3K/Akt and RAS/MAPK pathways resulting in increased cell survival and proliferation, respectively. Indeed, enhancement of PI3K/Akt pathway localizes Akt in the plasma membrane,[67] leading to $p27^{KIP1}$ inhibition and FOXO3a confinement in the cytoplasm.[68] PI3K/Akt pathway is regulated by PTEN, while BRCA1 contributes in controlling MAPK/ERK signaling cascade and in increasing expression and nuclear localization of activated EGFR. CTX binding to the extracellular domain of EGFR in TNBC cells interferes with receptor homo- and heterodimerization and inhibits the intracellular tyrosine kinase domain at Y1068 resulting in increased apoptosis.[19] In addition, CTX promotes p38 phosphorylation that leads to FOXO3 phosphorylation and nuclear translocation inducing $p27^{KIP1}$ upregulation, which results in decreased invasiveness and metastasis of cancer cells.[57] However, BRCA1 mutation activates Y1068 autophosphorylation conferring HCC1937 cells resistance to CTX.[48] In this picture, HC-CTX-NPs were able to exert multiple action by 1) re-establishing apoptotic events exploiting cell cycle arrest in G1 even under PTEN deletion, such as in MDA-MB-468 cells, reflecting the mechanism of CTX action and 2) allowing MAPK pathway-mediated inhibition of cell proliferation and migration also in BRCA1 mutated TNBC cells that are normally nonresponsive to CTX, by exploiting the beneficial effect of nanoconjugation in inducing EGFR degradation preventing its fast recycling, which resulted in a decrease of nuclear EGFR levels. On these bases, we are able to offer a comprehensive interpretation for the therapeutic effect of HC-CTX-NPs also in strongly resistant TNBC cells, which could be achieved exclusively through antibody nanoconjugation. Hence, our results allowed us to propose HC-CTX-NPs as a promising nanodrug suitable for widening the spectrum of TNBC responder patients.

Finally, the conjugation of HC-CTX to NPs did not negatively affect the antibody efficiency in promoting the PBMC-mediated ADCC response showing antitumor activity and improved selectivity toward CTX-sensitive TNBC cells, which is of great relevance in view of a future clinical translation. In conclusion, the results of our study provide robust evidence of the potential of compact HC-CTX-NPs in the treatment of TNBC, which could offer new therapeutic options for this highly aggressive life-threatening disease. Future directions of this work will be aimed to compare the results of this study with nanoconjugates bearing entire antibodies and to explore the effects of combining HC-CTX-NPs with conventional chemotherapy in vitro and in vivo.

METHODS

Synthesis and Characterization of Nanoparticles. All HC-mAb-NPs used in this study were synthesized following the protocol that we have previously published.[27] Briefly, mAb (CTX or IgG) dissolved in EDTA−PBS buffer (1 mg mL^{-1}) was added to the 2-mercaptoethanolamine kit (MEA, Thermo Fisher Scientific) in order to obtain thiol groups from the disulfide bridges reduction between the two heavy chains of the mAb (HCs). HCs were rapidly added to PDP-NPs (1 mg) and incubated 1 h at room temperature (RT). Nanoparticles surface was saturated with PEG_{500}-SH. The reagents excess was removed by dialysis, and HC-mAb-NPs were collected. PEG-NPs, used as control, were prepared incubating 1 mg of PDP-NPs with an excess of PEG_{500}-SH according to the protocol above. Hydrodynamic size and surface charge of HC-CTX-NPs were measured using a Malvern Zetasizer Nano ZS ZEN3600 (Worcestershire, UK). The measurements were performed in triplicate after dilution with Milli-Q water. SDS-PAGE electrophoresis was carried out using a 12% running gel and a 4% stacking gel and run for 2 h at 20 mA with a pH 8.3 running buffer (Buffer 10X: 1 L of deionized water, 30.28 g of Tris HCl, 144 g of glycine, final concentration SDS 0.1%). Proteins were revealed by Coomassie staining (Imperial protein staining, Euroclone).

Cell Culture. MDA-MB-468 and BT-474 cells were cultured in Dulbecco's Modified Eagle's Medium High Glucose (DMEM), supplemented with 10% FBS, L-glutamine (2 mM), penicillin (50 UI mL^{-1}), and streptomycin (50 mg mL^{-1}). MDA-MB-231 and HCC1937 cells were cultured in MEM Medium or in RPMI 1640 medium supplemented with 10% FBS, 2 mM L-glutamine, penicillin (50 UI mL^{-1}), and streptomycin (50 mg mL^{-1}), respectively. All cell lines grew at 37 °C and 5% CO_2 in a humidified atmosphere and were subcultured prior to confluence using trypsin/EDTA. Buffers, chemicals, and plastic disposables for cell culture were purchased from Euroclone.

EGFR Expression. MDA-MB-231, MDA-MB-468, HCC1937, and BT-474 cells (5×10^5) were immunodecorated in FACS tubes with cetuximab (CTX, 1 μg/tube) in phosphate buffer saline (PBS), 2% bovine serum albumin (BSA; Sigma), and 2% goat serum (Euroclone) for 30 min at room temperature (RT). Then, cells were washed thrice with PBS and immunodecorated with AlexaFluor488 (AF488) goat anti-human secondary antibody (1 μL/tube; Thermo Fischer Scientific) in PBS, 2% BSA, and 2% goat serum for 30 min at RT. After three washes with PBS cells were analyzed by a CytoFLEX flow cytometer (Beckman Coulter). 20,000 events were acquired for each analysis, after gating on viable cells and on singlets. A sample of cells immunodecorated with the secondary antibody only was used to set the region of positivity.

Cell Binding Assay. MDA-MB-231, MDA-MB-468, HCC1937, and BT-474 cells were seeded at a concentration of 2.5×10^5 cells/well. The day after, cells were incubated 1 h at 37 °C in culture medium supplemented with 5, 10, and 50 μg mL^{-1} of HC-CTX-NPs or HC-IgG-NPs. After incubation, cells were incubated in phosphate buffer (PBS), 2% Bovine Serum Albumin (BSA; Sigma), and 2% goat serum (Euroclone) for 15 min at RT. Then, cells were immunodecorated with AF488 antibody (1 μL/tube; Thermo Fischer Scientific) in PBS, 2% BSA, and 2% goat serum for 30 min at RT. AF488 anti-human and AF488 anti-rabbit antibodies have been used for samples treated with HC-CTX-NPs and HC-IgG-NPs, respectively. After three washes with PBS cells were analyzed by a CytoFLEX flow cytometer (Beckman Coulter). 20,000 events were acquired for each analysis, after gating on viable cells and on singlets. Samples of cells immunodecorated with the secondary antibodies only were used to set the regions of positivity.

Competition Assay. MDA-MB-231, MDA-MB-468, HCC1937, and BT-474 cells (5×10^5) were transferred in FACS tubes and washed twice with PBS. Then, cells were incubated with 10 μg mL^{-1} of HC-CTX-NPs labeled with FITC with or without CTX as competitor (1 mg mL^{-1}, 1 mL) in PBS supplemented with 2% BSA at 37 °C for 30 min. Cells were washed thrice and resuspended in PBS (500 μL) and analyzed by a CytoFLEX flow cytometer (Beckman Coulter). 10,000 events were acquired for each analysis, after gating on

DOI: 10.1021/acs.bioconjchem.8b00667
Bioconjugate Chem. XXXX, XXX, XXX−XXX

washed three times with TBS with 0.1% Tween 20 and reacted 1 h with the secondary antibody anti-rabbit conjugated with horseradish peroxidase (1:5000; Abcam). The bound antibody was revealed using ECL star reagent (Euroclone), and the chemiluminescence signal was detected using the Chemidoc System (Biorad). Then, EGFR Y1068 pho was stripped, and the membrane was blocked in 5% BSA in TBS with 0.1% Tween 20 for 1 h. For evaluation of total EGFR, the membrane was incubated 2 h with rabbit-polyclonal antibody against EGFR (EGFR (1005): sc-03; Santa Cruz) at 1:1000 dilution. The membranes were washed three times with TBS with 0.1% Tween 20, reacted 1 h with the secondary antibody anti-rabbit conjugated with horseradish peroxidase (1:5000; Abcam), and revealed as described above.

CTX-Mediated p38 Phosphorylation. Five × 10^5 cells were seeded in a 6-wells plate the day before. Cells were treated for 24 h with increasing concentration of CTX free or immobilized in HC-CTX-NPs (10, 50, and 100 μg mL^{-1}) in starvation medium. Negative control was represented by untreated cells. At the end of incubation, cells were washed with ice cold PBS, detached with Trypsin-EDTA, and harvested by centrifugation. Then, the pellet was resuspended in 100 μL of lysis buffer (10 mM Hepes pH 7.5, 10 mM KCl, 0.1 mM EDTA, 1 mM DTT, 0.5% NP-40, 1 mM Na_3VO_4, 10 mM NaF, Protease Inhibitor Cocktail, 0.5 mM PMSF) and incubated 20 min at 4 °C. Then, cells were vortexed and centrifuged 10 min at 12000 × g at 4 °C. The supernatants were collected and stored as cytoplasmic extracts. The pellet was washed thrice with lysis buffer, resuspended in 60 μL of nuclear extraction buffer (20 mM Hepes pH 7.5, 400 mM NaCl, 1 mM EDTA, 1 mM DTT, 1 mM PMSF, 1 mM Na_3VO_4, 10 mM NaF, Protease Inhibitor Cocktail), and incubated 30 min at 4 °C. Then, the samples were centrifuged 15 min at 12000 × g at 4 °C. The supernatant was collected as nuclear extract and processed for SDS-PAGE. Samples were separated by SDS-PAGE and transferred onto PVDF membrane. The membrane was blocked in 5% BSA in TBS for 1 h. For evaluation of phosphorylated p38, the membrane was incubated 2 h with rabbit-monoclonal antibody against phospho-p38 MAP kinase (Y180/Y182) (#9211; Cell Signaling) at 1:1000 dilution in 5% BSA in TBS with 0.1% Tween 20 for 1 h. The membranes were washed three times with TBS with 0.1% Tween 20 and reacted 1 h with the secondary antibody anti-rabbit conjugated with horseradish peroxidase (1:5000; Abcam) or with the secondary antibody anti-mouse conjugated with horseradish peroxidase (1:5000; Abcam), respectively. The bound antibody was revealed using ECL star reagent (Euroclone), and the chemiluminescence signal was detected using the Chemidoc System (Biorad).

Effector Cells Isolation. Peripheral blood mononuclear cells (PBMCs) were obtained by centrifugation on Ficoll−Paque of blood samples from a healthy donor (30 min at 1,500 rpm without brakes). At the end the PBMC layer was carefully transferred to a new tube, diluted with PBS, and centrifuged for 6 min at 1,400 rpm. Then supernatant was eliminated to remove platelets, and the procedure was repeated four times decreasing the centrifugation speed up to 1,000 rpm. Washed PBMCs were resuspended in RPMI-1640 medium with 10% of decomplemented FBS and 1,000 U mL^{-1} IL-2 (BioLegend, San Diego, CA, USA) for 24 h at 37 °C. The described procedure was approved by the Ethical Committee of the University of Milano-Bicocca (prot. #351, 13th November 2017) after submission of the project together with the informed consent by the healthy volunteer.

ADCC Assay. ADCC was performed using CytoTox 96 Non-Radioactive Cytotoxicity Assay (Promega Corporation, Madison, WI, USA). Firstly, target cells, plated at a density of 5 × 103 in 96-well plates, were coated with increasing concentration of CTX and IgG (0.5, 10, and 20 μg mL^{-1}) and with 5 μg mL^{-1} of PEG-NPs, HC-CTX-NPS, and HC-IgG-NPS for 30 min at 4 °C in RPMI-1640 medium. After coating, IL-2-activated PBMCs were added onto target cells at an effector:target (E:T) ratio of 20:1 and 40:1 and incubated 4 h at 37 °C. Then LDH release from target cells was measured by an EnSight multimode plate reader (Perkin Elmer, Waltham, MA, USA) setting the absorbance wavelength at 490 nm. The percentage of ADCC was calculated using the formula following protocol instructions:

$$\%\ \text{Specific Lysis} = \frac{\text{Experimental} - \text{Effector Spontaneous} - \text{Target Spontaneous}}{\text{Target Maximum} - \text{Target Spontaneous}} \times 100$$

Statistical Analysis. Statistical analyses were conducted using two-tailed Student's *t*-test. All plots show mean values ± standard error (s.e.). All tests assumed normal distribution, and the statistical significance threshold was set at $P < 0.05$.

■ ASSOCIATED CONTENT

Supporting Information

The Supporting Information is available free of charge on the ACS Publications website at DOI: 10.1021/acs.bioconjchem.8b00667.

DLS profiles of nanoparticles (Figure S1); electrophoresis gel (Figure S2, SDS-PAGE of HC-CTX-NPs, PEG-NPs, and CTX); EGFR expression determined by flow cytometry (Figure S3); viability assays of TNBC cells treated with HC-CTX-NPs, PEG-NPs, and CTX (Figure S4); immunofluorescence analysis of HCC1937 cells treated with HC-CTX-NPs and CTX (Figure S5); cell cycle analysis using PEG-NPs (Figure S6); p-values (Tables S1 and S2) (PDF)

■ AUTHOR INFORMATION

Corresponding Authors

*E-mail: davide.prosperi@unimib.it.
*E-mail: serena.mazzucchelli@unimi.it.

ORCID

Davide Prosperi: 0000-0003-4577-9575

Present Address

⊥Clinica di Malattie dell'Apparato Respiratorio, IRCCS Fondazione Policlinico San Matteo, Pavia, Italy.

Author Contributions

M.C. and M.A.R. contributed equally. The manuscript was written through contributions of all authors. All authors have given approval to the final version of the manuscript.

Notes

The authors declare no competing financial interest.

■ ACKNOWLEDGMENTS

We especially thank Raffaele Allevi (University of Milano) for help with electron microscopy. This project was partly supported by the Fondazione Regionale per la Ricerca Biomedica of Regione Lombardia (FRRB to D.P. and F.C.),

DOI: 10.1021/acs.bioconjchem.8b00667
Bioconjugate Chem. XXXX, XXX, XXX−XXX

Cariplo Foundation (grant no. 2016-0886 to M.C.), Pediatric Clinical Research Center "Romeo ed Enrica Invernizzi" to S.M., and by Academic Funding Unimib 2018 to M.C.

REFERENCES

(1) Ehrlich, P. (1906). *Collected Studies on Immunity*; J. Wiley & Sons, New York.

(2) Chames, P., Van Regenmortel, M., Weiss, E., and Baty, D. (2009) Therapeutic antibodies: successes, limitations and hopes for the future. *Br. J. Pharmacol. 157*, 220−233.

(3) Reichert, J. M. (2017) Antibodies to watch in 2017. *mAbs 9*, 167−181.

(4) Weiner, L. M., Surana, R., and Wang, S. (2010) Monoclonal antibodies: versatile platforms for cancer immunotherapy. *Nat. Rev. Immunol. 10*, 317−327.

(5) Carter, P. J., and Lazar, G. A. (2018) Next generation antibody drugs: pursuit of the 'high-hanging fruit'. *Nat. Rev. Drug Discovery 17*, 197−223.

(6) Jubb, A. M., Oates, A. J., Holden, S., and Koeppen, H. (2006) Predicting benefit from anti-angiogenic agents in malignancy. *Nat. Rev. Cancer 6*, 626−635.

(7) Jubb, A. M., and Harris, A. L. (2010) Biomarkers to predict the clinical efficacy of bevacizumab in cancer. *Lancet Oncol. 11*, 1172−1183.

(8) Wang, C., Wang, J. Q., Zhang, X. D., Yu, S. J., Wen, D., Hu, Q. Y., Ye, Y. Q., Bomba, H., Hu, X. L., Liu, Z., et al. (2018) In situ formed reactive oxygen species-responsive scaffold with gemcitabine and checkpoint inhibitor for combination therapy. *Sci. Transl. Med. 10*, eaan3682.

(9) Foster, J. B., and Maude, S. L. (2018) New developments in immunotherapy for pediatric leukemia. *Curr. Opin. Pediatr. 30*, 25−29.

(10) Ansell, S. M., Lesokhin, A. M., Borrello, I., Halwani, A., Scott, E. C., Gutierrez, M., Schuster, S. J., Millenson, M. M., Cattry, D., Freeman, G. J., et al. (2015) PD-1 Blockade with nivolumab in relapsed or refractory Hodgkin's lymphoma. *N. Engl. J. Med. 372*, 311−319.

(11) Smaglo, B. G., Aldeghaither, D., and Weiner, L. M. (2014) The development of immunoconjugates for targeted cancer therapy. *Nat. Rev. Clin. Oncol. 11*, 637−648.

(12) Jonker, D. J., O'Callaghan, C. J., Karapetis, C. S., Zalcberg, J. R., Tu, D., Au, H.-J., Berry, S. R., Krahn, M., Price, T., Simes, R. J., et al. (2007) Cetuximab for the treatment of colorectal cancer. *N. Engl. J. Med. 357*, 2040−2048.

(13) Vermorken, J. B., Mesia, R., Rivera, F., Remenar, E., Kawecki, A., Rottey, S., Erfan, J., Zabolotnyy, D., Kienzer, H.-R., Cupissol, D., et al. (2008) Platinum-based chemotherapy plus cetuximab in head and neck cancer. *N. Engl. J. Med. 359*, 1116−1127.

(14) Meira, D. D., Nóbrega, I., de Almeida, V. H., Mororó, J. S., Cardoso, A. M., Silva, R. L., Albano, R. M., and Ferreira, C. G. (2009) Different antiproliferative effects of matuzumab and cetuximab in a431 cells are associated with persistent activity of the MAPK pathway. *Eur. J. Cancer 45*, 1265−1273.

(15) Sunada, H., Magun, B. E., Mendelsohn, J., and MacLeod, C. L. (1986) Monoclonal antibody against epidermal growth factor receptor is internalized without stimulating receptor phosphorylation. *Proc. Natl. Acad. Sci. U. S. A. 83*, 3825−3829.

(16) Li, S., Schmitz, K. R., Jeffrey, P. D., Wiltzius, J. J., Kussie, P., and Ferguson, K. M. (2005) Structural basis for inhibition of the epidermal growth factor receptor by cetuximab. *Cancer Cell 7*, 301−311.

(17) Wiley, H. S. (2003) Trafficking of the ErbB receptors and its influence on signaling. *Exp. Cell Res. 284*, 78−88.

(18) Van Cutsem, E., Köhne, C.-H., Hitre, E., Zaluski, J., Chien, C.-R. C., Makhson, A., D'Haens, G., Pintér, T., Lim, R., Bodoky, G., et al. (2009) Cetuximab and chemotherapy as initial treatment for metastatic colorectal cancer. *N. Engl. J. Med. 360*, 1408−1417.

(19) El Guerrab, A., Bamdad, M., Kwiatkowski, F., Bignon, Y.-J., Penault-Llorca, F., and Aubel, C. (2016) Anti-EGFR monoclonal antibodies and EGFR tyrosine kinase inhibitors as combination therapy for triple-negative breast cancer. *Oncotarget 7*, 73618−73637.

(20) Weiner, G. J. (2015) Building better monoclonal antibody-based therapeutics. *Nat. Rev. Cancer 15*, 361−370.

(21) Montagut, C., Dalmases, A., Bellosillo, B., Crespo, M., Pairet, S., Iglesias, M., Salido, M., Gallen, M., Marsters, S., Ping Tsai, S., et al. (2012) Identification of a mutation in the extracellular domain of the Epidermal Growth Factor Receptor conferring cetuximab resistance in colorectal cancer. *Nat. Med. 18*, 221−223.

(22) Costa, R., Shah, A. N., Santa-Maria, C. A., Cruz, M. R., Mahalingam, D., Carneiro, B. A., Chae, Y. K., Cristofanilli, M., Gradishar, W. J., and Giles, F. J. (2017) Targeting Epidermal Growth Factor Receptor in triple negative breast cancer: new discoveries and practical insights for drug development. *Cancer Treat. Rev. 53*, 111−119.

(23) Occhipinti, E., Verderio, P., Natalello, A., Galbiati, E., Colombo, M., Mazzucchelli, S., Salvade, A., Tortora, P., Doglia, S. M., and Prosperi, D. (2011) Investigating the structural biofunctionality of antibodies conjugated to magnetic nanoparticles. *Nanoscale 3*, 387−390.

(24) Sousa, F., Castro, P., Fonte, P., Kennedy, P. J., Neves-Petersen, M. T., and Sarmento, B. (2017) Nanoparticles for the delivery of therapeutic antibodies: dogma or promising strategy? *Expert Opin. Drug Delivery 14*, 1163−1176.

(25) Colzani, B., Pandolfi, L., Hoti, A., Iovene, P. A., Natalello, A., Avvakumova, S., Colombo, M., and Prosperi, D. (2018) Investigation of antitumor activities of trastuzumab delivered by PLGA nanoparticles. *Int. J. Nanomed. 13*, 957−973.

(26) Alibakhshi, A., Kahaki, F. A., Ahangarzadeh, S., Yaghoobi, H., Yarian, F., Arezumand, R., Ranjbari, J., Mokhtarzadeh, A., and de la Guardia, M. (2017) Targeted cancer therapy through antibody fragments-decorated nanomedicines. *J. Controlled Release 268*, 323−334.

(27) Fiandra, L., Mazzucchelli, S., De Palma, C., Colombo, M., Allevi, R., Sommaruga, S., Clementi, E., Bellini, M., Prosperi, D., and Corsi, F. (2013) Assessing the in vivo targeting efficiency of multifunctional nanoconstructs bearing antibody-derived ligands. *ACS Nano 7*, 6092−6102.

(28) Colombo, M., Sommaruga, S., Mazzucchelli, S., Polito, L., Verderio, P., Galeffi, P., Corsi, F., Tortora, P., and Prosperi, D. (2012) Site-specific conjugation of ScFvs antibodies to nanoparticles by bioorthogonal strain-promoted alkyne-nitrone cycloaddition. *Angew. Chem., Int. Ed. 51*, 496−499.

(29) Colombo, M., Fiandra, L., Alessio, G., Mazzucchelli, S., Nebuloni, M., De Palma, C., Kantner, K., Pelaz, B., Rotem, R., Corsi, F., et al. (2016) Tumor homing and therapeutic effect of colloidal nanoparticles depend on the number of attached antibodies. *Nat. Commun. 7*, 13818.

(30) García-Fernández, L., Garcia-Pardo, J., Tort, O., Prior, I., Brust, M., Casals, E., Lorenzo, J., and Puntes, V. F. (2017) Conserved effects and altered trafficking of cetuximab antibodies conjugated to gold nanoparticles with precise control of their number and orientation. *Nanoscale 9*, 6111−6121.

(31) Truffi, M., Colombo, M., Sorrentino, L., Pandolfi, L., Mazzucchelli, S., Pappalardo, F., Pacini, C., Allevi, R., Bonizzi, A., Corsi, F., et al. (2018) Multivalent exposure of trastuzumab on iron oxide nanoparticles improves antitumor potential and reduces resistance in HER2-positive breast cancer cells. *Sci. Rep. 8*, 6563.

(32) Ahmed, S., Sami, A., and Xiang, J. (2015) HER2-directed therapy: current treatment options for her2-positive breast cancer. *Breast Cancer 22*, 101−116.

(33) Ning, S. T., Lee, S. Y., Wei, M. F., Peng, C. L., Lin, S. Y. F., Tsai, M. H., Lee, P. C., Shih, Y. H., Lin, C. Y., Luo, T. Y., et al. (2016) Targeting colorectal cancer stem-like cells with anti-CD133 antibody-conjugated SN-38 nanoparticles. *ACS Appl. Mater. Interfaces 8*, 17793−17804.

DOI: 10.1021/acs.bioconjchem.8b00667
Bioconjugate Chem. XXXX, XXX, XXX−XXX

(34) Berry, D. A., Cronin, K. A., Plevritis, S. K., Fryback, D. G., Clarke, L., Zelen, M., Mandelblatt, J. S., Yakovlev, A. Y., Habbema, J. D. F., and Feuer, E. J. (2005) Effect of screening and adjuvant therapy on mortality from breast cancer. *N. Engl. J. Med. 353*, 1784−1792.
(35) Ravdin, P. M., Cronin, K. A., Howlader, N., Berg, C. D., Chlebowski, R. T., Feuer, E. J., Edwards, B. K., and Berry, D. A. (2007) The decrease in breast-cancer incidence in 2003 in the United States. *N. Engl. J. Med. 356*, 1670−1674.
(36) Brenton, J. D., Carey, L. A., Ahmed, A. A., and Caldas, C. (2005) Molecular classification and molecular forecasting of breast cancer: ready for clinical application? *J. Clin. Oncol. 23*, 7350−7360.
(37) Bianchini, G., Balko, J. M., Mayer, I. A., Sanders, M. E., and Gianni, L. (2016) Triple-negative breast cancer: challenges and opportunities of a heterogeneous disease. *Nat. Rev. Clin. Oncol. 13*, 674−690.
(38) Foulkes, W. D., Smith, I. E., and Reis-Filho, J. S. (2010) Triple-negative breast cancer. *N. Engl. J. Med. 363*, 1938−1948.
(39) Jhan, J. R., and Andrechek, E. R. (2017) Triple-negative breast cancer and the potential for targeted therapy. *Pharmacogenomics 18*, 1595−1609.
(40) Chavez, K. J., Garimella, S. V., and Lipkowitz, S. (2011) Triple negative breast cancer cell lines: one tool in the search for better treatment of triple negative breast cancer. *Breast Dis. 32*, 35−48.
(41) Wang, Y. Y., Wang, Y. D., Chen, G. J., Li, Y. T., Xu, W., and Gong, S. Q. (2017) Quantum-dot-based theranostic micelles conjugated with an anti-EGFR nanobody for triple-negative breast cancer therapy. *ACS Appl. Mater. Interfaces 9*, 30297−30305.
(42) Mazzucchelli, S., Bellini, M., Fiandra, L., Truffi, M., Rizzuto, M. A., Sorrentino, L., Longhi, E., Nebuloni, M., Prosperi, D., and Corsi, F. (2017) Nanometronomic treatment of 4T1 breast cancer with nanocaged doxorubicin prevents drug resistance and circumvents cardiotoxicity. *Oncotarget 8*, 8383−8396.
(43) Pellegrino, T., Manna, L., Kudera, S., Liedl, T., Koktysh, D., Rogach, A. L., Keller, S., Rädler, J., Natile, G., and Parak, W. J. (2004) Hydrophobic nanocrystals coated with an amphiphilic polymer shell: a general route to water soluble nanocrystals. *Nano Lett. 4*, 703−707.
(44) Mazzucchelli, S., Colombo, M., Verderio, P., Rozek, E., Andreata, F., Galbiati, E., Tortora, P., Corsi, F., and Prosperi, D. (2013) Orientation-controlled conjugation of HALO-fused homing peptides to multifunctional nanoparticles for specific recognition of cancer cells. *Angew. Chem., Int. Ed. 52*, 3121−3125.
(45) Mazzucchelli, S., Colombo, M., De Palma, C., Verderio, P., Coghi, M. D., Clementi, E., Tortora, P., Corsi, F., and Prosperi, D. (2010) Synthesis of single-domain protein A-engineered magnetic nanoparticles: toward a universal strategy to site-specific labeling of antibodies for targeted detection of tumor cells. *ACS Nano 4*, 5693−5702.
(46) Hsu, H. C., Thiam, T. K., Lu, Y. J., Yeh, C. Y., Tsai, W. S., You, J. F., Hung, H. Y., Tsai, C. N., Hsu, A., Chen, H. C., et al. (2016) Mutations of KRAS/NRAS/BRAF predict cetuximab resistance in metastatic colorectal cancer patients. *Oncotarget 7*, 22257−22270.
(47) Schlessinger, J. (2000) Cell signaling by receptor tyrosine kinases. *Cell 103*, 211−25.
(48) Kumaraswamy, E., Wendt, K. L., Augustine, L. A., Stecklein, S. R., Sibala, E. C., Li, D., Gunewardena, S., and Jensen, R. A. (2015) BRCA1 regulation of epidermal growth factor receptor (EGFR) expression in human breast cancer cells involves microrna-146a and is critical for its tumor suppressor function. *Oncogene 34*, 4333−4346.
(49) Jorissen, R. N., Walker, F., Pouliot, N., Garrett, T. P., Ward, C. W., and Burgess, A. W. (2003) Epidermal growth factor receptor: mechanisms of activation and signalling. *Exp. Cell Res. 284*, 31−53.
(50) Vincenzi, B., Schiavon, G., Silletta, M., Santini, D., and Tonini, G. (2008) The biological properties of cetuximab. *Crit. Rev. Oncol. Hematol. 68*, 93−106.
(51) Lin, S.-Y., Makino, K., Xia, W., Matin, A., Wen, Y., Kwong, K. Y., Bourguignon, L., and Hung, M.-C. (2001) Nuclear localization of EGF receptor and its potential new role as a transcription factor. *Nat. Cell Biol. 3*, 802−808.
(52) Brand, T. M., Iida, M., Luthar, N., Starr, M. M., Huppert, E. J., and Wheeler, D. L. (2013) Nuclear EGFR as a molecular target in cancer. *Radiother. Oncol. 108*, 370−377.
(53) Roepstorff, K., Grandal, M. V., Henriksen, L., Knudsen, S. L. J., Lerdrup, M., Grøvdal, L., Willumsen, B. M., and van Deurs, B. (2009) Differential effects of EGFR ligands on endocytic sorting of the receptor. *Traffic 10*, 1115−1127.
(54) van Tilborg, G. A. F., Mulder, W. J. M., Chin, P. T. K., Storm, G., Reutelingsperger, C. P., Nicolay, K., and Strijkers, G. J. (2006) Annexin A5-conjugated quantum dots with a paramagnetic lipidic coating for the multimodal detection of apoptotic cells. *Bioconjugate Chem. 17*, 865−868.
(55) Wu, X., Rubin, M., Fan, Z., DeBlasio, T., Soos, T., Koff, A., and Mendelsohn, J. (1996) Involvement of $p27^{KIP1}$ in G1 arrest mediated by an anti-epidermal growth factor receptor monoclonal antibody. *Oncogene 12*, 1397−1403.
(56) McCubrey, J. A., Steelman, L. S., Chappell, W. H., Abrams, S. L., Wong, E. W., Chang, F., Lehmann, B., Terrian, D. M., Milella, M., Tafuri, A., et al. (2007) Roles of the Raf/MEK/ERK pathway in cell growth, malignant transformation and drug resistance. *Biochim. Biophys. Acta, Mol. Cell Res. 1773*, 1263−1284.
(57) Marzi, L., Combes, E., Vié, N., Ayrolles-Torro, A., Tosi, D., Desigaud, D., Perez-Gracia, E., Larbouret, C., Montagut, C., Iglesias, M., et al. (2016) FOXO3a and the MAPK p38 are activated by cetuximab to induce cell death and inhibit cell proliferation and their expression predicts cetuximab efficacy in colorectal cancer. *Br. J. Cancer 115*, 1223−1233.
(58) Kurai, J., Chikumi, H., and Hashimoto, K. (2007) Antibody-dependent cellular cytotoxicity mediated by cetuximab against lung cancer cell lines. *Clin. Cancer Res. 13*, 1552−1561.
(59) Kimura, H., Sakai, K., Arao, T., Shimoyama, T., Tamura, T., and Nishio, K. (2007) Antibody-dependent cellular cytotoxicity of cetuximab against tumor cells with wild-type or mutant epidermal growth factor receptor. *Cancer Sci. 98*, 1275−1280.
(60) Georgescu, M.-M. (2010) PTEN tumor suppressor network in PI3K-Akt pathway control. *Genes Cancer 1*, 1170−1177.
(61) Eckert, L. B., Repasky, G. A., Ülkü, A. S., McFall, A., Zhou, H., Sartor, C. I., and Der, C. J. (2004) Involvement of Ras activation in human breast cancer cell signaling, invasion, and anoikis. *Cancer Res. 64*, 4585−4592.
(62) Jaramillo, M. L., Leon, Z., Grothe, S., Paul-Roc, B., Abulrob, A., and O'Connor McCourt, M. (2006) Effect of the anti-receptor ligand-blocking 225 monoclonal antibody on EGF receptor endocytosis and sorting. *Exp. Cell Res. 312*, 2778−2790.
(63) Ho, K.-K., McGuire, V. A., Koo, C.-Y., Muir, K. W., de Olano, N., Maifoshie, E., Kelly, D. J., McGovern, U. B., Monteiro, L. J., Gomes, A. R., et al. (2012) Phosphorylation of FOXO3a on Ser-7 by p38 promotes its nuclear localization in response to doxorubicin. *J. Biol. Chem. 287*, 1545−1555.
(64) Yang, J.-Y., Zong, C. S., Xia, W., Yamaguchi, H., Ding, Q., Xie, X., Lang, J. Y., Lai, C. C., Chang, C. J., et al. (2008) ERK promotes tumorigenesis by inhibiting FOXO3a via MDM2-mediated degradation. *Nat. Cell Biol. 10*, 138−148.
(65) Biggs, W. H., Meisenhelder, J., Hunter, T., Cavenee, W. K., and Arden, K. C. (1999) Protein kinase B/Akt-mediated phosphorylation promotes nuclear exclusion of the winged helix transcription factor FKHR1. *Proc. Natl. Acad. Sci. U. S. A. 96*, 7421−7426.
(66) van der Vos, K. E., and Coffer, P. J. (2011) The extending network of FOXO transcriptional target genes. *Antioxid. Redox Signaling 14*, 579−592.
(67) King, D., Yeomanson, D., and Bryant, H. E. (2015) PI3King the lock: targeting the PI3K/Akt/mTOR pathway as a novel therapeutic strategy in neuroblastoma. *J. Pediatr. Hematol./Oncol. 37*, 245−251.
(68) Rafalski, V. A., and Brunet, A. (2011) Energy metabolism in adult neural stem cell fate. *Prog. Neurobiol. 93*, 182−203.

DOI: 10.1021/acs.bioconjchem.8b00667
Bioconjugate Chem. XXXX, XXX, XXX−XXX

LIST OF PUBLICATIONS

1) **Rizzuto M**.,[†] Colombo M.,[†] Pandolfi L., Pacini C., Bonizzi A., Truffi M., et al. (2018). Half-Chain Cetuximab Nanoconjugates Allow Multitarget Therapy of Triple Negative Breast Cancer. BIOCONJUGATE CHEMISTRY. in press. DOI: 10.1021/acs.bioconjchem.8b00667.

2) Riva, B., Bellini, M., Corvi, E., Verderio, P., Rozek, E., Colzani, B.,… **Rizzuto M**., et al. (2018). Impact of the strategy adopted for drug loading in nonporous silica nanoparticles on the drug release and cytotoxic activity. JOURNAL OF COLLOID AND INTERFACE SCIENCE, 519, 18-26.

3) Pandolfi, L., Bellini, M., Vanna, R., Morasso, C., Zago, A., Carcano, S.,… **Rizzuto M.**, et al. (2017). H-Ferritin Enriches the Curcumin Uptake and Improves the Therapeutic Efficacy in Triple Negative Breast Cancer Cells. BIOMACROMOLECULES, 18(10), 3318-3330.

4) Mazzucchelli, S., Truffi, M., Baccarini, F., Beretta, M., Sorrentino, L., Bellini, M., **Rizzuto M**., et al. (2017). H-Ferritin-nanocaged olaparib: A promising choice for both BRCA-mutated and sporadic triple negative breast cancer. SCIENTIFIC REPORTS, 7(1).

5) Mazzucchelli, S., Bellini, M., Fiandra, L., Truffi, M., **Rizzuto, M**., Sorrentino, L., et al. (2017). Nanometronomic treatment of 4T1 breast cancer with nanocaged doxorubicin prevents drug resistance and circumvents cardiotoxicity. ONCOTARGET, 8(5), 8383-8396.

6) Bellini, M., Mazzucchelli, S., Galbiati, E., Sommaruga, S., Fiandra, L., Truffi, M., **Rizzuto M**., et al. (2014). Protein nanocages for self-triggered nuclear delivery of DNA-targeted chemotherapeutics in Cancer Cells. JOURNAL OF CONTROLLED RELEASE, 196, 184-196.